

Strong Climate Control on the Millennial-Scale Dust Variability and Sediment Provenances in the Equatorial Indian Ocean inferred from Sr-Nd Isotopes

Arvind Shukla^{1,2}, Sunil Kumar Singh^{1*}, Dharmendra Pratap Singh³, Aka Sharma⁴, and A. P. Dimri⁴

¹CSIR-National Institute of Oceanography, Dona-Paula, Goa, India-403004,

²School of Earth Ocean and Atmospheric Sciences, Goa University, Dona-Paula, Goa, India-403004

³Department of Earth Sciences, IIT Roorkee, Roorkee, India-247667

⁴School of Environmental Sciences, Jawaharlal Nehru University, New Delhi 110067, India

*Corresponding author: Sunil Kumar Singh

Email: mail to: sunil@nio.org

Abstract

High-resolution Sr and Nd isotope compositions along with major and trace element abundances have been analyzed in silicate fraction of sediments core, SSD004-GC03, from the equatorial Indian Ocean (7.2 °N and 77.9 °E) at 1540 m water depth with a depositional history of ~38 ka to determine source variabilities and their controlling factors. $^{87}\text{Sr}/^{86}\text{Sr}$ (0.71978 to 0.72491), ϵ_{Nd} (-14.8 to -21.9), and a couple of source diagnostic elements display profound variability over the depositional time scale and point towards major sediment contribution from the Peninsular Gneissic Complex (PGC) and the Deccan Basalt along with aeolian dust flux, their relative proportions being determined by climate variability. The cold/arid periods are characterised by an enhanced proportion of aeolian dust and the Deccan Basalts, whereas the sediment contribution from the PGC is augmented during the warm/humid periods. The sediment provenance variations at the equatorial Indian Ocean coincide very well with known cold/arid (Heinrich Stadial events: HS 1-4, LGM, Younger Dryas, 8.2 ka, 5.2 ka, and 1.1 ka) and warm/humid (Early Deglacial, Holocene Intensified Monsoon) climatic events reported in the tropical region and sea-level change which are strongly captured by the Sr-Nd isotope and elemental composition of sediments. The present investigation underscores the significant role of climate, mainly the aridity, in modulating the dust fluxes and erosion intensity and the strong coupling between Indian monsoon and North Atlantic climatic oscillations and further demonstrates minimal time delay between the production and transport of sediment from source to sink.

Keywords

Equatorial Indian Ocean, Aeolian dust, Climate-weathering-erosion, Indian monsoon, Sr-Nd isotope

Key points

- 1) High-resolution $^{87}\text{Sr}/^{86}\text{Sr}$, ϵ_{Nd} and a few diagnostic elements track temporal variation of sediment sources in the equatorial Indian Ocean.
- 2) The cold periods are characterised by enhanced proportions of aeolian dust and the Deccan Basalts, whereas the PGC dominates warm periods.
- 3) North Atlantic climatic oscillations modulate Indian monsoon thereby controlling dust and erosional fluxes in the Equatorial Indian Ocean.

1. Introduction

The sediments deposited in the Indian Ocean (IO) archive information pertaining to provenance, erosion, transport, deposition and the factors impacting these processes and hence serve as a natural laboratory to study the erosional processes the surrounding land masses have undergone, variability in the aeolian fluxes of the basin and the records of climatic and sea-level variabilities influencing these processes (Clift et al., 2010; Goswami et al., 2012; Tripathy et al., 2011). The sediment composition at a given site is determined by, in addition to their sources, their proximity to the depositional site, ocean and atmospheric currents, and climatic and tectonic parameters. The landlocked northern Indian Ocean receives \sim 2000 metric tons of sediments annually from the Himalaya, the Deccan Basalt, the Peninsular Gneisses, and the Indo-Burman ranges (Clift et al., 2008; Colin et al., 1999; Derry & France-Lanord, 1996; Galy & France-Lanord, 2001; Goswami et al., 2012; Inam et al., 2007; Milliman & Syvitski, 1992; Peketi et al., 2021) and \sim 200 million tons of aeolian dust annually emanating from arid land masses of the Africa, Sahara, Arabia, and Indian continent (Figure 1; Ramaswamy & Nair, 1994; Sirocko & Sarnthein, 1989).

The climate plays a vital role in determining the erosion pattern of a drainage basin and aeolian dust fluxes. The Indian subcontinent experiences two phases of monsoon, the southwest (SW)-summer monsoon, and the northeast (NE)-winter monsoon. SW monsoon provides 80% of the annual rainfall (Gadgil, 2003) along with 85% of the yearly sediment discharge to the nearby basins. The impact of the SW monsoon is widespread over the entire India, whereas the NE monsoon has a more significant impact on the east coast of southern India (Rajeevan et al., 2012). The intensities and patterns of these monsoon phases have varied in the past (Fleitmann et al., 2003; Gupta et al., 2003) which controlled the erosion pattern of the surrounding drainage basins, the aeolian dust fluxes, and the supply of sediments to the nearby sea (Ahmad et al., 2005; Clift et al., 2008; Colin et al., 2006; Cruz et al., 2021; Goswami et al., 2012; Tripathy et al., 2011). In addition to impacting erosion, the monsoon also controls the surface water circulation and generates coastal currents (Shankar et al., 2002), which plays an essential role in the transportation and deposition of the sediments in the Arabian Sea (AS) and the Bay of Bengal (BoB) (Goswami et al., 2012; Tripathy et al., 2011). During the NE monsoon, low saline surface water flows from the BoB to the Arabian Sea, in terms of the East India Coastal Current (EICC) (Schott and McCreary, 2001, Shankar et al., 2002). This current transports suspended particulate matter from the western Bay of Bengal (WBoB) to the Eastern Arabian Sea (EAS) (Goswami et al., 2012), while in summer, the SW monsoon generates West India Coastal Current (WICC), which transports high saline water from the Arabian Sea to the western BoB (Schott and McCreary, 2001, Shankar et al., 2002). The intensity of the cross-basin exchange of water in the form of WICC and EICC has varied

in the past on the glacial-interglacial time scale (Yadav et al., 2021). Equatorial Indian Ocean (EIO) gets affected by these cross-basin exchanges of waters (Mahesh and Banakar 2014; Shankar et al., 2002; Tiwari et al., 2005; Yadav et al., 2021). Moreover, these coastal currents (WICC and EICC) play a crucial role in the transportation and deposition of the sediments in the AS and the BoB on the glacial-interglacial time scale (Sarkar et al., 1990; Goswami et al., 2012; Tripathy et al., 2011). EIO receives sediments mostly from its proximal sources, i.e., the Peninsular Gneisses and the Deccan Basalt, along with the material brought from the Himalaya by coastal currents through cross basin exchange and aeolian dust fluxes (Goswami et al., 2012; Sirocko & Sarnthein, 1989). Previously, variations of sediment provenance in the BoB and the AS on a glacial-interglacial time scale have been examined with the help of clay mineralogy, chemical composition, and Sr-Nd isotope compositions (Ahmad et al., 2005; Colin et al., 1999; France-Lanord et al., 1993; Goswami et al., 2012; Kessarkar et al., 2003; Tripathy et al., 2011) which serve as reliable tracers for sediment provenance. The $^{87}\text{Sr}/^{86}\text{Sr}$ and $^{143}\text{Nd}/^{144}\text{Nd}$ of the source rock vary according to Rb/Sr, Sm/Nd ratios, and their ages, respectively. Detrital materials coming to the ocean are the weathering products of continental rocks with a considerable variation in their Sr and Nd isotope ratios. Due to the distinct composition of Sr and Nd isotope ratios, ocean sediments are found suitable to trace their provenances. The major and trace element composition, along with Sr and Nd isotope, are also associated with the provenance characteristics and hence useful in identifying the source variabilities of sediments at the glacial-interglacial cycles.

Proximate sources of the sediments deposited in the EIO are characterised by considerable variation in Sr and Nd isotope ratios as the Indian peninsular region is categorized by varying lithology of different ages from Cretaceous Deccan basalt to Archean-Proterozoic gneissic complexes to the Himalayan sources (Figure 2 A & B). Major peninsular rivers like Krishna, Godavari, and the Cauvery, mainly contribute to sediments in the western BoB within the shelf and continental rise of the eastern coast (Einsele et al., 1996). Major dust sources delivering a quantifiable amount of dust in the Equatorial Indian Ocean such as the African, Sahara, Arabian, and the Thar are characterised by their distinct Sr, Nd isotope composition (Pease et al., 1998; Pourmand et al., 2004; Sirocko and Sarnthein, 1989; and Suresh et al., 2021). Any temporal variation in their relative proportions due to climatic variability could be tracked by Sr and Nd isotope composition archived in the sediment deposits.

The Equatorial Indian Ocean receives sediments from the EAS, the western BoB, and rivers draining Southern India. The sediments deposited in the Arabian Sea, the BoB, and EIO (off the southern tip of India) archive the paleo erosion history of the source region and factors affecting the dispersal and deposition of the sediments. Furthermore, the Gulf of Mannar region serves as a crucial

sedimentary depocenter for comprehending the impact of tectonic activity, climatic change, and sea level fluctuations on sediment provenance over geological time. While previous research has been conducted in the BoB and the Arabian Sea, this specific area warrants dedicated investigation into tracing sediment sources. This is particularly significant in the context of ascertaining the contribution of sediment originating from the Indian Peninsula, as other regions (BoB and AS) are significantly influenced by the substantial input of Himalayan sediments, thereby attenuating the discernibility of peninsular India's sedimentary contributions. It is imperative to highlight that this area experiences markedly reduced Himalayan sediment compared to BoB and Arabian Sea, falling within a shadow zone with minimal Himalayan input. Consequently, it offers an ideal opportunity to meticulously trace the contribution of sediments from the Indian Peninsula throughout glacial-interglacial time scales. The primary source of sediments to the core (SSD004-GC03) location may be from peninsular India, but detailed tracking is still required.

The major objectives of the present study are to (1) determine the temporal variation of sediment source deposited in EIO until the last ~38 ka BP, (2) assess the impact of climate on the sediment provenance in the EIO and (3) know the role of surface ocean currents (EICC & WICC) and sea level on the deposition and dispersal of sediments in the EIO. As per the knowledge, very few studies were found for tracing sediment sources in the EIO on the glacial-interglacial time scale. In this high-resolution study, tracing of sediment provenance in the EIO (off the southern tip of India) has been carried out for the first time to know the impact of climate on the weathering and erosion of the source rock. This study will be able to expand our understanding of the past variability of the sediment sources in the EIO and its climatic connection over the millennial time scale. Thus, the basic objectives of the present study are to determine the temporal variation in sources of sediments deposited in the Gulf of Mannar in the Equatorial Indian Ocean and the factors contributing to these variabilities utilizing major and trace elements and Sr-Nd isotopic composition in the sediments on the millennial time scale.

2. Study area, core details and chronology

The sediment samples of this study are taken from a 5.5 m long gravity core (SSD004-GC03) drilled off the Southern tip of India (7.2° N and 77.9° E) at a water depth of 1540 m (Figure 1). This core location is strategically selected to know the sediment provenance and to assess the impact of varying climatic events (cold/arid and warm/wet) on the sediment provenances over the EIO. The chronology of this sediment core was established using Accelerated Mass Spectrometer (AMS) radiocarbon dating of 18 mixed planktonic foraminifera (>350 μm size) (Singh, 2019; Singh et al., 2022). This core covers the depositional history of sediments up to ~38 ka with sedimentation rates varying from 4.4 cm/ka to 31.2 cm/ka (average: 16.0 cm/ka). The sedimentation rate during the Last Glacial Maxima (LGM) (~23

ka to ~20 ka) is 11.6 cm/ka, whereas it varies from 9.1 cm/ka to 31.2 cm/ka (mean value: 22 cm/ka) during the Holocene periods (~11 ka to present). The ages of the sediments between 9 to 22 ka are constrained better with an additional 13 number of AMS radiocarbon (^{14}C) dates on surface mixed layer planktic foraminifera (*Globigerinoides ruber* + *Trilobatus sacculifer*). The interpolated ages of samples collected between 0 to 9 and 22 to 38 ka will have comparatively larger uncertainties owing to a lesser number of dates; 3 and 2 samples, respectively used for constraining the ages. The interpolated ages of the samples used in this study are listed in Table 1.

3. Analysis of Major elements, trace elements, Sr, and Nd isotope

We have measured major and trace element concentrations and isotope composition of Sr and Nd in the silicate fraction of the GC03 core sediments. Bulk sediments were first desalinated with ultrapure grade water (Millipore^{®TM}), oven-dried at 90°C, powdered, and sieved (<100µm). These samples were subsequently analyzed for Sr-Nd isotope and concentrations in the silicate fraction of the sediments after removing carbonates, Fe-Mn hydroxides and organic matter (Bayon et al., 2002; Gutjahr et al., 2007, Singh et al., 2008). Briefly, approximately one gram of powdered sediment from each sample was treated with a 1M hydroxylamine hydrochloride mixture and 0.03M Na-EDTA solution in acetic acid (25% v/v) buffered to pH ≈ 4 with NaOH (Bayon et al., 2002; Gutjahr et al., 2007). The residual sediments were dried and decarbonated using 0.6 N HCl at 70 °C. The supernatants were discarded after centrifugation and residuals were washed with MQ 3 to 4 times to remove the acid. Subsequently, the samples were ashed in a muffle furnace at 600 °C to remove organic matter. A known amount (~50 mg) of the silicate fraction was digested with HF-HNO₃-HCl. An international rock standard (BCR-2) was digested for each batch along with the samples. The abundances of major and trace elements were determined using Inductively Coupled Plasma Optical Emission Spectroscopy (ICP-OES) and a High-Resolution Inductively Coupled Plasma Mass Spectrometer (HR-ICP-MS), respectively at CSIR-NIO, Goa. Sr and Nd were separated from the dissolved samples using AG50W-X8 (200-400 microns) and Eichrom Ln-specTM resins (50-100 microns) (Singh et al., 2008). Isotopic composition $^{87}\text{Sr}/^{86}\text{Sr}$ and $^{143}\text{Nd}/^{144}\text{Nd}$ were measured using the Multicollector Inductively Coupled Plasma Mass Spectrometer (MC-ICP-MS) (NU Plasma III) at CSIR-NIO, Goa in static mode. Mass-dependent fractionations for Sr and Nd were corrected by normalizing $^{86}\text{Sr}/^{88}\text{Sr}$ to 0.1194 and $^{146}\text{Nd}/^{144}\text{Nd}$ to 0.7219, respectively. $^{87}\text{Sr}/^{86}\text{Sr}$ and $^{143}\text{Nd}/^{144}\text{Nd}$ measured in reference standards SRM987 and JNd-1 yielded 0.710259 ± 0.000011 ; (1 σ , n = 22) and 0.512089 ± 0.000004 (1 σ , n = 22) respectively, agreeing well with the recommended values (Lei et al., 2019). An international rock standard (BCR-2) was also measured with each batch, yielding $^{87}\text{Sr}/^{86}\text{Sr}$ and $^{143}\text{Nd}/^{144}\text{Nd}$ values of 0.705034 ± 0.000006 (1 σ) and 0.512583 ± 0.000004 (1 σ) and compare well with the reported values (Lei et al., 2019). The internal

reproducibility of data was better than 10 ppm ($1\sigma_{\mu}$) for both Sr and Nd isotopes. The procedural blanks for Sr and Nd, measured along with samples, were orders of magnitude lower than the total Sr and Nd analyzed in the samples; hence, no blank corrections were made. The Nd isotopic composition is expressed as,

$$\epsilon_{\text{Nd}} = [((^{143}\text{Nd}/^{144}\text{Nd})_{\text{sample}} / (^{143}\text{Nd}/^{144}\text{Nd})_{\text{CHUR}}) - 1] \times 10^4$$

Where, $^{143}\text{Nd}/^{144}\text{Nd}$ is the measured Nd isotopic composition of the samples and $^{143}\text{Nd}/^{144}\text{Nd}_{\text{CHUR}}$ is the present-day $^{143}\text{Nd}/^{144}\text{Nd}$ value of Chondritic Uniform Reservoir (CHUR), which is 0.512638 (Jacobsen and Wasserburg, 1980).

Major oxides in the bulk sediments were analyzed using X-ray fluorescence (XRF) (S8 Tiger, Bruker) at IISER Pune by fusing them into glass beads (Samanta, 2022). The precision and accuracy of these measurements were monitored throughout the analysis by including two certified reference materials, namely USGS BCR-2 and BHVO-2 and were found to be better than 4%.

3.1. Modeling of change in precipitation over Peninsular India during LGM with respect to Present

Precipitation during LGM (20-23 ka) has been modelled using Max Planck Institute Earth System Model version 1.2 (MPI-ESM1-2-LR) from the modelling suite of Paleoclimate Modelling Intercomparison Project phase fourth (PMIP4) simulations in the Coupled Model Intercomparison Project (CMIP6) having spatial resolution of 250 km (Mauritsen et al., 2019; Figure S1). Whereas, the present day i.e. from 1980 to 2010 (Harris et al., 2020) rainfall dataset have been taken from Climate Research Unit (CRU) having spatial resolution of 50 km (Figure S2). The difference in the precipitation (LGM-Present) has been estimated by regridding the LGM data at 50 km spatial resolution.

4. Results

4.1. Major and trace element concentrations

To characterize the sediment provenance, the concentration of trace and major elements along with Sr and Nd isotopes were measured. The concentrations of major elements such as K, Ca, Al, Mg, Na and Ti, and trace elements Zr, Hf, Cr, Rb, and Sr are catalogued in Table 1. The relative abundance of these elements throughout the core was found in the order, Ca<Na<Ti<Mg<K<Al with significant temporal variations; K: 1.25 to 2.13 wt%, Ca: 0.03 to 0.39 wt%, Na: 0.20 to 0.71 wt%, Al: 7.15 to 8.72 wt%, Mg: 0.07 to 20.4 wt%, Ti: 0.55 to 0.97 wt% (Table 1). Abundances of Rb, Sr and Nd vary from 63 to 144 $\mu\text{g/g}$, 44 to 150 $\mu\text{g/g}$ and 12 to 33 $\mu\text{g/g}$ respectively. The Rb/Sr varies from 0.81 to 2.5.

4.2. Sr-Nd isotopic composition

The $^{87}\text{Sr}/^{86}\text{Sr}$ in these sediment samples display a range from 0.71978 to 0.72491 (mean value: 0.72257), and ϵ_{Nd} , from -21.9 to -14.8 (mean value of -17.8) (Table 1), suggesting varying relative contributions from different sediment sources to the core location. $^{87}\text{Sr}/^{86}\text{Sr}$ and ϵ_{Nd} values for Holocene sediments (~11 ka to present) vary from 0.71978 to 0.72491 (average value of 0.72256) and -21.9 to -16.5 (average value: -20.3), respectively. For pre-LGM (~23 ka to ~38 ka) sediments, $^{87}\text{Sr}/^{86}\text{Sr}$ varies from 0.72132 to 0.72394 (average value: 0.72304) and ϵ_{Nd} values are varying from -19.8 to -15.9 (average value: -17.5). LGM sediments are characterised by marginally less radiogenic Sr and more radiogenic Nd with $^{87}\text{Sr}/^{86}\text{Sr}$ varying from 0.71999 to 0.72349 (average value: 0.72121) and ϵ_{Nd} from -16.8 to 14.9 (average value: -15.6). Throughout the Early Deglaciation (ED) period, $^{87}\text{Sr}/^{86}\text{Sr}$ and ϵ_{Nd} data varies from 0.72205 to 0.72460 (average value: 0.72278) and -18.0 to -14.8 (average value: -16.9) respectively.

The concentrations and isotope compositions of Sr and Nd in the sediments of the core GC03 (Table 1) are comparable to those reported in earlier studies from the AS and the BoB (Goswami et al., 2012; Kessarkar et al., 2003; Peketi et al., 2021; Tripathy et al., 2011). Kessarkar et al., 2003 reported Sr isotope values, 0.7172 to 0.7229 and ϵ_{Nd} values, -12.6 to -20.3 for Holocene sediment and $^{87}\text{Sr}/^{86}\text{Sr}$, 0.7160 to 0.7230 and ϵ_{Nd} , -13.6 to -23.0 for late Pleistocene sediment from EAS. These values fall within the range of Sr-Nd isotope data of the present study. $^{87}\text{Sr}/^{86}\text{Sr}$ (~0.7250) and ϵ_{Nd} (~ -14) of LGM samples reported in western BoB (SK187/PC33) (Tripathy et al., 2011) are comparable with the present study. These values are within the range of the various sources supplying sediments to the core site (Figure 1). Potential dust sources delivering a significant amount of dust with their characteristics Sr-Nd isotopic values in the Equatorial Indian Ocean are the African ($^{87}\text{Sr}/^{86}\text{Sr}$: 0.708 to 0.747; ϵ_{Nd} : -17.9 to -3.1), Arabian ($^{87}\text{Sr}/^{86}\text{Sr}$: 0.7125 to 0.7105; ϵ_{Nd} : -8.2 to -4.6), and Thar Desert ($^{87}\text{Sr}/^{86}\text{Sr}$: 0.729 to 0.739; ϵ_{Nd} : -15.8 to -12.6). The Sr and Nd isotopic data for dust characterization have been tabulated in the supplementary information with their respective references (Table S3). The significant temporal variation in $^{87}\text{Sr}/^{86}\text{Sr}$ and ϵ_{Nd} observed in the core SSD004-GC03 sediments are well beyond the analytical uncertainties and can be used to track variability in the sediment provenance in the EIO. Some of the studies based in the Arabian Sea and the Bay of Bengal having similar sediment provenance and depositional characteristics utilized these proxies successfully to diagnose the sediment sources (France Lanord et al., 1993; Goswami et al., 2012; Li et al., 2018; Peketi et al., 2021; Tripathy et al., 2011). Chemical erosion and the minerals/size sorting during transport, however, might alter the source signatures of Sr and Nd isotopes; making the application of these proxies difficult in a few cases (Derry & France-Lanord, 1996; Meyer et al., 2011). To ensure whether Sr-Nd isotope data

of SSD004-GC03 were affected by grain size sorting and chemical weathering during erosion and transport, the Sr-Nd isotope data are plotted with $\text{SiO}_2/\text{Al}_2\text{O}_3$ ratio, Hf/Nd ratio, and chemical index of alteration (CIA) (Figure S3, S4 and S5), respectively. CIA can be used to quantify the chemical weathering intensity and provides information about the degree of chemical weathering of the rocks (Nesbitt & Young, 1982) and calculated as:

$$\text{CIA} = \text{Al}_2\text{O}_3 / (\text{K}_2\text{O} + \text{NaO} + \text{CaO}^* + \text{Al}_2\text{O}_3)$$

Where CaO^* represents the concentration of Ca from the silicate fraction of the sediment only.

Sr-Nd versus $\text{SiO}_2/\text{Al}_2\text{O}_3$, Hf/Nd and CIA plots of these sediments (Figs S3, S4, S5) display almost no correlation suggesting little impact of size sorting and chemical alteration on their isotope composition. Marginal apparent correlations observed between ε_{Nd} vs CIA and ε_{Nd} vs $\text{SiO}_2/\text{Al}_2\text{O}_3$ could result from their source variability, basalt vs granite/gneisses as these sources possess distinct $\text{SiO}_2/\text{Al}_2\text{O}_3$, CIA and ε_{Nd} . The $\text{SiO}_2/\text{Al}_2\text{O}_3$ ratio in PGC consistently exhibits higher values compared to Deccan. The observed correlations in these plots (Figure S4) reflect changes originating partly from the source rock variation and not because of grain size variation.

In addition to the aforementioned discussion, we also employed Hf/Nd ratios to assess the influence of grain size on the Sr and Nd isotopes within the silicate fraction. During the silicate weathering, a large inventory of Hf in the crustal rocks remains locked in zircon which tends to be sorted into the coarser size fraction (silt and sand) during the sediment transport. Conversely, Nd is more inclined to be associated with the finer sediment fractions during the weathering and transportation processes (Bayon et al., 2009; Carter et al., 2020; Meyer et al., 2011; Patchett et al., 1984). Therefore, the Hf/Nd ratio can also be used as a grain size verification indicator along with the $\text{SiO}_2/\text{Al}_2\text{O}_3$. The scatter plot of Hf/Nd vs Sr-Nd isotope (Figure S5) shows a very poor correlation (R^2 : 0.004 to 0.432).

The absence of any significant correlation of Sr-Nd isotope with $\text{SiO}_2/\text{Al}_2\text{O}_3$, CIA and Hf/Nd (Figure S3, S4 and S5) affirms that Sr-Nd isotopic composition of these sediments remains unaffected by size sorting and chemical weathering, therefore can be used as excellent geochemical proxy for tracing the sediment provenance in the basin. In addition, the concomitant change in both $^{87}\text{Sr}/^{86}\text{Sr}$ and ε_{Nd} values argue in favour of provenance changes and not due to the particle sorting/weathering process (Colin et al., 2006; Tütken et al., 2002; Walter et al., 2000). Therefore, it can be asserted with confidence that the fluctuations in Sr-Nd isotope ratios and elemental concentrations do not result from differences in grain size but rather stem from shifts in the sediment's provenance. These results gave us the confidence to use Sr and Nd isotope data in the silicate fraction of the sediment as a provenance indicator over the past ~38 kyr.

The $^{87}\text{Sr}/^{86}\text{Sr}$, Σ_{Nd} , Rb/Sr, CIA, and Al normalized major and trace elements data display a noticeable temporal variation coinciding with the known climatic intervals, such as the Heinrich events, LGM, Early Deglacial, Younger Dryas, and other various cooling events. An earlier study (Singh et al., 2022), based on the samples of this core GC03, demonstrated $\sim 4^{\circ}\text{C}$ temperature variation during glacial-interglacial time scale in the time interval of 9 to 22 ka. In addition, during the same time interval, the sea level has increased by ~ 120 m from the Glacial to the Holocene. These variabilities have significantly impacted sediment provenances.

5. Discussion

5.1. The Provenance of the Sediments

Major potential sources of sediments at the core site of this study are (i) Peninsular Gneisses, (ii) Deccan Basalt, (iii) the aeolian dust from Africa, Arabian Peninsula, and the Thar desert (Figure 1A & B). The Mahanadi, Godavari, Krishna, Nethravathi and the Narmada bring sediments mixture from the Deccan and the Peninsular Gneisses. The Cauvery, Periyar, Vaigai, and the Thamirabarani deliver sediments from the Peninsular Gneisses. The abundant Himalayan sediments brought by the Ganga-Brahmaputra River system may contribute a little to the core location due to its location. The sediments delivered at the west and east coasts are brought to the Equatorial Indian Ocean by the WICC and EICC respectively (Figure 1A).

Sr and Nd isotope compositions, the diagnostic proxies of the potential major sources of the sediments; of the Peninsular Gneisses, Deccan Basalt, Higher and Lesser Himalaya, and the aeolian dust, are characterised based on the available data in the literature as discussed in the supplementary sections (Table S1; Figure S6 & S7). Endmembers' characterization of sediment sources is validated by the similar isotope compositions of sediments delivered by the rivers draining them (Figure S8).

Sr-Nd isotope composition of the sediments and the potential endmembers are plotted on the binary mixing plots (Figure 3 and Figure S8) to trace and quantify the sediment provenances. It is evident from the mixing plots that most of the samples are lying in the mixing field defined by the Deccan Basalts, the PGC and the aeolian dust suggesting the dominant contribution from aeolian dust and the Deccan Basalt compared to the PGC (Figure 3). The contribution from the Himalayan sources appears to be negligible as the core site in the Gulf of Mannar is a restricted basin with minimal contribution from the Himalayan sediments through the EICC and hence the Himalayan endmembers are not considered in the mixing diagram (Figure 3). Due to the restricted nature of the Mannar basin in the equatorial Indian Ocean, fluvial sediments are derived mostly from local rivers with smaller sediment fluxes such as the Periyar, Vaigai and Thamirabarani (Figure 1A), resulting in an enhanced impact of

aeolian dust on sediment budget. The Holocene sediments are characterised by contributions from the PGC and the Deccan Basalt, whereas sediments deposited during LGM, Younger Dryas, and other cold/arid events are defined by enhanced aeolian contributions from the Arabian Peninsula, African, and Thar desert and the Deccan Basalt (Figure 3). During the Last Glacial Maximum, the relative contribution from the Deccan stands at approximately 28-16%, 42-24% from the Peninsular Gneiss Complex, and 30-60% from aeolian dust. Similarly, the Holocene period exhibits proportions of 40-60% Deccan, 60-40% PGC, and negligible Dust source contributions. In the Younger Dryas phase, the relative contributions are approximately 12% Deccan, 48% PGC, and 40% Dust sources. For the Early Deglacial period, the composition comprises 24% Deccan, 30% PGC, and 46% Dust sources. Lastly, spanning the pre-LGM time the sediments reveal contributions of 18-36% Deccan, 12-24% PGC, and 40-70% dust sources to the core site. This comprehensive analysis distinctly illustrates those colder climatic events such as the Last Glacial Maximum and Younger Dryas are characterized by a more pronounced presence of Deccan-derived and dust sediments relative to the Peninsular Gneiss Complex. Conversely, Holocene samples show almost negligible signature (0-10%) of dust and are dominated by the PGC sediment source.

The higher dust fluxes to the Arabian Sea could result from weakened southwest (SW) monsoon and/or strengthened north-westerly (Cruz et al., 2021; Pourmand et al., 2004; Sirocko & Sarnthein, 1989; Suresh et al., 2021). The higher sediment proportion from the Deccan Basalt compared to the PGC during the colder/arid period could result due to a lesser reduction of rainfall over the Deccan region compared to the PGC during the cold/arid period with respect to the wet period (Ota et al., 2019). Based on contemporary observations of precipitation over peninsular India, it is evident that during the drought year of 2002, the Deccan region received approximately 20% less rainfall, while the PGC region experienced a reduction of around 34%, as compared to the higher rainfall year of 2007 (Figure S9 & S10).

Precipitation over peninsular India during LGM (20-23 ka) has been modelled (see section 3.1) which varied in the range of 0.6 to 5.1 and 0.1 to 1.6 mm/day over the Deccan and PGC regions respectively during LGM (Figure S1). In contrast, present-day precipitation ranges between 2.1 to 7.6 mm/day over the Deccan region, while PGC region experiences precipitation exceeds 7.6 mm/day (Figure S2).

The difference in annual precipitation between the LGM and the present (Figure 4) clearly indicates a more pronounced reduction in rainfall over the PGC region compared to the Deccan region. This observation aligns with the findings of the modelling study of Broccoli et al., (2006), Yan et al., 2015, and the observation of Ota et al. (2019). Broccoli et al., (2006) indicated that a southward shift in the

Inter Tropical Convergence Zone (ITCZ) resulted in lower precipitation in the northeastern and eastern parts of the Indian peninsula and slightly higher precipitation in western parts during LGM compared to the present, which has further been supported by Ota et al., (2019).

The discernible trend suggests that the Deccan region experienced a comparatively smaller reduction in rainfall during the LGM and analogous colder climatic events compared to the PGC region (Figure 4). Consequently, there is a more pronounced relative decrease in rainfall over the PGC compared to the Deccan, leading to a lower supply of sediments from the PGC to the core location (SSD004-GC03) and resulting in a higher fraction of Deccan-derived sediments during colder climatic events. Moreover, a sediment proportion study conducted by Ota et al., (2019), in the Bay of Bengal, reinforces this observation. The study clearly indicates that more decreased precipitation over PGC led to an increased sediment proportion form Deccan region to the western Bay of Bengal during LGM. This increased relative contribution of sediments from Deccan region stems from a more significant decrease in monsoonal precipitation in the eastern and northeastern regions compared to the western part of the Indian peninsula.

The weatherability of lithology also plays a significant role in sediment contribution to the nearby ocean basins (Xie et al., 2022 and reference there in). In similar climatic conditions, differential weathering processes manifest, influenced by the inherent lithological variations (Ibarra et al., 2016 and reference therein). The granitic composition of PGC renders more resistant to weathering in comparison to the basaltic nature of the Deccan rocks (Babechuk et al., 2014; Ibarra et al., 2016). The higher weathering products associated with basalt weathering are expounded by high reactivity of basaltic mafic minerals (Dessert et al., 2003; Gislason and Oelkers, 2003). Consequently, it is anticipated that, under similar climatic conditions, the Deccan rocks would exhibit a greater degree of weathering compared to PGC rocks, leading to an increased contribution of sediments to the adjacent ocean basin. The higher erodibility of Deccan compared to PGC also favour the higher sediments flux from Deccan in addition to higher precipitation. The modeling observations presented in this study robustly support our Sr-Nd isotope data, confirming the presence of more Deccan sediment at the core location during LGM and analogous colder climatic events.

5.2. Control of Climate Variability on the Sediment Sources

Sr-Nd isotope composition of GC03 sediments displays large temporal variability (Figure 6A & 6B). The periodic decrease in $^{87}\text{Sr}/^{86}\text{Sr}$ is complimented with a corresponding increase in ϵ_{Nd} of the sediments and vice versa for the entire 38 ka record. The coupled variations, i.e., the lower $^{87}\text{Sr}/^{86}\text{Sr}$ and higher ϵ_{Nd} , are observed at ~38, 32, 26, 20-23, 16-18, 11-12, 8.2, 5.2, and 1.1 ka. The coherency

in Sr-Nd isotope variation records (Figure 6A & 6B) reflect relation with their provenances as the Sr and Nd isotope composition of the three main sources of these sediments, the aeolian dust, the Deccan and the PGC, have opposite Sr-Nd isotope signatures. The lower $^{87}\text{Sr}/^{86}\text{Sr}$ coupled with higher ϵ_{Nd} at the time intervals detailed above could result from a relative increase either in the aeolian dust or sediment proportions from the Deccan Basalt relative to the PGC. Such source variability in the sediment deposition could be facilitated by climatic variabilities, particularly the monsoonal intensity controlled mainly by atmosphere-ocean-climate coupling. Many such millennial-scale climate variabilities, warm/humid and cold/arid events reported during this period are four north Atlantic cold events, i.e., Heinrich events (H1-H4), LGM, Younger Dryas, and cooling events at 8.2 ka, 5.1 ka, 4.2 and 1.1 ka (Dixit et al., 2014; Kathayat et al., 2017; Rashid et al., 2011; Roland et al., 2015) and the Early Deglacial, B/A and Holocene Intense Monsoon (HIM) periods (Fleitmann et al., 2003; Tiwari et al., 2005). It is interesting to note that all the events marked with lower $^{87}\text{Sr}/^{86}\text{Sr}$ and higher ϵ_{Nd} coincide with cold/arid climatic events, i.e., 1.1 ka, 5.2 ka, 8.2 ka, Younger Dryas (YD; 11.3 ka), Heinrich Stadial 1 (HS 1; 16 ka), LGM (22 ka), Heinrich Stadial 2 (HS 2; 26 ka), Heinrich Stadial 3 (HS 2; 32ka) and Heinrich Stadial 4 (HS 4; 38 ka) (Figure 6). Whereas relatively higher $^{87}\text{Sr}/^{86}\text{Sr}$ and lower ϵ_{Nd} represent the warm/humid period such as HIM (9 ka), B-A (Bølling- Allerød; 14 ka) and Early Deglacial period (17-19 ka) (Figure 6A & B). Such a strong one-to-one correlation of Sr-Nd isotope signatures of the sediments from the Indian Ocean advocates for very strong control of climate particularly the rainfall on the sediment sources. Periods marked with cold/arid events at 1.1, 5.2, 8.2, 11.3, 16, 22, 26, 32, and 38 ka, favour higher dust fluxes and relatively higher sediment proportion from the Deccan Basalt region, whereas higher precipitation erodes relatively more sediments from the PGC as has been discussed in the above section. Sr and Nd isotope mixing diagram (Figure 5), however, support enhanced dust flux from Africa, Sahara, Arabia, or the Thar Desert during cold/arid periods, the impact of which is more pronounced during the Younger Dryas (Roux et al., 2012) (Figure 5 & 6). Intensification of dust flux over the globe as well as in the Arabian Sea has been reported during cold/arid periods, including YD (Cruz et al., 2021; Kinsley et al., 2022; DeMenocal, 2000; Pourmand et al., 2004; Sirocko & Sarnthein, 1989; Thompson et al., 2002). On the contrary, the warm and humid periods such as the ED (17-19 ka) with higher $^{87}\text{Sr}/^{86}\text{Sr}$ and lower ϵ_{Nd} , imply reduced dust fluxes and enhanced sediment proportion from the PGC. ED, a glacial-interglacial transition, is marked by higher precipitation, particularly under the influence of the NE monsoon (Tiwari et al., 2005) eroding more PGC across the southern region of India, characterized by less radiogenic Nd and more radiogenic Sr values.

The temporal variation of Sr-Nd isotope ratios shows a considerable change during ~9 ka, coinciding with the HIM, with higher $^{87}\text{Sr}/^{86}\text{Sr}$ and lower ϵ_{Nd} implying a larger sediment proportion from the PGC region compared to other time intervals. The intensified SW monsoon triggered higher erosion over the PGC leading to the enhanced sediment discharge by south-flowing rivers into the nearby ocean basin and to the core site reflected by the high sedimentation rate (~29 cm/ka) during this climatic window. It is evident that the core site receives a higher sediments proportion of PGC during the warm/humid periods (e.g., HIM and ED). This study is unable to get Sr-Nd isotope variability at the well-reported cold/dry period at 4.2 ka and warm/humid B-A event at 14 ka due to the poor resolution of data during this interval. Further, sea-level change also seems to play an essential role in sediment provenance via their transport. During the LGM, the sea level was ~120 meters below the present, exposing the western and eastern shelves of India (Clark & Mix, 2002). Due to the lowering of the sea level, the base level of erosion deepened, intensifying the erosion within the source regions of rivers. This phenomenon prompted rivers in India, flowing both westward and eastward, to discharge into the ocean at more advanced points beyond the continental shelf. This altered configuration facilitated an enhanced progress of sediments into the open ocean. Consequently, the rivers flowing eastward, primarily the Krishna and Godavari rivers originating from the Deccan region, likely deposited more Deccan-origin sediments into the WBoB (Tripathy et al., 2011; Ota et al., 2019). This sediment contribution could have been further carried to our core site through the EICC due to the strengthened Indian winter monsoon (Yadav et al., 2022). Along with that which could explain the manifestation of a distinct signal characterized by more radiogenic Nd and less radiogenic Sr isotopes during the LGM. Furthermore, during the LGM, the drop in sea levels facilitated a direct influx of Deccan sediment to the core site from the Eastern Arabian Sea and the Bay of Bengal. This occurred as sediment deposition was not impeded within the shelf area. While it is acknowledged that the EICC exerted a greater influence in transporting Deccan sediment due to the intensified Northeast monsoon (Tripathy et al., 2011; Ota et al., 2019; Yadav et al., 2022). It should be noted that a certain proportion of Deccan sediment could also directly reach the core site.

Notably, the southern tip of India is drained by smaller rivers like the Thamirabarani (Tamraparni), Vaigai (Porunai), Gudar, Vaipar, Karamaniar, and Nambiyar. These predominantly rain-fed rivers contribute a relatively minor fraction of sediments to the offshore region of the southern tip (Jonathan et al., 2004). Most of the sediments from the Peninsular Gneiss Complex (PGC) are likely retained within the shelf region. Consequently, during the LGM, the isotopic composition of GC03 reveals a lesser radiogenic Sr and a more radiogenic Nd signature, indicative of Deccan sediment influences rather than the more radiogenic Sr and less radiogenic Nd isotopes associated with the PGC

highlighting the intricate interplay of sea level changes, river dynamics, and sediment transport in shaping the isotopic signatures observed in GC03 during the Last Glacial Maximum.

Further, the strong correlation between isotope signature and climatic events argues against any significant time delay between erosion and sediment deposition, as suggested based on U-Th isotope studies in the Ganga Plain (Chabaux et al., 2006). Sediments may be transferred from the source to sink well within the temporal uncertainties of the sediment deposition.

5.3. Temporal Variation in Major and Trace Elements and their Correlation with Climatic Events

Some of the Al normalized major and trace elements abundances display considerable temporal variation similar to the Sr-Nd isotope composition suggesting the strong impact of climate variability on them and correlate strongly with known climate events (Figure 6). Chemical Index of Alteration exhibits low-frequency fluctuation in phase with sea-level changes, suggesting higher Deccan basalt contribution owing to lower sea-level during the LGM. As suggested for Sr-Nd isotopes, the Mg/Al of the sediments respond to all the climatic variabilities. Higher Mg/Al during all the cold/drier periods suggests higher sediment contribution from the aeolian dust or the Deccan Basalt with higher Magnesian minerals. Similarly, the Rb/Sr ratio displays noticeable temporal variation in tune with the reported climatic events, such as LGM, pre-LGM and the Holocene. Al normalized trace elements Cr, Ti, Zr, and Hf, correlate very well with short-term climatic events such as at 1.1ka, 5.2 ka, 8.2 ka, and HIM, also known as Holocene Intensified Monsoon phase (Goswami et al., 2012), Younger Dryas Heinrich Stadials 1 to 4, Early deglacial and LGM, coinciding in part with 7 to 19 ka records from Iran (Safaierad et al., 2020). Higher values of Cr/Al during the cold/arid period suggest higher dust contribution as suggested earlier by Sr-Nd isotopes. Very high Cr/Al during YD supports strong aeolian contribution from the Oman region (Pease et al., 1998). Higher Ti/Al, Hf/Al and Zr/Al during cold events further support higher dust input in this basin.

To examine the cyclicity of the Sr and Nd isotope data, we have performed spectral analysis on the $^{87}\text{Sr}/^{86}\text{Sr}$ and Σ_{Nd} of the GC03 core using the REDFIT method (Schulz & Mudelsee, 2002). Spectral analysis is a powerful tool to detangle the various signals contributing to the observed climatic variabilities. The temporal variation in $^{87}\text{Sr}/^{86}\text{Sr}$ and $^{143}\text{Nd}/^{144}\text{Nd}$ shows significant periodicities of 17 kyr, 8.3 kyr, 5.5 kyr, 3.8 kyr, 2.9 kyr, and 1.6 kyr, (Figure S11 & S12), indicating the impact of precession cyclicity along with other millennial scale, mainly Bond cyclicity on sediment source variability.

5. Conclusion

The major and trace elements and Sr-Nd isotope composition of silicate fraction of the sediments of a gravity core SSD004-GC03 from the equatorial Indian Ocean have been used to reconstruct the past variation in the sediment provenance. Sr-Nd isotopes show remarkable temporal variation in the sediment provenance since ~38 ka, in phase with known short-term climatic events highlighting the significant influence of climate (warm/humid and cold/arid), especially deposition of the dust and the weathering and erosion over the Deccan and PGC regions. Sr and Nd isotope and diagnostic elemental data show remarkable variability during warm and cold events. Cold/arid events like HS1- 4, LGM, YD, 8.2 ka, 5.2 ka, and 1.1 ka provide higher aeolian dust fluxes from the Sahara, South Africa, Arabian, and Thar deserts, along with sediment from the Deccan Basalt contributing significantly to the Gulf of Mannar basin. On the contrary, warm/humid events like ED, B-A, and HIM show more PGC sediment contribution to the core location.

Enhanced periodical dust intensity observed in this study underscores the teleconnection between the North Atlantic climatic oscillations and the Indian summer monsoon. Enhanced freshwater discharge into the North Atlantic Ocean during Heinrich and other colder events lowered the equatorial heat transported northward by thermohaline circulation, increased the north-westerly wind intensity and shifted the intertropical conversion zone southward in the Indian Ocean leading to a decrease in Indian summer monsoon intensity.

A significant correlation observed between most of the known climatic events and the provenance of the sediments of the equatorial Indian Ocean suggests almost no time lag between erosion and deposition of the sediments. This study emphasizes the importance of the high-resolution isotopic study of sediments in underpinning the driving role of the climate in modulating the intensity of aeolian dust fluxes. There is a need to further look into the role of increased dust fluxes in influencing the regional climate by regulating the radiative forcing, cloud and precipitation formation processes, and carbon cycle by ocean fertilization (Cruz et al., 2021).

Acknowledgments

We thank Dr. Rajeev Saraswat for providing the samples and Mr. Nikhil Mohan & Mr. Robin John for helping during isotope and elemental analyses. The author would like to acknowledge Dr. Gyana Ranjan Tripathy for his indispensable contribution to XRF measurements and Prof. Ashok Dimri for his help in precipitation modelling. Furthermore, the author expresses their appreciation to Prof. M. G. Yadava for graciously providing the oxygen isotope data of caves located in Peninsular India. These

collaborations and data contributions have greatly enriched the scientific endeavours undertaken in this study. Finally, AS thanks DST-INSPIRE for the partial financial support during this period.

Open Research

The data used in this study are available in the Supplementary Information and their archiving is underway in the institutional (National Institute of Oceanography) data center. Sr and Nd isotopic data were downloaded and compiled from the published papers, Ahmad & Harris, (2000), Argles et al. (2003), Bhanot, et al. (1979), Bikramaditya et al. (2020), Brook, & Snelling, (1976), Chu et al. (2006), Clift et al. (2010), Dai et al. (2008), Das et al. (2022), Debon, et al. (1986), Deniel et al. (1987), Derry and France-Lanord (1996), East et al. (2015), Einfalt et al. (1993), Fank, et al. (1977), France-Lanord & Le Fort, (1988), France-Lanord et al. (1993), Gao & Zeng, (2014) Gazis et al. (1998), George & Ray, (2017), Goodbred et al. (2014), Hao et al. (2022), Haproff et al. (2019) Hu et al. (2018), Imayama & Arita, (2008), Inger & Harris, (1993), Jager, et al. (1971), Jain et al. (2022), Kingson et al. (2019), Kwatra, et al. (1999), Le Fort, et al. (1983), Lee et al. (2012), Li et al. (2019), Licht et al., (2013), Lin et al. (2012), Lupker et al. (2012), McKenzie et al. (2011), Martin et al. (2005), Miller et al. (2001), Murphy, (2007), Oliver et al. (2003), Parrish and Hodges, (1996), Pognante et al. (1990), Rai, et al. (1993), Rao, et al. (1990), Richards et al. (2005), Robinson et al. (2001), Roddaz et al. (2011), Shukla, (2011), Singh (2018) thesis work, Singh et al. (2016), Singh et al. (2008), Stutz & Thöni, (1987), Szulc et al. (2006), Tobisch et al. (1994), Tripathi et al. (2013), Trivedi, et al. (1984), Williams, (2004), Zeng et al. (2015), Zhang et al. (2004), Zhao et al. (2001). In addition to that Sr-Nd isotope have also been downloaded and complied from the GEOROC Database on 1 July 2021 under geological settings: Archean Craton, Continental Flood Basalt, and Intraplate volcanics. All these data have been tabulated in Table S2. NGRIP oxygen data have been downloaded from the World Data Center for Paleoclimatology, Boulder, and NOAA Paleoclimatology Program (North Greenland Ice Core Project Members, 2004). Further Oxygen isotope data form the different carbonate caves (Himalayan and Peninsular regions of India) have been compiled from the earlier published work of Band et al. (2018), Berkelhammer et al. (2012), Berkelhammer et al. (2010), Gautam et al., (2019), Kathayat et al. (2016), Lone et al. (2013), Sinha et al. (2011), Yadava et al. (2004), Yadava & Ramesh, (2005) to produce figure 5c. QGIS software was used for creating the maps. Rainfall data used for creating precipitation map (Figure S9 and S10) have been taken from Goddard Earth Sciences Data and Information Service Center (2016), TMPA_3B42RT_Daily [Dataset]. Precipitation data has been taken from Climate Research Unit (CRU TS v.4.07) (Harris et al., 2020). Published Sr-Nd isotope data for characterizing dust end member used in this study are taken from Ayalew et al. (2018), Gili et al. (2022), Grousset & Biscaye, (2005), Grousset et al. (1992, 1998), Kunkelova et al. (2022), Skonieczny et al. (2011),

Tripathi et al. (2013), Zhao et al. (2018) and tabulated in Table S3. “PAST 4.03” (<https://past.en.lo4d.com/windows>) software was used for the spectral analysis (Figure S11 and S12).

References

- Ahmad, S. M., Anil Babu, G., Padmakumari, V. M., Dayal, A. M., Sukhija, B. S., & Nagabhushanam, P. (2005). Sr, Nd isotopic evidence of terrigenous flux variations in the Bay of Bengal: Implications of monsoons during the last ~34,000 years. *Geophysical Research Letters*, 32(22). <https://doi.org/10.1029/2005GL024519>
- Arz, H. W., Lamy, F., Ganopolski, A., Nowaczyk, N., & Pätzold, J. (2007). Dominant Northern Hemisphere climate control over millennial-scale glacial sea-level variability. *Quaternary Science Reviews*, 26(3–4), 312–321. <https://doi.org/10.1016/j.quascirev.2006.07.016>
- Babechuk, M. G., Widdowson, M., & Kamber, B. S. (2014). Quantifying chemical weathering intensity and trace element release from two contrasting basalt profiles, Deccan Traps, India. *Chemical Geology*, 363, 56–75. <http://dx.doi.org/10.1016/j.chemgeo.2013.10.027>
- Band, S., Yadava, M. G., Lone, M. A., Shen, C.-C., Sree, K., & Ramesh, R. (2018). Highresolution mid-Holocene Indian Summer Monsoon recorded in a stalagmite from the Kotumsar Cave, Central India. *Quaternary International*, 479, 19–24. <https://doi.org/10.1016/j.quaint.2018.01.026>
- Bayon, G., German, C. R., Boella, R. M., Milton, J. A., Taylor, R. N., & Nesbitt, R. W. (2002). An improved method for extracting marine sediment fractions and its application to Sr and Nd isotopic analysis. *Chemical Geology*, 187(3–4), 179–199. [https://doi.org/10.1016/S0009-2541\(01\)00416-8](https://doi.org/10.1016/S0009-2541(01)00416-8)
- Bayon, G., Burton, K. W., Soulet, G., Vigier, N., Dennielou, B., Etoubleau, J., et al. (2009). Hf and Nd isotopes in marine sediments: Constraints on global silicate weathering. *Earth and Planetary Science Letters*, 277(3–4), 318–326. <https://doi.org/10.1016/j.epsl.2008.10.028>
- Berkelhammer, Max, Sinha, A., Mudelsee, M., Cheng, H., Edwards, R., & Cannariato, K. (2010). Persistent multidecadal power of the Indian Summer Monsoon. *Earth and Planetary Science Letters*, 290, 166–172. <https://doi.org/10.1016/j.epsl.2009.12.017>
- Berkelhammer, M., Sinha, A., Stott, L., Cheng, H., Pausata, F. S. R., & Yoshimura, K. (2012). An Abrupt Shift in the Indian Monsoon 4000 Years Ago. *Geophysical Monograph Series*, 75–88. <https://doi.org/10.1029/2012GM001207>
- Broccoli, A. J., Dahl, K. A., & Stouffer, R. J. (2006). Response of the ITCZ to Northern Hemisphere cooling. *Geophysical Research Letters*, 33, L01702. <https://doi.org/10.1029/2005GL024546>
- Carter, S. C., Griffith, E. M., Clift, P. D., Scher, H. D., & Dellapenna, T. M. (2020). Clayfraction strontium and neodymium isotopes in the Indus Fan: implications for sediment transport and provenance. *Geological Magazine*, 157(6), 879–894. <https://doi.org/10.1017/S0016756820000394>
- Chabaux, F., Granet, M., Pelt, E., France-Lanord, C., & Galy, V. (2006). ^{238}U - ^{234}U - ^{230}Th disequilibria and timescale of sedimentary transfers in rivers: Clues from the Gangetic plain rivers. *Journal of Geochemical Exploration*, 88(1–3), 373–375. <https://doi.org/10.1016/j.gexplo.2005.08.078>

Clark, P. U., & Mix, A. C. (2002). Ice sheets and sea level of the Last Glacial Maximum. *Quaternary Science Reviews*, 7. [https://doi.org/10.1016/S0277-3791\(01\)00118-4](https://doi.org/10.1016/S0277-3791(01)00118-4)

Clift, P. D., Giosan, L., Blusztajn, J., Campbell, I. H., Allen, C., Pringle, M., et al. (2008). Holocene erosion of the Lesser Himalaya triggered by intensified summer monsoon. *Geology*, 36(1), 79. <https://doi.org/10.1130/G24315A.1>

Clift, P. D., Giosan, L., Carter, A., Garzanti, E., Galy, V., Tabrez, A. R., et al. (2010). Monsoon control over erosion patterns in the Western Himalaya: possible feed-back into the tectonic evolution. *Geological Society, London, Special Publications*, 342(1), 185– 218. <https://doi.org/10.1144/SP342.12>

Colin, C., Turpin, L., Bertaux, J., Desprairies, A., & Kissel, C. (1999). Erosional history of the Himalayan and Burman ranges during the last two glacial–interglacial cycles. *Earth and Planetary Science Letters*, 171(4), 647–660. [https://doi.org/10.1016/S0012821X\(99\)00184-3](https://doi.org/10.1016/S0012821X(99)00184-3)

Colin, C., Turpin, L., Blamart, D., Frank, N., Kissel, C., & Duchamp, S. (2006). Evolution of weathering patterns in the Indo-Burman Ranges over the last 280 kyr: Effects of sediment provenance on $^{87}\text{Sr}/^{86}\text{Sr}$ ratios tracer. *Geochemistry, Geophysics, Geosystems*, 7(3). <https://doi.org/10.1029/2005GC000962>

Cruz, J. A., McDermott, F., Turrero, M. J., Edwards, R. L., & Martín-Chivelet, J. (2021). Strong links between Saharan dust fluxes, monsoon strength, and North Atlantic climate during the last 5000 years. *Science Advances*, 7(26), eabe6102. <https://doi.org/10.1126/sciadv.abe6102>

Derry, L. A., & France-Lanord, C. (1996). Neogene Himalayan weathering history and river $^{87}\text{Sr}/^{86}\text{Sr}$: impact on the marine Sr record. *Earth and Planetary Science Letters*, 142(1–2), 59–74. [https://doi.org/10.1016/0012-821X\(96\)00091-X](https://doi.org/10.1016/0012-821X(96)00091-X)

Dessert, C., Dupré, B., Gaillardet, J., François, L. M., & Allègre, C. J. (2003). Basalt weathering laws and the impact of basalt weathering on the global carbon cycle. *Chemical Geology*, 202(3-4), 257–273. <https://doi.org/10.1016/j.chemgeo.2002.10.001>

Demenocal, P., Ortiz, J., Guilderson, T., Adkins, J., Sarnthein, M., Baker, L., & Yarusinsky, M. (2000). Abrupt onset and termination of the African Humid Period: rapid climate responses to gradual insolation forcing. *Quaternary science reviews*, 19(1–5), 347–361

DIGIS Team, (2021), "GEOROC Compilation: Archaean Cratons", Goettingen Research Online. <https://doi.org/10.25625/1KRR1P>

DIGIS Team, (2021), "GEOROC Compilation: Continental Flood Basalts", Goettingen Research Online. <https://doi.org/10.25625/WSTPOX>

DIGIS Team, (2021), "GEOROC Compilation: Intraplate Volcanic Rocks", Goettingen Research Online. <https://doi.org/10.25625/RZZ9VM>

Dixit, Y., Hodell, D. A., Sinha, R., & Petrie, C. A. (2014). Abrupt weakening of the Indian summer monsoon at 8.2 kyr B.P. *Earth and Planetary Science Letters*, 391, 16–23. <https://doi.org/10.1016/j.epsl.2014.01.026>

Einsele, G., Ratschbacher, L., & Wetzel, A. (1996). The Himalaya-Bengal Fan denudationaccumulation system during the past 20 Ma. *the Journal of Geology*, 104(2), 163-184. <https://doi.org/10.1086/629812>

Fleitmann, D., Burns, S. J., Mudelsee, M., Neff, U., Kramers, J., Mangini, A., & Matter, A. (2003). Holocene Forcing of the Indian Monsoon Recorded in a Stalagmite from Southern Oman. *Science*, 300(5626), 1737–1739. <https://doi.org/10.1126/science.1083130>

France-Lanord, C., Derry, L., & Michard, A. (1993). Evolution of the Himalaya since Miocene time: isotopic and sedimentological evidence from the Bengal Fan. *Geological Society, London, Special Publications*, 74(1), 603–621. <https://doi.org/10.1144/GSL.SP.1993.074.01.40>

Gadgil, S. (2003). The Indian Monsoon and Its Variability. *Annual Review of Earth and Planetary Sciences*, 31(1), 429–467. <https://doi.org/10.1146/annurev.earth.31.100901.141251>

Galy, A., & France-Lanord, C. (2001). Higher erosion rates in the Himalaya: Geochemical constraints on riverine fluxes. *Geology*, 29(1), 23. [https://doi.org/10.1130/0091-7613\(2001\)029<0023:HERITH>2.0.CO;2](https://doi.org/10.1130/0091-7613(2001)029<0023:HERITH>2.0.CO;2)

Goddard Earth Sciences Data and Information Services Center (2016). TRMM (TMPA-RT) Near Real-Time Precipitation L3 1 day 0.25 degree x 0.25 degree V7, TMPA (3B42RT_Daily) [Dataset] Goddard Earth Sciences Data and Information Services Center (GES DISC). <https://doi.org/10.5067/TRMM/TMPA/DAY-E/7>

Goswami, V., Singh, S. K., Bhushan, R., & Rai, V. K. (2012). Temporal variations in $^{87}\text{Sr}/^{86}\text{Sr}$ and ϵ_{Nd} in sediments of the southeastern Arabian Sea: Impact of monsoon and surface water circulation. *Geochemistry, Geophysics, Geosystems*, 13(1). <https://doi.org/10.1029/2011GC003802>

Gautam, P. K., Narayana, A. C., Band, S. T., Yadava, M. G., Ramesh, R., Wu, C. C., & Shen, C.-C. (2019). High-resolution reconstruction of Indian summer monsoon during the Bølling-Allerød from a central Indian stalagmite. *Palaeogeography, Palaeoclimatology, Palaeoecology*, 514, 567–576. <https://doi.org/10.1016/j.palaeo.2018.11.006>

Gislason, S. R., & Oelkers, E. H. (2003). Mechanism, rates, and consequences of basaltic glass dissolution: II. An experimental study of the dissolution rates of basaltic glass as a function of pH and temperature. *Geochimica et Cosmochimica Acta*, 67(20), 3817-3832. [https://doi.org/10.1016/S0016-7037\(03\)00176-5](https://doi.org/10.1016/S0016-7037(03)00176-5)

Gutjahr, M., Frank, M., Stirling, C. H., Klemm, V., van de Flierdt, T., & Halliday, A. N. (2007). Reliable extraction of a deepwater trace metal isotope signal from Fe–Mn oxyhydroxide coatings of marine sediments. *Chemical Geology*, 242(3–4), 351–370. <https://doi.org/10.1016/j.chemgeo.2007.03.021>

Gupta, A. K., Anderson, D. M., & Overpeck, J. T. (2003). Abrupt changes in the Asian southwest monsoon during the Holocene and their links to the North Atlantic Ocean. *Nature*, 421(6921), 354–357. <https://doi.org/10.1038/nature01340>

Harris, I., Osborn, T. J., Jones, P., & Lister, D. (2020). Version 4 of the CRU TS monthly high-resolution gridded multivariate climate dataset. *Scientific Data*, 7(1), 109. <https://doi.org/10.1038/s41597-020-0453-3>

Ibarra, D. E., Caves, J. K., Moon, S., Thomas, D. L., Hartmann, J., Chamberlain, C. P., & Maher, K. (2016). Differential weathering of basaltic and granitic catchments from concentration–discharge relationships. *Geochimica et Cosmochimica Acta*, 190, 265–293. <http://dx.doi.org/10.1016/j.gca.2016.07.006>

Inam, A., Clift, P. D., Giosan, L., Tabrez, A. R., Tahir, M., Rabbani, M. M., & Danish, M. (2007). The Geographic, Geological and Oceanographic Setting of the Indus River. In A. Gupta (Ed.), Large Rivers (pp. 333–346). Chichester, UK: John Wiley & Sons, Ltd. <https://doi.org/10.1002/9780470723722.ch16>

Jacobsen, S. B., & Wasserburg, G. J. (1980). Sm-Nd isotopic evolution of chondrites. *Earth and Planetary Science Letters*, 50(1), 139–155. [https://doi.org/10.1016/0012821X\(80\)90125-9](https://doi.org/10.1016/0012821X(80)90125-9)

Jonathan, M. P., Ram-Mohan, V., & Srinivasulu, S. (2004). Geochemical variations of major and trace elements in recent sediments, off the Gulf of Mannar, the southeast coast of India. *Environmental Geology*, 45(4), 466–480. <https://doi.org/10.1007/s00254-0030898-7>

Kathayat, G., Cheng, H., Sinha, A., Spötl, C., Edwards, R. L., Zhang, H., et al. (2016). Indian monsoon variability on millennial-orbital timescales. *Scientific Reports*, 6(1), 24374. <https://doi.org/10.1038/srep24374>

Kathayat, G., Cheng, H., Sinha, A., Yi, L., Li, X., Zhang, H., et al. (2017). The Indian monsoon variability and civilization changes in the Indian subcontinent. *Science Advances*, 3(12), e1701296. <https://doi.org/10.1126/sciadv.1701296>

Kessarkar, P. M., Rao, V. P., Ahmad, S. M., & Babu, G. A. (2003). Clay minerals and Sr–Nd isotopes of the sediments along the western margin of India and their implication for sediment provenance. *Marine Geology*, 202(1–2), 55–69. [https://doi.org/10.1016/S00253227\(03\)00240-8](https://doi.org/10.1016/S00253227(03)00240-8)

Kinsley, C. W., Bradtmiller, L. I., McGee, D., Galgay, M., Stuut, J., Tjallingii, R. (2022). Orbital- and Millennial-Scale Variability in Northwest African Dust Emissions Over the Past 67,000 years. *Paleoceanography and Paleoceanography*, 37(1). <https://doi.org/10.1029/2020PA004137>

Lone, M., Ahmad, S., Nguyen, D., Shen, C.-C., Raza, W., & Kumar, A. (2013). Speleothem based 1,000-year high resolution record of Indian monsoon variability during the last deglaciation. *Palaeogeography Palaeoclimatology Palaeoecology*. <https://doi.org/10.1016/j.palaeo.2013.12.010>

Li, J., Liu, S., Shi, X., Zhang, H., Fang, X., Chen, M.T. (2018). Clay minerals and Sr–Nd isotopic composition of the Bay of Bengal sediments: Implications for sediment provenance and climate control since 40 ka. *Quaternary International*, 493, 50–58. <https://doi.org/10.1016/j.quaint.2018.06.044>

Mahesh, B. S., & Banakar, V. K. (2014). Change in the intensity of low-salinity water inflow from the Bay of Bengal into the Eastern Arabian Sea from the Last Glacial Maximum to the Holocene: Implications for monsoon variations. *Palaeogeography, Palaeoclimatology, Palaeoecology*, 397, 31–37. <https://doi.org/10.1016/j.palaeo.2013.05.024>

Mauritsen, T., Bader, J., Becker, T., Behrens, J., Bittner, M., Brokopf, R., Brovkin, V., Claussen, M., Crueger, T., Esch, M., Fast, I., Fiedler, S., Fläschner, D., Gayler, V., Giorgetta, M., Goll, D. S., Haak, H., Hagemann, S., Hedemann, C., ... Roeckner, E. (2019). Developments in the MPI-M Earth System Model version 1.2 (MPI-ESM1.2) and Its Response to Increasing CO₂. *Journal of Advances in Modeling Earth Systems*, 11(4), 998–1038. <https://doi.org/10.1029/2018MS001400>

Meyer, I., Davies, G. R., & Stuut, J. B. W. (2011). Grain size control on Sr-Nd isotope provenance studies and impact on paleoclimate reconstructions: An example from deepsea sediments offshore NW Africa. *Geochemistry, Geophysics, Geosystems*, 12(3). <https://doi.org/10.1029/2010GC003355>

Milliman, J. D., & Syvitski, J. P. M. (1992). Geomorphic/Tectonic Control of Sediment Discharge to the Ocean: The Importance of Small Mountainous Rivers. *The Journal of Geology*, 100(5), 525–544. <https://doi.org/10.1086/629606>

Nesbitt, H., & Young, G. M. (1982). Early Proterozoic climates and plate motions inferred from major element chemistry of lutites. *Nature*, 299(5885), 715–717. <https://doi.org/10.1038/299715a0>

North Greenland Ice Core Project members (2004). NOAA/WDS Paleoclimatology - North GRIP - 50-year Averaged Oxygen Isotope Data. [Dataset]. NOAA National Centers for Environmental Information. <https://doi.org/10.25921/g2m5-qd24>

Ota, Y., Kawahata, H., Kuroda, J., Yamaguchi, A., Suzuki, A., Araoka, D., et al., (2019). Indian monsoonal variations during the past 80 kyr recorded in NGHP-02 Hole 19B, western Bay of Bengal: Implications from chemical and mineral properties. *Geochemistry, Geophysics, Geosystems*, 20, 148–165. <https://doi.org/10.1029/2018GC007772>

Patchett, P. J., White, W. M., Feldmann, H., Kielinczuk, S., & Hofmann, A. W. (1984). Hafnium/rare earth element fractionation in the sedimentary system and crustal recycling into the Earth's mantle. *Earth and Planetary Science Letters*, 69(2), 365–378. [https://doi.org/10.1016/0012-821X\(84\)90195-X](https://doi.org/10.1016/0012-821X(84)90195-X)

Pease, P. P., Tchakerian, V. P., & Tindale, N. W. (1998). Aerosols over the Arabian Sea: geochemistry and source areas for aeolian desert dust. *Journal of Arid Environments*, 39(3), 477–496. <https://doi.org/10.1006/jare.1997.0368>

Peketi, A., Mazumdar, A., Pillutla, S. P. K., Sawant, B., & Gupta, H. (2021). Climatic and Tectonic Control on the Bengal Fan Sedimentation Since the Pliocene. *Geochemistry, Geophysics, Geosystems*, 22(3). <https://doi.org/10.1029/2020GC009448>

Pourmand, A., Marcantonio, F., & Schulz, H. (2004). Variations in productivity and eolian fluxes in the northeastern Arabian Sea during the past 110 ka. *Earth and Planetary Science Letters*, 221(1–4), 39–54. [https://doi.org/10.1016/S0012-821X\(04\)00109-8](https://doi.org/10.1016/S0012-821X(04)00109-8)

QGIS Development Team. (2022). QGIS Geographic Information System [QGIS 3.24, Tisler]. Open Source Geospatial Foundation. <https://qgis.org/en/site/>

Rajeevan, M., Unnikrishnan, C. K., Bhate, J., Niranjan Kumar, K., & Sreekala, P. P. (2012). Northeast monsoon over India: variability and prediction. *Meteorological Applications*, 19(2), 226–236. <https://doi.org/10.1002/met.1322>

Ramaswamy, V., & Nair, R. R. (1994). Fluxes of material in the Arabian Sea and Bay of Bengal - Sediment trap studies. *Journal of Earth System Science*, 103(2), 189–210. <https://doi.org/10.1007/BF02839536>

Roux, G., Fagel, N., De Vleeschouwer, F., Krachler, M., Debaille, V., Stille, P. (2012). Volcano- and climate-driven changes in atmospheric dust sources and fluxes since the Late Glacial in Central Europe. *Geology*, 40(4), 335–338. <https://doi.org/10.1130/G32586.1>

Rashid, H., England, E., Thompson, L., & Polyak, L. (2011). Late Glacial to Holocene Indian Summer Monsoon Variability Based upon Sediment Records Taken from the Bay of Bengal. *Terrestrial, Atmospheric and Oceanic Sciences*, 22(2), 215–228. [https://doi.org/10.3319/TAO.2010.09.17.02\(TibXS\)](https://doi.org/10.3319/TAO.2010.09.17.02(TibXS))

Roland, T. P., Daley, T. J., Caseldine, C. J., Charman, D. J., Turney, C. S. M., Amesbury, M. J., et al. (2015). The 5.2 ka climate event: Evidence from stable isotope and multi-proxy palaeoecological peatland records in Ireland. *Quaternary Science Reviews*, 124, 209–223. <https://doi.org/10.1016/j.quascirev.2015.07.026>

Safaierad, R., Mohtadi, M., Zolitschka, B., Yokoyama, Y., Vogt, C., & Schefuß, E. (2020). Elevated dust depositions in West Asia linked to ocean–atmosphere shifts during North Atlantic cold events. *Proceedings of the National Academy of Sciences*, 117(31), 18272–18277. <https://doi.org/10.1073/pnas.2004071117>

Samanta, A. (2022, February). Weathering and climate linkage at seasonal to kilo-year timescales: Evidence from water and sediment chemistry (Thesis). Dept. of Earth and Climate Science. Retrieved from <http://dr.iiserpune.ac.in:8080/xmlui/handle/123456789/7247>

Schott, F. A., & McCreary Jr, J. P. (2001). The monsoon circulation of the Indian Ocean. *Progress in Oceanography*, 51(1), 1–123. [https://doi.org/10.1016/S0079-6611\(01\)00083-0](https://doi.org/10.1016/S0079-6611(01)00083-0)

Schulz, M., Mudelsee, M., 2002. REDFIT: estimating red-noise spectra directly from unevenly spaced paleoclimatic time series. *Computers & Geosciences* 28, 421–426. [https://doi.org/10.1016/S0098-3004\(01\)00044-9](https://doi.org/10.1016/S0098-3004(01)00044-9)

Shankar, D., Vinayachandran, P. N., & Unnikrishnan, A. S. 2002. The monsoon currents in the north Indian Ocean. *Progress in Oceanography*, 52(1), 63–120. [https://doi.org/10.1016/S0079-6611\(02\)00024-1](https://doi.org/10.1016/S0079-6611(02)00024-1)

Singh, S. K., Rai, S. K., & Krishnaswami, S. (2008). Sr and Nd isotopes in river sediments from the Ganga Basin: Sediment provenance and spatial variability in physical erosion. *Journal of Geophysical Research*, 113(F3), F03006. <https://doi.org/10.1029/2007JF000909>

Singh, D. P., Saraswat, R., Mohtadi, M., & Kumar, P. (2022). Warm northern tropical Indian Ocean strengthened the ocean circulation prior to the last glacial termination. *Global and Planetary Change*, 209, 103733. <https://doi.org/10.1016/j.gloplacha.2021.103733>

Singh D. P. (2019), Foraminiferal distribution off the southern tip of India to understand its response to cross basin water exchange and to reconstruct seasonal monsoon intensity during the Late Quaternary, PhD thesis, Goa University, Goa, India, <http://hdl.handle.net/10603/281649>

Sinha, A., Berkelhammer, M., Stott, L., Mudelsee, M., Cheng, H., & Biswas, J. (2011). The leading mode of Indian Summer Monsoon precipitation variability during the last millennium. *Geophysical Research Letters - GEOPHYS RES LETT*, 38. <https://doi.org/10.1029/2011GL047713>

Sirocko, F., & Sarnthein, M. (1989). Wind-borne deposits in the northwestern Indian Ocean: Record of Holocene sediments versus modern satellite data. In *Paleoclimatology and Paleometeorology: modern and past patterns of global atmospheric transport* (pp. 401-433). Springer, Dordrecht. https://doi.org/10.1007/978-94-009-0995-3_17

Stanford, J. D., Hemingway, R., Rohling, E. J., Challenor, P. G., Medina-Elizalde, M., & Lester, A. J. (2011). Sea-level probability for the last deglaciation: A statistical analysis of far-field records. *Global and Planetary Change*, 79(3–4), 193–203. <https://doi.org/10.1016/j.gloplacha.2010.11.002>

Suresh, K., Singh, U., Kumar, A., Karri, D., Peketi, A., & Ramaswamy, V. (2021). Provenance tracing of long-range transported dust over the Northeastern Arabian Sea during the southwest monsoon. *Atmospheric Research*, 250, 105377. <https://doi.org/10.1016/j.atmosres.2020.105377>

Thompson, L. G., Mosley-Thompson, E., Davis, M. E., Henderson, K. A., Brecher, H. H., Zagorodnov, V. S., et al. (2002). Kilimanjaro Ice Core Records: Evidence of Holocene Climate Change in Tropical Africa. *Science*, 298(5593), 589–593. <https://doi.org/10.1126/science.1073198>

Tiwari, M., Ramesh, R., Somayajulu, B. L. K., Jull, A. J. T., & Burr, G. S. (2005). Paleomonsoon precipitation deduced from a sediment core from the equatorial Indian Ocean. *Geo-Marine Letters*, 26(1), 23–30. <https://doi.org/10.1007/s00367-005-0012-0>

Tripathy, G. R., Singh, S. K., Bhushan, R., & Ramaswamy, V. (2011). Sr–Nd isotope composition of the Bay of Bengal sediments: impact of climate on erosion in the Himalaya. *Geochemical Journal*, 45(3), 175–186. <https://doi.org/10.2343/geochemj.1.0112>

Walter, H. J., Hegner, E., Diekmann, B., Kuhn, G., & Rutgers van der loeff, M. M. (2000). Provenance and transport of terrigenous sediment in the south Atlantic Ocean and their relations to glacial and interglacial cycles: Nd and Sr isotopic evidence. *Geochimica et Cosmochimica Acta*, 64(22), 3813–3827. [https://doi.org/10.1016/S0016-037\(00\)00476-2](https://doi.org/10.1016/S0016-037(00)00476-2)

Xie, C., Antić, N., Nadal-Romero, E., Yan, L., Tosti, T., Djogo Mračević, S., ... & Kašanin-Grubin, M. (2022). The Influences of Climatic and Lithological Factors on Weathering of Sediments in Humid Badland Areas. *Frontiers in Earth Science*, 10, 900314. <http://dx.doi.org/10.3389/feart.2022.900314>

Yadava, M., Ramesh, R., & Pant, G. B. (2004). Past monsoon rainfall variations in peninsular India recorded in a 331-year-old speleothem. *Holocene*, 14. <https://doi.org/10.1191/0959683604hl728rp>

Yadava, M. G., & Ramesh, R. (2005). Monsoon reconstruction from radiocarbon dated tropical Indian speleothems. *The Holocene*, 15(1), 48–59. <https://doi.org/10.1191/0959683605h1783rp>

Yadav, R., Naik, S. S., & Narvekar, J. (2021). The equatorial Indian Ocean upper watercolumn structure influenced by cross-basinal water exchange over the last~ 40000. <https://doi.org/10.1016/j.quaint.2021.04.002>

Yan, M., Wang, B., & Liu, J. (2016). Global monsoon change during the Last Glacial Maximum: a multi-model study. *Climate Dynamics*, 47, 359–374. <https://link.springer.com/article/10.1007/s00382-015-2841-5>

References from Supporting Information

- Ahmad, T., & Harris, N. (2000). Isotopic constraints on the structural relationships between the Lesser Himalayan Series and the High Himalayan Crystalline Series, Garhwal Himalaya. *Geological Society of America Bulletin*, 111. [https://doi.org/10.1130/0016-7606\(2000\)112<0467:ICOTSR>2.3.CO;2](https://doi.org/10.1130/0016-7606(2000)112<0467:ICOTSR>2.3.CO;2)
- Argles, T., Foster, G., Whittington, A., Harris, N., & George, M. (2003). Isotope studies reveal a complete Himalayan section in the Nanga Parbat syntaxis. *Geology*, 31(12), 1109. <https://doi.org/10.1130/G19937.1>
- Ayalew, D., Jung, S., Romer, R. L., & Garbe-Schönberg, D. (2018). Trace element systematics and Nd, Sr and Pb isotopes of Pliocene flood basalt magmas (Ethiopian rift): A case for Afar plume-lithosphere interaction. *Chemical Geology*, 493, 172–188. <https://doi.org/10.1016/j.chemgeo.2018.05.037>
- Bhanot, V. B., Bhandari, A. K., Singh, V. P., & Kansal, A. K. (1979). Geochronological and geological studies on a granite of Higher Himalaya, northeast of Manikaran, Himachal Pradesh. *Journal of the Geological Society of India*, 20, 90. Retrieved from <https://www.geosocindia.org/index.php/jgsi/article/view/64591>
- Bikramaditya, R. K., Chung, S.L., Singh, A. K., Lee, H.-Y., Lin, T.-H., & Iizuka, Y. (2020). Age and isotope geochemistry of magmatic rocks of the Lohit Plutonic Complex, eastern Himalaya: implications for the evolution of Transhimalayan arc magmatism. *Journal of the Geological Society*, 177(2), 379–394. <https://doi.org/10.1144/jgs2018-214>
- Brook, M. & Snelling, N.J. (1976). K/Ar and Rb/Sr Age Determinations on Rocks and Minerals from Burma. Report of the Isotope Geology Unit 76/12. Institute of Geological Sciences, Keyworth, Nottingham, UK.
- Chu, M. F., Chung, S.L., Song, B., Liu, D., O'Reilly, S. Y., Pearson, N. J. (2006). Zircon U-Pb and Hf isotope constraints on the Mesozoic tectonics and crustal evolution of southern Tibet. *Geology*, 34(9), 745. <https://doi.org/10.1130/G22725.1>
- Dai, J., Yin, A., Liu, W., and Wang, C. (2008). Nd Isotopic Compositions of the Tethyan Himalayan Sequence in Southeastern Tibet. *Science in China Series D: Earth Sciences*, 51, 1306-1316. <https://doi.org/10.1007/s11430-008-0103-7>
- Das, S., Rai, S. K., Rahaman, W., Singhal, S., & Sarangi, S. (2022). Chemical weathering and Sr flux from the silicate lithology dominated fluvial system: Insights from major ions, dissolved Sr and $^{87}\text{Sr}/^{86}\text{Sr}$ of the Teesta headwaters, Sikkim Himalaya. *Applied Geochemistry*, 137, 105171. <https://doi.org/10.1016/j.apgeochem.2021.105171>
- Debon, F., Le Fort, P., & Sonet, J. (1986). Granitoid belts West and South of Tibet. About their geochemical trends and Rb-Sr isotopic studies. *Science Press*, Beijing, 1(395–4). [https://doi.org/10.1016/0040-1951\(87\)90248-4](https://doi.org/10.1016/0040-1951(87)90248-4)

- Deniel, C., Vidal, P., Fernandez, A., Le Fort, P., & Peucat, J.J. (1987). Isotopic study of the Manaslu granite (Himalaya, Nepal): inferences on the age and source of Himalayan leucogranites. Contributions to Mineralogy and Petrology, 96(1), 78–92. <https://doi.org/10.1007/BF00375529>
- East, A. E., Clift, P. D., Carter, A., Alizai, A., & VanLaningham, S. (2015). Fluvial–eolian interactions in sediment routing and sedimentary signal buffering: an example from the Indus Basin and Thar Desert. Journal of Sedimentary Research, 85, 715–728. <https://doi.org/10.2110/jsr.2015.42>
- Einfalt, H. C., Hoehndorf, A., & Kaphle, K. P. (1993). Radiometric age determination of the Dadeldhura granite, Lesser Himalaya, far western Nepal. Schweizerische Mineralogische und Petrographische Mitteilungen, 73(1), 97–106. <https://doi.org/10.5169/SEALS-55564>
- Fank, W., Thoni, M., & Purtscheller, F. (1977). Geology and petrography of Kullu–south Lahul area. Science de La Terre, 268, 147–72.
- France-Lanord, C., & Le Fort, P. (1988). Crustal melting and granite genesis during the Himalayan collision orogenesis. Earth and Environmental Science Transactions of the Royal Society of Edinburgh, 79(2–3), 183–195. <https://doi.org/10.1017/S0263593300014206>
- Gao, L. E., & Zeng, L. (2014). Fluxed melting of metapelite and the formation of Miocene high-CaO two-mica granites in the Malashan gneiss dome, southern Tibet. Geochimica et Cosmochimica Acta, 130, 136–155. <https://doi.org/10.1016/j.gca.2014.01.003>
- Gazis, C.A, Blum, J.D, Chamberlain, C.P, & Poage, M. (1998). Isotope systematics of granites and gneisses of the Nanga Parbat massif, Pakistan Himalaya.pdf. American Journal of Science, 298, 673–698. <https://doi.org/10.2475/ajs.298.8.673>
- George, B. G., & Ray, J. S. (2017). Provenance of sediments in the Marwar Supergroup, Rajasthan, India: Implications for basin evolution and Neoproterozoic global events. Journal of Asian Earth Sciences, 147, 254–270. <https://doi.org/10.1016/j.jseaes.2017.07.027>
- Gili, S. A., Vanderstraeten, A., Chaput, J., King, D. M., Gaiero, B., Delmonte, & Mattielli, N. (2022). South African dust contribution to the high southern latitudes and East Antarctica during interglacial stages. Communications Earth & Environment, 3 (1), 129. <https://doi.org/10.1038/s43247-022-00464-z>
- Goodbred, S. L., Paolo, P. M., Ullah, M. S., Pate, R. D., Khan, S. R., Kuehl, S. A. (2014). Piecing together the Ganges-Brahmaputra-Meghna River delta: Use of sediment provenance to reconstruct the history and interaction of multiple fluvial systems during Holocene delta evolution. Geological Society of America Bulletin, 126(11–12), 1495–1510. <https://doi.org/10.1130/B30965.1>
- Grousset, F. E., & Biscaye, P. E. (2005). Tracing dust sources and transport patterns using Sr, Nd and Pb isotopes: Chemical Geology, 222, 149–167. <https://doi.org/10.1016/j.chemgeo.2005.05.006>
- Grousset, F. E., Parra, M., Bory, A., Martinez, P., Bertrand, P., Shimmield, G., & Ellam, R. M. (1998). Saharan wind regimes traced by the Sr–Nd isotopic composition of subtropical Atlantic sediments: last glacial maximum vs today: Quaternary Science Reviews, 17, 395–409. [https://doi.org/10.1016/S0277-3791\(97\)00048-6](https://doi.org/10.1016/S0277-3791(97)00048-6)
- Grousset, F. E., Rognon, P., Coudé-Gaussen, G., & Pédehay, P. (1992). Origins of peri-Saharan dust deposits traced by their Nd and Sr isotopic composition. Palaeogeography, Palaeoclimatology, Palaeoecology, 93, 203–212. [https://doi.org/10.1016/0031-0182\(92\)90097-O](https://doi.org/10.1016/0031-0182(92)90097-O)

Hao, L.L., Wang, Q., Kerr, A. C., Wei, G.J., Huang, F., Zhang, M.Y. (2022). Contribution of continental subduction to very light B isotope signatures in post-collisional magmas: Evidence from southern Tibetan ultrapotassic rocks. *Earth and Planetary Science Letters*, 584, 117508. <https://doi.org/10.1016/j.epsl.2022.117508>

Haproff, P. J., Zuza, A. V., Yin, A., Harrison, T. M., Manning, C. E., Dubey, C. S. (2019). Geologic framework of the northern Indo-Burma Ranges and lateral correlation of Himalayan-Tibetan lithologic units across the eastern Himalayan syntaxis. *Geosphere*. <https://doi.org/10.1130/GES02054.1>

Harris, N. B. W., Santosh, M., & Taylor, P. N. (1994). Crustal Evolution in South India: Constraints from Nd Isotopes. *The Journal of Geology*, 102(2), 139–150. <https://doi.org/10.1086/629659>

Hu, G., Zeng, L., Gao, L.E., Liu, Q., Chen, H., & Guo, Y. (2018). Diverse magma sources for the Himalayan leucogranites: Evidence from B-Sr-Nd isotopes. *Lithos*, 314–315, 88–99. <https://doi.org/10.1016/j.lithos.2018.05.022>

Imayama, T., & Arita, K. (2008). Nd isotopic data reveal the material and tectonic nature of the Main Central Thrust zone in Nepal Himalaya. *Tectonophysics*, 451(1–4), 265–281. <https://doi.org/10.1016/j.tecto.2007.11.051>

Inger, S., & Harris, N. (1993). Geochemical Constraints on Leucogranite Magmatism in the Langtang Valley, Nepal Himalaya. *Journal of Petrology*, 34(2), 345–368. <https://doi.org/10.1093/petrology/34.2.345>

Jager, E., Bhandari, A. K., & Bhanot, V. (1971). Rb-Sr age determinations on biotites and Whole Rock samples from Mandi and Chor granites, Himachal Pradesh. India. *Eclogae Geologicae Helvetiae*. <https://doi.org/10.5169/seals-163993>

Jain, V., Wasson, R., McCulloch, M., Kaushal, R. K., & Singhvi, A. K. (2022). Controls on sediment provenance in the Baghmati river catchment, Central Himalaya, India. *Journal of Earth System Science*, 131(1), 14. <https://doi.org/10.1007/s12040-021-01759-z>

Jayananda, M., Moyen, J. F., Martin, H., Peucat, J. J., Auvray, B., & Mahabaleswar, B. (2000). Late Archaean (2550–2520 Ma) juvenile magmatism in the Eastern Dharwar craton, southern India: constraints from geochronology, Nd–Sr isotopes and whole rock geochemistry. *Precambrian Research*, 99(3–4), 225–254. [https://doi.org/10.1016/S0301-9268\(99\)00063-7](https://doi.org/10.1016/S0301-9268(99)00063-7)

Kingson, O., Bhutani, R., Balakrishnan, S., Dash, J. K., & Shukla, A. D. (2019). Subduction-related Manipur Ophiolite Complex, Indo-Myanmar Ranges: elemental and isotopic record of mantle metasomatism. *Geological Society, London, Special Publications*, 481(1), 195–210. <https://doi.org/10.1144/SP481.9>

Kunkelova, T., Crocker, A. J., Jewell, A. M., Breeze, P. S., Drake, N. A., Cooper, M. J., et al. (2022). Dust sources in Westernmost Asia have a different geochemical fingerprint to those in the Sahara. *Quaternary Science Reviews*, 294, 107717. <https://doi.org/10.1016/j.quascirev.2022.107717>

Kwatra, S. K., Singh, S., Singh, V.P, Sharma, R. K., Rai, B., & Kishor, N. (1999). Geochemical and geochronological characteristics of the Early Palaeozoic granitoids from Sutlej-Baspa Valleys, Himachal Himalaya. *Gondwana Research Group Memoirs*, 6, 145–58.

Le Fort, P., Debon, F., & Sonet, J. (1983). The Lower palaeozoic Lesser Himalayan granitic belt: emphasis of the Simchar pluton of Central Nepal. In *Granites of Himalayas Karakorum and Hindu Kush*, 235–255.

Lee, H. Y., Chung, S. L., Ji, J., Qian, Q., Gallet, S., Lo, C. H., et al. (2012). Geochemical and Sr–Nd isotopic constraints on the genesis of the Cenozoic Linzizong volcanic successions, southern Tibet. *Journal of Asian Earth Sciences*, 53, 96–114. <https://doi.org/10.1016/j.jseaes.2011.08.019>

Li, J. X., Fan, W. M., Zhang, L. Y., Evans, N. J., Sun, Y. L., Ding, L., & Sein, K. (2019). Geochronology, geochemistry and Sr–Nd–Hf isotopic compositions of Late Cretaceous–Eocene granites in southern Myanmar: Petrogenetic, tectonic and metallogenic implications. *Ore Geology Reviews*, 112, 103031. <https://doi.org/10.1016/j.oregeorev.2019.103031>

Licht, A., France-Lanord, C., Reisberg, L., Fontaine, C., Soe, A. N., & Jaeger, J. J. (2013). A palaeo Tibet–Myanmar connection? Reconstructing the Late Eocene drainage system of central Myanmar using a multi-proxy approach. *Journal of the Geological Society*, 170(6), 929–939. <https://doi.org/10.1144/jgs2012-126>

Lin, C., Zhang, J., Wang, X., Huang, T., Zhang, B., & Fan, Y. (2021). Himalayan Miocene adakitic rocks, a case study of the Mayum pluton: Insights into geodynamic processes within the subducted Indian continental lithosphere and Himalayan mid-Miocene tectonic regime transition. *GSA Bulletin*, 133(3–4), 591–611. <https://doi.org/10.1130/B35640.1>

Lin, I. J., Chung, S. L., Chu, C. H., Lee, H. Y., Gallet, S., Wu, G. (2012). Geochemical and Sr–Nd isotopic characteristics of Cretaceous to Paleocene granitoids and volcanic rocks, SE Tibet: Petrogenesis and tectonic implications. *Journal of Asian Earth Sciences*, 53, 131–150. <https://doi.org/10.1016/j.jseaes.2012.03.010>

Lupker M., France-Lanord C., Galy V., Lave' J., Gaillardet J., Gajurel A.P., Guilmette C. , Rahman M., Singh S.K. and Sinha R. (2012) Predominant floodplain over mountain weathering of Himalayan sediments (Ganga basin). *Geochimica et Cosmochimica Acta* 84, 410-432. <https://doi.org/10.1016/j.gca.2012.02.001>

Martin, A. J., DeCelles, P.G., Gehrels, G. E., Patchett, P. J., and Isachsen, C. (2005). Isotopic and Structural Constraints on the Location of the Main Central Thrust in the Annapurna Range, Central Nepal Himalaya. *Geological Society of America Bulletin*, 117, 926-944. <https://doi.org/10.1130/B25646.1>

McKenzie, N. R., Hughes, N. C., Myrow, P. M., Xiao, S., and Sharma, M. (2011). Correlation of Precambrian-Cambrian Sedimentary Successions across Northern India and the Utility of Isotopic Signatures of Himalayan Lithotectonic Zones. *Earth and Planetary Science Letters*, 312, 471-483. <https://doi.org/10.1016/j.epsl.2011.10.027>

Miller, C., Thöni, M., Frank, W., Grasemann, B., Klötzli, U., Guntli, P., & Draganits, E. (2001). The early Palaeozoic magmatic event in the Northwest Himalaya, India: source, tectonic setting and age of emplacement. *Geological Magazine*, 138(3), 237–251. <https://doi.org/10.1017/S0016756801005283>

Murphy, M. A. (2007). Isotopic characteristics of the Gurla Mandhata metamorphic core complex: Implications for the architecture of the Himalayan orogen. *Geology*, 35(11), 983. <https://doi.org/10.1130/G23774A.1>

Oliver, L., Harris, N., Bickle, M., Chapman, H., Dise, N., & Horstwood, M. (2003). Silicate weathering rates decoupled from the $^{87}\text{Sr}/^{86}\text{Sr}$ ratio of the dissolved load during Himalayan erosion. *Chemical Geology*, 201(1–2), 119–139. [https://doi.org/10.1016/S0009-2541\(03\)00236-5](https://doi.org/10.1016/S0009-2541(03)00236-5)

Pandey, B. K., Gupta, J. N., Sarma, K. J., & Sastry, C. A. (1997). Sm-Nd, Pb-Pb and Rb-Sr geochronology and petrogenesis of the mafic dyke swarm of Mahbubnagar, South India: implications for Paleoproterozoic crustal evolution of the Eastern Dharwar Craton. *Precambrian Research*, 84(3–4), 181–196. [https://doi.org/10.1016/S0301-9268\(97\)00027-2](https://doi.org/10.1016/S0301-9268(97)00027-2)

Parrish, R.R., and Hodges, V. (1996). Isotopic Constraints on the Age and Provenance of the Lesser and Greater Himalayan Sequences, Nepalese Himalaya. *Geological Society of America Bulletin*, 108, 904–911. [https://doi.org/10.1130/0016-7606\(1996\)108<0904:ICOTAA>2.3.CO;2](https://doi.org/10.1130/0016-7606(1996)108<0904:ICOTAA>2.3.CO;2)

Peketi, A., Mazumdar, A., Pillutla, S. P. K., Sawant, B., & Gupta, H. (2021). Climatic and Tectonic Control on the Bengal Fan Sedimentation Since the Pliocene. *Geochemistry, Geophysics, Geosystems*, 22(3). <https://doi.org/10.1029/2020GC009448>

Peucat, J. J., Vidal, P., Bernard-Griffiths, J., & Condie, K. C. (1989). Sr, Nd, and Pb Isotopic Systematics in the Archean Low- to High-Grade Transition Zone of Southern India: Syn-Accretion vs. Post-Accretion Granulites. *The Journal of Geology*, 97(5), 537–549. <https://doi.org/10.1086/629333>

Pognante, U., Castelli, D., Benna, P., Genovese, G., Oberli, F., Meier, M., & Tonarini, S. (1990). The crystalline units of the High Himalayas in the Lahul-Zanskar region (northwest India): metamorphic–tectonic history and geochronology of the collided and imbricated Indian plate. *Geological Magazine*, 127(2), 101–116. <https://doi.org/10.1017/S0016756800013807>

Rai, B., Kwatra, S. K., Singh, V. P., & Sharma, N. K. (1993). Whole rock Rb–Sr age for granitic rocks of Khadrala area, district Shimla, Himachal Pradesh, India. Preprint Volume 6th National Symposium Mass Spectrometry, 8, 1–4.

Ramaswamy, V., & Nair, R. R. (1994). Fluxes of material in the Arabian Sea and Bay of Bengal Sediment trap studies. *Journal of Earth System Science*, 103(2), 189–210. <https://doi.org/10.1007/BF02839536>

Rao, D. R., Sharma, K. K., Sivaraman, T. V., Gopalan, K., & Trivedi, J. R. (1990). Rb/Sr dating and petrochemistry of Hante granite (Baramulla area) Kashmir Himalaya. *Journal of Himalayan Geology*, 1, 57–63.

Richards, A., Argles, T., Harris, N., Parrish, R., Ahmad, T., Darbyshire, F., & Draganits, E. (2005). Himalayan architecture constrained by isotopic tracers from clastic sediments. *Earth and Planetary Science Letters*, 236(3–4), 773–796. <https://doi.org/10.1016/j.epsl.2005.05.034>

Robinson, D. M., DeCelles, P. G., Patchett, P. J., and Garzione, C. N., (2001). The Kinematic Evolution of the Nepalese Himalaya Interpreted from Nd Isotopes. *Earth and Planetary Science Letters*, 192, 507–521. [https://doi.org/10.1016/S0012-821X\(01\)00451-4](https://doi.org/10.1016/S0012-821X(01)00451-4)

Roddaz, M., Said, A., Guillot, S., Antoine, P.-O., Montel, J.-M., Martin, F., & Darrozes, J. (2011). Provenance of Cenozoic sedimentary rocks from the Sulaiman fold and thrust belt, Pakistan: implications for the palaeogeography of the Indus drainage system. *Journal of the Geological Society*, 168(2), 499–516. <https://doi.org/10.1144/0016-76492010-100>

Shukla. (2011). Geochemical and isotopic studies of some sedimentary sequences of the vindhyan supergroup India. M.S. University of Baroda, Vadodara, Gujarat, India. <http://hdl.handle.net/10603/58046>

Singh, A., Paul, D., Sinha, R., Thomsen, K. J., & Gupta, S. (2016). Geochemistry of buried river sediments from Ghaggar Plains, NW India: Multi-proxy records of variations in provenance, paleoclimate, and paleovegetation patterns in the Late Quaternary. *Palaeogeography, Palaeoclimatology, Palaeoecology*, 449, 85–100. <https://doi.org/10.1016/j.palaeo.2016.02.012>

Singh, K. (2018). Sr, Nd isotopic and geochemical studies of the rocks in the Manipur Ophiolite complex, Indo-Myanmar Range, India. Pondicherry University, Pondicherry. <http://hdl.handle.net/10603/284323>

Singh, S. K., Kumar, A., & France-Lanord, C. (2006). Sr and $^{87}\text{Sr}/^{86}\text{Sr}$ in waters and sediments of the Brahmaputra river system: silicate weathering, CO₂ consumption and Sr flux. *Chemical Geology*, 234(3-4), 308-320. <http://doi.org/10.1016/j.chemgeo.2006.05.009>

Sirocko, F. (1995). Abrupt Change in Monsoonal Climate: Evidence from the Geochemical Composition of Arabian Sea Sediments. habilitation thesis. Univ. of Kiel, Kiel, Germany. <https://epic.awi.de/id/eprint/21173/1/Sir1994a.pdf>

Skonieczny, C., Bory, A., Bout-Roumazeilles, V., Abouchami, W., Galer, S. J., Crosta, X., & Ndiaye, T. (2011). The 7–13 March 2006 major Saharan outbreak: Multiproxy characterization of mineral dust deposited on the West African margin. *Journal of Geophysical Research: Atmospheres*, 116(D18). <https://doi.org/10.1029/2011JD016173>

Stutz, E., & Thöni, M. (1987). The lower Paleozoic Nyimaling Granite in the Indian Himalaya (Ladakh): New Rb/Sr data versus zircon typology. *Geologische Rundschau*, 76(2), 307–315. <https://doi.org/10.1007/BF01821076>

Szulc, A. G., Najman, Y., Sinclair, H. D., Pringle, M., Bickle, M., Chapman, H., et al. (2006). Tectonic evolution of the Himalaya constrained by detrital 40Ar-39Ar, Sm-Nd and petrographic data from the Siwalik foreland basin succession, SW Nepal: Tectonic evolution of the Himalaya. *Basin Research*, 18(4), 375–391. <https://doi.org/10.1111/j.1365-2117.2006.00307.x>

Taylor, P. N., Chadwick, B., Moorbath, S., Ramakrishnan, M., & Viswanatha, M. N. (1984). Petrography, chemistry and isotopic ages of Peninsular Gneiss, Dharwar acid volcanic rocks and the Chitradurga granite with special reference to the late Archean evolution of the Karnataka craton, southern India. *Precambrian Research*, 23(3), 349–375. [https://doi.org/10.1016/0301-9268\(84\)90050-0](https://doi.org/10.1016/0301-9268(84)90050-0)

Tobisch, O. T., Collerson, K. D., Bhattacharyya, T., & Mukhopadhyay, D. (1994). Structural relationships and Sr-Nd isotope systematics of polymetamorphic granitic gneisses and granitic rocks from central Rajasthan, India: implications for the evolution of the Aravalli craton. *Precambrian Research*, 65(1–4), 319–339. [https://doi.org/10.1016/0301-9268\(94\)90111-2](https://doi.org/10.1016/0301-9268(94)90111-2)

Tripathi, J. K., Bock, B., & Rajamani, V. (2013). Nd and Sr isotope characteristics of Quaternary Indo-Gangetic plain sediments: Source distinctiveness in different geographic regions and its geological significance. *Chemical Geology*, 344, 12–22. <https://doi.org/10.1016/j.chemgeo.2013.02.016>

Trivedi, J. R., Gopalan, K., & Valdiya, K. S. (1984). Rb-Sr ages of granitic rocks within the Lesser Himalayan nappes, Kumaun, India. *Journal of the Geological Society of India*, 25, 641–654. Retrieved from <https://www.geosocindia.org/index.php/jgsi/article/view/65318>

Vimal R., Banerjee R., Gupta S., Krishna V., Achar K.K., Babu P.V., Parihar, P. S., Maithani, P. B. (2012). Geochemistry and Sr and Pb isotope systematics of basement granitoids from north and west of Palnad Sub-basin, Guntur and Nalgonda districts, Andhra Pradesh: *Journal of Applied Geochemistry*, 14(3), 295–315.

Williams, H. M. (2004). Nature of the Source Regions for Post-collisional, Potassic Magmatism in Southern and Northern Tibet from Geochemical Variations and Inverse Trace Element Modelling. *Journal of Petrology*, 45(3), 555–607. <https://doi.org/10.1093/petrology/egg094>

Zeng, L., Gao, L. E., Tang, S., Hou, K., Guo, C., & Hu, G. (2015). Eocene magmatism in the Tethyan Himalaya, southern Tibet. *Geological Society, London, Special Publications*, 412(1), 287–316. <https://doi.org/10.1144/SP412.8>

Zhang, H., Harris, N., Parrish, R., Kelley, S., Zhang, L., Rogers, N. (2004). Causes and consequences of protracted melting of the mid-crust exposed in the North Himalayan antiform. *Earth and Planetary Science Letters*, 228(1–2), 195–212. <https://doi.org/10.1016/j.epsl.2004.09.031>

Zhao, W., Balsam, W., Williams, E., Long, X., & Ji, J. (2018). Sr-Nd-Hf isotopic fingerprinting of transatlantic dust derived from North Africa. *Earth and Planetary Science Letters*, 486, 23–31. <https://doi.org/10.1016/j.epsl.2018.01.004>

Zhao, Z., Mo, X., Zhang, S., Guo, T., Zhou, S., Dong, G., & Wang, Y. (2001). Post-collisional magmatism in Wuyu basin, central Tibet: evidence for recycling of subducted Tethyan oceanic crust. *Science in China Series D: Earth Sciences*, 44(S1), 27–34. <https://doi.org/10.1007/BF02911968>

Table 1: Sr and Nd isotopic values of core SSD 004-GC03 with the concentration of Al, Mg, Ti, K, Na, Ca, Zr, Hf, Cr, Sr, Rb, Nd

Sr. No.	Sample dept h (cm)	Age (ka)	Al	Mg	Ti	K	Na	Ca	Zr	Hf	Cr	Sr	Rb	Nd	$^{87}\text{Sr}/^{86}\text{Sr}$	2σ	$^{143}\text{Nd}/^{144}\text{Nd}$	2σ	ϵ_{Nd}
			wt (%)						($\mu\text{g/g}$)										
1	1-2	0.10	7.44	1.2	0.68	1.37	0.45	0.16	48.3	1.52	132.4	74.	94.0	18.8	0.72491	0.000017	0.5116015	0.000008	-20.2
2	11-12	0.74	7.58	1.2	0.66	1.40	0.46	0.21	49.5	1.51	143.1	79.	93.2	19.4	0.72477	0.000012	0.5115786	0.000016	-20.7
3	21-22	1.37	7.21	1.3	0.57	1.25	0.32	0.13	48.2	1.45	155.2	84.	90.2	18.0	0.72000	0.000018	0.5116211	0.000010	-19.8
4	29-30	1.65	7.32	1.2	0.61	1.32	0.34	0.09	48.7	1.50	148.7	80.	91.4	17.1	0.72172	0.000016	0.5116033	0.000010	-20.2
5	61-62	2.93	7.47	1.2	0.61	1.37	0.39	0.15	48.5	1.49	145.8	73.	93.7	17.3	0.72320	0.000014	0.5115638	0.000009	-21.0
6	79-80	3.89	7.64	1.3	0.64	1.43	0.36	0.09	53.8	1.70	170.8	77.	95.3	17.2	0.72189	0.000014	0.5115508	0.000008	-21.2
7	87-88	4.31	8.02	1.4	0.64	1.45	0.32	0.11	51.8	1.63	173.3	82.	99.2	17.5	0.72059	0.000018	0.5115690	0.000010	-20.9
8	99-100	4.95	7.65	1.5	0.64	1.49	0.31	0.10	50.1	1.55	174.1	69.	98.2	18.5	0.71978	0.000011	0.5115981	0.000009	-20.3
9	109-110	5.47	7.25	1.4	0.57	1.43	0.30	0.09	52.7	1.63	157.9	76.	96.3	16.2	0.72090	0.000016	0.5115740	0.000009	-20.3
10	114-115	5.74	7.72	1.5	0.66	1.60	0.40	0.15	59.9	1.83	165.7	75.	100.6	17.8	0.72113	0.000012	0.5115640	0.000009	-20.8
11	120-121	6.06	7.60	1.3	0.63	1.53	0.33	0.10	62.0	1.91	161.0	68.	99.1	18.0	0.72184	0.000010	0.5115597	0.000010	-21.0
12	130-131	6.59	7.64	1.4	0.65	1.56	0.29	0.07	57.9	1.76	164.8	44.	101.3	18.9	0.72124	0.000014	0.5115962	0.000009	-21.0
13	140-141	7.11	8.43	1.5	0.58	1.58	0.20	0.05	57.2	1.82	172.7	68.	110.5	13.7	0.72424	0.000020	0.5115880	0.000011	-20.3
14	150-151	7.71	8.18	1.4	0.70	1.75	0.28	0.09	61.8	1.91	165.5	70.	115.7	18.9	0.72297	0.000015	0.5115539	0.000009	-20.5
15	160-161	8.81	8.13	1.4	0.68	1.74	0.32	0.08	61.1	1.85	157.5	71.	112.1	21.3	0.72430	0.000010	0.5115128	0.000009	-21.1
16	170-171	9.28	7.77	1.2	0.68	1.59	0.30	0.05	66.2	2.02	157.2	54.	106.1	23.5	0.72286	0.000012	0.5116371	0.000011	-21.9
17	180-181	9.63	8.20	1.2	0.65	1.43	0.25	0.09	70.2	2.15	167.1	66.	111.8	17.7	0.72355	0.000011	0.5116221	0.000014	-19.5
18	190-191	9.99	8.12	1.3	0.70	1.52	0.26	0.05	69.4	2.12	169.0	59.	107.2	22.5	0.72148	0.000018	0.5116259	0.000011	-19.8
19	200-201	10.31	8.56	1.1	0.78	1.47	0.29	0.08	75.5	2.29	164.7	59.	110.8	21.0	0.72405	0.000011	0.5116195	0.000011	-19.7
20	210-211	10.63	8.38	1.2	0.84	1.52	0.28	0.03	84.9	2.57	180.0	58.	117.9	23.6	0.72332	0.000015	0.5117006	0.000010	-19.9
21	220-221	10.95	8.59	1.4	0.87	1.70	0.32	0.06	78.9	2.46	183.7	59.	124.3	20.5	0.72352	0.000014	0.5117940	0.000013	-18.3
22	230-231	11.25	8.72	1.4	0.95	1.71	0.38	0.09	83.4	2.56	181.6	59.	126.8	19.3	0.72410	0.000010	0.5117976	0.000012	-16.5
23	240-241	11.74	8.18	1.4	0.97	1.66	0.40	0.11	90.7	2.74	181.8	61.	125.7	20.0	0.72422	0.000011	0.5117729	0.000011	-16.4
24	250-251	12.24	8.61	1.5	0.87	1.71	0.35	0.07	82.9	2.55	187.1	79.	127.3	20.6	0.72356	0.000013	0.5116925	0.000015	-16.9
25	260-261	12.71	7.89	1.4	0.76	1.74	0.38	0.12	78.7	2.42	182.7	89.	123.9	24.6	0.72231	0.000010	0.5118180	0.000012	-18.4
26	280-281	14.99	7.27	1.8	0.68	1.94	0.61	0.23	71.8	2.16	155.7	90.	123.7	21.9	0.72243	0.000009	0.5118124	0.000013	-16.0
27	290-291	16.67	7.35	1.9	0.69	2.09	0.70	0.28	79.8	2.37	155.5	125.9	22.5	0.72312	0.000012	0.000009	0.000009	-16.1	

28	293-294	17.33	8.00	2.0	0.62	2.00	0.40	0.08	77.5	2.34	170.6	62.	129.4	17.8	0.72275	0.000012	0.5118817	0.000010	-14.8	
29	295-296	17.65	7.51	1.9	0.59	1.82	0.38	0.09	75.1	2.31	175.6	66.	126.4	17.0	0.72225	0.000008	0.5118772	0.000009	-14.8	
30	297-298	17.74	7.23	1.7	0.70	2.05	0.65	0.31	66.8	2.05	155.2	116	122.2	24.5	0.72272	0.000014	0.5117753	0.000009	-16.8	
31	301-302	17.94	7.24	1.6	0.71	2.08	0.59	0.36	70.3	2.13	157.5	127	123.8	25.4	0.72380	0.000013	0.5117527	0.000009	-17.3	
32	303-304	18.03	7.52	1.7	0.74	2.11	0.60	0.37	79.8	2.41	171.4	75.	127.1	26.8	0.72296	0.000012	0.5118539	0.000007	-17.6	
33	305-306	18.13	8.19	1.9	0.61	1.94	0.43	0.12	71.9	2.17	195.3	123	129.1	17.7	0.72238	0.000017	0.5117719	0.000011	-15.3	
34	307-308	18.39	7.43	1.5	0.73	2.01	0.55	0.31	78.9	2.39	163.3	130	123.8	23.5	0.72460	0.000010	0.5117906	0.000012	-16.9	
35	309-310	18.70	7.47	1.7	0.69	2.02	0.59	0.39	75.3	2.28	170.7	124	124.3	25.7	0.72282	0.000013	0.5117394	0.000006	-16.5	
36	311-312	19.02	8.40	2.0	0.72	2.13	0.62	0.28	90.1	2.76	201.8	135	143.6	27.0	0.72249	0.000015	0.5117668	0.000010	-17.5	
37	313-314	19.35	7.29	1.7	0.70	2.00	0.71	0.39	80.7	2.44	166.6	130	120.7	25.0	0.72241	0.000007	0.5117230	0.000012	-17.0	
38	315-316	19.67	7.35	1.5	0.68	1.96	0.66	0.36	77.1	2.36	158.8	135	120.5	23.8	0.72238	0.000017	0.5117150	0.000010	-17.8	
39	317-318	20.00	7.26	1.5	0.69	1.96	0.55	0.39	76.0	2.30	161.7	140	122.6	26.1	0.72253	0.000014	0.5117566	0.000006	-18.0	
40	319-320	20.11	7.48	1.7	0.67	2.00	0.70	0.38	75.9	2.24	168.6	134	124.7	24.3	0.72204	0.000017	0.5117475	0.000008	-17.2	
41	321-322	20.22	7.24	1.5	0.69	1.98	0.56	0.36	76.4	2.29	159.8	146	121.2	23.6	0.72310	0.000012	0.5118578	0.000005	-17.4	
42	323-324	20.33	7.86	2.0	0.66	2.01	0.65	0.27	89.6	2.60	195.3	135	125.4	32.2	0.71999	0.000015	0.5118746	0.000009	-15.2	
43	325-326	20.44	7.52	1.9	0.65	2.00	0.64	0.25	86.6	2.48	197.2	141	122.6	31.0	0.72047	0.000014	0.5118684	0.000007	-14.9	
44	327-328	20.55	7.66	1.9	0.67	2.03	0.64	0.30	81.2	2.36	193.0	149	122.8	30.7	0.72104	0.000017	0.5118393	0.000005	-15.0	
45	329-330	20.66	7.41	1.8	0.66	2.02	0.63	0.30	84.2	2.45	186.3	137	120.9	30.7	0.72051	0.000010	0.5117844	0.000007	-15.6	
46	331-332	20.77	7.81	1.9	0.67	2.03	0.67	0.29	86.4	2.52	199.8	122	124.9	30.7	0.72127	0.000013	0.5118697	0.000008	-16.7	
47	333-334	20.88	7.60	2.0	0.64	1.93	0.54	0.19	84.7	2.47	206.1	146	122.9	29.5	0.72033	0.000013	0.5118211	0.000009	-15.0	
48	337-338	20.99	7.74	2.0	0.67	2.05	0.69	0.32	82.7	2.45	204.4	133	124.7	32.7	0.72231	0.000016	0.5118490	0.000009	-15.9	
49	335-336	21.30	7.52	1.9	0.66	2.02	0.52	0.33	92.5	2.66	199.9	134	122.8	30.7	0.72099	0.000015	0.5118265	0.000008	-15.4	
50	339-340	21.61	7.57	1.9	0.66	1.98	0.68	0.31	88.3	2.52	199.7		119.0	30.9	0.72184	0.000010		0.000010	-15.8	

51	341-342	21.92	7.48	1.8	0.66	1.96	0.67	0.29	89.9	2.59	198.8	134	119.0	30.6	0.72095	0.000010	0.5118409	0.000004	-15.5	
52	343-344	22.19	7.87	1.9	0.66	2.03	0.55	0.31	89.4	2.53	194.3	145	121.1	32.3	0.72086	0.000013	0.5118482	0.000008	-15.4	
53	345-346	22.38	7.53	1.8	0.66	1.97	0.64	0.25	92.4	2.67	199.7	126	120.3	30.3	0.72167	0.000013	0.5118216	0.000009	-15.9	
54	347-348	22.58	7.27	1.1	0.72	1.87	0.64	0.20	94.6	2.69	153.8	96.	108.7	22.0	0.72349	0.000011	0.5117978	0.000009	-16.8	
55	349-350	22.77	7.46	1.3	0.68	1.87	0.58	0.16	92.4	2.65	175.3	93.	115.0	21.5	0.72321	0.000013	0.5118063	0.000006	-16.4	
56	351-352	22.97	7.44	1.2	0.69	1.86	0.56	0.15	89.4	2.59	162.6	90.	114.4	20.4	0.72353	0.000011	0.5118229	0.000010	-16.2	
57	353-354	23.16	7.58	1.2	0.69	1.84	0.63	0.14	94.4	2.69	159.3	92.	110.8	20.2	0.72394	0.000012	0.5117859	0.000005	-15.9	
58	357-358	23.55	7.25	1.2	0.69	1.89	0.61	0.21	94.5	2.66	154.7	94.	110.6	20.0	0.72393	0.000013	0.5117785	0.000013	-16.6	
59	359-360	23.74	7.26	1.2	0.69	1.90	0.61	0.17	96.0	2.81	157.0	114	117.2	21.3	0.72360	0.000013	0.5117778	0.000011	-16.8	
60	360-361	23.84	7.40	1.2	0.73	1.93	0.65	0.20	89.9	2.61	153.9	78.	113.5	21.9	0.72291	0.000013	0.5117986	0.000009	-16.8	
61	370-371	24.81	7.57	1.3	0.69	1.83	0.49	0.10	92.8	2.68	172.5	95.	113.7	19.6	0.72378	0.000014	0.5117960	0.000010	-16.4	
62	380-381	25.78	7.47	1.3	0.71	1.90	0.59	0.17	94.4	2.72	168.3	110	114.4	21.7	0.72261	0.000012	0.5117753	0.000009	-16.4	
63	390-391	26.75	7.32	1.1	0.72	1.85	0.66	0.19	95.0	2.71	162.5	80.	109.2	21.8	0.72338	0.000015	0.5117460	0.000010	-16.8	
64	400-401	27.72	8.24	1.4	0.68	1.75	0.42	0.11	90.3	2.63	185.1	94.	114.4	19.3	0.72286	0.000013	0.5117212	0.000009	-17.4	
65	410-411	28.69	7.62	1.1	0.69	1.76	0.56	0.15	86.1	2.55	156.3	88.	108.1	21.7	0.72389	0.000012	0.5117815	0.000005	-17.9	
66	420-421	29.67	7.80	1.6	0.66	1.92	0.58	0.18	88.9	2.60	155.2	87.	119.4	24.2	0.72357	0.000011	0.5117150	0.000006	-16.7	
67	430-431	30.64	7.84	1.6	0.65	1.86	0.48	0.13	83.2	2.44	108.2	49.	120.9	23.2	0.72263	0.000014	0.5117635	0.000009	-18.0	
68	440-441	31.61	7.97	1.6	0.63	1.83	0.43	0.14	82.4	2.38	90.0	87.	62.7	11.8	0.72227	0.000009	0.5117393	0.000008	-17.1	
69	450-451	32.58	8.11	1.6	0.60	1.75	0.52	0.09	82.1	2.40	69.7	113	114.7	24.7	0.72188	0.000012	0.5116826	0.000005	-17.5	
70	460-461	33.55	7.67	1.4	0.66	1.76	0.53	0.16	80.2	2.33	180.8	83.	111.8	25.7	0.72292	0.000019	0.5117072	0.000006	-18.6	
71	470-471	34.43	7.73	1.6	0.60	1.74	0.40	0.09	76.2	2.23	149.6	79.	112.5	21.8	0.72262	0.000013	0.5116452	0.000007	-18.2	
72	480-481	34.87	7.15	1.4	0.55	1.65	0.46	0.15	79.8	2.29	67.9	85.	103.6	20.9	0.72367	0.000010	0.5116226	0.000008	-19.4	
73	490-491	35.30	7.77	1.5	0.57	1.66	0.37	0.08	74.9	2.25	139.6	69.	113.7	21.3	0.72195	0.000010	0.5117140	0.000006	-19.8	
74	500-501	35.73	7.99	1.6	0.56	1.62	0.31	0.03	74.1	2.14	167.2	78.	109.2	18.6	0.72266	0.000014	0.5117454	0.000010	-18.0	
75	510-511	36.17	7.51	1.7	0.63	1.88	0.51	0.15	79.3	2.29	75.0	82.	115.7	22.0	0.72385	0.000010	0.5117441	0.000014	-17.4	
76	520-521	36.60	7.60	1.6	0.62	1.82	0.49	0.14	79.6	2.33	54.7	89.	115.2	21.9	0.72337	0.000010	0.5117371	0.000012	-17.4	
77	530-531	37.04	8.31	1.6	0.65	1.84	0.47	0.12	82.6	2.39	44.1	129	120.0	23.2	0.72250	0.000016	0.5117179	0.000010	-17.6	
78	540-541	37.47	7.67	1.5	0.67	1.84	0.53	0.17	79.4	2.28	82.9	114.7	24.8	0.72132	0.000012	0.5116353	0.000010	-17.9		
79	550-551	37.91													0.72313	0.000011	0.5116353	0.000008	-19.6	

BCR -2 Reported	7.1	2.2	1.4	1.5	2.3	5.1	186.5	4.97	15.9	³³⁷	46	28.3	0.70502	0.51263		
BCR-2 measured	7.3	2.3	1.3	1.4	2.2	5.0	171.1	4.65	14.0	³⁴⁴	40.1	31.1	0.70503	0.000007	0.51258	0.000004

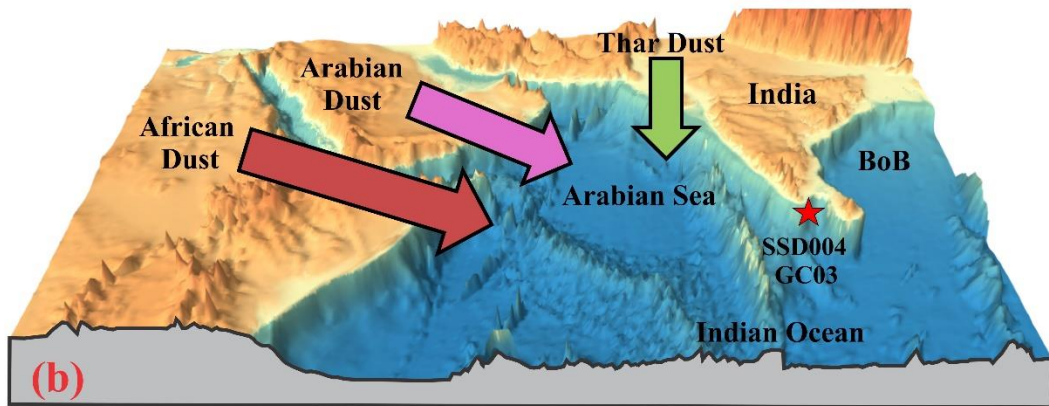
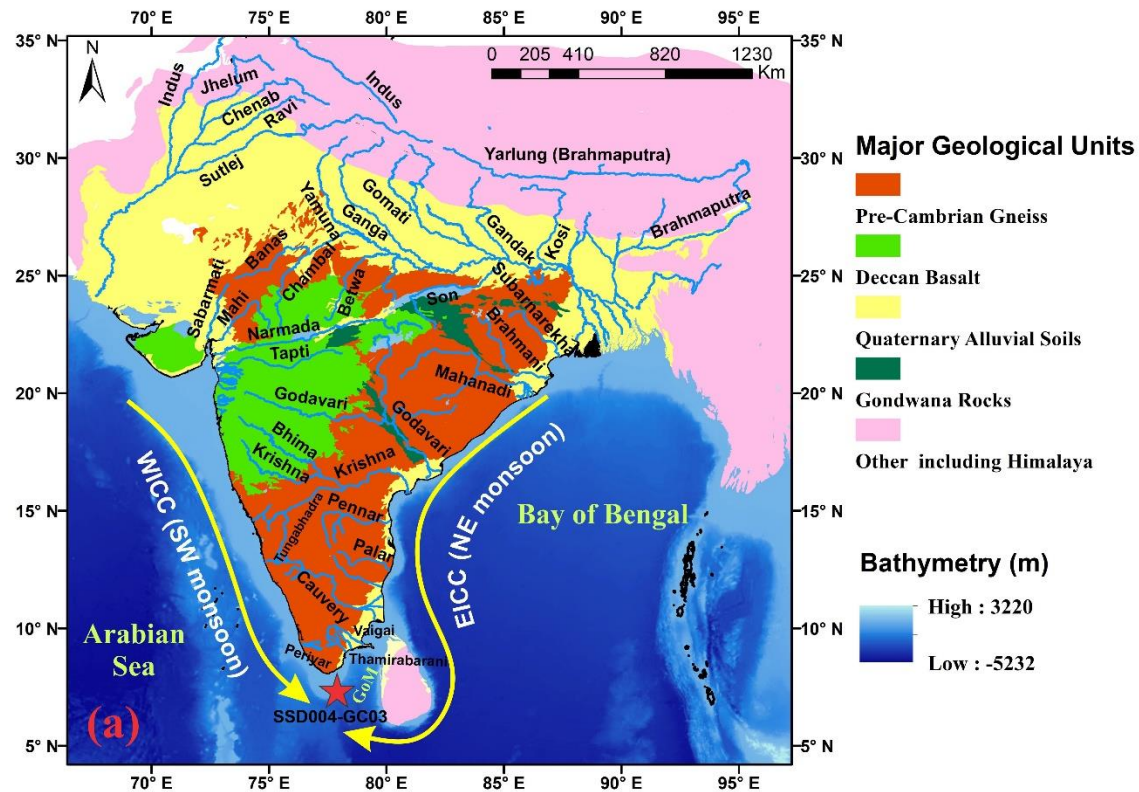


Figure 1. Possible riverine (a) and dust (b) sources of sediments to the Indian Ocean along with coastal currents (yellow arrows) and the core location of the present study; SSD004GC03 (Red Star). EICC: East India Coastal Currents; WICC: West India Coastal Currents; GoM: Gulf of Mannar; BoB: Bay of Bengal. The base map is taken from USGS and created in Q GIS 3.24 environment (WGS84).

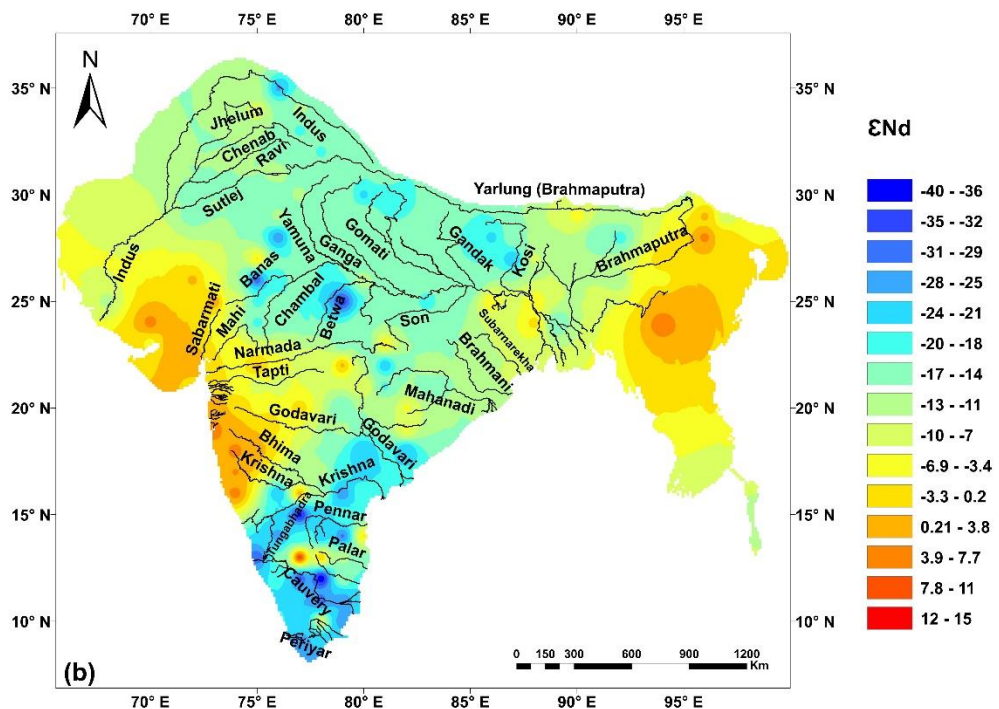
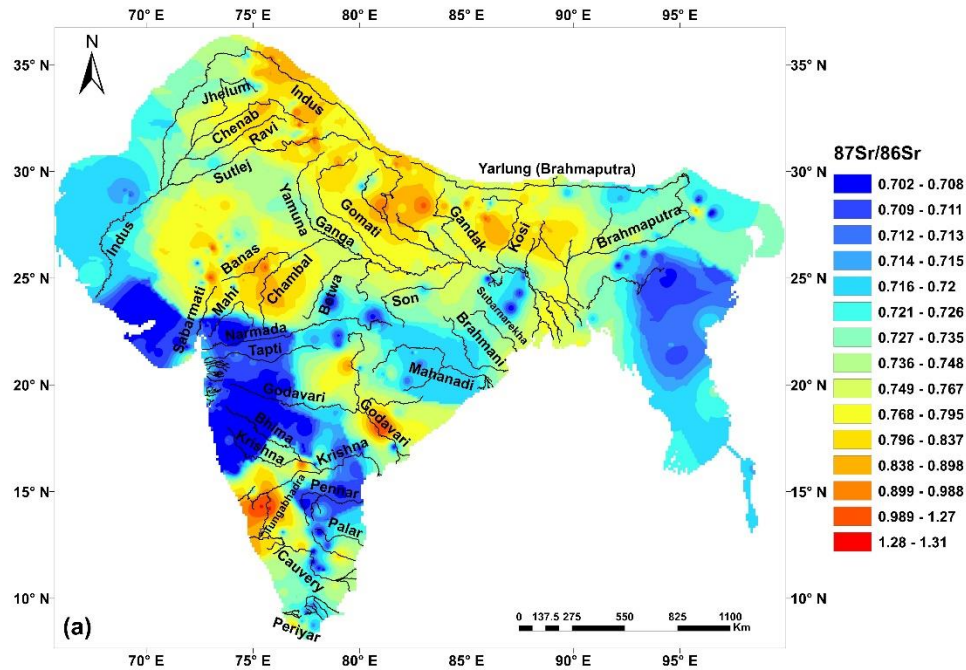


Figure 2. Spatial distribution map of (a) $^{87}\text{Sr}/^{86}\text{Sr}$ and (b) ϵ_{Nd} over Indian continent, created by Inverse Distance Weighting (IDW) interpolation method in Q GIS 3.24 environment (WGS84).

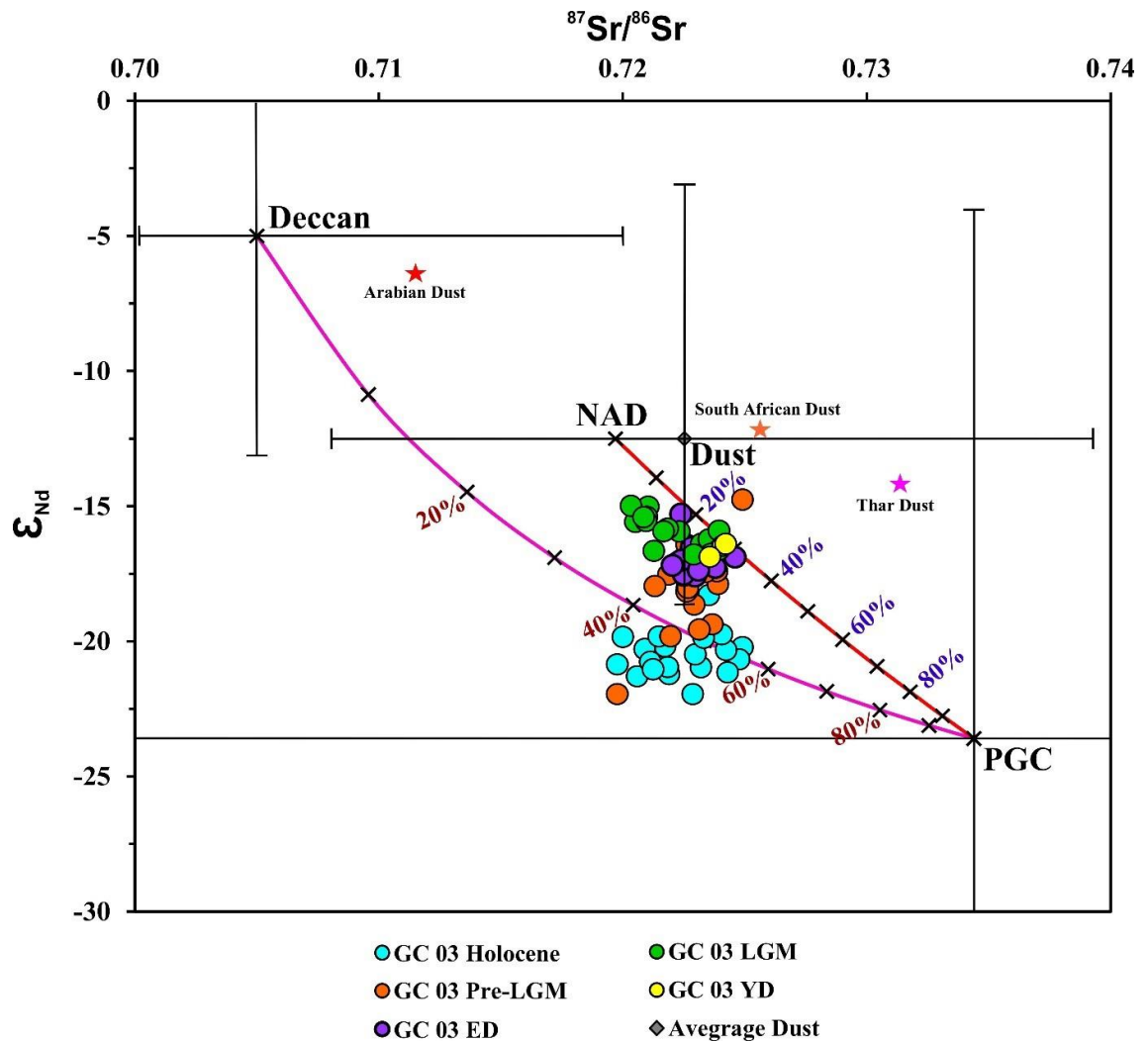


Figure 3. Binary mixing plot of Sr-Nd isotopes of the sediments of core SSD004-GC03 along with the potential end members. The end members are taken from the literature (Supplementary information Text, and Table S1) and represent their average value with 2σ variation. PGC: Peninsular Gneissic Complex; NAD: North African Dust (includes Saharan dust).

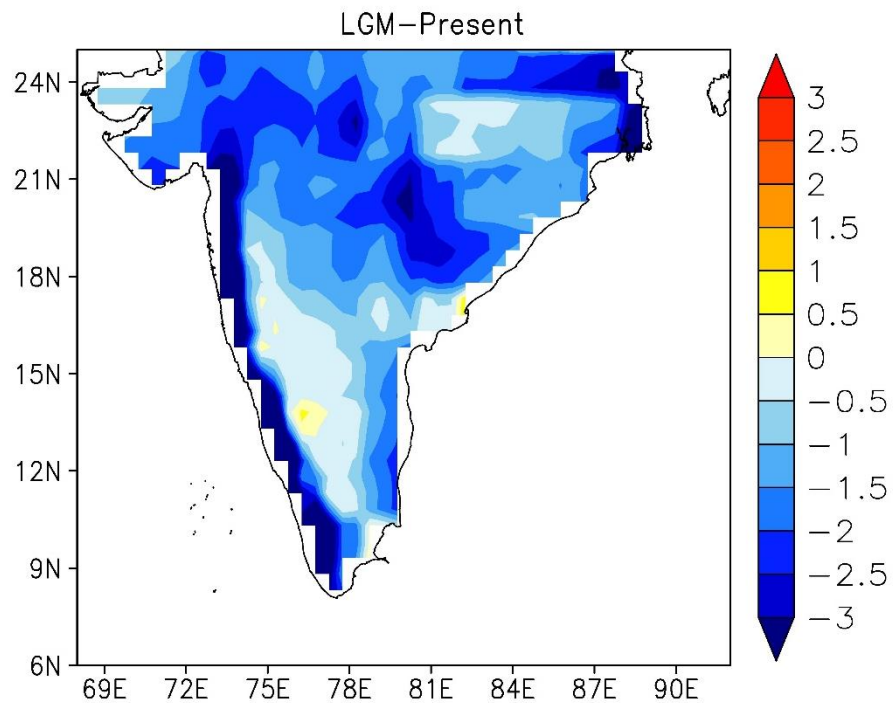


Figure 4. Difference in the annual mean precipitation (mm/day) between LGM and present time over peninsular India. LGM precipitation is averaged during 20-23 Kyr using MPI-ESM1-2-LR model and present is averaged during 1980-2010 using CRU observation.

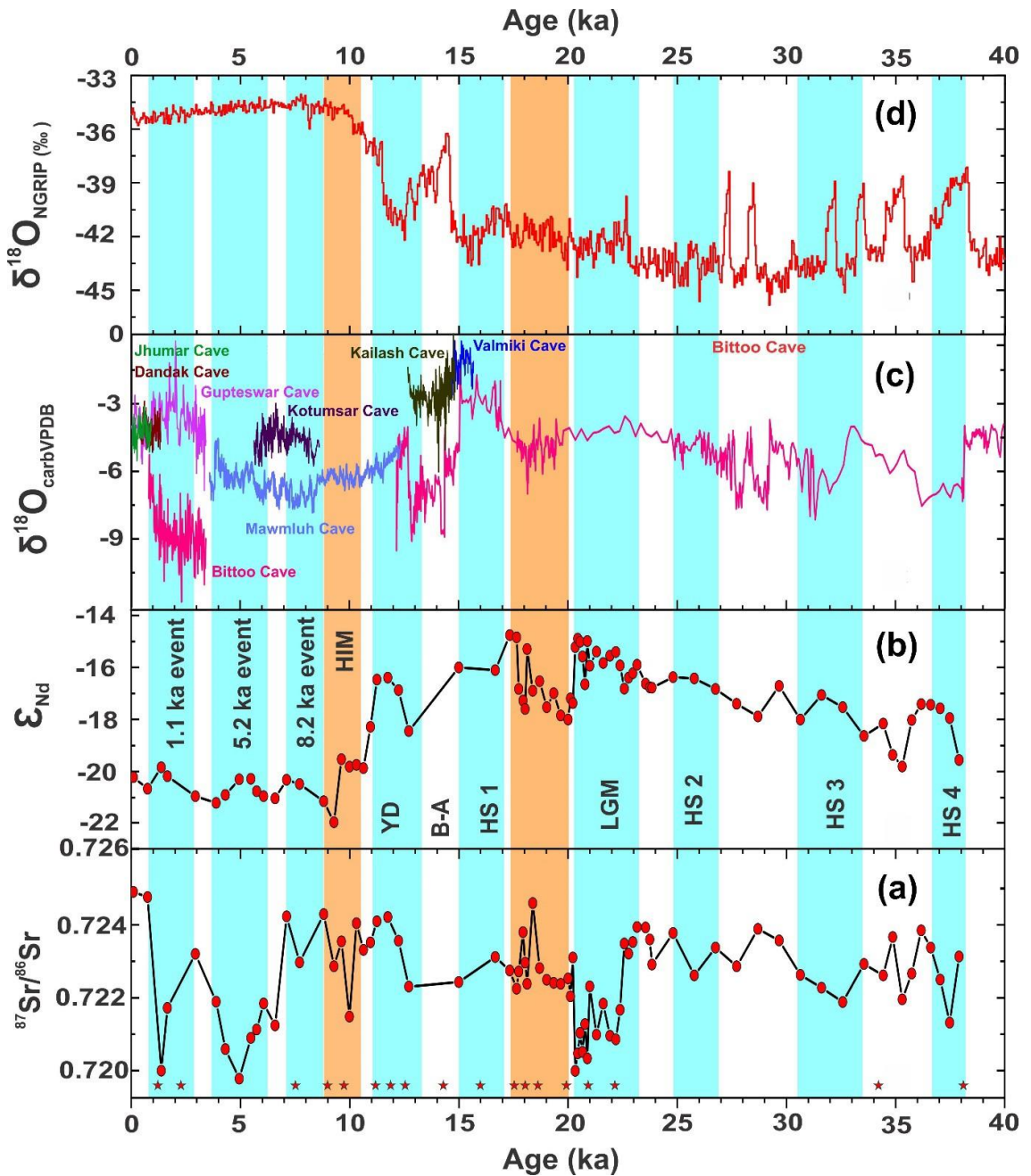


Figure 5. Comparison of Sr (a) and Nd (b) isotope variations with oxygen isotope of $\delta^{18}\text{O}_{\text{carbVPDB}}$ (Oxygen isotope measured in the Carbonates of Vienna PeeDee Belemnite) (c) from different caves in the Himalayan and Peninsular regions of India (Band et al., 2018; Berkelhammer et al., 2012; Berkelhammer et al., 2010; Gautam et al., 2019; Kathayat et al., 2016; Lone et al., 2013; Sinha et al., 2011; Yadava et al., 2004; Yadava & Ramesh, 2005) and NGRIP (<https://www.ncei.noaa.gov/access/paleo-search/study/2481>) (d). The variation in Sr-Nd isotope data correlates with well-known cold and warm climatic events marked with different colour shades. The red star in the plot denotes ^{14}C dated ages.

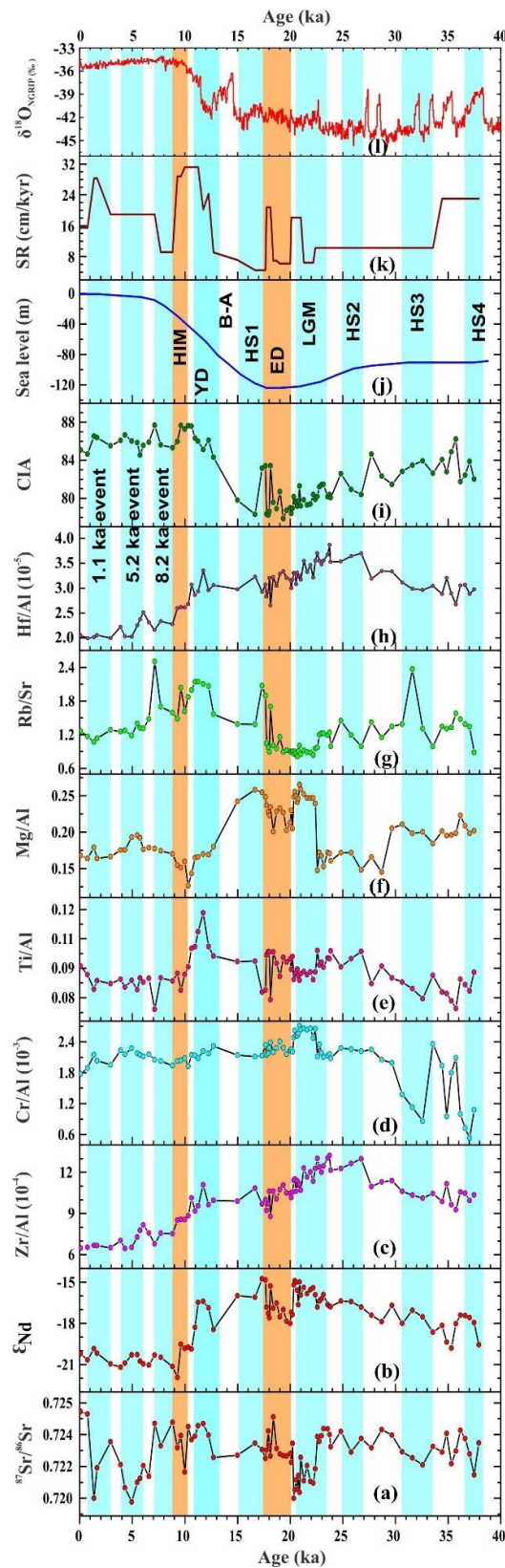


Figure 6. Variations in major and trace element composition of sediments correlate with climatic events and sea level (Arz et al., 2007; Stanford et al., 2011). The elemental ratios are calculated in $\mu\text{g/g}$.

[Paleoceanography and Paleoclimatology]

Supplementary Information

Strong Climate Control on the Millennial-Scale Dust Variability and Sediment Provenances in the Equatorial Indian Ocean inferred from Sr-Nd Isotopes

Arvind Shukla^{1,2}, Sunil Kumar Singh^{1*}, Dharmendra Pratap Singh³, Aka Sharma⁴, and A. P. Dimri⁴

¹CSIR-National Institute of Oceanography, Dona-Paula, Goa, India-403004,

²School of Earth Ocean and Atmospheric Sciences, Goa University, Dona-Paula, Goa, India-403004

³Department of Earth Sciences, IIT Roorkee, Roorkee, India-247667

⁴School of Environmental Sciences, Jawaharlal Nehru University, New Delhi 110067, India

*Corresponding author: **Sunil Kumar Singh**

Email: mail to: sunil@nio.org

Table of Contents

Text S1 to S3

Figures S1 to S12

Table S1 to S3

Supplementary Text

S1. End-members Characterization of Potential Sources

As discussed in the main text, the core location of the present study (GC03) may receive the sediments from different sources mainly from the (1) Lower Himalaya (LH), (2) Higher Himalaya (HH), (3) Deccan basalt, (4) Peninsular Gneissic complex (PGC) and (5) Aeolian dust. Therefore, to trace the provenances of the sediments deposited at the core site and to quantify them, end member of Sr and Nd isotope composition of different sources have been characterized with the available data set from the earlier published literature.

I.Himalaya

Several studies report the Sr and Nd isotopic compositions of the Himalayan lithology which have been summarized by Singh et al. (2008). The end members of the Lower and Higher Himalaya have been assigned from Singh et al. (2008) and directly incorporated in binary mixing plot.

II.Deccan

Deccan basalt is a major source of sediment in the Northern and Equatorial Indian Ocean and hence can be a prominent sediment source to the core location (off the southern tip of India: GC03). Sr and Nd isotopic endmember characterization of Deccan basalt has already been fixed by (Singh et al., 2008), and hence directly incorporated in the present study, listed in Table S1.

III.Peninsular Gneissic complex (PGC)

PGC consists of rocks of different ages (Archean to Proterozoic) and of varying lithologies. The major geology of the PGC consists of Southern Granulitic Terrane (SGT), which is a Proterozoic mobile belt, Western Dharwar and Eastern Dharwar Craton (Archean Cratons), Closepet Granite (Neoarchean granitoid) and Paleoproterozoic to Neoproterozoic basins (Cuddapah Basin). Having complex lithology, PGC can contribute sediments to the equatorial Indian Ocean with large-scale variations in Sr and Nd isotopic composition. $^{87}\text{Sr}/^{86}\text{Sr}$ and ε_{Nd} data of the peninsular lithologies are available in literature and data repositories. Therefore, the Sr and Nd isotopic endmember characterization of PGC has been done using the GEOROC data repository (<https://georoc.mpch-mainz.gwdg.de//georoc/CompFiles.aspx>) and other data sets available in earlier publications (Harris et al., 1994; Jayananda et al., 2000; Pandey et al., 1997; Peucat et al., 1989; Taylor et al., 1984; Vimal et al., 2012) as mentioned in Table S1. Based on the available $^{87}\text{Sr}/^{86}\text{Sr}$ ($n=487$) and ε_{Nd} ($n=528$) data, the histograms for both ($^{87}\text{Sr}/^{86}\text{Sr}$ and ε_{Nd}) have been plotted (Figure S4). The mean value for $^{87}\text{Sr}/^{86}\text{Sr}$ is 0.7344 (from 0.7010 to 1.600; total range, i.e., 100% data consideration) and ε_{Nd} is -23.6 (from -46 to -4.1; total range, i.e., 100% data consideration).

IV.Dust

Along with detrital sediment fluxes from major lithologies (Deccan, LH, HH, and PGC), huge dust flux from arid land masses of the African, Saharan, Arabian, and Indian continents (Ramaswamy & Nair, 1994; Sirocko & Sarnthein, 1989) can also significantly control the Sr and Nd isotope budget of sediments of Equatorial Indian Ocean. The core location GC03 (off the southern tip of India) receives aeolian dust from the different sources mentioned above. The Sr and Nd isotope compositions of these dust sources have been characterized in the earlier publications, which have been listed below with their respective references in Table S3. The Histograms have been plotted for $^{87}\text{Sr}/^{86}\text{Sr}$ ($n = 145$) and ε_{Nd} ($n = 131$) shown in figure S5. The average value of $^{87}\text{Sr}/^{86}\text{Sr}$ is 0.72252 (from 0.74715 to 0.70800) and ε_{Nd} is -12.5 (from -18.7 to -3.1).

S2. Binary Mixing plot

The Sr-Nd isotope composition of sediments have been plotted on mixing diagram along with the possible end members (*viz.* Deccan, PGC, LH and HH) (Figure S6) to determine their provenances. Along with the Sr-Nd isotope data of the sediments of GC03, the mixing plot also incorporates isotope

data of river sediments from respective outflows. The Sr and Nd isotope composition of the rivers confirms the end members of the sources they drain.

S3. Rainfall distribution map over Indian peninsula

To show the impact of dry and wet periods on the sediment source variability to the core site, the average precipitation map of the Indian peninsula for year 2002 (Figure S7), considered as drought year and 2007 (Figure S8), a wet period (defined by India Meteorological Department: IMD) have been prepared. Rainfall data for creating precipitation map (Figure S7 and S8) have been taken from Goddard Earth Sciences Data and Information Service Centre (2016) and can be accessed through this link: https://disc.gsfc.nasa.gov/datasets/TRMM_3B42RT_Daily_7/summary. The map is marked with Deccan and PGC regions to quantify the rainfall over both regions and for further comparison. It is observed from the maps that in the contemporary scenario, rainfall over the Indian subcontinent is highly variable in time and place and hence different areas (Deccan and Peninsular Gneissic complex) receive different amounts of rainfall throughout the years. The average precipitation over the Deccan region during drought year (2002) and high rainfall year (2007) is 28 mm/year and 35 mm/year respectively. Similarly, the average precipitation over the PGC region during 2002 and 2007 is 25 mm/year and 38 mm/year respectively. Therefore, it is noticed that during the drought year (2002) Deccan region receives 20% less rainfall, whereas the PGC receives ~34% less during the drought year of 2002 compared to the higher rainfall year 2007. This implies that during the drought period (cold period), Deccan region receives more rainfall than PGC, which could result in the enhanced erosion of the Deccan basalt compared to PGC during the cold and dry periods.

In addition to contemporary precipitation, the rainfall over peninsular India during LGM (20-23 Ka) has been modelled using Max Planck Institute Earth System Model version 1.2 (MPI-ESM1-2-LR) from the modelling suite of Paleoclimate Modelling Intercomparison Project phase fourth (PMIP4) simulations in the Coupled Model Intercomparison Project (CMIP6) having spatial resolution of 250 km (Figure S1), which varied in the range of 0.6 to 5.1 and 0.1 to 1.6 mm/day over the Deccan and PGC regions respectively. In contrast, present-day precipitation (1980 to 2010) ranges between 2.1 to 7.6 mm/day over the Deccan region, while PGC region experiences precipitation exceeds 7.6 mm/day (Figure S2). The difference in annual precipitation between the LGM and the present clearly indicates a more pronounced reduction in rainfall over the PGC region compared to the Deccan region.

Supplementary Figure

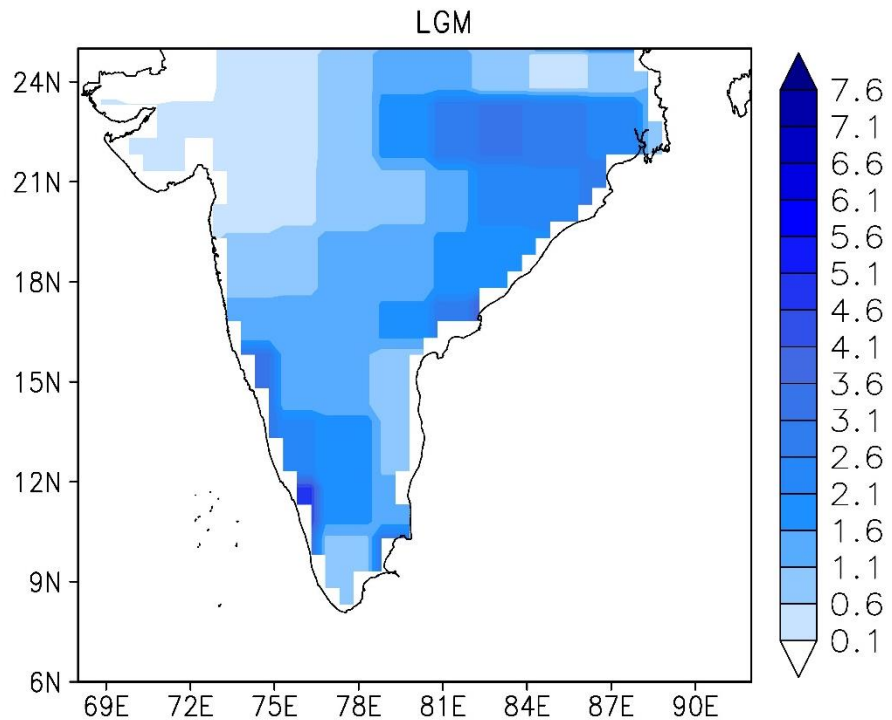


Figure S1. Annual mean precipitation (mm/day) over peninsular India during LGM (20-23 ka) using MPI-ESM1-2-LR model.

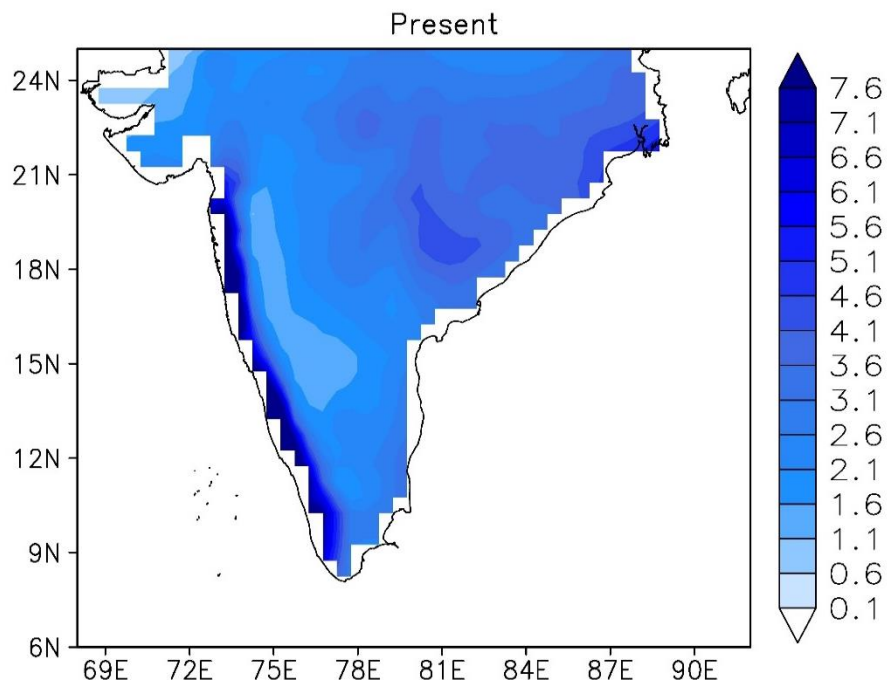


Figure S2. Annual mean precipitation (mm/day) over peninsular India during present time (1980-2010) using CRU observations.

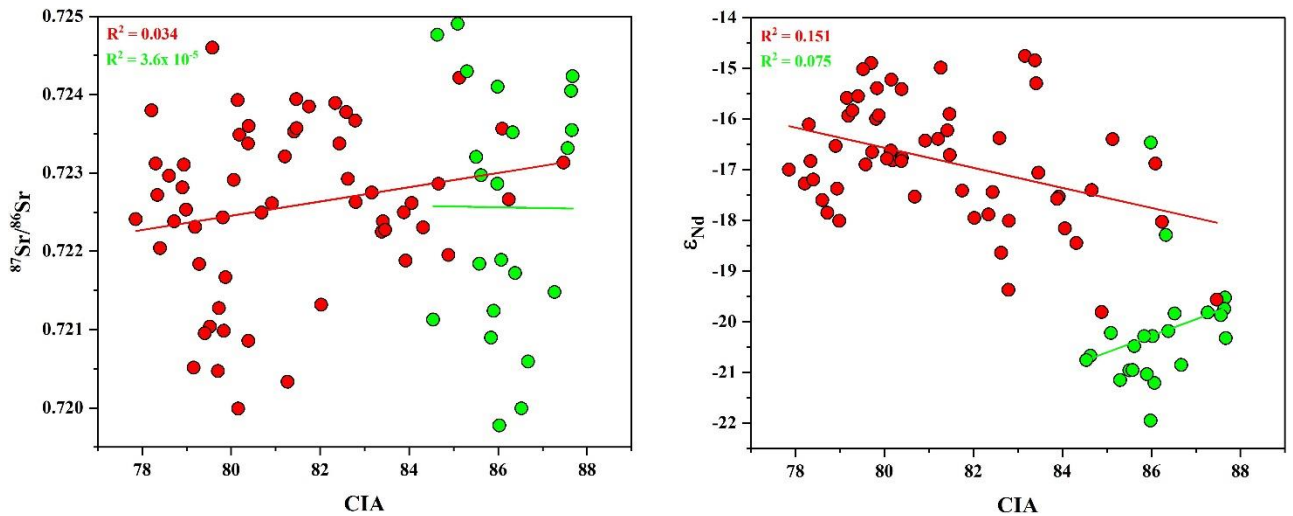


Figure S3. Scatter plots of $^{87}\text{Sr}/^{86}\text{Sr}$ and ϵ_{Nd} with CIA.

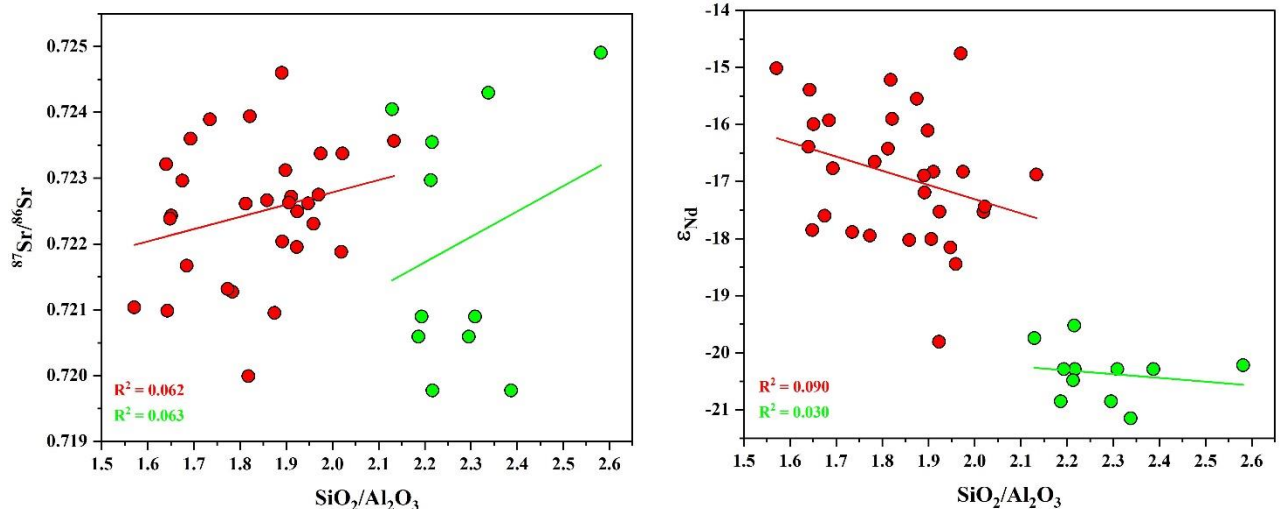


Figure S4. Scatter plots of $^{87}\text{Sr}/^{86}\text{Sr}$ and ϵ_{Nd} with $\text{SiO}_2/\text{Al}_2\text{O}_3$

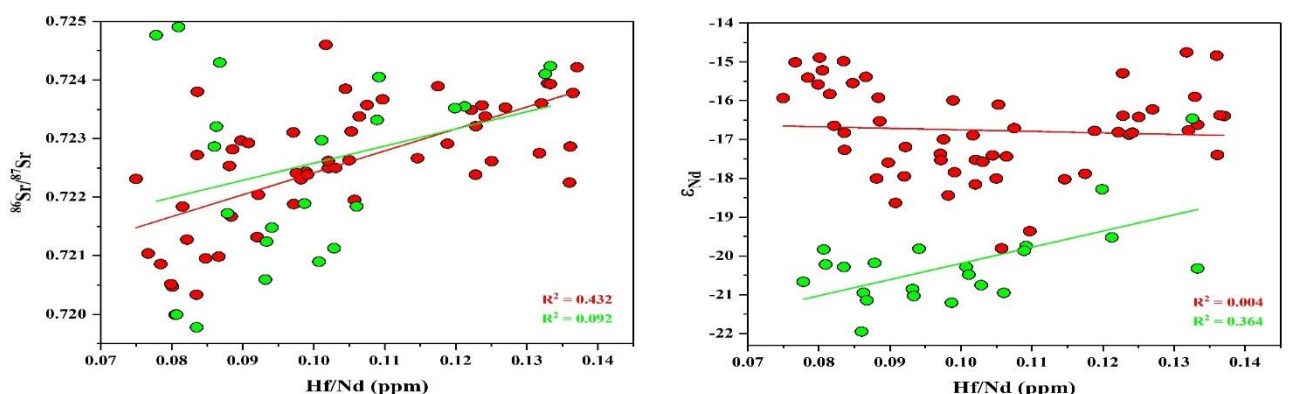


Figure S5. Scatter plots of $^{87}\text{Sr}/^{86}\text{Sr}$ and ϵ_{Nd} with Hf/Nd

*Green circles represent samples from the Holocene time and rest of the sample of GC03 core are represented by the red circles in the all the above plots.

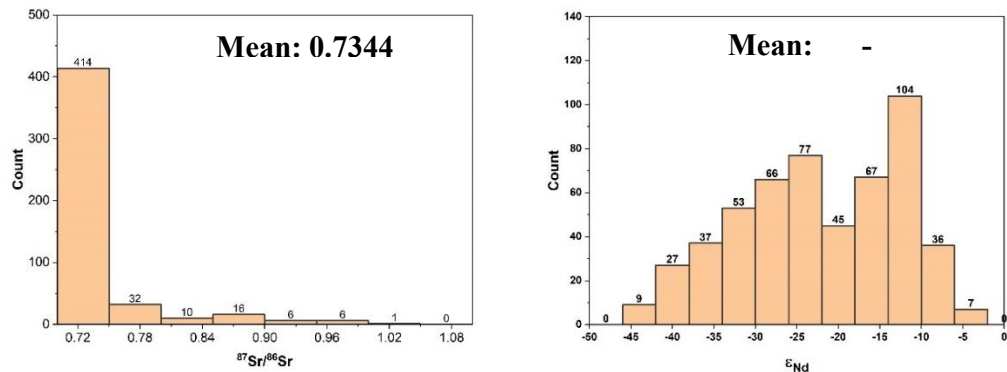


Figure S6: Histogram of $^{87}\text{Sr}/^{86}\text{Sr}$ and ϵ_{Nd} for PGC end member.

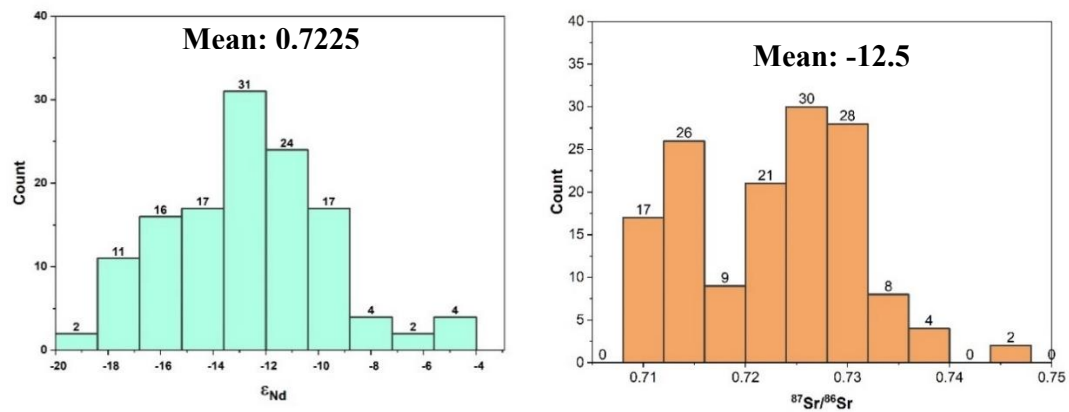


Figure S7: Histogram of $^{87}\text{Sr}/^{86}\text{Sr}$ and ϵ_{Nd} for dust end member.

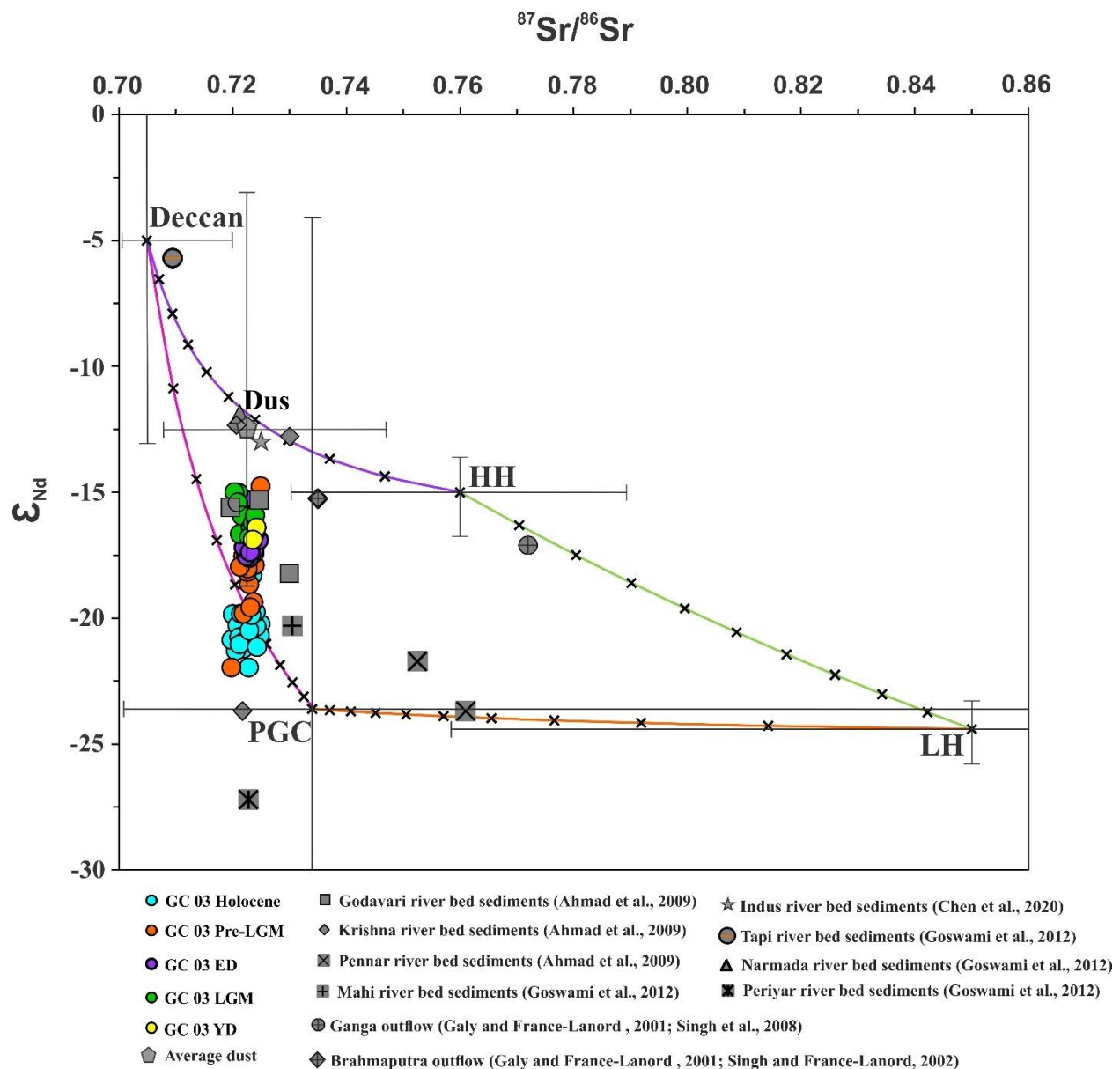


Figure S8: Binary mixing plot of the sediments of SSD004-GC 03 core with the potential endmembers, such as the Deccan, PGC, LH, HH, and the aeolian dust. Sr-Nd isotope composition of river sediments at their outflow is also incorporated in the mixing plot. Error for end members have been considered the full range of literature values.

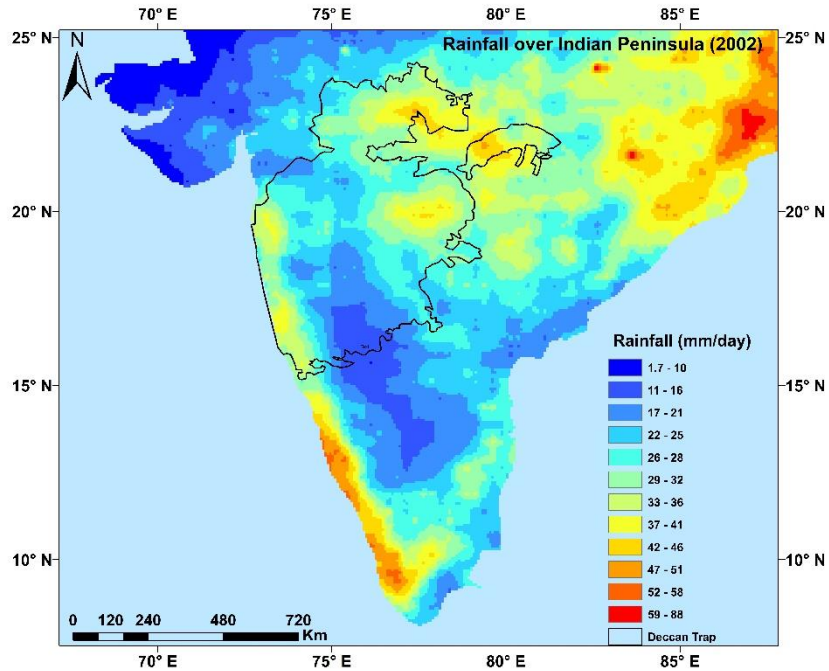


Figure S9: Rainfall distribution over the Indian peninsula during the drought year 2002. The map has been created in Q GIS 3.24 environment (WGS84).

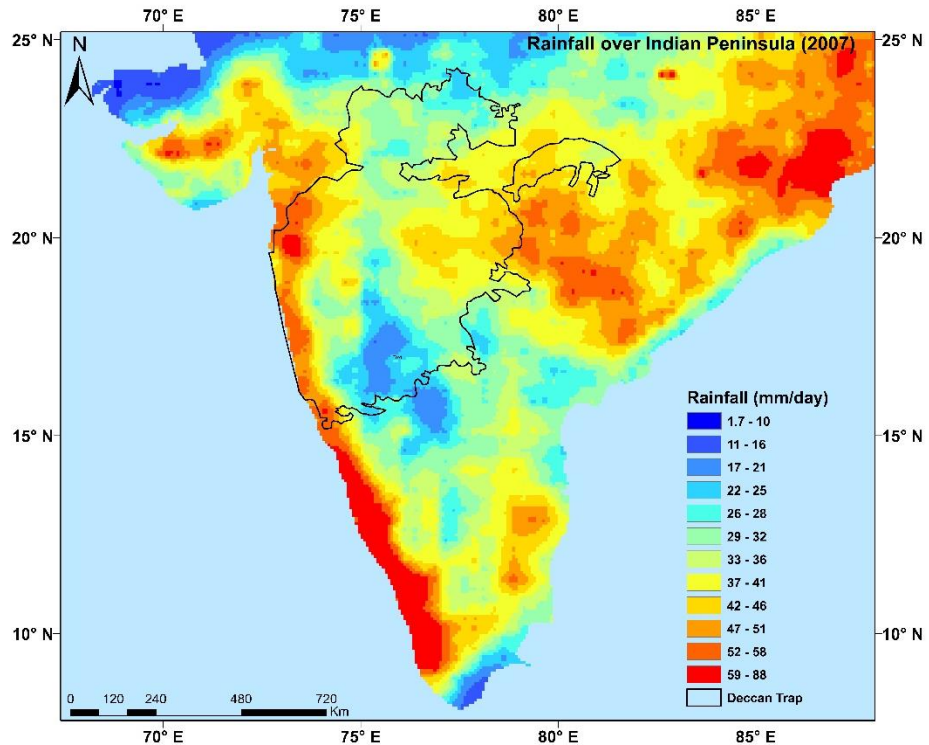


Figure S10: Rainfall distribution over the Indian peninsula during the high rainfall year 2007. The map has been created in Q GIS 3.24 environment (WGS84).

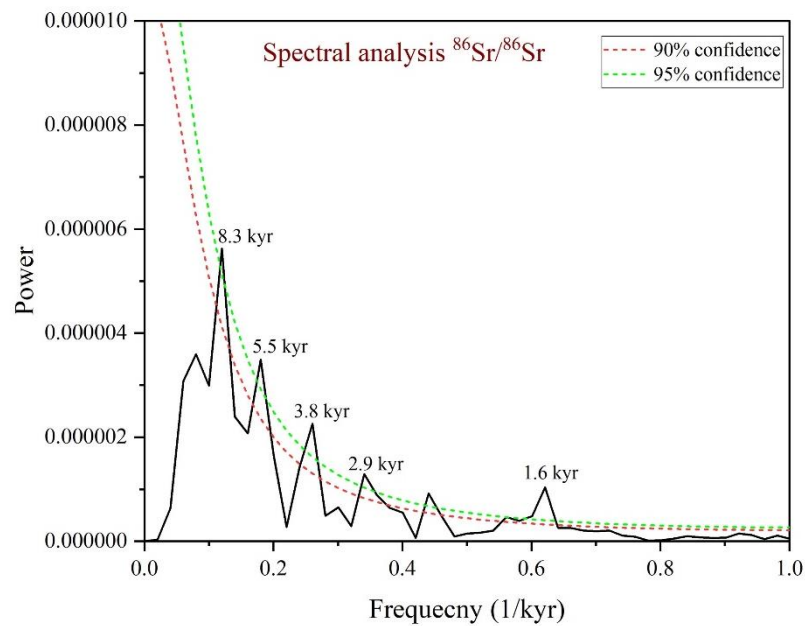


Figure S11: Spectral analysis of $^{87}\text{Sr}/^{86}\text{Sr}$ data for the SSD004-GC03 core (~38 kyr) showing most significant periodicities at 8.3 kyr, 5.5 kyr, 3.8 kyr, 2.9 kyr, and 1.6 kyr. Spectral analysis was done using PAST 4.03 software (Hammer et al., 2001).

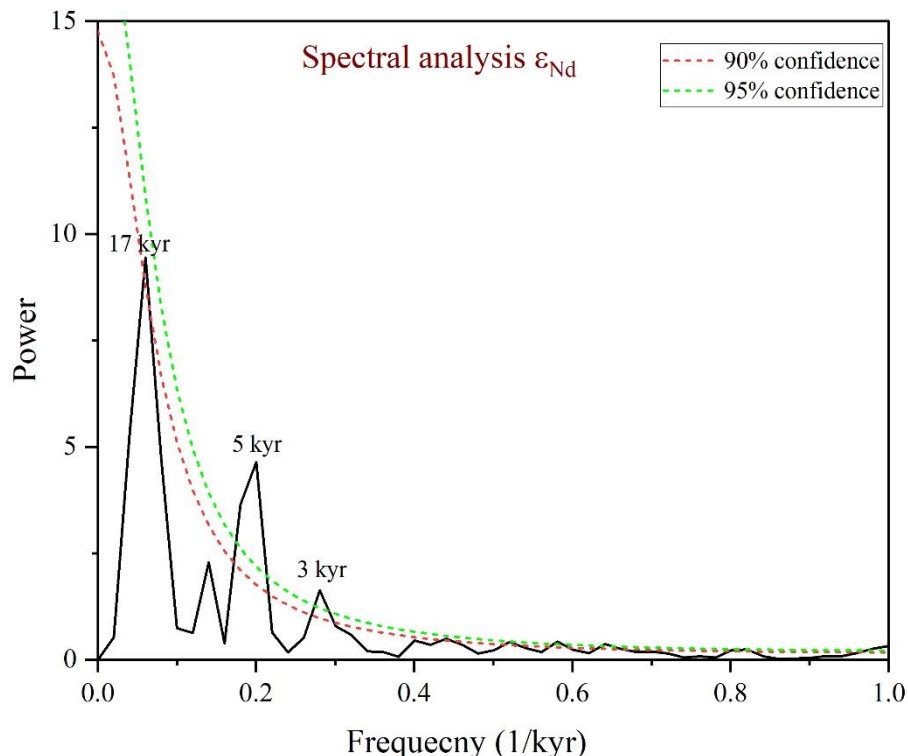


Figure S12: Spectral analysis of $^{143}\text{Nd}/^{144}\text{Nd}$ data for the SSD004-GC03 core (~38 kyr) showing most significant periodicities at 17 kyr, 5 kyr and 3 kyr. Spectral analysis was done using PAST 4.03 software (Hammer et al., 2001).

Supplementary Table

Table 1: End members characterisation of potential sources used in binary mixing plot.

End Member	$^{87}\text{Sr}/^{86}\text{Sr}$	Sr ($\mu\text{g/g}$)	ϵ_{Nd}	Nd ($\mu\text{g/g}$)	Reference
Deccan	0.705	228	-5.0	11	(Singh et al., 2008)
Higher Himalaya	0.760	80	-15.0	18	(Singh et al., 2008)
Lower Himalaya	0.850	94	-24.4	26	(Singh et al., 2008)
Peninsular Gneissic Complexes (PGC)	0.734	378	-23.6	46	Data used for the characterizing this end member have been tabulated in Table S2 and referenced are attached
North African Dust	0.720	327	-12.5	34	(Ayalew et al., 2018; Zhao et al., 2018)

Table 2: $^{87}\text{Sr}/^{86}\text{Sr}$ and ϵ_{Nd} data used for preparation of map and fixing end member of the PGC.

Sr. No.	Latitude	Longitude	$^{87}\text{Sr}/^{86}\text{Sr}$	Reference	Latitude	Longitude	ϵ_{Nd}	Reference
1	21.0	82.8	0.7120	GEOROC	21.0	82.8	-15.7	GEOROC
2	21.0	82.8	0.7110	GEOROC	21.0	82.8	-15.9	GEOROC
3	21.0	82.8	0.7120	GEOROC	21.0	82.8	-16.2	GEOROC
4	21.0	82.8	0.7110	GEOROC	21.0	82.8	-15.9	GEOROC
5	21.0	82.8	0.7140	GEOROC	21.0	82.8	-15.8	GEOROC
6	21.0	82.8	0.7110	GEOROC	21.0	82.8	-14.7	GEOROC
7	21.0	82.8	0.7110	GEOROC	21.0	82.8	-15.6	GEOROC
8	21.0	80.0	0.9130	GEOROC	20.4	81.1	-15.4	GEOROC
9	21.0	80.0	1.0680	GEOROC	20.3	81.2	-6.8	GEOROC
10	21.0	80.0	1.1430	GEOROC	20.3	81.2	-10.8	GEOROC
11	21.0	80.0	1.2200	GEOROC	20.4	81.1	-3.8	GEOROC
12	21.0	80.0	1.4170	GEOROC	20.5	81.1	-4.2	GEOROC
13	21.0	80.0	1.6390	GEOROC	21.2	80.6	-19.7	GEOROC
14	21.0	80.0	0.7330	GEOROC	21.2	80.6	-20.2	GEOROC
15	21.0	80.0	0.7380	GEOROC	21.2	80.6	-20.7	GEOROC
16	21.0	80.0	0.7510	GEOROC	21.2	80.6	-20.5	GEOROC
17	21.0	80.0	0.7650	GEOROC	21.2	80.6	-21.8	GEOROC
18	21.0	80.0	0.7760	GEOROC	21.2	80.6	-21.8	GEOROC
19	21.0	80.0	0.7920	GEOROC	21.2	80.6	-22.0	GEOROC

20	18.0	81.0	0.8050	GEOROC	21.1	80.5	-12.3	GEOROC
21	18.0	81.0	0.8900	GEOROC	21.1	80.5	-11.9	GEOROC
22	18.0	81.0	0.9270	GEOROC	21.1	80.5	-11.5	GEOROC
23	18.0	81.0	1.0540	GEOROC	21.1	80.5	-12.3	GEOROC
24	18.0	81.0	1.1590	GEOROC	21.1	80.5	-12.6	GEOROC
25	20.4	81.1	0.7150	GEOROC	21.1	80.5	-12.0	GEOROC
26	20.3	81.2	0.7130	GEOROC	21.1	80.5	-9.5	GEOROC
27	20.3	81.2	0.7220	GEOROC	21.1	80.5	-9.6	GEOROC
28	20.4	81.1	0.7170	GEOROC	21.1	80.5	-9.4	GEOROC
29	20.5	81.1	0.7160	GEOROC	21.1	80.5	-9.7	GEOROC
30	20.5	81.4	0.7470	GEOROC	21.1	80.5	-9.6	GEOROC
31	20.3	81.1	0.7480	GEOROC	21.8	80.5	-23.5	GEOROC
32	20.3	81.2	0.7210	GEOROC	21.8	80.5	-23.5	GEOROC
33	20.3	81.2	0.7260	GEOROC	21.8	80.5	-24.3	GEOROC
34	21.5	82.6	0.7290	GEOROC	21.8	80.5	-23.5	GEOROC
35	21.4	82.6	0.7150	GEOROC	21.8	80.5	-24.2	GEOROC
36	21.5	82.6	0.7180	GEOROC	21.4	80.7	-19.2	GEOROC
37	21.5	82.5	0.7100	GEOROC	21.4	80.7	-16.2	GEOROC
38	21.4	82.7	0.7150	GEOROC	21.4	80.7	-19.2	GEOROC
39	21.4	82.6	0.7190	GEOROC	21.4	80.7	-17.5	GEOROC
40	20.4	81.1	0.7390	GEOROC	21.4	80.7	-17.7	GEOROC
41	20.4	81.1	0.7490	GEOROC	21.4	80.7	-16.1	GEOROC
42	20.4	81.1	0.7460	GEOROC	21.4	80.7	-17.4	GEOROC
43	20.4	81.1	0.7330	GEOROC	21.4	80.7	-17.6	GEOROC
44	20.3	81.1	0.7380	GEOROC	21.4	80.7	-18.8	GEOROC
45	20.9	79.5	0.7120	GEOROC	21.8	80.5	-22.2	GEOROC
46	20.8	80.0	0.7080	GEOROC	20.5	81.4	-31.6	GEOROC
47	20.8	80.0	0.7100	GEOROC	20.3	81.1	-17.6	GEOROC
48	20.8	80.0	0.7070	GEOROC	20.3	81.2	-12.1	GEOROC
49	20.9	79.5	0.8260	GEOROC	20.3	81.2	-18.9	GEOROC
50	20.9	79.5	0.8460	GEOROC	21.5	82.6	-12.8	GEOROC
51	20.9	79.5	0.9140	GEOROC	21.4	82.6	-9.9	GEOROC
52	20.9	79.5	0.8290	GEOROC	21.5	82.6	-22.2	GEOROC
53	18.7	81.8	0.7190	GEOROC	21.5	82.5	2.8	GEOROC
54	18.7	81.8	0.7220	GEOROC	21.4	82.7	-8.4	GEOROC
55	18.7	81.8	0.7210	GEOROC	21.4	82.6	-10.0	GEOROC
56	18.7	81.8	0.7280	GEOROC	20.4	81.1	-16.7	GEOROC
57	18.7	81.8	0.7380	GEOROC	20.4	81.1	-19.3	GEOROC
58	18.7	81.8	0.7260	GEOROC	20.4	81.1	-20.2	GEOROC
59	18.7	81.8	0.7200	GEOROC	20.4	81.1	-9.7	GEOROC
60	24.5	83.0	0.7150	GEOROC	20.3	81.1	-18.4	GEOROC
61	24.5	83.0	0.7210	GEOROC	20.9	79.5	-6.5	GEOROC
62	24.5	83.0	0.7240	GEOROC	20.8	80.0	-3.2	GEOROC
63	24.5	83.0	0.7270	GEOROC	20.8	80.0	-7.6	GEOROC

64	24.5	83.0	0.7270	GEOROC	20.8	80.0	-3.8	GEOROC
65	24.5	83.0	0.7340	GEOROC	20.9	79.5	-19.4	GEOROC
66	20.2	82.2	0.7080	GEOROC	20.9	79.5	-20.0	GEOROC
67	20.2	82.2	0.7110	GEOROC	20.9	79.5	-13.8	GEOROC
68	20.2	82.2	0.7080	GEOROC	20.9	79.5	-16.2	GEOROC
69	20.2	82.2	0.7090	GEOROC	18.7	81.8	-6.2	GEOROC
70	20.2	82.2	0.7090	GEOROC	18.7	81.8	-8.1	GEOROC
71	20.2	82.2	0.7090	GEOROC	18.7	81.8	-5.9	GEOROC
72	20.2	82.2	0.7080	GEOROC	18.7	81.8	-8.9	GEOROC
73	20.2	82.2	0.7080	GEOROC	18.7	81.8	-8.1	GEOROC
74	24.8	72.8	0.7060	GEOROC	18.7	81.8	-7.4	GEOROC
75	24.8	72.8	0.7150	GEOROC	18.7	81.8	-7.1	GEOROC
76	24.8	72.8	0.7340	GEOROC	24.5	82.5	-12.5	GEOROC
77	24.8	72.8	0.7080	GEOROC	24.5	82.5	-11.5	GEOROC
78	24.8	72.8	0.8170	GEOROC	24.5	82.5	-13.9	GEOROC
79	24.8	72.8	0.8420	GEOROC	24.5	82.5	-11.8	GEOROC
80	24.8	72.8	0.8150	GEOROC	24.5	82.5	-14.7	GEOROC
81	24.8	72.8	0.8580	GEOROC	24.5	82.5	-12.6	GEOROC
82	24.9	73.8	0.7960	GEOROC	24.5	82.5	-13.3	GEOROC
83	25.8	73.5	0.7420	GEOROC	24.5	82.5	-14.6	GEOROC
84	25.8	73.5	0.7380	GEOROC	24.5	82.5	-15.0	GEOROC
85	25.8	73.5	0.7210	GEOROC	24.5	82.5	-15.4	GEOROC
86	25.8	73.5	0.7360	GEOROC	20.2	82.2	-6.4	GEOROC
87	24.8	72.8	0.8790	GEOROC	20.2	82.2	-10.5	GEOROC
88	24.8	72.8	0.9760	GEOROC	20.2	82.2	-6.4	GEOROC
89	24.8	72.8	0.8370	GEOROC	20.2	82.2	-6.3	GEOROC
90	24.8	72.8	0.7700	GEOROC	20.2	82.2	-6.7	GEOROC
91	25.0	73.5	0.7720	GEOROC	20.2	82.2	-7.3	GEOROC
92	25.0	73.5	0.8310	GEOROC	20.2	82.2	-6.4	GEOROC
93	25.0	73.5	0.7710	GEOROC	20.2	82.2	-6.1	GEOROC
94	25.0	73.0	1.1380	GEOROC	24.9	73.8	-19.3	GEOROC
95	25.0	73.0	1.1120	GEOROC	24.9	73.8	-16.5	GEOROC
96	25.0	73.0	0.8910	GEOROC	24.9	73.8	-19.5	GEOROC
97	24.6	74.1	0.7020	GEOROC	24.9	73.8	-22.4	GEOROC
98	24.6	74.1	0.7020	GEOROC	24.9	73.8	-28.1	GEOROC
99	24.6	74.1	0.7020	GEOROC	24.9	73.8	-18.7	GEOROC
100	24.6	74.1	0.7020	GEOROC	24.9	73.8	-2.4	GEOROC
101	24.6	74.1	0.7020	GEOROC	24.9	73.8	-8.2	GEOROC
102	24.6	74.1	0.7020	GEOROC	24.9	73.8	-24.6	GEOROC
103	24.6	74.1	0.7030	GEOROC	24.9	73.8	-25.9	GEOROC
104	24.6	74.1	0.7030	GEOROC	24.9	73.8	-19.9	GEOROC
105	24.6	74.1	0.7030	GEOROC	24.9	73.8	-21.2	GEOROC
106	24.6	74.1	0.7030	GEOROC	24.9	73.8	-12.0	GEOROC
107	24.6	74.1	0.7020	GEOROC	24.9	73.8	-20.8	GEOROC

108	24.6	74.1	0.7020	GEOROC	24.9	73.8	-24.0	GEOROC
109	24.6	74.1	0.7020	GEOROC	24.8	72.8	-3.5	GEOROC
110	24.6	74.1	0.7030	GEOROC	24.8	72.8	-4.2	GEOROC
111	24.6	74.1	0.7030	GEOROC	24.8	72.8	-6.1	GEOROC
112	24.6	74.1	0.7020	GEOROC	24.8	72.8	-7.1	GEOROC
113	24.6	74.1	0.7020	GEOROC	24.8	72.8	-10.6	GEOROC
114	24.6	74.1	0.7020	GEOROC	24.8	72.8	-11.0	GEOROC
115	24.6	74.1	0.7020	GEOROC	24.8	72.8	-7.8	GEOROC
116	24.6	74.1	0.7020	GEOROC	24.8	72.8	-8.9	GEOROC
117	19.0	72.9	0.7280	GEOROC	24.9	73.8	-10.0	GEOROC
118	19.0	72.9	0.7800	GEOROC	25.8	73.5	-15.1	GEOROC
119	19.0	72.9	0.7070	GEOROC	25.8	73.5	-14.6	GEOROC
120	22.0	74.1	0.7080	GEOROC	25.8	73.5	-14.3	GEOROC
121	22.0	74.1	0.7090	GEOROC	25.8	73.5	-14.0	GEOROC
122	22.0	74.1	0.7060	GEOROC	24.8	72.8	1.2	GEOROC
123	22.0	74.1	0.7060	GEOROC	24.8	72.8	-0.6	GEOROC
124	22.0	74.1	0.7060	GEOROC	24.8	72.8	6.8	GEOROC
125	22.0	74.1	0.7060	GEOROC	24.8	72.8	1.9	GEOROC
126	22.0	74.1	0.7060	GEOROC	25.0	73.5	-4.9	GEOROC
127	22.0	74.1	0.7060	GEOROC	25.0	73.5	-7.9	GEOROC
128	22.0	74.1	0.7220	GEOROC	25.0	73.5	-6.1	GEOROC
129	22.0	74.1	0.7080	GEOROC	25.0	73.0	-9.3	GEOROC
130	22.0	74.1	0.7100	GEOROC	25.0	73.0	-9.8	GEOROC
131	22.0	74.1	0.7090	GEOROC	25.0	73.0	-8.9	GEOROC
132	22.0	74.1	0.7080	GEOROC	26.0	73.0	-5.0	GEOROC
133	22.0	74.1	0.7110	GEOROC	26.0	73.0	-4.8	GEOROC
134	22.0	74.1	0.7060	GEOROC	24.6	74.1	-20.9	GEOROC
135	22.0	74.1	0.7070	GEOROC	24.6	74.1	-25.4	GEOROC
136	22.0	74.1	0.7060	GEOROC	24.6	74.1	-23.4	GEOROC
137	22.0	74.1	0.7060	GEOROC	24.6	74.1	-24.0	GEOROC
138	22.0	74.1	0.7080	GEOROC	24.6	74.1	-11.0	GEOROC
139	22.0	74.1	0.7080	GEOROC	24.6	74.1	-14.6	GEOROC
140	22.1	77.9	0.7060	GEOROC	24.6	74.1	-16.3	GEOROC
141	22.1	77.9	0.7070	GEOROC	24.6	74.1	-22.4	GEOROC
142	22.1	77.9	0.7070	GEOROC	24.6	74.1	-21.3	GEOROC
143	22.1	77.9	0.7110	GEOROC	24.6	74.1	-21.9	GEOROC
144	22.1	77.9	0.7110	GEOROC	24.6	74.1	-22.6	GEOROC
145	22.1	77.9	0.7100	GEOROC	24.6	74.1	-22.3	GEOROC
146	22.1	77.9	0.7100	GEOROC	24.6	74.1	-21.6	GEOROC
147	22.1	77.9	0.7130	GEOROC	24.6	74.1	-16.2	GEOROC
148	22.1	77.9	0.7110	GEOROC	24.6	74.1	-11.5	GEOROC
149	22.1	77.9	0.7100	GEOROC	24.6	74.1	-19.5	GEOROC
150	18.3	72.9	0.7040	GEOROC	25.8	73.5	-6.4	GEOROC
151	18.3	72.9	0.7040	GEOROC	25.8	73.5	-9.1	GEOROC

152	18.3	72.9	0.7040	GEOROC	25.8	73.5	-5.5	GEOROC
153	18.3	72.9	0.7050	GEOROC	25.8	73.5	0.3	GEOROC
154	18.3	72.9	0.7050	GEOROC	25.8	73.5	0.9	GEOROC
155	18.3	72.9	0.7050	GEOROC	25.8	73.5	3.0	GEOROC
156	18.3	72.9	0.7050	GEOROC	25.8	73.5	2.4	GEOROC
157	18.3	72.9	0.7090	GEOROC	25.8	73.5	2.7	GEOROC
158	18.3	72.9	0.7060	GEOROC	24.8	72.8	-4.0	GEOROC
159	22.0	74.1	0.7060	GEOROC	24.8	72.8	-2.1	GEOROC
160	22.0	74.1	0.7060	GEOROC	24.8	72.8	-5.1	GEOROC
161	22.0	74.1	0.7060	GEOROC	24.8	72.8	-3.7	GEOROC
162	22.0	74.1	0.7060	GEOROC	24.8	72.8	-6.3	GEOROC
163	22.0	74.1	0.7060	GEOROC	24.8	72.8	-1.6	GEOROC
164	22.0	74.1	0.7060	GEOROC	25.8	73.5	0.3	GEOROC
165	22.0	74.1	0.7060	GEOROC	25.8	73.5	-0.2	GEOROC
166	22.0	74.1	0.7060	GEOROC	24.9	73.8	-18.5	GEOROC
167	22.0	74.1	0.7060	GEOROC	25.2	78.5	1.0	GEOROC
168	22.0	74.1	0.7060	GEOROC	25.2	78.5	3.9	GEOROC
169	22.0	74.1	0.7060	GEOROC	25.2	78.5	-4.4	GEOROC
170	22.0	74.1	0.7070	GEOROC	25.2	78.5	-7.9	GEOROC
171	22.0	74.1	0.7060	GEOROC	25.2	78.5	-23.3	GEOROC
172	22.0	74.1	0.7070	GEOROC	25.2	78.5	-9.8	GEOROC
173	22.0	74.1	0.7060	GEOROC	25.2	79.2	-1.2	GEOROC
174	22.0	74.1	0.7060	GEOROC	25.2	79.2	-5.2	GEOROC
175	22.0	74.1	0.7060	GEOROC	25.2	79.2	-2.0	GEOROC
176	22.0	74.1	0.7060	GEOROC	25.2	79.2	-2.5	GEOROC
177	22.0	74.1	0.7060	GEOROC	25.2	79.2	-1.2	GEOROC
178	22.0	74.1	0.7060	GEOROC	25.4	78.6	-29.1	GEOROC
179	22.0	74.1	0.7060	GEOROC	25.4	78.6	-26.7	GEOROC
180	22.0	74.1	0.7060	GEOROC	25.4	78.9	-33.5	GEOROC
181	22.0	74.1	0.7060	GEOROC	19.0	72.9	0.6	GEOROC
182	22.0	74.1	0.7060	GEOROC	19.0	72.9	-4.3	GEOROC
183	22.0	74.1	0.7060	GEOROC	22.0	74.1	-6.1	GEOROC
184	22.0	74.1	0.7070	GEOROC	22.0	74.1	-2.8	GEOROC
185	22.0	74.1	0.7060	GEOROC	22.0	74.1	-3.2	GEOROC
186	22.0	74.1	0.7060	GEOROC	22.0	74.1	-2.3	GEOROC
187	22.0	74.1	0.7070	GEOROC	22.0	74.1	-3.1	GEOROC
188	22.0	74.1	0.7060	GEOROC	22.0	74.1	-5.0	GEOROC
189	22.0	74.1	0.7060	GEOROC	22.0	74.1	-5.0	GEOROC
190	22.0	74.1	0.7060	GEOROC	22.0	74.1	-2.9	GEOROC
191	22.0	74.1	0.7060	GEOROC	22.0	74.1	-4.5	GEOROC
192	22.0	74.1	0.7060	GEOROC	22.0	74.1	-4.6	GEOROC
193	22.0	74.1	0.7080	GEOROC	22.0	74.1	-8.5	GEOROC
194	22.0	74.1	0.7060	GEOROC	22.0	74.1	-3.8	GEOROC
195	22.0	74.1	0.7070	GEOROC	22.0	74.1	-6.4	GEOROC

196	22.0	74.1	0.7060	GEOROC	22.0	74.1	-14.1	GEOROC
197	22.0	74.1	0.7060	GEOROC	22.0	74.1	-5.1	GEOROC
198	22.0	74.1	0.7090	GEOROC	22.0	74.1	-10.8	GEOROC
199	22.0	74.1	0.7090	GEOROC	22.0	74.1	0.4	GEOROC
200	22.0	74.1	0.7060	GEOROC	22.0	74.1	-8.8	GEOROC
201	22.0	74.1	0.7060	GEOROC	22.0	74.1	0.3	GEOROC
202	22.0	74.1	0.7070	GEOROC	22.1	77.9	-3.6	GEOROC
203	22.0	74.1	0.7070	GEOROC	22.1	77.9	-0.3	GEOROC
204	22.0	74.1	0.7080	GEOROC	22.1	77.9	-2.6	GEOROC
205	22.0	74.1	0.7050	GEOROC	22.1	77.9	-10.1	GEOROC
206	22.0	74.1	0.7100	GEOROC	22.1	77.9	-25.1	GEOROC
207	22.0	74.1	0.7110	GEOROC	22.1	77.9	-8.9	GEOROC
208	22.0	74.1	0.7110	GEOROC	22.1	77.9	-8.8	GEOROC
209	22.0	74.1	0.7110	GEOROC	22.1	77.9	-9.5	GEOROC
210	22.0	74.0	0.7070	GEOROC	22.1	77.9	-15.0	GEOROC
211	22.0	74.0	0.7080	GEOROC	22.1	77.9	-16.7	GEOROC
212	22.0	74.0	0.7070	GEOROC	18.3	72.9	3.4	GEOROC
213	22.0	74.0	0.7070	GEOROC	18.3	72.9	3.0	GEOROC
214	22.0	74.0	0.7080	GEOROC	18.3	72.9	-17.3	GEOROC
215	22.1	74.1	0.7060	GEOROC	18.3	72.9	-15.4	GEOROC
216	22.1	74.1	0.7060	GEOROC	18.3	72.9	-16.5	GEOROC
217	22.1	74.1	0.7060	GEOROC	18.3	72.9	-13.2	GEOROC
218	22.8	74.1	0.7070	GEOROC	22.0	74.1	-4.9	GEOROC
219	22.8	74.1	0.7070	GEOROC	22.0	74.1	-6.0	GEOROC
220	22.3	74.0	0.7080	GEOROC	22.0	74.1	-5.9	GEOROC
221	22.3	74.0	0.7070	GEOROC	22.0	74.1	-2.8	GEOROC
222	22.3	74.0	0.7070	GEOROC	22.0	74.1	-2.7	GEOROC
223	22.3	74.0	0.7110	GEOROC	22.0	74.1	-2.5	GEOROC
224	22.2	73.9	0.7070	GEOROC	22.0	74.1	-3.7	GEOROC
225	22.2	73.9	0.7070	GEOROC	22.0	74.1	-2.4	GEOROC
226	22.1	73.8	0.7080	GEOROC	22.0	74.1	-2.8	GEOROC
227	22.1	73.8	0.7070	GEOROC	22.0	74.1	-4.7	GEOROC
228	22.0	74.0	0.7070	GEOROC	22.0	74.1	-4.1	GEOROC
229	22.3	74.0	0.7080	GEOROC	22.0	74.1	-4.8	GEOROC
230	22.4	74.2	0.7080	GEOROC	22.0	74.1	-3.9	GEOROC
231	22.4	74.2	0.7080	GEOROC	22.0	74.1	-2.4	GEOROC
232	21.8	69.8	0.7100	GEOROC	22.0	74.1	-2.9	GEOROC
233	21.8	69.8	0.7110	GEOROC	22.0	74.1	-2.5	GEOROC
234	21.8	69.8	0.7080	GEOROC	22.0	74.1	-2.2	GEOROC
235	21.8	69.8	0.7110	GEOROC	22.0	74.1	-2.6	GEOROC
236	21.8	69.8	0.7100	GEOROC	22.0	74.1	-4.5	GEOROC
237	21.8	70.0	0.7130	GEOROC	22.0	74.1	-2.5	GEOROC
238	21.8	70.0	0.7110	GEOROC	22.0	74.1	-2.4	GEOROC
239	21.8	70.0	0.7090	GEOROC	22.0	74.1	-4.7	GEOROC

240	21.8	70.0	0.7070	GEOROC	22.0	74.1	-3.7	GEOROC
241	21.8	70.0	0.7080	GEOROC	22.0	74.1	-2.9	GEOROC
242	17.3	73.5	0.7040	GEOROC	22.0	74.1	-2.4	GEOROC
243	17.3	73.5	0.7040	GEOROC	22.0	74.1	-3.8	GEOROC
244	18.9	72.3	0.7060	GEOROC	22.0	74.1	-3.0	GEOROC
245	18.9	73.1	0.7090	GEOROC	22.0	74.1	-3.0	GEOROC
246	18.9	73.1	0.7130	GEOROC	22.0	74.1	-3.3	GEOROC
247	18.6	73.5	0.7040	GEOROC	22.0	74.1	-1.9	GEOROC
248	21.5	70.5	0.7060	GEOROC	22.0	74.1	-2.7	GEOROC
249	21.5	70.6	0.7070	GEOROC	22.0	74.1	-2.6	GEOROC
250	21.5	70.6	0.7060	GEOROC	22.0	74.1	-3.1	GEOROC
251	21.5	70.5	0.7060	GEOROC	22.0	74.1	-3.0	GEOROC
252	21.5	70.6	0.7070	GEOROC	22.0	74.1	-6.1	GEOROC
253	21.5	70.5	0.7360	GEOROC	22.0	74.1	-6.5	GEOROC
254	21.5	70.5	0.7100	GEOROC	22.0	74.1	-3.2	GEOROC
255	21.2	72.1	0.7140	GEOROC	22.0	74.1	1.3	GEOROC
256	21.2	72.1	0.7460	GEOROC	22.0	74.1	0.3	GEOROC
257	21.2	72.1	0.7070	GEOROC	22.0	74.1	-3.9	GEOROC
258	21.2	72.1	0.7630	GEOROC	22.0	74.1	-1.2	GEOROC
259	21.2	72.1	0.7110	GEOROC	22.0	74.1	-19.4	GEOROC
260	21.2	72.1	0.7310	GEOROC	22.0	74.1	-16.4	GEOROC
261	21.2	72.1	0.7230	GEOROC	22.0	74.0	-2.5	GEOROC
262	21.2	72.1	0.7200	GEOROC	22.0	74.0	-5.5	GEOROC
263	21.2	72.1	0.7180	GEOROC	22.0	74.0	-3.5	GEOROC
264	21.2	72.1	0.7440	GEOROC	22.0	74.0	-2.7	GEOROC
265	19.7	73.6	0.7130	GEOROC	22.0	74.0	1.4	GEOROC
266	16.0	74.2	0.7040	GEOROC	22.1	74.1	-5.8	GEOROC
267	17.4	73.8	0.7110	GEOROC	22.1	74.1	0.4	GEOROC
268	17.4	73.8	0.7120	GEOROC	22.1	74.1	-2.2	GEOROC
269	17.4	73.8	0.7100	GEOROC	22.8	74.1	-9.4	GEOROC
270	23.6	87.1	0.7060	GEOROC	22.8	74.1	-5.7	GEOROC
271	23.6	87.1	0.7070	GEOROC	22.3	74.0	-4.6	GEOROC
272	23.6	87.1	0.7060	GEOROC	22.3	74.0	-3.0	GEOROC
273	23.6	87.1	0.7060	GEOROC	22.3	74.0	-3.8	GEOROC
274	23.6	87.1	0.7060	GEOROC	22.2	73.9	-4.4	GEOROC
275	23.6	87.1	0.7060	GEOROC	22.2	73.9	-4.5	GEOROC
276	21.5	70.5	0.7100	GEOROC	22.1	73.8	-4.9	GEOROC
277	21.5	70.5	0.7070	GEOROC	22.1	73.8	-3.0	GEOROC
278	21.5	70.5	0.7070	GEOROC	22.0	74.0	-5.4	GEOROC
279	21.5	70.5	0.7070	GEOROC	22.4	74.2	-5.2	GEOROC
280	21.5	70.5	0.7070	GEOROC	22.4	74.2	-4.7	GEOROC
281	20.0	73.0	0.7050	GEOROC	21.8	69.8	-0.5	GEOROC
282	20.0	73.0	0.7050	GEOROC	21.8	69.8	0.7	GEOROC
283	22.0	71.5	0.7050	GEOROC	21.8	69.8	-30.7	GEOROC

284	20.0	76.5	0.7060	GEOROC	21.8	69.8	0.4	GEOROC
285	20.0	76.5	0.7060	GEOROC	21.8	69.8	0.0	GEOROC
286	20.0	76.5	0.7060	GEOROC	21.8	69.8	0.6	GEOROC
287	20.0	76.5	0.7060	GEOROC	21.8	69.8	-0.2	GEOROC
288	20.0	76.5	0.7070	GEOROC	21.8	70.0	1.3	GEOROC
289	20.0	76.5	0.7080	GEOROC	21.8	70.0	-1.9	GEOROC
290	20.0	76.5	0.7080	GEOROC	21.8	70.0	-1.5	GEOROC
291	20.0	76.5	0.7080	GEOROC	21.8	70.0	-1.3	GEOROC
292	20.0	76.5	0.7070	GEOROC	21.8	70.0	-1.3	GEOROC
293	23.0	71.0	0.7040	GEOROC	21.5	70.5	2.4	GEOROC
294	23.0	71.0	0.7040	GEOROC	21.5	70.6	0.4	GEOROC
295	23.0	71.0	0.7040	GEOROC	21.5	70.6	2.3	GEOROC
296	23.0	71.0	0.7060	GEOROC	21.5	70.5	2.8	GEOROC
297	23.0	71.0	0.7040	GEOROC	21.5	70.6	2.6	GEOROC
298	23.0	71.0	0.7040	GEOROC	21.5	70.5	0.0	GEOROC
299	23.0	71.0	0.7050	GEOROC	21.5	70.5	1.8	GEOROC
300	23.3	69.7	0.7040	GEOROC	21.2	72.1	-10.0	GEOROC
301	23.7	69.7	0.7040	GEOROC	21.2	72.1	-20.3	GEOROC
302	23.3	69.7	0.7040	GEOROC	21.2	72.1	-0.1	GEOROC
303	23.3	69.5	0.7040	GEOROC	21.2	72.1	-20.4	GEOROC
304	23.0	71.0	0.7050	GEOROC	21.2	72.1	-7.0	GEOROC
305	23.3	69.7	0.7070	GEOROC	21.2	72.1	-19.5	GEOROC
306	23.3	69.7	0.7100	GEOROC	21.2	72.1	-20.6	GEOROC
307	16.7	74.1	0.7040	GEOROC	21.2	72.1	-12.9	GEOROC
308	16.0	74.1	0.7040	GEOROC	21.2	72.1	-16.7	GEOROC
309	16.0	74.1	0.7040	GEOROC	21.2	72.1	-20.3	GEOROC
310	16.0	74.1	0.7040	GEOROC	19.7	73.6	-3.7	GEOROC
311	16.0	74.1	0.7050	GEOROC	16.0	74.2	5.1	GEOROC
312	16.0	74.1	0.7050	GEOROC	21.5	70.5	-6.5	GEOROC
313	16.0	74.1	0.7050	GEOROC	21.5	70.5	2.0	GEOROC
314	19.3	72.8	0.7670	GEOROC	21.5	70.5	2.3	GEOROC
315	19.3	72.8	0.7680	GEOROC	21.5	70.5	-2.2	GEOROC
316	19.3	72.8	0.7780	GEOROC	21.5	70.5	0.2	GEOROC
317	19.2	72.9	0.7070	GEOROC	20.0	73.0	2.3	GEOROC
318	19.2	72.9	0.7070	GEOROC	20.0	73.0	3.4	GEOROC
319	19.2	72.8	0.7060	GEOROC	22.0	71.5	1.5	GEOROC
320	19.2	72.8	0.7060	GEOROC	20.0	76.5	2.0	GEOROC
321	19.2	72.8	0.7110	GEOROC	20.0	76.5	1.8	GEOROC
322	20.7	75.0	0.7050	GEOROC	20.0	76.5	2.8	GEOROC
323	20.7	75.0	0.7280	GEOROC	20.0	76.5	0.4	GEOROC
324	20.7	75.0	0.7850	GEOROC	20.0	76.5	-3.8	GEOROC
325	20.7	75.0	0.7330	GEOROC	20.0	76.5	-2.4	GEOROC
326	20.7	75.0	0.7140	GEOROC	20.0	76.5	-3.1	GEOROC
327	20.7	75.0	0.7090	GEOROC	20.0	76.5	-1.7	GEOROC

328	19.1	72.9	0.7070	GEOROC	20.0	76.5	-0.9	GEOROC
329	17.6	73.5	0.7050	GEOROC	23.0	71.0	1.8	GEOROC
330	19.3	72.8	0.7680	GEOROC	23.0	71.0	2.3	GEOROC
331	19.3	72.8	0.7860	GEOROC	23.0	71.0	2.5	GEOROC
332	19.3	72.8	0.8010	GEOROC	23.0	71.0	2.6	GEOROC
333	19.2	72.9	0.7090	GEOROC	23.0	71.0	2.3	GEOROC
334	19.2	72.9	0.7150	GEOROC	23.0	71.0	2.7	GEOROC
335	19.3	72.8	0.7280	GEOROC	23.0	71.0	3.0	GEOROC
336	19.3	72.8	0.7800	GEOROC	23.3	69.7	0.4	GEOROC
337	19.3	72.8	0.7070	GEOROC	23.7	69.7	4.9	GEOROC
338	19.3	72.8	0.7090	GEOROC	23.3	69.7	4.8	GEOROC
339	19.2	72.9	0.7090	GEOROC	23.3	69.5	5.0	GEOROC
340	19.3	72.8	0.7200	GEOROC	23.0	71.0	0.7	GEOROC
341	19.2	72.8	0.7070	GEOROC	23.3	69.7	-2.7	GEOROC
342	16.9	77.4	0.7050	GEOROC	23.3	69.7	-5.0	GEOROC
343	17.9	77.5	0.7040	GEOROC	16.7	74.1	3.6	GEOROC
344	17.9	77.5	0.7050	GEOROC	16.0	74.1	1.2	GEOROC
345	19.5	74.3	0.7060	GEOROC	16.0	74.1	1.6	GEOROC
346	19.5	74.3	0.7060	GEOROC	16.0	74.1	1.8	GEOROC
347	19.5	74.3	0.7050	GEOROC	16.0	74.1	-1.7	GEOROC
348	19.5	74.3	0.7060	GEOROC	16.0	74.1	-2.3	GEOROC
349	19.5	74.3	0.7060	GEOROC	16.0	74.1	0.0	GEOROC
350	19.5	74.3	0.7060	GEOROC	17.5	74.0	-1.5	GEOROC
351	19.5	74.3	0.7090	GEOROC	17.5	74.0	7.1	GEOROC
352	19.5	74.3	0.7120	GEOROC	17.5	74.0	4.5	GEOROC
353	19.5	74.3	0.7090	GEOROC	17.5	74.0	3.9	GEOROC
354	19.5	74.3	0.7050	GEOROC	17.5	74.0	3.6	GEOROC
355	22.0	75.0	0.7060	GEOROC	17.5	74.0	2.0	GEOROC
356	22.0	75.0	0.7060	GEOROC	17.5	74.0	4.7	GEOROC
357	22.0	75.0	0.7070	GEOROC	17.5	74.0	2.0	GEOROC
358	22.0	75.0	0.7070	GEOROC	17.5	74.0	0.0	GEOROC
359	22.0	75.0	0.7060	GEOROC	19.3	72.8	1.0	GEOROC
360	22.0	75.0	0.7040	GEOROC	19.3	72.8	-1.3	GEOROC
361	22.0	75.0	0.7040	GEOROC	19.2	72.9	-0.5	GEOROC
362	22.0	75.0	0.7050	GEOROC	19.2	72.8	1.6	GEOROC
363	22.0	75.0	0.7050	GEOROC	19.2	72.8	-0.9	GEOROC
364	22.0	75.0	0.7060	GEOROC	19.2	72.8	-4.6	GEOROC
365	22.0	75.0	0.7060	GEOROC	19.1	72.9	1.2	GEOROC
366	22.0	75.0	0.7090	GEOROC	19.2	72.8	-1.1	GEOROC
367	22.0	75.0	0.7070	GEOROC	17.6	73.5	-16.9	GEOROC
368	22.0	75.0	0.7080	GEOROC	17.6	73.5	-17.9	GEOROC
369	22.0	75.0	0.7070	GEOROC	19.3	72.8	-1.9	GEOROC
370	22.0	75.0	0.7050	GEOROC	19.3	72.8	-1.3	GEOROC
371	22.0	75.0	0.7050	GEOROC	19.2	72.9	-5.0	GEOROC

372	22.0	74.1	0.7050	GEOROC	19.3	72.8	0.6	GEOROC
373	22.0	74.1	0.7060	GEOROC	19.3	72.8	-4.3	GEOROC
374	23.2	69.9	0.7040	GEOROC	19.2	72.8	-4.3	GEOROC
375	23.2	69.9	0.7040	GEOROC	19.5	74.3	-1.8	GEOROC
376	23.2	69.9	0.7040	GEOROC	19.5	74.3	0.0	GEOROC
377	23.2	69.9	0.7040	GEOROC	19.5	74.3	1.3	GEOROC
378	24.8	72.6	0.7060	GEOROC	19.5	74.3	-2.5	GEOROC
379	24.8	72.6	0.7050	GEOROC	19.5	74.3	-2.8	GEOROC
380	24.8	72.6	0.7050	GEOROC	19.5	74.3	-0.8	GEOROC
381	24.8	72.6	0.7050	GEOROC	19.5	74.3	-6.2	GEOROC
382	24.8	72.6	0.7050	GEOROC	19.5	74.3	-15.1	GEOROC
383	25.7	72.4	0.7050	GEOROC	19.5	74.3	-7.9	GEOROC
384	25.7	72.4	0.7040	GEOROC	19.5	74.3	-0.2	GEOROC
385	25.7	72.4	0.7040	GEOROC	22.0	75.0	1.1	GEOROC
386	25.7	72.4	0.7040	GEOROC	22.0	75.0	0.6	GEOROC
387	25.7	72.4	0.7040	GEOROC	22.0	75.0	-2.4	GEOROC
388	25.7	72.4	0.7040	GEOROC	22.0	75.0	-2.0	GEOROC
389	23.3	69.7	0.7060	GEOROC	22.0	75.0	1.1	GEOROC
390	23.3	69.7	0.7050	GEOROC	22.0	75.0	3.4	GEOROC
391	23.9	78.6	0.7060	GEOROC	22.0	75.0	3.6	GEOROC
392	23.9	78.6	0.7050	GEOROC	22.0	75.0	3.1	GEOROC
393	23.9	78.6	0.7050	GEOROC	22.0	75.0	1.7	GEOROC
394	23.9	78.6	0.7050	GEOROC	22.0	75.0	1.8	GEOROC
395	23.9	78.6	0.7050	GEOROC	22.0	75.0	1.2	GEOROC
396	23.9	78.6	0.7050	GEOROC	22.0	75.0	-5.1	GEOROC
397	23.9	78.6	0.7050	GEOROC	22.0	75.0	-3.7	GEOROC
398	23.9	78.6	0.7050	GEOROC	22.0	75.0	-0.3	GEOROC
399	23.9	78.6	0.7040	GEOROC	22.0	75.0	-0.2	GEOROC
400	23.9	78.6	0.7070	GEOROC	22.0	75.0	3.1	GEOROC
401	23.9	78.6	0.7080	GEOROC	22.0	75.0	3.2	GEOROC
402	23.9	78.6	0.7080	GEOROC	22.0	74.1	4.7	GEOROC
403	23.9	78.6	0.7060	GEOROC	22.0	74.1	-1.6	GEOROC
404	23.9	78.6	0.7050	GEOROC	23.2	69.9	4.4	GEOROC
405	17.9	73.6	0.7080	GEOROC	23.2	69.9	5.5	GEOROC
406	17.9	73.6	0.7050	GEOROC	23.2	69.9	4.7	GEOROC
407	17.9	73.6	0.7050	GEOROC	23.2	69.9	5.3	GEOROC
408	17.9	73.6	0.7080	GEOROC	24.8	72.6	2.5	GEOROC
409	21.5	70.5	0.7080	GEOROC	24.8	72.6	3.1	GEOROC
410	21.5	70.5	0.7080	GEOROC	24.8	72.6	2.6	GEOROC
411	21.5	70.5	0.7070	GEOROC	24.8	72.6	3.0	GEOROC
412	21.5	70.5	0.7100	GEOROC	24.8	72.6	2.0	GEOROC
413	21.5	70.5	0.7050	GEOROC	25.7	72.4	3.2	GEOROC
414	21.5	70.5	0.7060	GEOROC	25.7	72.4	3.5	GEOROC
415	21.5	70.5	0.7090	GEOROC	25.7	72.4	3.5	GEOROC

416	21.5	70.5	0.7280	GEOROC	25.7	72.4	1.5	GEOROC
417	21.5	70.5	0.7330	GEOROC	25.7	72.4	1.7	GEOROC
418	21.5	70.5	0.7310	GEOROC	25.7	72.4	0.8	GEOROC
419	22.0	74.1	0.7060	GEOROC	23.3	69.7	1.1	GEOROC
420	22.0	74.1	0.7060	GEOROC	23.3	69.7	-0.6	GEOROC
421	22.0	74.1	0.7060	GEOROC	17.9	73.6	0.8	GEOROC
422	22.0	74.1	0.7060	GEOROC	17.9	73.6	-5.4	GEOROC
423	22.0	74.1	0.7060	GEOROC	22.0	74.1	-2.5	GEOROC
424	22.0	74.1	0.7060	GEOROC	22.0	74.1	-1.5	GEOROC
425	22.0	74.1	0.7060	GEOROC	22.0	74.1	-2.3	GEOROC
426	22.0	74.1	0.7060	GEOROC	22.0	74.1	-2.3	GEOROC
427	22.0	74.1	0.7060	GEOROC	22.0	74.1	-1.5	GEOROC
428	24.8	72.6	0.7050	GEOROC	22.0	74.1	-2.3	GEOROC
429	24.8	72.6	0.7050	GEOROC	22.0	74.1	-2.1	GEOROC
430	25.7	72.4	0.7050	GEOROC	22.0	74.1	-1.9	GEOROC
431	23.2	80.6	0.7070	GEOROC	22.0	74.1	-2.5	GEOROC
432	22.3	79.0	0.7060	GEOROC	22.3	79.0	1.5	GEOROC
433	22.3	79.0	0.7080	GEOROC	22.3	79.0	2.3	GEOROC
434	22.3	79.0	0.7160	GEOROC	22.3	79.0	2.5	GEOROC
435	22.3	79.0	0.7080	GEOROC	22.3	79.0	1.0	GEOROC
436	22.3	79.0	0.7080	GEOROC	22.3	79.0	0.5	GEOROC
437	22.3	79.0	0.7090	GEOROC	22.3	79.0	0.6	GEOROC
438	22.3	79.0	0.7070	GEOROC	22.3	79.0	0.3	GEOROC
439	22.3	79.0	0.7070	GEOROC	22.3	79.0	2.8	GEOROC
440	22.3	79.0	0.7050	GEOROC	19.3	73.7	4.4	GEOROC
441	22.3	79.0	0.7060	GEOROC	19.3	73.7	-7.7	GEOROC
442	22.0	74.1	0.7060	GEOROC	18.8	73.3	1.5	GEOROC
443	22.0	75.0	0.7050	GEOROC	18.8	73.3	1.3	GEOROC
444	18.3	74.2	0.7050	GEOROC	18.8	73.3	2.1	GEOROC
445	18.3	74.2	0.7070	GEOROC	18.8	73.3	0.6	GEOROC
446	18.3	74.2	0.7080	GEOROC	18.3	73.0	3.7	GEOROC
447	18.3	74.2	0.7110	GEOROC	18.5	72.9	4.0	GEOROC
448	18.3	74.2	0.7090	GEOROC	18.3	74.2	0.6	GEOROC
449	19.3	73.7	0.7040	GEOROC	20.0	73.7	1.7	GEOROC
450	19.3	73.7	0.7090	GEOROC	18.0	75.0	-4.1	GEOROC
451	18.8	73.3	0.7050	GEOROC	18.0	75.0	-1.2	GEOROC
452	18.8	73.3	0.7050	GEOROC	18.0	75.0	-15.0	GEOROC
453	18.8	73.3	0.7050	GEOROC	19.0	73.3	0.8	GEOROC
454	18.8	73.3	0.7060	GEOROC	19.0	73.3	-5.2	GEOROC
455	18.3	73.0	0.7040	GEOROC	18.8	73.3	1.1	GEOROC
456	18.5	72.9	0.7050	GEOROC	18.9	73.4	-5.3	GEOROC
457	18.3	74.2	0.7060	GEOROC	19.0	73.3	0.4	GEOROC
458	20.0	73.7	0.7060	GEOROC	18.9	73.3	-12.3	GEOROC
459	18.0	75.0	0.7090	GEOROC	19.7	73.7	-0.4	GEOROC

460	18.0	75.0	0.7070	GEOROC	18.8	73.8	0.6	GEOROC
461	18.0	75.0	0.7120	GEOROC	18.8	73.8	-0.1	GEOROC
462	19.0	73.3	0.7050	GEOROC	19.2	73.7	1.1	GEOROC
463	19.0	73.3	0.7080	GEOROC	19.0	73.5	0.0	GEOROC
464	18.8	73.3	0.7050	GEOROC	19.0	73.5	0.4	GEOROC
465	18.9	73.4	0.7080	GEOROC	19.1	73.4	-7.5	GEOROC
466	19.0	73.3	0.7080	GEOROC	19.1	73.4	0.5	GEOROC
467	19.0	73.3	0.7060	GEOROC	19.0	73.3	-1.5	GEOROC
468	18.9	73.3	0.7090	GEOROC	18.0	75.0	0.4	GEOROC
469	19.7	73.7	0.7070	GEOROC	18.0	75.0	-8.2	GEOROC
470	18.8	73.8	0.7050	GEOROC	18.0	75.0	4.1	GEOROC
471	18.8	73.8	0.7050	GEOROC	18.0	75.0	-5.5	GEOROC
472	19.2	73.7	0.7050	GEOROC	18.0	75.0	-11.5	GEOROC
473	19.0	73.5	0.7070	GEOROC	18.0	75.0	-2.6	GEOROC
474	19.0	73.5	0.7060	GEOROC	18.0	75.0	-7.4	GEOROC
475	19.1	73.4	0.7080	GEOROC	18.0	75.0	-6.7	GEOROC
476	19.1	73.4	0.7060	GEOROC	18.0	75.0	0.6	GEOROC
477	19.0	73.3	0.7080	GEOROC	18.0	75.0	3.2	GEOROC
478	18.0	75.0	0.7060	GEOROC	18.0	75.0	3.1	GEOROC
479	18.0	75.0	0.7120	GEOROC	18.0	75.0	0.8	GEOROC
480	18.0	75.0	0.7040	GEOROC	18.0	75.0	-6.7	GEOROC
481	18.0	75.0	0.7060	GEOROC	21.4	74.2	-15.2	GEOROC
482	18.0	75.0	0.7090	GEOROC	21.4	74.1	-6.4	GEOROC
483	18.0	75.0	0.7090	GEOROC	21.3	74.3	-5.4	GEOROC
484	18.0	75.0	0.7110	GEOROC	19.8	73.0	-11.9	GEOROC
485	18.0	75.0	0.7060	GEOROC	18.3	74.2	-11.2	GEOROC
486	18.0	75.0	0.7050	GEOROC	18.3	74.2	-15.8	GEOROC
487	18.0	75.0	0.7050	GEOROC	18.3	74.2	-0.9	GEOROC
488	18.0	75.0	0.7060	GEOROC	18.3	74.2	-0.6	GEOROC
489	18.0	75.0	0.7100	GEOROC	18.3	74.2	-2.6	GEOROC
490	21.4	74.2	0.7150	GEOROC	18.3	74.2	-12.8	GEOROC
491	21.4	74.1	0.7100	GEOROC	18.3	74.2	-6.8	GEOROC
492	21.3	74.3	0.7110	GEOROC	18.3	74.2	-6.8	GEOROC
493	19.8	73.0	0.7170	GEOROC	18.3	74.2	-9.4	GEOROC
494	18.3	74.2	0.7090	GEOROC	18.3	74.2	-10.5	GEOROC
495	18.3	74.2	0.7230	GEOROC	18.3	74.2	2.0	GEOROC
496	18.3	74.2	0.7080	GEOROC	18.3	74.2	-3.4	GEOROC
497	18.3	74.2	0.7080	GEOROC	18.3	74.2	-5.9	GEOROC
498	18.3	74.2	0.7080	GEOROC	18.3	74.2	0.6	GEOROC
499	18.3	74.2	0.7100	GEOROC	18.3	74.2	0.1	GEOROC
500	18.3	74.2	0.7090	GEOROC	18.3	74.2	-10.4	GEOROC
501	18.3	74.2	0.7100	GEOROC	18.3	74.2	1.3	GEOROC
502	18.3	74.2	0.7160	GEOROC	18.3	74.2	2.3	GEOROC
503	18.3	74.2	0.7170	GEOROC	18.3	74.2	-0.2	GEOROC

504	18.3	74.2	0.7060	GEOROC	18.3	74.2	4.6	GEOROC
505	18.3	74.2	0.7080	GEOROC	18.3	74.2	0.9	GEOROC
506	18.3	74.2	0.7040	GEOROC	18.3	74.2	2.5	GEOROC
507	18.3	74.2	0.7050	GEOROC	18.0	75.0	0.9	GEOROC
508	18.3	74.2	0.7070	GEOROC	18.0	75.0	2.1	GEOROC
509	18.3	74.2	0.7140	GEOROC	21.8	71.9	0.0	GEOROC
510	18.3	74.2	0.7050	GEOROC	21.8	71.9	-3.6	GEOROC
511	18.3	74.2	0.7050	GEOROC	21.8	71.9	-1.7	GEOROC
512	18.3	74.2	0.7070	GEOROC	21.8	71.9	-1.7	GEOROC
513	18.3	74.2	0.7040	GEOROC	21.8	71.9	2.2	GEOROC
514	18.3	74.2	0.7060	GEOROC	21.8	71.9	-0.6	GEOROC
515	18.3	74.2	0.7050	GEOROC	21.8	71.9	-0.6	GEOROC
516	18.0	75.0	0.7060	GEOROC	21.8	71.9	0.4	GEOROC
517	18.0	75.0	0.7050	GEOROC	21.8	71.9	-13.0	GEOROC
518	21.8	71.9	0.7290	GEOROC	21.8	71.9	-14.5	GEOROC
519	21.8	71.9	0.7300	GEOROC	21.7	70.3	-7.1	GEOROC
520	21.8	71.9	0.7090	GEOROC	21.7	70.3	-3.7	GEOROC
521	21.8	71.9	0.7080	GEOROC	21.7	70.3	-6.8	GEOROC
522	21.8	71.9	0.7060	GEOROC	21.7	70.3	2.3	GEOROC
523	21.8	71.9	0.7060	GEOROC	21.7	70.3	1.0	GEOROC
524	21.8	71.9	0.7070	GEOROC	21.7	70.3	-1.6	GEOROC
525	21.8	71.9	0.7080	GEOROC	23.3	69.7	5.5	GEOROC
526	21.8	71.9	0.7370	GEOROC	23.3	69.7	5.1	GEOROC
527	21.8	71.9	0.7340	GEOROC	23.3	69.7	0.2	GEOROC
528	21.7	70.3	0.7860	GEOROC	23.3	69.7	5.4	GEOROC
529	21.7	70.3	0.7690	GEOROC	23.3	69.7	-4.5	GEOROC
530	21.7	70.3	0.7630	GEOROC	23.3	69.7	-1.8	GEOROC
531	21.7	70.3	0.7090	GEOROC	23.3	69.7	4.6	GEOROC
532	21.7	70.3	0.7080	GEOROC	23.3	69.7	5.0	GEOROC
533	21.7	70.3	0.7080	GEOROC	21.5	73.8	-8.5	GEOROC
534	23.3	69.7	0.7040	GEOROC	21.5	73.8	-8.3	GEOROC
535	23.3	69.7	0.7040	GEOROC	21.5	73.8	-12.2	GEOROC
536	23.3	69.7	0.7040	GEOROC	21.5	73.8	-12.1	GEOROC
537	23.3	69.7	0.7040	GEOROC	21.5	73.8	-7.6	GEOROC
538	23.3	69.7	0.7090	GEOROC	21.5	73.8	-6.7	GEOROC
539	23.3	69.7	0.7060	GEOROC	21.5	73.8	-8.1	GEOROC
540	23.3	69.7	0.7040	GEOROC	21.5	73.8	-13.5	GEOROC
541	23.3	69.7	0.7040	GEOROC	21.5	73.8	-13.9	GEOROC
542	21.5	73.8	0.7110	GEOROC	21.3	72.3	-18.0	GEOROC
543	21.5	73.8	0.7110	GEOROC	21.3	72.3	-5.7	GEOROC
544	21.5	73.8	0.7120	GEOROC	21.3	72.3	-18.6	GEOROC
545	21.5	73.8	0.7120	GEOROC	21.3	72.3	0.8	GEOROC
546	21.5	73.8	0.7120	GEOROC	21.3	72.3	-0.9	GEOROC
547	21.5	73.8	0.7150	GEOROC	21.3	72.3	0.5	GEOROC

548	21.5	73.8	0.7110	GEOROC	21.3	72.3	-1.1	GEOROC
549	21.5	73.8	0.7130	GEOROC	21.3	72.3	0.5	GEOROC
550	21.5	73.8	0.7130	GEOROC	18.3	74.2	-19.4	GEOROC
551	21.3	72.3	0.7300	GEOROC	17.9	73.6	1.0	GEOROC
552	21.3	72.3	0.7100	GEOROC	16.7	74.1	3.7	GEOROC
553	21.3	72.3	0.7320	GEOROC	16.7	74.1	3.6	GEOROC
554	21.3	72.3	0.7080	GEOROC	16.0	74.1	3.0	GEOROC
555	21.3	72.3	0.7080	GEOROC	16.0	74.1	1.8	GEOROC
556	21.3	72.3	0.7070	GEOROC	16.0	74.1	0.4	GEOROC
557	21.3	72.3	0.7080	GEOROC	16.0	74.1	1.0	GEOROC
558	21.3	72.3	0.7070	GEOROC	17.5	74.0	-13.4	GEOROC
559	18.3	74.2	0.7190	GEOROC	17.5	74.0	-13.6	GEOROC
560	17.9	73.6	0.7060	GEOROC	17.5	74.0	-15.2	GEOROC
561	16.7	74.1	0.7040	GEOROC	17.5	74.0	0.6	GEOROC
562	16.7	74.1	0.7040	GEOROC	17.5	74.0	-2.3	GEOROC
563	16.0	74.1	0.7040	GEOROC	17.5	74.0	-6.0	GEOROC
564	16.0	74.1	0.7050	GEOROC	17.5	74.0	0.2	GEOROC
565	16.0	74.1	0.7050	GEOROC	17.5	74.0	-6.0	GEOROC
566	16.0	74.1	0.7050	GEOROC	17.5	74.0	-2.3	GEOROC
567	19.0	72.9	0.7090	GEOROC	17.5	74.0	-2.3	GEOROC
568	19.0	72.9	0.7070	GEOROC	17.5	74.0	-6.2	GEOROC
569	19.0	72.9	0.7090	GEOROC	17.5	74.0	0.8	GEOROC
570	15.0	75.0	0.7190	GEOROC	17.9	73.7	-5.2	GEOROC
571	15.0	75.0	0.7150	GEOROC	19.0	72.9	-5.0	GEOROC
572	15.0	75.0	0.7190	GEOROC	25.7	72.4	2.4	GEOROC
573	15.0	75.0	0.7170	GEOROC	18.3	74.2	-5.0	GEOROC
574	15.0	75.0	0.7170	GEOROC	18.3	74.2	-3.4	GEOROC
575	15.0	75.0	0.7160	GEOROC	18.3	74.2	-8.1	GEOROC
576	24.8	72.6	0.7050	GEOROC	23.2	80.6	-6.2	GEOROC
577	24.8	72.6	0.7040	GEOROC	23.2	80.6	-7.7	GEOROC
578	24.8	72.6	0.7050	GEOROC	23.2	80.6	-5.9	GEOROC
579	24.8	72.6	0.7050	GEOROC	23.2	80.6	-6.3	GEOROC
580	24.8	72.6	0.7060	GEOROC	23.2	80.6	-5.1	GEOROC
581	24.8	72.6	0.7040	GEOROC	23.2	80.6	-11.4	GEOROC
582	22.0	75.0	0.7090	GEOROC	23.2	80.6	-4.8	GEOROC
583	22.0	75.0	0.7100	GEOROC	23.2	80.6	-4.1	GEOROC
584	22.0	75.0	0.7060	GEOROC	23.2	80.6	-13.1	GEOROC
585	25.7	72.4	0.7040	GEOROC	23.2	80.6	-4.4	GEOROC
586	18.3	74.2	0.7080	GEOROC	23.2	80.6	-13.9	GEOROC
587	18.3	74.2	0.7070	GEOROC	23.2	80.6	-6.0	GEOROC
588	18.3	74.2	0.7130	GEOROC	19.1	72.9	-4.5	GEOROC
589	23.2	80.6	0.7070	GEOROC	19.1	72.9	-5.3	GEOROC
590	23.2	80.6	0.7080	GEOROC	19.1	72.9	-5.8	GEOROC
591	23.2	80.6	0.7070	GEOROC	19.1	72.9	-5.8	GEOROC

592	23.2	80.6	0.7070	GEOROC	19.1	72.9	5.0	GEOROC
593	23.2	80.6	0.7070	GEOROC	19.1	72.9	-4.6	GEOROC
594	23.2	80.6	0.7180	GEOROC	19.1	72.9	2.2	GEOROC
595	23.2	80.6	0.7090	GEOROC	19.1	72.9	-4.2	GEOROC
596	23.2	80.6	0.7070	GEOROC	19.1	72.9	5.5	GEOROC
597	23.2	80.6	0.7340	GEOROC	19.1	72.9	4.8	GEOROC
598	23.2	80.6	0.7070	GEOROC	19.1	72.9	-4.6	GEOROC
599	23.2	80.6	0.7090	GEOROC	19.1	72.9	-4.4	GEOROC
600	23.2	80.6	0.7120	GEOROC	20.5	74.5	-6.2	GEOROC
601	18.6	73.5	0.7060	GEOROC	20.5	74.5	-7.2	GEOROC
602	18.9	73.4	0.7040	GEOROC	20.5	74.5	-6.0	GEOROC
603	18.9	73.4	0.7130	GEOROC	20.5	74.5	-3.9	GEOROC
604	18.9	72.9	0.7080	GEOROC	21.0	75.0	-5.6	GEOROC
605	19.1	72.9	0.7070	GEOROC	21.0	75.0	-7.1	GEOROC
606	19.1	72.9	0.7060	GEOROC	21.0	75.0	-8.2	GEOROC
607	19.1	72.9	0.7060	GEOROC	21.0	75.0	-9.9	GEOROC
608	19.1	72.9	0.7060	GEOROC	20.0	75.0	-5.1	GEOROC
609	19.1	72.9	0.7050	GEOROC	20.0	75.0	-3.6	GEOROC
610	19.1	72.9	0.7060	GEOROC	20.5	75.5	-9.0	GEOROC
611	19.1	72.9	0.7050	GEOROC	20.5	75.5	-6.1	GEOROC
612	19.1	72.9	0.7060	GEOROC	20.5	75.5	1.0	GEOROC
613	19.1	72.9	0.7040	GEOROC	20.5	75.5	-1.2	GEOROC
614	19.1	72.9	0.7040	GEOROC	20.0	75.0	-4.9	GEOROC
615	19.1	72.9	0.7060	GEOROC	21.9	79.0	-0.2	GEOROC
616	19.1	72.9	0.7060	GEOROC	21.9	79.0	1.1	GEOROC
617	20.5	74.5	0.7080	GEOROC	21.9	79.0	-0.3	GEOROC
618	20.5	74.5	0.7070	GEOROC	21.9	79.0	0.5	GEOROC
619	20.5	74.5	0.7070	GEOROC	21.9	79.0	1.1	GEOROC
620	20.5	74.5	0.7060	GEOROC	21.9	79.0	-0.3	GEOROC
621	21.0	75.0	0.7080	GEOROC	18.0	73.0	-7.3	GEOROC
622	21.0	75.0	0.7080	GEOROC	22.0	72.0	-8.4	GEOROC
623	21.0	75.0	0.7090	GEOROC	22.0	72.0	-4.1	GEOROC
624	21.0	75.0	0.7120	GEOROC	22.0	72.0	-4.2	GEOROC
625	20.0	75.0	0.7070	GEOROC	22.0	72.0	-12.7	GEOROC
626	20.0	75.0	0.7070	GEOROC	22.0	72.0	-2.9	GEOROC
627	20.5	75.5	0.7080	GEOROC	22.0	72.0	-1.4	GEOROC
628	20.5	75.5	0.7070	GEOROC	22.0	72.0	4.4	GEOROC
629	20.5	75.5	0.7060	GEOROC	22.0	72.0	-5.7	GEOROC
630	20.5	75.5	0.7070	GEOROC	22.0	72.0	1.1	GEOROC
631	20.0	75.0	0.7070	GEOROC	22.0	72.0	-2.7	GEOROC
632	21.9	79.0	0.7070	GEOROC	22.0	72.0	-2.5	GEOROC
633	21.9	79.0	0.7060	GEOROC	22.0	72.0	-4.0	GEOROC
634	21.9	79.0	0.7070	GEOROC	14.0	78.0	-1.1	GEOROC
635	21.9	79.0	0.7060	GEOROC	14.0	78.0	-9.1	GEOROC

636	21.9	79.0	0.7060	GEOROC	14.0	78.0	-25.0	GEOROC
637	21.9	79.0	0.7070	GEOROC	14.0	78.0	-28.9	GEOROC
638	22.0	74.1	0.7060	GEOROC	14.0	78.0	-31.3	GEOROC
639	22.0	74.1	0.7060	GEOROC	14.0	78.0	-34.2	GEOROC
640	22.0	74.1	0.7060	GEOROC	14.0	78.0	-9.1	GEOROC
641	22.0	74.1	0.7070	GEOROC	14.0	76.3	-17.8	GEOROC
642	22.0	74.1	0.7070	GEOROC	14.0	76.3	8.1	GEOROC
643	22.0	74.1	0.7160	GEOROC	14.0	76.3	25.3	GEOROC
644	22.0	74.1	0.7070	GEOROC	14.0	76.3	20.7	GEOROC
645	22.0	74.1	0.7120	GEOROC	14.0	76.3	-28.6	GEOROC
646	22.0	74.1	0.7060	GEOROC	14.0	76.3	11.4	GEOROC
647	22.0	74.1	0.7060	GEOROC	14.0	76.3	39.7	GEOROC
648	22.0	74.1	0.7060	GEOROC	14.0	76.3	33.9	GEOROC
649	22.0	74.1	0.7060	GEOROC	14.0	76.3	34.3	GEOROC
650	22.0	74.1	0.7060	GEOROC	14.0	76.3	6.0	GEOROC
651	22.0	74.1	0.7070	GEOROC	14.0	76.3	-19.2	GEOROC
652	22.0	74.1	0.7060	GEOROC	14.0	76.3	-19.6	GEOROC
653	22.0	74.1	0.7060	GEOROC	13.8	78.5	-1.2	GEOROC
654	18.0	73.0	0.7090	GEOROC	13.8	78.5	-1.2	GEOROC
655	22.0	72.0	0.7150	GEOROC	13.8	78.5	-0.9	GEOROC
656	22.0	72.0	0.7080	GEOROC	13.8	78.5	-4.6	GEOROC
657	22.0	72.0	0.7080	GEOROC	13.8	78.5	-2.0	GEOROC
658	22.0	72.0	0.7180	GEOROC	13.8	78.4	0.4	GEOROC
659	22.0	72.0	0.7070	GEOROC	13.8	78.4	-3.7	GEOROC
660	22.0	72.0	0.7060	GEOROC	13.8	78.4	-5.2	GEOROC
661	22.0	72.0	0.7050	GEOROC	14.0	78.5	-2.3	GEOROC
662	22.0	72.0	0.7100	GEOROC	14.0	78.5	-0.3	GEOROC
663	22.0	72.0	0.7050	GEOROC	14.0	78.5	3.4	GEOROC
664	22.0	72.0	0.7070	GEOROC	14.0	78.4	-27.5	GEOROC
665	22.0	72.0	0.7070	GEOROC	14.1	78.4	-23.0	GEOROC
666	22.0	72.0	0.7080	GEOROC	14.2	78.4	-8.5	GEOROC
667	13.1	78.1	0.7020	GEOROC	14.2	78.4	-8.1	GEOROC
668	13.1	78.1	0.7020	GEOROC	14.2	78.4	-12.4	GEOROC
669	13.1	78.1	0.7020	GEOROC	14.2	78.4	-19.5	GEOROC
670	13.1	78.1	0.7040	GEOROC	13.8	78.5	-25.4	GEOROC
671	13.1	78.1	0.7080	GEOROC	14.0	78.5	-12.3	GEOROC
672	13.1	78.1	0.7160	GEOROC	14.0	78.5	-29.7	GEOROC
673	13.1	78.1	0.7080	GEOROC	14.0	78.5	-29.7	GEOROC
674	13.1	78.1	0.7080	GEOROC	13.8	78.5	-4.6	GEOROC
675	13.1	78.1	0.7190	GEOROC	14.2	78.4	-6.5	GEOROC
676	13.1	78.1	0.7030	GEOROC	14.1	78.4	-23.1	GEOROC
677	13.1	78.1	0.7360	GEOROC	14.0	75.5	6.3	GEOROC
678	13.1	78.1	0.7120	GEOROC	14.0	75.5	-0.3	GEOROC
679	13.1	78.1	0.7140	GEOROC	14.0	75.5	-13.5	GEOROC

680	13.1	78.1	0.7200	GEOROC	14.0	75.5	-0.4	GEOROC
681	13.1	76.4	0.7100	GEOROC	14.0	75.5	8.5	GEOROC
682	13.1	76.4	0.7150	GEOROC	14.0	75.5	-29.0	GEOROC
683	13.1	76.4	0.7160	GEOROC	14.0	75.5	5.4	GEOROC
684	13.1	76.4	0.7060	GEOROC	14.0	75.5	-29.1	GEOROC
685	13.1	76.4	0.7170	GEOROC	14.0	75.5	-5.8	GEOROC
686	13.1	76.4	0.7060	GEOROC	14.0	75.5	-3.6	GEOROC
687	13.1	76.4	0.7280	GEOROC	14.0	75.5	-12.9	GEOROC
688	13.1	76.4	0.7060	GEOROC	14.0	75.5	-7.0	GEOROC
689	13.1	76.4	0.7060	GEOROC	14.0	75.5	-3.8	GEOROC
690	13.1	76.4	0.7060	GEOROC	14.0	75.5	-11.3	GEOROC
691	13.1	76.4	0.7260	GEOROC	14.3	77.6	1.2	GEOROC
692	13.1	76.4	0.7150	GEOROC	14.3	77.6	-0.2	GEOROC
693	13.1	76.4	0.7240	GEOROC	14.3	77.5	4.0	GEOROC
694	13.5	75.8	0.7080	GEOROC	14.3	77.5	3.9	GEOROC
695	13.5	75.8	0.7310	GEOROC	14.3	77.6	5.5	GEOROC
696	13.5	75.8	0.7860	GEOROC	14.3	77.6	-23.0	GEOROC
697	13.1	77.8	0.7090	GEOROC	14.3	77.5	-20.5	GEOROC
698	13.1	77.8	0.7120	GEOROC	14.3	77.6	-25.3	GEOROC
699	14.3	75.4	0.7040	GEOROC	14.3	77.6	-25.2	GEOROC
700	14.3	75.4	0.7250	GEOROC	14.3	77.5	-13.1	GEOROC
701	14.3	75.4	1.3120	GEOROC	14.3	77.6	8.7	GEOROC
702	14.0	76.3	0.8430	GEOROC	14.3	77.6	-14.4	GEOROC
703	14.0	76.3	0.8960	GEOROC	14.3	77.6	15.5	GEOROC
704	14.0	76.3	1.1200	GEOROC	14.3	77.6	-39.8	GEOROC
705	14.0	76.3	0.7090	GEOROC	14.3	77.6	16.6	GEOROC
706	14.0	76.3	0.7270	GEOROC	14.3	77.6	-33.9	GEOROC
707	16.3	77.3	0.7010	GEOROC	13.1	78.1	-0.8	GEOROC
708	16.3	77.3	0.7640	GEOROC	13.1	78.1	-0.1	GEOROC
709	16.3	77.3	0.8560	GEOROC	13.1	78.1	0.6	GEOROC
710	16.3	77.3	0.9040	GEOROC	13.1	78.1	-3.3	GEOROC
711	15.1	76.6	0.7060	GEOROC	13.1	78.1	-2.8	GEOROC
712	15.1	76.6	0.7180	GEOROC	13.1	78.1	1.2	GEOROC
713	15.1	76.6	0.7580	GEOROC	13.1	78.1	1.0	GEOROC
714	16.3	77.3	0.7190	GEOROC	13.1	78.1	0.1	GEOROC
715	16.3	77.3	1.0530	GEOROC	13.1	78.1	-11.2	GEOROC
716	16.3	77.3	0.9370	GEOROC	13.1	78.1	5.5	GEOROC
717	16.3	77.3	0.7360	GEOROC	13.1	78.1	18.2	GEOROC
718	16.3	77.3	0.7780	GEOROC	13.1	78.1	20.0	GEOROC
719	16.3	77.3	0.9280	GEOROC	13.1	78.1	13.8	GEOROC
720	16.3	77.3	0.8560	GEOROC	13.1	78.1	14.1	GEOROC
721	16.3	77.3	1.0290	GEOROC	13.1	78.1	13.4	GEOROC
722	16.3	77.3	0.7380	GEOROC	13.1	78.1	13.3	GEOROC
723	16.3	77.3	0.7510	GEOROC	13.1	78.1	6.8	GEOROC

724	16.3	77.3	0.9200	GEOROC	13.1	78.1	24.0	GEOROC
725	13.5	75.8	0.7030	GEOROC	13.1	78.1	-9.7	GEOROC
726	13.5	75.8	0.7520	GEOROC	13.1	78.1	-12.4	GEOROC
727	13.5	75.8	0.7800	GEOROC	13.1	78.1	-9.4	GEOROC
728	13.5	75.8	0.8070	GEOROC	13.1	78.1	-11.3	GEOROC
729	13.5	75.8	0.8150	GEOROC	13.1	78.1	-4.3	GEOROC
730	13.5	75.8	0.8470	GEOROC	13.2	76.3	2.9	GEOROC
731	13.3	75.8	0.7100	GEOROC	13.2	76.3	1.9	GEOROC
732	13.1	77.8	0.7120	GEOROC	13.2	76.3	3.3	GEOROC
733	14.3	75.4	0.7080	GEOROC	13.2	76.3	2.3	GEOROC
734	14.3	75.4	0.7190	GEOROC	13.2	76.3	2.7	GEOROC
735	14.2	75.8	1.3490	GEOROC	13.2	76.3	2.6	GEOROC
736	14.3	75.4	1.5280	GEOROC	13.2	76.3	2.5	GEOROC
737	14.2	76.4	0.7090	GEOROC	13.2	76.3	1.8	GEOROC
738	14.2	76.4	0.8500	GEOROC	13.2	76.3	1.4	GEOROC
739	14.0	76.3	0.9770	GEOROC	13.2	76.3	2.2	GEOROC
740	14.0	76.3	0.7130	GEOROC	13.2	76.5	1.3	GEOROC
741	14.0	76.3	0.7310	GEOROC	13.2	76.5	1.7	GEOROC
742	14.0	76.3	0.7130	GEOROC	13.2	76.5	1.4	GEOROC
743	16.3	77.3	0.7010	GEOROC	13.2	76.5	1.3	GEOROC
744	16.3	77.3	0.7040	GEOROC	13.2	76.5	1.8	GEOROC
745	16.3	77.3	0.7240	GEOROC	13.1	76.4	-15.8	GEOROC
746	16.3	77.3	0.7720	GEOROC	13.1	76.4	-22.2	GEOROC
747	16.3	77.3	0.8740	GEOROC	13.1	76.4	-18.2	GEOROC
748	16.3	77.3	0.8720	GEOROC	13.1	76.4	-1.5	GEOROC
749	16.3	77.3	0.8870	GEOROC	13.1	76.4	-22.6	GEOROC
750	15.1	76.6	0.7070	GEOROC	13.1	76.4	-3.7	GEOROC
751	15.1	76.6	0.7070	GEOROC	13.1	76.4	-21.0	GEOROC
752	15.1	76.6	0.7070	GEOROC	13.1	76.4	-20.1	GEOROC
753	15.1	76.6	0.7100	GEOROC	13.1	76.4	-16.5	GEOROC
754	15.1	76.6	0.7100	GEOROC	13.1	76.4	-22.7	GEOROC
755	15.1	76.6	0.7350	GEOROC	13.1	76.4	-0.2	GEOROC
756	13.3	75.8	0.7340	GEOROC	13.1	76.4	-15.9	GEOROC
757	13.3	75.8	0.7280	GEOROC	13.1	76.4	-15.6	GEOROC
758	13.3	75.8	0.7260	GEOROC	13.1	76.4	-17.8	GEOROC
759	13.3	75.8	0.7170	GEOROC	13.1	76.4	-14.7	GEOROC
760	13.3	75.8	0.7330	GEOROC	15.1	76.7	-8.8	GEOROC
761	13.3	75.8	0.7370	GEOROC	15.1	76.7	0.7	GEOROC
762	13.3	75.8	0.7040	GEOROC	15.1	76.7	1.8	GEOROC
763	13.3	75.8	0.7120	GEOROC	15.1	76.7	1.2	GEOROC
764	13.3	75.8	0.7060	GEOROC	15.1	76.7	5.6	GEOROC
765	13.3	75.8	0.7190	GEOROC	15.1	76.7	3.6	GEOROC
766	13.3	75.8	0.7090	GEOROC	15.1	76.7	3.8	GEOROC
767	16.3	77.3	0.7210	GEOROC	15.1	76.7	3.2	GEOROC

768	16.3	77.3	1.1030	GEOROC	13.1	78.1	9.7	GEOROC
769	16.3	77.3	1.0350	GEOROC	13.1	78.1	-4.2	GEOROC
770	16.3	77.3	0.7420	GEOROC	13.1	78.1	8.6	GEOROC
771	16.3	77.3	0.8750	GEOROC	13.1	78.1	14.4	GEOROC
772	16.3	77.3	0.9980	GEOROC	13.1	78.1	-4.2	GEOROC
773	16.3	77.3	0.7420	GEOROC	13.1	78.1	16.4	GEOROC
774	16.3	77.3	0.7810	GEOROC	13.1	78.1	-10.5	GEOROC
775	16.3	77.3	0.7340	GEOROC	13.1	78.1	-9.2	GEOROC
776	16.3	77.3	0.7230	GEOROC	14.3	77.6	-20.2	GEOROC
777	13.1	78.1	0.7020	GEOROC	14.3	77.6	-23.2	GEOROC
778	13.1	78.1	0.7030	GEOROC	14.3	77.6	-19.4	GEOROC
779	13.1	78.1	0.7020	GEOROC	14.3	77.6	-20.9	GEOROC
780	13.1	78.1	0.7060	GEOROC	14.3	77.6	-13.5	GEOROC
781	13.1	78.1	0.7030	GEOROC	14.3	77.6	-18.6	GEOROC
782	13.1	78.1	0.7080	GEOROC	14.3	77.6	-24.4	GEOROC
783	13.1	78.1	0.7030	GEOROC	14.3	77.6	-24.2	GEOROC
784	13.1	78.1	0.7030	GEOROC	14.3	77.6	-21.7	GEOROC
785	14.0	76.3	0.7030	GEOROC	14.3	77.6	-17.9	GEOROC
786	14.0	76.3	0.7070	GEOROC	14.3	77.6	-26.9	GEOROC
787	14.0	76.3	0.7030	GEOROC	14.3	77.6	2.7	GEOROC
788	14.2	76.4	0.7170	GEOROC	14.3	77.6	5.5	GEOROC
789	14.2	76.4	0.7170	GEOROC	14.3	77.6	6.3	GEOROC
790	14.2	76.4	0.7240	GEOROC	14.3	77.6	5.0	GEOROC
791	14.2	76.4	0.8720	GEOROC	14.3	77.6	6.7	GEOROC
792	16.3	76.8	0.7030	GEOROC	14.3	77.6	5.7	GEOROC
793	16.3	76.8	0.7030	GEOROC	14.3	77.6	5.6	GEOROC
794	16.3	76.8	0.7020	GEOROC	14.3	77.6	4.5	GEOROC
795	16.3	76.8	0.7020	GEOROC	14.3	77.6	6.3	GEOROC
796	16.3	76.8	0.7100	GEOROC	14.3	77.6	4.7	GEOROC
797	16.3	76.8	0.7050	GEOROC	14.3	77.5	3.1	GEOROC
798	16.3	76.8	0.7090	GEOROC	14.3	77.5	-0.7	GEOROC
799	16.3	76.8	0.7080	GEOROC	14.3	77.5	0.7	GEOROC
800	16.3	76.8	0.7030	GEOROC	14.3	77.5	3.5	GEOROC
801	16.3	76.8	0.7340	GEOROC	14.3	77.5	3.5	GEOROC
802	16.3	76.8	0.7020	GEOROC	14.3	77.5	1.0	GEOROC
803	16.3	76.8	0.7090	GEOROC	14.3	77.5	4.3	GEOROC
804	16.3	76.8	0.7840	GEOROC	14.3	77.5	3.0	GEOROC
805	16.3	76.8	0.7100	GEOROC	14.3	77.5	1.4	GEOROC
806	13.1	78.1	0.7020	GEOROC	14.3	77.5	1.3	GEOROC
807	13.1	78.1	0.7020	GEOROC	14.3	77.5	2.1	GEOROC
808	13.1	78.1	0.7020	GEOROC	14.3	77.5	2.3	GEOROC
809	13.1	78.1	0.7040	GEOROC	14.3	77.5	1.4	GEOROC
810	13.1	78.1	0.7080	GEOROC	14.3	77.5	1.6	GEOROC
811	13.1	78.1	0.7160	GEOROC	14.0	76.3	-15.2	GEOROC

812	13.1	78.1	0.7080	GEOROC	14.0	76.3	-9.3	GEOROC
813	13.1	78.1	0.7080	GEOROC	13.5	76.5	-2.8	GEOROC
814	13.1	78.1	0.7190	GEOROC	13.5	76.5	-20.9	GEOROC
815	13.1	78.1	0.7030	GEOROC	13.5	76.5	-2.7	GEOROC
816	13.1	78.1	0.7360	GEOROC	13.5	76.5	9.9	GEOROC
817	13.1	78.1	0.7120	GEOROC	13.5	76.5	-5.6	GEOROC
818	13.1	78.1	0.7140	GEOROC	13.5	76.5	11.0	GEOROC
819	13.1	78.1	0.7200	GEOROC	13.3	76.7	10.6	GEOROC
820	13.1	76.4	0.7100	GEOROC	13.3	76.7	12.9	GEOROC
821	13.1	76.4	0.7150	GEOROC	13.3	76.7	12.8	GEOROC
822	13.1	76.4	0.7160	GEOROC	14.0	76.3	27.3	GEOROC
823	13.1	76.4	0.7060	GEOROC	13.3	76.7	20.4	GEOROC
824	13.1	76.4	0.7170	GEOROC	12.9	78.3	-20.5	GEOROC
825	13.1	76.4	0.7060	GEOROC	12.9	78.3	6.8	GEOROC
826	13.1	76.4	0.7280	GEOROC	12.9	78.3	14.5	GEOROC
827	13.1	76.4	0.7060	GEOROC	12.9	78.3	16.2	GEOROC
828	13.1	76.4	0.7060	GEOROC	13.1	76.4	-0.4	GEOROC
829	13.1	76.4	0.7060	GEOROC	13.1	76.4	-14.9	GEOROC
830	13.1	76.4	0.7260	GEOROC	13.1	76.4	9.5	GEOROC
831	13.1	76.4	0.7150	GEOROC	14.0	76.3	10.3	GEOROC
832	13.1	76.4	0.7240	GEOROC	14.0	76.3	-4.0	GEOROC
833	13.5	75.8	0.7080	GEOROC	14.0	76.3	0.1	GEOROC
834	13.5	75.8	0.7310	GEOROC	14.2	76.4	-3.8	GEOROC
835	13.5	75.8	0.7860	GEOROC	14.2	76.4	-3.6	GEOROC
836	13.1	77.8	0.7090	GEOROC	14.2	76.4	4.4	GEOROC
837	13.1	77.8	0.7120	GEOROC	14.2	76.4	-33.3	GEOROC
838	14.3	75.4	0.7040	GEOROC	14.2	79.7	-9.1	GEOROC
839	14.3	75.4	0.7250	GEOROC	14.2	79.7	-11.4	GEOROC
840	14.3	75.4	1.3120	GEOROC	14.2	79.7	-10.6	GEOROC
841	14.0	76.3	0.8430	GEOROC	14.2	79.7	-14.1	GEOROC
842	14.0	76.3	0.8960	GEOROC	14.2	79.7	-10.1	GEOROC
843	14.0	76.3	1.1200	GEOROC	14.2	79.7	-13.6	GEOROC
844	14.0	76.3	0.7090	GEOROC	14.2	79.7	-13.8	GEOROC
845	14.0	76.3	0.7270	GEOROC	14.2	79.7	-11.3	GEOROC
846	16.3	77.3	0.7010	GEOROC	14.2	79.7	-11.4	GEOROC
847	16.3	77.3	0.7640	GEOROC	14.2	79.7	-13.1	GEOROC
848	16.3	77.3	0.8560	GEOROC	14.2	79.7	-25.7	GEOROC
849	16.3	77.3	0.9040	GEOROC	14.2	79.7	-27.5	GEOROC
850	15.1	76.6	0.7060	GEOROC	14.2	79.7	-27.1	GEOROC
851	15.1	76.6	0.7180	GEOROC	14.2	79.7	-16.2	GEOROC
852	15.1	76.6	0.7580	GEOROC	14.2	79.7	-0.9	GEOROC
853	16.3	77.3	0.7190	GEOROC	14.2	79.7	-2.7	GEOROC
854	16.3	77.3	1.0530	GEOROC	14.2	79.7	-16.1	GEOROC
855	16.3	77.3	0.9370	GEOROC	14.2	79.7	-12.7	GEOROC

856	16.3	77.3	0.7360	GEOROC	14.2	79.7	-3.0	GEOROC
857	16.3	77.3	0.7780	GEOROC	14.2	79.7	-10.2	GEOROC
858	16.3	77.3	0.9280	GEOROC	14.2	79.7	-1.7	GEOROC
859	16.3	77.3	0.8560	GEOROC	14.2	79.7	-3.6	GEOROC
860	16.3	77.3	1.0290	GEOROC	14.2	79.7	-13.2	GEOROC
861	16.3	77.3	0.7380	GEOROC	14.2	79.7	-12.9	GEOROC
862	16.3	77.3	0.7510	GEOROC	14.2	79.7	-10.7	GEOROC
863	16.3	77.3	0.9200	GEOROC	14.2	79.7	-16.1	GEOROC
864	13.5	75.8	0.7030	GEOROC	14.2	79.7	1.4	GEOROC
865	13.5	75.8	0.7520	GEOROC	14.2	79.7	-9.3	GEOROC
866	13.5	75.8	0.7800	GEOROC	14.2	79.7	-27.3	GEOROC
867	13.5	75.8	0.8070	GEOROC	14.2	79.7	-21.0	GEOROC
868	13.5	75.8	0.8150	GEOROC	16.3	76.8	1.5	GEOROC
869	13.5	75.8	0.8470	GEOROC	16.3	76.8	1.3	GEOROC
870	13.3	75.8	0.7100	GEOROC	16.3	76.8	-0.1	GEOROC
871	13.1	77.8	0.7120	GEOROC	16.3	76.8	1.1	GEOROC
872	14.3	75.4	0.7080	GEOROC	16.3	76.8	-26.2	GEOROC
873	14.3	75.4	0.7190	GEOROC	16.3	76.8	5.8	GEOROC
874	14.2	75.8	1.3490	GEOROC	16.3	76.8	7.2	GEOROC
875	14.3	75.4	1.5280	GEOROC	16.3	76.8	-0.9	GEOROC
876	14.2	76.4	0.7090	GEOROC	16.3	76.8	2.3	GEOROC
877	14.2	76.4	0.8500	GEOROC	16.3	76.8	-8.8	GEOROC
878	14.0	76.3	0.9770	GEOROC	16.3	76.8	4.7	GEOROC
879	14.0	76.3	0.7130	GEOROC	16.3	76.8	-34.4	GEOROC
880	14.0	76.3	0.7310	GEOROC	16.3	76.8	-31.2	GEOROC
881	14.0	76.3	0.7130	GEOROC	16.3	76.8	-27.7	GEOROC
882	16.3	77.3	0.7010	GEOROC	15.1	76.8	-37.8	GEOROC
883	16.3	77.3	0.7040	GEOROC	15.1	76.8	-41.4	GEOROC
884	16.3	77.3	0.7240	GEOROC	15.1	76.8	-34.1	GEOROC
885	16.3	77.3	0.7720	GEOROC	15.9	76.2	-30.5	GEOROC
886	16.3	77.3	0.8740	GEOROC	15.9	76.2	-30.4	GEOROC
887	16.3	77.3	0.8720	GEOROC	15.9	76.2	-24.5	GEOROC
888	16.3	77.3	0.8870	GEOROC	16.1	76.8	-31.3	GEOROC
889	15.1	76.6	0.7070	GEOROC	16.1	76.8	-27.3	GEOROC
890	15.1	76.6	0.7070	GEOROC	16.1	76.8	-34.2	GEOROC
891	15.1	76.6	0.7070	GEOROC	15.1	76.8	-36.2	GEOROC
892	15.1	76.6	0.7100	GEOROC	15.1	76.8	-31.9	GEOROC
893	15.1	76.6	0.7100	GEOROC	15.9	76.2	-33.9	GEOROC
894	15.1	76.6	0.7350	GEOROC	15.9	76.2	-42.1	GEOROC
895	13.3	75.8	0.7340	GEOROC	15.9	76.2	-31.1	GEOROC
896	13.3	75.8	0.7280	GEOROC	16.1	76.8	-26.5	GEOROC
897	13.3	75.8	0.7260	GEOROC	16.1	76.8	-46.0	GEOROC
898	13.3	75.8	0.7170	GEOROC	16.1	76.8	-36.1	GEOROC
899	13.3	75.8	0.7330	GEOROC	16.1	76.8	4.4	GEOROC

900	13.3	75.8	0.7370	GEOROC	16.1	76.8	4.1	GEOROC
901	13.3	75.8	0.7040	GEOROC	16.1	78.8	-9.8	GEOROC
902	13.3	75.8	0.7120	GEOROC	16.1	78.8	-7.0	GEOROC
903	13.3	75.8	0.7060	GEOROC	16.1	78.8	34.6	GEOROC
904	13.3	75.8	0.7190	GEOROC	16.1	78.8	-7.6	GEOROC
905	13.3	75.8	0.7090	GEOROC	16.1	78.8	2.5	GEOROC
906	16.3	77.3	0.7210	GEOROC	16.1	78.8	1.2	GEOROC
907	16.3	77.3	1.1030	GEOROC	16.1	78.8	-2.3	GEOROC
908	16.3	77.3	1.0350	GEOROC	16.1	78.8	-5.4	GEOROC
909	16.3	77.3	0.7420	GEOROC	16.1	78.8	-1.4	GEOROC
910	16.3	77.3	0.8750	GEOROC	16.1	78.8	-4.7	GEOROC
911	16.3	77.3	0.9980	GEOROC	16.1	78.8	-26.7	GEOROC
912	16.3	77.3	0.7420	GEOROC	16.1	78.8	-32.8	GEOROC
913	16.3	77.3	0.7810	GEOROC	16.1	78.8	-28.1	GEOROC
914	16.3	77.3	0.7340	GEOROC	16.1	78.8	-27.8	GEOROC
915	16.3	77.3	0.7230	GEOROC	16.1	78.8	-25.4	GEOROC
916	13.1	78.1	0.7020	GEOROC	16.1	78.8	-25.7	GEOROC
917	13.1	78.1	0.7030	GEOROC	16.1	78.8	-29.4	GEOROC
918	13.1	78.1	0.7020	GEOROC	16.1	78.8	-32.9	GEOROC
919	13.1	78.1	0.7060	GEOROC	16.1	78.8	-28.9	GEOROC
920	13.1	78.1	0.7030	GEOROC	14.3	76.3	-30.0	GEOROC
921	13.1	78.1	0.7080	GEOROC	14.3	76.3	-31.4	GEOROC
922	13.1	78.1	0.7030	GEOROC	14.3	76.3	-26.8	GEOROC
923	13.1	78.1	0.7030	GEOROC	14.3	76.3	-36.8	GEOROC
924	14.0	76.3	0.7030	GEOROC	12.9	78.3	-35.7	GEOROC
925	14.0	76.3	0.7070	GEOROC	12.9	78.3	-33.4	GEOROC
926	14.0	76.3	0.7030	GEOROC	12.9	78.3	-38.7	GEOROC
927	14.2	76.4	0.7170	GEOROC	12.9	78.3	-25.3	GEOROC
928	14.2	76.4	0.7170	GEOROC	14.0	78.0	-32.4	GEOROC
929	14.2	76.4	0.7240	GEOROC	14.0	78.0	-33.6	GEOROC
930	14.2	76.4	0.8720	GEOROC	14.0	78.5	-29.6	GEOROC
931	16.3	76.8	0.7030	GEOROC	15.3	77.6	-21.0	GEOROC
932	16.3	76.8	0.7030	GEOROC	16.7	79.2	-21.1	GEOROC
933	16.3	76.8	0.7020	GEOROC	14.2	76.4	-32.5	GEOROC
934	16.3	76.8	0.7020	GEOROC	14.2	76.4	-31.0	GEOROC
935	16.3	76.8	0.7100	GEOROC	14.2	76.4	-31.1	GEOROC
936	16.3	76.8	0.7050	GEOROC	14.2	76.4	-30.5	GEOROC
937	16.3	76.8	0.7090	GEOROC	13.5	75.8	-31.0	GEOROC
938	16.3	76.8	0.7080	GEOROC	13.5	75.8	-23.6	GEOROC
939	16.3	76.8	0.7030	GEOROC	13.5	75.8	-20.4	GEOROC
940	16.3	76.8	0.7340	GEOROC	13.5	75.8	-19.4	GEOROC
941	16.3	76.8	0.7020	GEOROC	13.5	75.8	-15.7	GEOROC
942	16.3	76.8	0.7090	GEOROC	13.5	75.8	-26.7	GEOROC
943	16.3	76.8	0.7840	GEOROC	13.4	75.6	-23.8	GEOROC

944	16.3	76.8	0.7100	GEOROC	13.4	75.6	-20.2	GEOROC
945	34.0	74.9	0.7630	GEOROC	13.4	75.6	-19.6	GEOROC
946	34.0	75.0	0.7140	GEOROC	13.4	75.6	-17.9	GEOROC
947	34.0	75.0	0.7130	GEOROC	13.4	75.6	-0.4	GEOROC
948	34.0	75.0	0.7110	GEOROC	13.4	75.6	-19.1	GEOROC
949	34.0	75.0	0.7110	GEOROC	13.4	75.6	-16.2	GEOROC
950	34.0	75.0	0.7150	GEOROC	13.4	75.6	-20.9	GEOROC
951	34.0	75.0	0.7150	GEOROC	13.4	75.6	-19.4	GEOROC
952	34.0	75.0	0.7120	GEOROC	14.0	78.0	-1.1	GEOROC
953	34.0	75.0	0.7120	GEOROC	14.0	78.0	-9.1	GEOROC
954	34.0	75.0	0.7120	GEOROC	14.0	78.0	-25.0	GEOROC
955	34.0	75.0	0.7120	GEOROC	14.0	78.0	-28.9	GEOROC
956	34.1	74.8	0.7090	GEOROC	14.0	78.0	-31.3	GEOROC
957	34.1	74.8	0.7120	GEOROC	14.0	78.0	-34.2	GEOROC
958	34.1	74.8	0.7090	GEOROC	14.0	78.0	-9.1	GEOROC
959	34.1	74.8	0.7090	GEOROC	14.0	76.3	-17.8	GEOROC
960	34.1	74.8	0.7090	GEOROC	14.0	76.3	8.1	GEOROC
961	34.1	74.8	0.7110	GEOROC	14.0	76.3	25.3	GEOROC
962	34.1	74.8	0.7100	GEOROC	14.0	76.3	20.7	GEOROC
963	34.1	74.8	0.7100	GEOROC	14.0	76.3	-28.6	GEOROC
964	34.1	74.8	0.7100	GEOROC	14.0	76.3	11.4	GEOROC
965	34.1	74.8	0.7090	GEOROC	14.0	76.3	39.7	GEOROC
966	34.1	74.8	0.7050	GEOROC	14.0	76.3	33.9	GEOROC
967	34.1	74.8	0.7050	GEOROC	14.0	76.3	34.3	GEOROC
968	34.0	75.3	0.7090	GEOROC	14.0	76.3	6.0	GEOROC
969	34.0	75.3	0.7100	GEOROC	14.0	76.3	-19.2	GEOROC
970	34.0	75.3	0.7060	GEOROC	14.0	76.3	-19.6	GEOROC
971	34.0	75.3	0.7140	GEOROC	13.8	78.5	-1.2	GEOROC
972	34.0	75.3	0.7130	GEOROC	13.8	78.5	-1.2	GEOROC
973	34.0	75.3	0.7160	GEOROC	13.8	78.5	-0.9	GEOROC
974	34.0	75.3	0.7080	GEOROC	13.8	78.5	-4.6	GEOROC
975	34.0	75.3	0.7070	GEOROC	13.8	78.5	-2.0	GEOROC
976	34.0	74.9	0.7500	GEOROC	13.8	78.4	0.4	GEOROC
977	34.0	74.9	0.7580	GEOROC	13.8	78.4	-3.7	GEOROC
978	34.0	74.9	0.7300	GEOROC	13.8	78.4	-5.2	GEOROC
979	34.0	74.9	0.7300	GEOROC	14.0	78.5	-2.3	GEOROC
980	34.0	74.9	0.7260	GEOROC	14.0	78.5	-0.3	GEOROC
981	34.0	74.9	0.7300	GEOROC	14.0	78.5	3.4	GEOROC
982	17.1	81.6	0.7060	GEOROC	14.0	78.4	-27.5	GEOROC
983	17.1	81.6	0.7050	GEOROC	14.1	78.4	-23.0	GEOROC
984	17.1	81.6	0.7050	GEOROC	14.2	78.4	-8.5	GEOROC
985	17.1	81.6	0.7050	GEOROC	14.2	78.4	-8.1	GEOROC
986	17.1	81.6	0.7060	GEOROC	14.2	78.4	-12.4	GEOROC
987	17.1	81.6	0.7060	GEOROC	14.2	78.4	-19.5	GEOROC

988	26.0	92.5	0.7070	GEOROC	13.8	78.5	-25.4	GEOROC
989	26.0	92.5	0.7070	GEOROC	14.0	78.5	-12.3	GEOROC
990	26.0	92.5	0.7090	GEOROC	14.0	78.5	-29.7	GEOROC
991	26.0	92.5	0.7070	GEOROC	14.0	78.5	-29.7	GEOROC
992	26.0	92.5	0.7080	GEOROC	13.8	78.5	-4.6	GEOROC
993	26.2	93.3	0.7080	GEOROC	14.2	78.4	-6.5	GEOROC
994	26.2	93.3	0.7100	GEOROC	14.1	78.4	-23.1	GEOROC
995	26.2	93.3	0.7060	GEOROC	14.0	75.5	6.3	GEOROC
996	26.2	93.3	0.7090	GEOROC	14.0	75.5	-0.3	GEOROC
997	26.2	93.3	0.7070	GEOROC	14.0	75.5	-13.5	GEOROC
998	26.2	93.3	0.7080	GEOROC	14.0	75.5	-0.4	GEOROC
999	25.6	92.1	0.7050	GEOROC	14.0	75.5	8.5	GEOROC
1000	25.6	92.1	0.7080	GEOROC	14.0	75.5	-29.0	GEOROC
1001	25.6	92.1	0.7060	GEOROC	14.0	75.5	5.4	GEOROC
1002	25.6	92.1	0.7050	GEOROC	14.0	75.5	-29.1	GEOROC
1003	25.6	92.1	0.7050	GEOROC	14.0	75.5	-5.8	GEOROC
1004	25.6	92.1	0.7050	GEOROC	14.0	75.5	-3.6	GEOROC
1005	25.6	92.1	0.7050	GEOROC	14.0	75.5	-12.9	GEOROC
1006	25.6	92.1	0.7050	GEOROC	14.0	75.5	-7.0	GEOROC
1007	25.2	87.7	0.7080	GEOROC	14.0	75.5	-3.8	GEOROC
1008	25.2	87.7	0.7070	GEOROC	14.0	75.5	-11.3	GEOROC
1009	25.2	87.7	0.7060	GEOROC	14.3	77.6	1.2	GEOROC
1010	25.2	87.7	0.7070	GEOROC	14.3	77.6	-0.2	GEOROC
1011	25.2	87.7	0.7070	GEOROC	14.3	77.5	4.0	GEOROC
1012	25.2	87.7	0.7070	GEOROC	14.3	77.5	3.9	GEOROC
1013	25.0	87.7	0.7080	GEOROC	14.3	77.6	5.5	GEOROC
1014	25.0	87.7	0.7040	GEOROC	14.3	77.6	-23.0	GEOROC
1015	25.0	87.7	0.7040	GEOROC	14.3	77.5	-20.5	GEOROC
1016	25.0	87.7	0.7080	GEOROC	14.3	77.6	-25.3	GEOROC
1017	25.0	87.7	0.7080	GEOROC	14.3	77.6	-25.2	GEOROC
1018	25.0	87.7	0.7080	GEOROC	14.3	77.5	-13.1	GEOROC
1019	25.0	87.7	0.7040	GEOROC	14.3	77.6	8.7	GEOROC
1020	25.0	87.7	0.7050	GEOROC	14.3	77.6	-14.4	GEOROC
1021	25.0	87.7	0.7050	GEOROC	14.3	77.6	15.5	GEOROC
1022	25.0	87.7	0.7210	GEOROC	14.3	77.6	-39.8	GEOROC
1023	25.1	87.7	0.7090	GEOROC	14.3	77.6	16.6	GEOROC
1024	25.1	87.7	0.7080	GEOROC	14.3	77.6	-33.9	GEOROC
1025	25.1	87.7	0.7040	GEOROC	13.1	78.1	-0.8	GEOROC
1026	25.1	87.7	0.7050	GEOROC	13.1	78.1	-0.1	GEOROC
1027	25.1	87.7	0.7060	GEOROC	13.1	78.1	0.6	GEOROC
1028	25.0	86.0	0.7060	GEOROC	13.1	78.1	-3.3	GEOROC
1029	25.0	86.0	0.7050	GEOROC	13.1	78.1	-2.8	GEOROC
1030	25.0	86.0	0.7070	GEOROC	13.1	78.1	1.2	GEOROC
1031	27.3	88.3	0.7070	GEOROC	13.1	78.1	1.0	GEOROC

1032	27.3	88.3	0.7120	GEOROC	13.1	78.1	0.1	GEOROC
1033	27.3	88.3	0.7060	GEOROC	13.1	78.1	-11.2	GEOROC
1034	27.3	88.3	0.7090	GEOROC	13.1	78.1	5.5	GEOROC
1035	27.3	88.3	0.7080	GEOROC	13.1	78.1	18.2	GEOROC
1036	27.3	88.3	0.7070	GEOROC	13.1	78.1	20.0	GEOROC
1037	27.3	88.3	0.7070	GEOROC	13.1	78.1	13.8	GEOROC
1038	27.3	88.3	0.7070	GEOROC	13.1	78.1	14.1	GEOROC
1039	27.3	88.3	0.7070	GEOROC	13.1	78.1	13.4	GEOROC
1040	27.3	88.3	0.7070	GEOROC	13.1	78.1	13.3	GEOROC
1041	27.3	88.3	0.7080	GEOROC	13.1	78.1	6.8	GEOROC
1042	27.3	88.3	0.7090	GEOROC	13.1	78.1	24.0	GEOROC
1043	27.3	88.3	0.7150	GEOROC	13.1	78.1	-9.7	GEOROC
1044	27.0	94.0	0.7050	GEOROC	13.1	78.1	-12.4	GEOROC
1045	27.0	94.0	0.7050	GEOROC	13.1	78.1	-9.4	GEOROC
1046	27.0	94.0	0.7050	GEOROC	13.1	78.1	-11.3	GEOROC
1047	27.0	94.0	0.7060	GEOROC	13.1	78.1	-4.3	GEOROC
1048	27.0	94.0	0.7100	GEOROC	13.2	76.3	2.9	GEOROC
1049	27.0	94.0	0.7070	GEOROC	13.2	76.3	1.9	GEOROC
1050	27.0	94.0	0.7070	GEOROC	13.2	76.3	3.3	GEOROC
1051	27.0	94.0	0.7110	GEOROC	13.2	76.3	2.3	GEOROC
1052	27.0	94.0	0.7140	GEOROC	13.2	76.3	2.7	GEOROC
1053	27.0	94.0	0.7080	GEOROC	13.2	76.3	2.6	GEOROC
1054	27.0	94.0	0.7080	GEOROC	13.2	76.3	2.5	GEOROC
1055	27.0	94.0	0.7040	GEOROC	13.2	76.3	1.8	GEOROC
1056	27.0	94.0	0.7290	GEOROC	13.2	76.3	1.4	GEOROC
1057	27.0	94.0	0.7120	GEOROC	13.2	76.3	2.2	GEOROC
1058	27.0	94.0	0.7070	GEOROC	13.2	76.5	1.3	GEOROC
1059	26.0	94.0	0.7070	GEOROC	13.2	76.5	1.7	GEOROC
1060	26.0	94.0	0.7070	GEOROC	13.2	76.5	1.4	GEOROC
1061	26.0	94.0	0.7080	GEOROC	13.2	76.5	1.3	GEOROC
1062	26.0	94.0	0.7060	GEOROC	13.2	76.5	1.8	GEOROC
1063	26.0	94.0	0.7080	GEOROC	13.1	76.4	-15.8	GEOROC
1064	26.0	94.0	0.7160	GEOROC	13.1	76.4	-22.2	GEOROC
1065	26.0	94.0	0.7090	GEOROC	13.1	76.4	-18.2	GEOROC
1066	26.0	94.0	0.7160	GEOROC	13.1	76.4	-1.5	GEOROC
1067	26.0	94.0	0.7140	GEOROC	13.1	76.4	-22.6	GEOROC
1068	26.0	94.0	0.7120	GEOROC	13.1	76.4	-3.7	GEOROC
1069	25.6	92.1	0.7050	GEOROC	13.1	76.4	-21.0	GEOROC
1070	25.6	92.1	0.7050	GEOROC	13.1	76.4	-20.1	GEOROC
1071	25.6	92.1	0.7050	GEOROC	13.1	76.4	-16.5	GEOROC
1072	25.6	92.1	0.7040	GEOROC	13.1	76.4	-22.7	GEOROC
1073	25.6	92.1	0.7040	GEOROC	13.1	76.4	-0.2	GEOROC
1074	25.6	92.1	0.7060	GEOROC	13.1	76.4	-15.9	GEOROC
1075	25.6	92.1	0.7060	GEOROC	13.1	76.4	-15.6	GEOROC

1076	25.6	92.1	0.7070	GEOROC	13.1	76.4	-17.8	GEOROC
1077	25.6	92.1	0.7060	GEOROC	13.1	76.4	-14.7	GEOROC
1078	25.6	92.1	0.7120	GEOROC	15.1	76.7	-8.8	GEOROC
1079	25.6	92.1	0.7120	GEOROC	15.1	76.7	0.7	GEOROC
1080	25.6	92.1	0.7110	GEOROC	15.1	76.7	1.8	GEOROC
1081	25.6	92.1	0.7110	GEOROC	15.1	76.7	1.2	GEOROC
1082	25.6	92.1	0.7060	GEOROC	15.1	76.7	5.6	GEOROC
1083	25.6	92.1	0.7160	GEOROC	15.1	76.7	3.6	GEOROC
1084	25.6	92.1	0.7090	GEOROC	15.1	76.7	3.8	GEOROC
1085	25.6	92.1	0.7260	GEOROC	15.1	76.7	3.2	GEOROC
1086	25.6	92.1	0.8030	GEOROC	13.1	78.1	9.7	GEOROC
1087	24.3	87.5	0.7090	GEOROC	13.1	78.1	-4.2	GEOROC
1088	24.3	87.5	0.7040	GEOROC	13.1	78.1	8.6	GEOROC
1089	24.3	87.5	0.7080	GEOROC	13.1	78.1	14.4	GEOROC
1090	24.3	87.5	0.7080	GEOROC	13.1	78.1	-4.2	GEOROC
1091	24.3	87.5	0.7070	GEOROC	13.1	78.1	16.4	GEOROC
1092	24.3	87.5	0.7050	GEOROC	13.1	78.1	-10.5	GEOROC
1093	24.3	87.5	0.7080	GEOROC	13.1	78.1	-9.2	GEOROC
1094	24.3	87.5	0.7050	GEOROC	14.3	77.6	-20.2	GEOROC
1095	24.3	87.5	0.7050	GEOROC	14.3	77.6	-23.2	GEOROC
1096	24.3	87.5	0.7080	GEOROC	14.3	77.6	-19.4	GEOROC
1097	25.6	92.1	0.7050	GEOROC	14.3	77.6	-20.9	GEOROC
1098	25.6	92.1	0.7050	GEOROC	14.3	77.6	-13.5	GEOROC
1099	25.6	92.1	0.7060	GEOROC	14.3	77.6	-18.6	GEOROC
1100	25.6	92.1	0.7110	GEOROC	14.3	77.6	-24.4	GEOROC
1101	25.6	92.1	0.7090	GEOROC	14.3	77.6	-24.2	GEOROC
1102	25.6	92.1	0.7050	GEOROC	14.3	77.6	-21.7	GEOROC
1103	24.3	87.5	0.7080	GEOROC	14.3	77.6	-17.9	GEOROC
1104	24.3	87.5	0.7040	GEOROC	14.3	77.6	-26.9	GEOROC
1105	24.3	87.5	0.7050	GEOROC	14.3	77.6	2.7	GEOROC
1106	24.3	87.5	0.7100	GEOROC	14.3	77.6	5.5	GEOROC
1107	24.3	87.5	0.7080	GEOROC	14.3	77.6	6.3	GEOROC
1108	24.3	87.5	0.7050	GEOROC	14.3	77.6	5.0	GEOROC
1109	24.3	87.5	0.7080	GEOROC	14.3	77.6	6.7	GEOROC
1110	31.0	77.5	0.7280	GEOROC	14.3	77.6	5.7	GEOROC
1111	31.0	77.5	0.7160	GEOROC	14.3	77.6	5.6	GEOROC
1112	31.8	77.3	0.7320	GEOROC	14.3	77.6	4.5	GEOROC
1113	12.5	78.5	0.7060	GEOROC	14.3	77.6	6.3	GEOROC
1114	12.5	78.5	0.7060	GEOROC	14.3	77.6	4.7	GEOROC
1115	12.5	78.5	0.7060	GEOROC	14.3	77.5	3.1	GEOROC
1116	12.5	78.5	0.7070	GEOROC	14.3	77.5	-0.7	GEOROC
1117	12.5	78.5	0.7130	GEOROC	14.3	77.5	0.7	GEOROC
1118	12.5	78.5	0.7090	GEOROC	14.3	77.5	3.5	GEOROC
1119	12.5	78.5	0.7190	GEOROC	14.3	77.5	3.5	GEOROC

1120	12.5	78.5	0.7050	GEOROC	14.3	77.5	1.0	GEOROC
1121	12.5	78.5	0.7100	GEOROC	14.3	77.5	4.3	GEOROC
1122	15.0	77.4	0.7140	GEOROC	14.3	77.5	3.0	GEOROC
1123	14.5	77.6	0.7030	GEOROC	14.3	77.5	1.4	GEOROC
1124	15.0	77.2	0.7030	GEOROC	14.3	77.5	1.3	GEOROC
1125	14.9	77.3	0.7060	GEOROC	14.3	77.5	2.1	GEOROC
1126	14.9	77.3	0.7100	GEOROC	14.3	77.5	2.3	GEOROC
1127	14.9	77.3	0.7050	GEOROC	14.3	77.5	1.4	GEOROC
1128	14.5	77.3	0.7040	GEOROC	14.3	77.5	1.6	GEOROC
1129	16.8	77.3	0.7040	GEOROC	14.0	76.3	-15.2	GEOROC
1130	16.9	77.3	0.7080	GEOROC	14.0	76.3	-9.3	GEOROC
1131	16.8	77.3	0.7050	GEOROC	13.5	76.5	-2.8	GEOROC
1132	17.1	77.3	0.7070	GEOROC	13.5	76.5	-20.9	GEOROC
1133	15.5	77.3	0.7450	GEOROC	13.5	76.5	-2.7	GEOROC
1134	15.5	77.3	0.7220	GEOROC	13.5	76.5	9.9	GEOROC
1135	15.3	77.3	0.7410	GEOROC	13.5	76.5	-5.6	GEOROC
1136	12.4	78.5	0.7050	GEOROC	13.5	76.5	11.0	GEOROC
1137	12.4	78.5	0.7050	GEOROC	13.3	76.7	10.6	GEOROC
1138	12.4	78.5	0.7050	GEOROC	13.3	76.7	12.9	GEOROC
1139	12.4	78.5	0.7070	GEOROC	13.3	76.7	12.8	GEOROC
1140	12.4	78.5	0.7050	GEOROC	14.0	76.3	27.3	GEOROC
1141	12.4	78.5	0.7050	GEOROC	13.3	76.7	20.4	GEOROC
1142	16.8	77.5	0.7040	GEOROC	12.9	78.3	-20.5	GEOROC
1143	16.8	77.7	0.7050	GEOROC	12.9	78.3	6.8	GEOROC
1144	14.9	77.3	0.7060	GEOROC	12.9	78.3	14.5	GEOROC
1145	15.0	77.5	0.7060	GEOROC	12.9	78.3	16.2	GEOROC
1146	15.0	77.5	0.7090	GEOROC	13.1	76.4	-0.4	GEOROC
1147	15.0	77.3	0.7060	GEOROC	13.1	76.4	-14.9	GEOROC
1148	15.0	77.3	0.7100	GEOROC	13.1	76.4	9.5	GEOROC
1149	14.8	77.3	0.7120	GEOROC	14.0	76.3	10.3	GEOROC
1150	14.5	77.7	0.7120	GEOROC	14.0	76.3	-4.0	GEOROC
1151	14.5	77.7	0.7080	GEOROC	14.0	76.3	0.1	GEOROC
1152	15.1	77.4	0.7140	GEOROC	14.2	76.4	-3.8	GEOROC
1153	15.1	77.4	0.7080	GEOROC	14.2	76.4	-3.6	GEOROC
1154	25.3	72.6	0.7140	GEOROC	14.2	76.4	4.4	GEOROC
1155	25.3	72.6	0.7140	GEOROC	14.2	76.4	-33.3	GEOROC
1156	16.8	77.4	0.7110	GEOROC	14.2	79.7	-9.1	GEOROC
1157	16.8	77.4	0.7110	GEOROC	14.2	79.7	-11.4	GEOROC
1158	16.8	77.4	0.7080	GEOROC	14.2	79.7	-10.6	GEOROC
1159	16.8	77.4	0.7070	GEOROC	14.2	79.7	-14.1	GEOROC
1160	16.8	77.4	0.7080	GEOROC	14.2	79.7	-10.1	GEOROC
1161	16.8	77.5	0.7130	GEOROC	14.2	79.7	-13.6	GEOROC
1162	16.8	77.7	0.7110	GEOROC	14.2	79.7	-13.8	GEOROC
1163	16.8	77.6	0.7130	GEOROC	14.2	79.7	-11.3	GEOROC

1164	16.8	77.3	0.7150	GEOROC	14.2	79.7	-11.4	GEOROC
1165	16.8	77.4	0.7180	GEOROC	14.2	79.7	-13.1	GEOROC
1166	16.8	77.4	0.7110	GEOROC	14.2	79.7	-25.7	GEOROC
1167	16.8	77.5	0.7070	GEOROC	14.2	79.7	-27.5	GEOROC
1168	16.7	77.6	0.7110	GEOROC	14.2	79.7	-27.1	GEOROC
1169	16.7	77.6	0.7100	GEOROC	14.2	79.7	-16.2	GEOROC
1170	12.5	78.5	0.7080	GEOROC	14.2	79.7	-0.9	GEOROC
1171	12.5	78.5	0.7190	GEOROC	14.2	79.7	-2.7	GEOROC
1172	12.5	78.5	0.7130	GEOROC	14.2	79.7	-16.1	GEOROC
1173	12.5	78.5	0.7090	GEOROC	14.2	79.7	-12.7	GEOROC
1174	12.5	78.5	0.7070	GEOROC	14.2	79.7	-3.0	GEOROC
1175	12.5	78.5	0.7320	GEOROC	14.2	79.7	-10.2	GEOROC
1176	12.5	78.5	0.7120	GEOROC	14.2	79.7	-1.7	GEOROC
1177	12.5	78.5	0.7250	GEOROC	14.2	79.7	-3.6	GEOROC
1178	12.5	78.5	0.7120	GEOROC	14.2	79.7	-13.2	GEOROC
1179	12.4	78.5	0.7060	GEOROC	14.2	79.7	-12.9	GEOROC
1180	12.4	78.5	0.7050	GEOROC	14.2	79.7	-10.7	GEOROC
1181	12.4	78.5	0.7420	GEOROC	14.2	79.7	-16.1	GEOROC
1182	12.4	78.5	0.7130	GEOROC	14.2	79.7	1.4	GEOROC
1183	12.5	78.5	0.7080	GEOROC	14.2	79.7	-9.3	GEOROC
1184	15.0	77.0	0.7090	GEOROC	14.2	79.7	-27.3	GEOROC
1185	15.0	77.0	0.7090	GEOROC	14.2	79.7	-21.0	GEOROC
1186	15.0	77.0	0.7110	GEOROC	16.3	76.8	1.5	GEOROC
1187	16.9	79.1	0.7090	GEOROC	16.3	76.8	1.3	GEOROC
1188	16.9	79.1	0.7080	GEOROC	16.3	76.8	-0.1	GEOROC
1189	16.9	79.1	0.7070	GEOROC	16.3	76.8	1.1	GEOROC
1190	16.9	79.1	0.7150	GEOROC	16.3	76.8	-26.2	GEOROC
1191	16.9	79.1	0.7120	GEOROC	16.3	76.8	5.8	GEOROC
1192	16.9	79.1	0.7130	GEOROC	16.3	76.8	7.2	GEOROC
1193	16.9	79.2	0.7070	GEOROC	16.3	76.8	-0.9	GEOROC
1194	16.9	79.0	0.7070	GEOROC	16.3	76.8	2.3	GEOROC
1195	14.1	78.1	0.7150	GEOROC	16.3	76.8	-8.8	GEOROC
1196	14.1	78.1	0.7190	GEOROC	16.3	76.8	4.7	GEOROC
1197	12.0	79.0	0.8110	GEOROC	16.3	76.8	-34.4	GEOROC
1198	18.7	78.9	0.7140	GEOROC	16.3	76.8	-31.2	GEOROC
1199	18.7	78.9	0.7220	GEOROC	16.3	76.8	-27.7	GEOROC
1200	18.7	78.9	0.7150	GEOROC	15.1	76.8	-37.8	GEOROC
1201	18.8	79.0	0.7150	GEOROC	15.1	76.8	-41.4	GEOROC
1202	18.8	79.0	0.7150	GEOROC	15.1	76.8	-34.1	GEOROC
1203	18.8	79.0	0.7150	GEOROC	15.9	76.2	-30.5	GEOROC
1204	18.8	79.0	0.7150	GEOROC	15.9	76.2	-30.4	GEOROC
1205	15.0	77.3	0.7070	GEOROC	15.9	76.2	-24.5	GEOROC
1206	15.0	77.3	0.7100	GEOROC	16.1	76.8	-31.3	GEOROC
1207	15.0	77.3	0.7110	GEOROC	16.1	76.8	-27.3	GEOROC

1208	15.0	77.3	0.7110	GEOROC	16.1	76.8	-34.2	GEOROC
1209	10.1	77.2	0.7540	GEOROC	15.1	76.8	-36.2	GEOROC
1210	10.1	77.2	0.7360	GEOROC	15.1	76.8	-31.9	GEOROC
1211	10.1	77.2	0.7450	GEOROC	15.9	76.2	-33.9	GEOROC
1212	10.1	77.2	0.7220	GEOROC	15.9	76.2	-42.1	GEOROC
1213	10.1	77.2	0.7180	GEOROC	15.9	76.2	-31.1	GEOROC
1214	10.1	77.2	0.7370	GEOROC	16.1	76.8	-26.5	GEOROC
1215	10.1	77.2	0.7130	GEOROC	16.1	76.8	-46.0	GEOROC
1216	10.1	77.2	0.7120	GEOROC	16.1	76.8	-36.1	GEOROC
1217	10.1	77.2	0.7110	GEOROC	16.1	76.8	4.4	GEOROC
1218	10.1	77.2	0.7200	GEOROC	16.1	76.8	4.1	GEOROC
1219	10.1	77.1	0.7230	GEOROC	16.1	78.8	-9.8	GEOROC
1220	10.1	77.1	0.7240	GEOROC	16.1	78.8	-7.0	GEOROC
1221	10.1	77.1	0.7390	GEOROC	16.1	78.8	-7.6	GEOROC
1222	10.1	77.1	0.7230	GEOROC	16.1	78.8	2.5	GEOROC
1223	10.1	77.1	0.7530	GEOROC	16.1	78.8	1.2	GEOROC
1224	10.1	77.1	0.7540	GEOROC	16.1	78.8	-2.3	GEOROC
1225	10.1	77.1	0.7160	GEOROC	16.1	78.8	-5.4	GEOROC
1226	10.1	77.1	0.7410	GEOROC	16.1	78.8	-1.4	GEOROC
1227	12.4	78.5	0.7050	GEOROC	16.1	78.8	-4.7	GEOROC
1228	12.4	78.5	0.7050	GEOROC	16.1	78.8	-26.7	GEOROC
1229	12.4	78.5	0.7050	GEOROC	16.1	78.8	-32.8	GEOROC
1230	12.4	78.5	0.7050	GEOROC	16.1	78.8	-28.1	GEOROC
1231	12.4	78.5	0.7050	GEOROC	16.1	78.8	-27.8	GEOROC
1232	12.4	78.5	0.7050	GEOROC	16.1	78.8	-25.4	GEOROC
1233	12.4	78.5	0.7050	GEOROC	16.1	78.8	-25.7	GEOROC
1234	12.4	78.5	0.7050	GEOROC	16.1	78.8	-29.4	GEOROC
1235	12.5	78.5	0.7050	GEOROC	16.1	78.8	-32.9	GEOROC
1236	12.5	78.5	0.7050	GEOROC	16.1	78.8	-28.9	GEOROC
1237	11.7	77.8	0.7050	GEOROC	14.3	76.3	-30.0	GEOROC
1238	12.4	78.5	0.7140	GEOROC	14.3	76.3	-31.4	GEOROC
1239	12.4	78.5	0.7130	GEOROC	14.3	76.3	-26.8	GEOROC
1240	12.4	78.5	0.7060	GEOROC	14.3	76.3	-36.8	GEOROC
1241	12.5	78.5	0.7150	GEOROC	12.9	78.3	-35.7	GEOROC
1242	12.5	78.5	0.7090	GEOROC	12.9	78.3	-33.4	GEOROC
1243	12.5	78.5	0.9340	GEOROC	12.9	78.3	-38.7	GEOROC
1244	12.5	78.5	0.7080	GEOROC	12.9	78.3	-25.3	GEOROC
1245	12.5	78.5	0.7210	GEOROC	14.0	78.0	-32.4	GEOROC
1246	12.5	78.5	0.7150	GEOROC	14.0	78.0	-33.6	GEOROC
1247	12.4	78.5	0.7070	GEOROC	14.0	78.5	-29.6	GEOROC
1248	12.2	77.8	0.7030	GEOROC	15.3	77.6	-21.0	GEOROC
1249	12.2	77.8	0.7020	GEOROC	16.7	79.2	-21.1	GEOROC
1250	12.2	77.8	0.7010	GEOROC	14.2	76.4	-32.5	GEOROC
1251	12.2	77.8	0.7020	GEOROC	14.2	76.4	-31.0	GEOROC

1252	16.3	77.9	0.7040	GEOROC	14.2	76.4	-31.1	GEOROC
1253	16.3	77.9	0.7040	GEOROC	14.2	76.4	-30.5	GEOROC
1254	12.2	77.8	0.7020	GEOROC	13.5	75.8	-31.0	GEOROC
1255	12.2	77.8	0.7020	GEOROC	13.5	75.8	-23.6	GEOROC
1256	12.2	77.8	0.7020	GEOROC	13.5	75.8	-20.4	GEOROC
1257	12.2	77.8	0.7020	GEOROC	13.5	75.8	-19.4	GEOROC
1258	12.2	77.8	0.7020	GEOROC	13.5	75.8	-15.7	GEOROC
1259	12.2	77.8	0.7020	GEOROC	13.5	75.8	-26.7	GEOROC
1260	12.2	77.8	0.7170	GEOROC	13.4	75.6	-23.8	GEOROC
1261	12.2	77.8	0.7100	GEOROC	13.4	75.6	-20.2	GEOROC
1262	12.2	77.8	0.7220	GEOROC	13.4	75.6	-19.6	GEOROC
1263	12.2	77.8	0.7140	GEOROC	13.4	75.6	-17.9	GEOROC
1264	12.2	77.8	0.7110	GEOROC	13.4	75.6	-0.4	GEOROC
1265	12.4	78.5	0.7050	GEOROC	13.4	75.6	-19.1	GEOROC
1266	12.4	78.5	0.7050	GEOROC	13.4	75.6	-16.2	GEOROC
1267	12.4	78.5	0.7050	GEOROC	13.4	75.6	-20.9	GEOROC
1268	12.4	78.5	0.7050	GEOROC	13.4	75.6	-19.4	GEOROC
1269	12.4	78.5	0.7050	GEOROC	34.0	74.9	-11.2	GEOROC
1270	12.4	78.5	0.7080	GEOROC	34.5	85.0	0.5	GEOROC
1271	12.4	78.5	0.7100	GEOROC	34.5	85.0	0.0	GEOROC
1272	12.4	78.5	0.7090	GEOROC	34.5	85.0	1.1	GEOROC
1273	12.4	78.5	0.7090	GEOROC	34.5	85.0	1.1	GEOROC
1274	12.4	78.5	0.7060	GEOROC	34.5	85.0	0.7	GEOROC
1275	12.4	78.5	0.7090	GEOROC	34.0	75.0	-2.6	GEOROC
1276	12.4	78.5	0.7060	GEOROC	34.0	75.0	-0.2	GEOROC
1277	15.0	79.0	0.7070	GEOROC	34.0	75.0	-1.0	GEOROC
1278	17.1	77.3	0.7080	GEOROC	34.0	75.0	-2.5	GEOROC
1279	16.8	80.2	0.7050	GEOROC	34.0	75.0	-2.4	GEOROC
1280	16.9	80.1	0.7070	GEOROC	34.0	75.0	-2.8	GEOROC
1281	15.0	79.0	0.7070	GEOROC	34.0	75.0	-1.0	GEOROC
1282	16.8	80.3	0.7360	GEOROC	34.0	75.0	1.6	GEOROC
1283	16.8	80.2	0.7070	GEOROC	34.0	75.0	-2.6	GEOROC
1284	17.0	80.0	0.7060	GEOROC	34.1	74.8	-4.3	GEOROC
1285	16.9	80.1	0.7070	GEOROC	34.1	74.8	-7.2	GEOROC
1286	16.8	80.2	0.7070	GEOROC	34.1	74.8	-4.5	GEOROC
1287	16.8	78.0	0.7400	GEOROC	34.1	74.8	-4.2	GEOROC
1288	16.8	78.0	0.7480	GEOROC	34.1	74.8	-4.2	GEOROC
1289	16.7	78.0	0.7460	GEOROC	34.1	74.8	-5.8	GEOROC
1290	16.7	78.0	0.7470	GEOROC	34.1	74.8	-5.7	GEOROC
1291	16.7	78.0	0.7500	GEOROC	34.1	74.8	-5.6	GEOROC
1292	16.9	77.7	0.7130	GEOROC	34.1	74.8	-8.3	GEOROC
1293	16.8	77.7	0.7260	GEOROC	34.1	74.8	-4.4	GEOROC
1294	16.8	77.7	0.7220	GEOROC	34.1	74.8	0.1	GEOROC
1295	16.8	77.7	0.7230	GEOROC	34.1	74.8	0.4	GEOROC

1296	15.0	77.2	0.7090	GEOROC	34.0	75.3	-3.7	GEOROC
1297	15.0	77.0	0.7070	GEOROC	34.0	75.3	-5.2	GEOROC
1298	15.0	77.4	0.7050	GEOROC	34.0	75.3	-1.9	GEOROC
1299	16.1	79.9	0.7090	GEOROC	34.0	75.3	-1.4	GEOROC
1300	16.1	79.9	0.7110	GEOROC	34.0	75.3	-4.9	GEOROC
1301	16.1	79.9	0.7080	GEOROC	34.0	75.3	-6.7	GEOROC
1302	16.1	79.9	0.7050	GEOROC	34.0	75.3	-8.3	GEOROC
1303	16.1	79.9	0.7090	GEOROC	34.0	75.3	-2.4	GEOROC
1304	16.1	79.9	0.7140	GEOROC	34.0	75.3	-0.9	GEOROC
1305	16.1	79.9	0.7130	GEOROC	34.0	74.9	-11.3	GEOROC
1306	16.1	79.9	0.7190	GEOROC	34.0	74.9	-11.3	GEOROC
1307	16.1	79.9	0.7180	GEOROC	34.0	74.9	-11.5	GEOROC
1308	16.1	79.9	0.7270	GEOROC	34.0	74.9	-11.2	GEOROC
1309	16.1	79.9	0.7070	GEOROC	34.0	74.9	-11.3	GEOROC
1310	16.1	79.9	0.7070	GEOROC	34.0	74.9	-11.3	GEOROC
1311	16.1	79.9	0.7150	GEOROC	26.0	92.5	-2.9	GEOROC
1312	16.1	79.9	0.7080	GEOROC	26.0	92.5	-2.1	GEOROC
1313	16.1	79.9	0.7090	GEOROC	26.0	92.5	-4.7	GEOROC
1314	16.1	79.9	0.7100	GEOROC	26.0	92.5	-5.9	GEOROC
1315	16.1	79.9	0.7130	GEOROC	26.0	92.5	-3.7	GEOROC
1316	12.2	77.8	0.7020	GEOROC	26.2	93.3	-1.5	GEOROC
1317	12.2	77.8	0.7020	GEOROC	26.2	93.3	-5.5	GEOROC
1318	12.4	78.5	0.7050	GEOROC	26.2	93.3	-1.3	GEOROC
1319	12.4	78.5	0.7050	GEOROC	26.2	93.3	-6.4	GEOROC
1320	12.5	78.5	0.7050	GEOROC	26.2	93.3	-2.8	GEOROC
1321	12.5	78.5	0.7060	GEOROC	26.2	93.3	-3.1	GEOROC
1322	12.5	78.5	0.7060	GEOROC	25.2	87.7	-4.4	GEOROC
1323	11.7	77.8	0.7070	GEOROC	25.2	87.7	-3.9	GEOROC
1324	11.7	77.8	0.7050	GEOROC	25.2	87.7	-4.8	GEOROC
1325	14.5	77.7	0.7080	GEOROC	25.2	87.7	-4.6	GEOROC
1326	13.1	78.1	0.7020	GEOROC	25.2	87.7	-6.0	GEOROC
1327	13.1	78.1	0.7020	GEOROC	25.2	87.7	-6.2	GEOROC
1328	13.1	78.1	0.7020	GEOROC	25.0	87.7	-5.6	GEOROC
1329	13.1	78.1	0.7040	GEOROC	25.0	87.7	2.8	GEOROC
1330	13.1	78.1	0.7080	GEOROC	25.0	87.7	1.6	GEOROC
1331	13.1	78.1	0.7160	GEOROC	25.0	87.7	-7.8	GEOROC
1332	13.1	78.1	0.7080	GEOROC	25.0	87.7	-8.0	GEOROC
1333	13.1	78.1	0.7080	GEOROC	25.0	87.7	-5.8	GEOROC
1334	13.1	78.1	0.7190	GEOROC	25.0	87.7	2.8	GEOROC
1335	13.1	78.1	0.7030	GEOROC	25.0	87.7	0.6	GEOROC
1336	13.1	78.1	0.7360	GEOROC	25.0	87.7	1.4	GEOROC
1337	13.1	78.1	0.7120	GEOROC	25.0	87.7	-7.0	GEOROC
1338	13.1	78.1	0.7140	GEOROC	25.1	87.7	-5.0	GEOROC
1339	13.1	78.1	0.7200	GEOROC	25.1	87.7	-7.0	GEOROC

1340	13.1	76.4	0.7100	GEOROC	25.1	87.7	2.8	GEOROC
1341	13.1	76.4	0.7150	GEOROC	25.1	87.7	1.6	GEOROC
1342	13.1	76.4	0.7160	GEOROC	25.1	87.7	-4.6	GEOROC
1343	13.1	76.4	0.7060	GEOROC	25.0	86.0	-3.9	GEOROC
1344	13.1	76.4	0.7170	GEOROC	25.0	86.0	2.2	GEOROC
1345	13.1	76.4	0.7060	GEOROC	25.0	86.0	0.6	GEOROC
1346	13.1	76.4	0.7280	GEOROC	27.3	88.3	-6.6	GEOROC
1347	13.1	76.4	0.7060	GEOROC	27.3	88.3	-5.0	GEOROC
1348	13.1	76.4	0.7060	GEOROC	27.3	88.3	-6.4	GEOROC
1349	13.1	76.4	0.7060	GEOROC	27.3	88.3	-5.8	GEOROC
1350	13.1	76.4	0.7260	GEOROC	27.3	88.3	-7.8	GEOROC
1351	13.1	76.4	0.7150	GEOROC	27.3	88.3	-5.2	GEOROC
1352	13.1	76.4	0.7240	GEOROC	27.3	88.3	-8.7	GEOROC
1353	13.5	75.8	0.7080	GEOROC	27.3	88.3	-7.4	GEOROC
1354	13.5	75.8	0.7310	GEOROC	27.3	88.3	-8.9	GEOROC
1355	13.5	75.8	0.7860	GEOROC	27.3	88.3	-7.8	GEOROC
1356	13.1	77.8	0.7090	GEOROC	27.3	88.3	-7.8	GEOROC
1357	13.1	77.8	0.7120	GEOROC	27.3	88.3	-9.7	GEOROC
1358	14.3	75.4	0.7040	GEOROC	27.3	88.3	-8.3	GEOROC
1359	14.3	75.4	0.7250	GEOROC	27.0	94.0	-0.7	GEOROC
1360	14.0	76.3	0.8430	GEOROC	27.0	94.0	-1.1	GEOROC
1361	14.0	76.3	0.8960	GEOROC	27.0	94.0	-0.2	GEOROC
1362	14.0	76.3	0.7090	GEOROC	27.0	94.0	-3.9	GEOROC
1363	14.0	76.3	0.7270	GEOROC	27.0	94.0	-3.7	GEOROC
1364	16.3	77.3	0.7010	GEOROC	27.0	94.0	-0.2	GEOROC
1365	16.3	77.3	0.7640	GEOROC	27.0	94.0	-2.9	GEOROC
1366	16.3	77.3	0.8550	GEOROC	27.0	94.0	-5.6	GEOROC
1367	16.3	77.3	0.9040	GEOROC	27.0	94.0	-16.0	GEOROC
1368	15.1	76.6	0.7060	GEOROC	27.0	94.0	-2.9	GEOROC
1369	15.1	76.6	0.7180	GEOROC	27.0	94.0	-4.3	GEOROC
1370	15.1	76.6	0.7580	GEOROC	27.0	94.0	-12.4	GEOROC
1371	16.3	77.3	0.7190	GEOROC	27.0	94.0	-19.1	GEOROC
1372	16.3	77.3	0.9370	GEOROC	27.0	94.0	-7.6	GEOROC
1373	16.3	77.3	0.7360	GEOROC	27.0	94.0	-4.3	GEOROC
1374	16.3	77.3	0.7780	GEOROC	26.0	94.0	-3.3	GEOROC
1375	16.3	77.3	0.9280	GEOROC	26.0	94.0	-1.5	GEOROC
1376	16.3	77.3	0.8560	GEOROC	26.0	94.0	-5.2	GEOROC
1377	16.3	77.3	0.7380	GEOROC	26.0	94.0	-2.5	GEOROC
1378	16.3	77.3	0.7510	GEOROC	26.0	94.0	-4.8	GEOROC
1379	16.3	77.3	0.9200	GEOROC	26.0	94.0	-5.2	GEOROC
1380	13.5	75.8	0.7030	GEOROC	26.0	94.0	-5.8	GEOROC
1381	13.5	75.8	0.7520	GEOROC	26.0	94.0	-11.7	GEOROC
1382	13.5	75.8	0.7800	GEOROC	26.0	94.0	-13.4	GEOROC
1383	13.5	75.8	0.8060	GEOROC	26.0	94.0	-5.4	GEOROC

1384	13.5	75.8	0.8150	GEOROC	25.6	92.1	-0.4	GEOROC
1385	13.5	75.8	0.8460	GEOROC	25.6	92.1	0.2	GEOROC
1386	13.3	75.8	0.7100	GEOROC	25.6	92.1	-0.4	GEOROC
1387	13.1	77.8	0.7110	GEOROC	25.6	92.1	0.2	GEOROC
1388	14.3	75.4	0.7080	GEOROC	25.6	92.1	-1.9	GEOROC
1389	14.3	75.4	0.7190	GEOROC	25.6	92.1	-0.4	GEOROC
1390	14.2	76.4	0.7090	GEOROC	25.6	92.1	-2.5	GEOROC
1391	14.2	76.4	0.8500	GEOROC	25.6	92.1	-1.9	GEOROC
1392	14.0	76.3	0.9760	GEOROC	25.6	92.1	-13.0	GEOROC
1393	14.0	76.3	0.7130	GEOROC	25.6	92.1	-14.0	GEOROC
1394	14.0	76.3	0.7310	GEOROC	25.6	92.1	-11.5	GEOROC
1395	14.0	76.3	0.7130	GEOROC	25.6	92.1	-11.9	GEOROC
1396	16.3	77.3	0.7010	GEOROC	25.6	92.1	-10.9	GEOROC
1397	16.3	77.3	0.7040	GEOROC	25.6	92.1	-6.8	GEOROC
1398	16.3	77.3	0.7240	GEOROC	25.6	92.1	-2.9	GEOROC
1399	16.3	77.3	0.7720	GEOROC	25.6	92.1	-7.2	GEOROC
1400	16.3	77.3	0.8740	GEOROC	25.6	92.1	-7.8	GEOROC
1401	16.3	77.3	0.8720	GEOROC	24.3	87.5	-0.8	GEOROC
1402	16.3	77.3	0.8870	GEOROC	24.3	87.5	1.7	GEOROC
1403	15.1	76.6	0.7070	GEOROC	24.3	87.5	-6.3	GEOROC
1404	15.1	76.6	0.7070	GEOROC	24.3	87.5	-5.3	GEOROC
1405	15.1	76.6	0.7070	GEOROC	24.3	87.5	-4.7	GEOROC
1406	15.1	76.6	0.7100	GEOROC	24.3	87.5	-2.2	GEOROC
1407	15.1	76.6	0.7100	GEOROC	24.3	87.5	-6.4	GEOROC
1408	15.1	76.6	0.7350	GEOROC	24.3	87.5	-3.0	GEOROC
1409	13.3	75.8	0.7340	GEOROC	24.3	87.5	-2.3	GEOROC
1410	13.3	75.8	0.7280	GEOROC	24.3	87.5	-5.7	GEOROC
1411	13.3	75.8	0.7260	GEOROC	25.6	92.1	-0.5	GEOROC
1412	13.3	75.8	0.7170	GEOROC	25.6	92.1	-0.5	GEOROC
1413	13.3	75.8	0.7330	GEOROC	25.6	92.1	-2.0	GEOROC
1414	13.3	75.8	0.7370	GEOROC	25.6	92.1	-12.2	GEOROC
1415	13.3	75.8	0.7040	GEOROC	25.6	92.1	-13.9	GEOROC
1416	13.3	75.8	0.7120	GEOROC	25.6	92.1	-5.2	GEOROC
1417	13.3	75.8	0.7060	GEOROC	24.3	87.5	0.0	GEOROC
1418	13.3	75.8	0.7190	GEOROC	24.3	87.5	1.9	GEOROC
1419	13.3	75.8	0.7090	GEOROC	24.3	87.5	-0.9	GEOROC
1420	16.3	77.3	0.7210	GEOROC	24.3	87.5	-7.5	GEOROC
1421	16.3	77.3	0.7420	GEOROC	24.3	87.5	-6.5	GEOROC
1422	16.3	77.3	0.8750	GEOROC	24.3	87.5	0.7	GEOROC
1423	16.3	77.3	0.9980	GEOROC	31.0	77.5	-14.7	GEOROC
1424	16.3	77.3	0.7420	GEOROC	31.0	77.5	-8.7	GEOROC
1425	16.3	77.3	0.7810	GEOROC	31.0	77.5	-18.6	GEOROC
1426	16.3	77.3	0.7340	GEOROC	31.0	77.5	-15.2	GEOROC
1427	16.3	77.3	0.7230	GEOROC	31.0	77.5	2.9	GEOROC

1428	13.1	78.1	0.7020	GEOROC	31.8	77.3	-16.1	GEOROC
1429	13.1	78.1	0.7020	GEOROC	31.8	77.3	-16.2	GEOROC
1430	13.1	78.1	0.7020	GEOROC	31.8	77.3	-14.5	GEOROC
1431	13.1	78.1	0.7060	GEOROC	31.8	77.3	-13.6	GEOROC
1432	13.1	78.1	0.7030	GEOROC	31.8	77.3	-16.6	GEOROC
1433	13.1	78.1	0.7080	GEOROC	30.3	79.0	2.1	GEOROC
1434	13.1	78.1	0.7030	GEOROC	30.3	79.0	1.9	GEOROC
1435	13.1	78.1	0.7030	GEOROC	30.3	79.0	-12.1	GEOROC
1436	14.0	76.3	0.7030	GEOROC	30.3	79.0	-13.5	GEOROC
1437	14.0	76.3	0.7070	GEOROC	30.3	79.0	-8.4	GEOROC
1438	14.0	76.3	0.7030	GEOROC	30.3	79.0	-14.7	GEOROC
1439	14.2	76.4	0.7170	GEOROC	30.3	79.0	-15.1	GEOROC
1440	14.2	76.4	0.7170	GEOROC	30.3	79.0	-13.8	GEOROC
1441	14.2	76.4	0.7240	GEOROC	30.3	79.0	-13.9	GEOROC
1442	14.2	76.4	0.8720	GEOROC	30.3	79.0	-13.7	GEOROC
1443	16.3	76.8	0.7030	GEOROC	30.2	79.2	0.4	GEOROC
1444	16.3	76.8	0.7030	GEOROC	30.3	79.0	-14.6	GEOROC
1445	16.3	76.8	0.7020	GEOROC	29.4	79.5	-13.6	GEOROC
1446	16.3	76.8	0.7020	GEOROC	29.4	79.5	-16.8	GEOROC
1447	16.3	76.8	0.7100	GEOROC	12.5	78.5	-11.2	GEOROC
1448	16.3	76.8	0.7050	GEOROC	12.5	78.5	-13.8	GEOROC
1449	16.3	76.8	0.7090	GEOROC	12.5	78.5	-13.5	GEOROC
1450	16.3	76.8	0.7080	GEOROC	12.5	78.5	-15.4	GEOROC
1451	16.3	76.8	0.7020	GEOROC	12.5	78.5	-16.7	GEOROC
1452	16.3	76.8	0.7340	GEOROC	12.5	78.5	-22.1	GEOROC
1453	16.3	76.8	0.7020	GEOROC	12.5	78.5	-17.9	GEOROC
1454	16.3	76.8	0.7090	GEOROC	12.5	78.5	-9.1	GEOROC
1455	16.3	76.8	0.7840	GEOROC	12.5	78.5	-17.4	GEOROC
1456	16.3	76.8	0.7100	GEOROC	15.0	77.4	-12.3	GEOROC
1457	11.2	78.3	0.7340	GEOROC	14.5	77.6	-12.4	GEOROC
1458	11.3	78.3	0.7020	GEOROC	15.0	77.2	-13.0	GEOROC
1459	11.4	78.1	0.7050	GEOROC	14.9	77.3	-14.2	GEOROC
1460	11.3	78.3	0.7130	GEOROC	14.9	77.3	-16.0	GEOROC
1461	11.3	78.3	0.7130	GEOROC	14.9	77.3	-13.2	GEOROC
1462	11.3	78.3	0.7120	GEOROC	14.5	77.3	-13.0	GEOROC
1463	11.3	78.3	0.7110	GEOROC	16.8	77.3	-13.0	GEOROC
1464	9.7	77.8	0.7100	GEOROC	16.9	77.3	-12.4	GEOROC
1465	10.0	77.8	0.7240	GEOROC	16.8	77.3	-13.0	GEOROC
1466	10.1	76.7	0.7260	GEOROC	17.1	77.3	-25.3	GEOROC
1467	9.1	77.5	0.7300	GEOROC	15.5	77.3	-28.8	GEOROC
1468	9.3	77.5	0.7060	GEOROC	15.3	77.3	-27.7	GEOROC
1469	10.0	76.4	0.7330	GEOROC	12.4	78.5	-14.5	GEOROC
1470	9.9	76.5	0.7260	GEOROC	12.4	78.5	-13.4	GEOROC
1471	10.2	76.5	0.7480	GEOROC	12.4	78.5	-14.8	GEOROC

1472	9.8	76.4	0.7310	GEOROC	12.4	78.5	-20.1	GEOROC
1473	9.6	76.8	0.7230	GEOROC	12.4	78.5	-15.3	GEOROC
1474	8.7	76.9	0.8300	GEOROC	12.4	78.5	-14.4	GEOROC
1475	8.9	77.3	0.7100	GEOROC	16.8	77.5	-13.1	GEOROC
1476	8.9	77.5	0.7270	GEOROC	16.8	77.7	-13.0	GEOROC
1477	8.7	77.4	0.7560	GEOROC	14.9	77.3	-14.1	GEOROC
1478	8.8	77.8	0.7120	GEOROC	12.5	78.5	-15.7	GEOROC
1479	8.7	77.8	0.7110	GEOROC	12.5	78.5	-15.5	GEOROC
1480	8.2	77.5	0.7120	GEOROC	12.5	78.5	-14.6	GEOROC
1481	8.2	77.5	0.7420	GEOROC	12.5	78.5	-22.7	GEOROC
1482	8.2	77.4	0.7400	GEOROC	12.5	78.5	-14.6	GEOROC
1483	10.6	78.8	0.7670	GEOROC	12.5	78.5	-17.9	GEOROC
1484	10.5	78.8	0.7890	GEOROC	12.5	78.5	-20.3	GEOROC
1485	10.4	78.7	0.7520	GEOROC	12.5	78.5	-22.3	GEOROC
1486	10.4	78.7	0.7390	GEOROC	12.4	78.5	-14.6	GEOROC
1487	10.4	78.7	0.7230	GEOROC	12.4	78.5	-15.0	GEOROC
1488	10.5	78.8	0.7550	GEOROC	12.4	78.5	-12.5	GEOROC
1489	10.6	78.8	0.7640	GEOROC	12.4	78.5	-33.4	GEOROC
1490	10.6	78.8	0.7510	GEOROC	12.5	78.5	-30.4	GEOROC
1491	10.4	78.7	0.7280	GEOROC	15.0	77.0	-37.1	GEOROC
1492	10.5	78.8	0.8030	GEOROC	15.0	77.0	-35.1	GEOROC
1493	10.6	78.8	0.7180	GEOROC	15.0	77.0	-35.3	GEOROC
1494	10.6	78.8	0.7160	GEOROC	16.9	79.1	-31.5	GEOROC
1495	12.0	77.1	0.7160	GEOROC	16.9	79.1	-32.0	GEOROC
1496	12.4	77.3	0.8400	GEOROC	16.9	79.1	-32.2	GEOROC
1497	12.0	77.1	0.7340	GEOROC	16.9	79.1	-32.8	GEOROC
1498	13.8	76.3	0.8620	GEOROC	16.9	79.1	-32.0	GEOROC
1499	13.9	76.3	0.8460	GEOROC	16.9	79.1	-32.1	GEOROC
1500	13.9	76.3	0.8780	GEOROC	16.9	79.2	-30.4	GEOROC
1501	13.9	76.3	0.8730	GEOROC	16.9	79.0	-30.9	GEOROC
1502	14.0	76.3	0.9740	GEOROC	14.1	78.1	-22.7	GEOROC
1503	13.9	76.3	0.8820	GEOROC	14.1	78.1	-29.0	GEOROC
1504	13.9	76.3	0.8500	GEOROC	12.0	79.0	-39.0	GEOROC
1505	13.9	76.3	0.7750	GEOROC	18.7	78.9	-12.7	GEOROC
1506	13.9	76.3	0.7350	GEOROC	18.7	78.9	-13.3	GEOROC
1507	13.9	76.3	0.7770	GEOROC	18.7	78.9	-12.7	GEOROC
1508	27.2	74.4	0.9200	(George & Ray, 2017)	18.8	79.0	-13.0	GEOROC
1509	26.7	73.7	0.7080	(George & Ray, 2017)	18.8	79.0	-12.8	GEOROC
1510	26.5	73.8	0.7080	(George & Ray, 2017)	18.8	79.0	-12.8	GEOROC
1511	26.9	73.5	0.7080	(George & Ray, 2017)	18.8	79.0	-13.3	GEOROC
1512	26.6	73.4	0.7930	(George & Ray, 2017)	15.0	77.3	-11.9	GEOROC

1513	26.4	73.1	0.7220	(George & Ray, 2017)	15.0	77.3	-12.6	GEOROC
1514	26.4	73.1	0.7220	(George & Ray, 2017)	15.0	77.3	-12.1	GEOROC
1515	26.4	73.1	0.7140	(George & Ray, 2017)	15.0	77.3	-14.0	GEOROC
1516	26.3	73.0	0.7140	(George & Ray, 2017)	10.1	77.2	-21.7	GEOROC
1517	26.6	73.4	0.8410	(George & Ray, 2017)	10.1	77.2	-20.9	GEOROC
1518	26.6	73.4	0.7920	(George & Ray, 2017)	10.1	77.2	-21.4	GEOROC
1519	26.9	71.9	0.7850	(George & Ray, 2017)	10.1	77.2	-14.3	GEOROC
1520	26.3	72.9	0.7130	(George & Ray, 2017)	10.1	77.2	-15.1	GEOROC
1521	26.3	73.0	0.7140	(George & Ray, 2017)	10.1	77.2	-15.2	GEOROC
1522	27.1	74.3	0.7170	(George & Ray, 2017)	10.1	77.2	-14.3	GEOROC
1523	27.2	74.4	0.7380	(George & Ray, 2017)	10.1	77.2	-12.6	GEOROC
1524	27.2	74.4	0.8740	(George & Ray, 2017)	10.1	77.2	-13.3	GEOROC
1525	26.4	73.1	0.7160	(George & Ray, 2017)	10.1	77.2	-11.1	GEOROC
1526	26.2	73.7	0.7290	(George & Ray, 2017)	10.1	77.1	-26.3	GEOROC
1527	26.8	73.7	0.8130	(George & Ray, 2017)	10.1	77.1	-20.4	GEOROC
1528	26.8	73.7	0.7480	(George & Ray, 2017)	10.1	77.1	-29.9	GEOROC
1529	26.8	73.7	0.7260	(George & Ray, 2017)	10.1	77.1	-31.1	GEOROC
1530	28.4	73.7	0.8100	(George & Ray, 2017)	10.1	77.1	-24.3	GEOROC
1531	26.6	73.8	0.8450	(George & Ray, 2017)	10.1	77.1	-24.1	GEOROC
1532	26.6	73.8	0.7340	(George & Ray, 2017)	10.1	77.1	-13.4	GEOROC
1533	26.6	73.8	0.7380	(George & Ray, 2017)	10.1	77.1	-30.1	GEOROC
1534	26.4	73.1	1.1580	(George & Ray, 2017)	12.4	78.5	-14.2	GEOROC
1535	26.6	72.3	0.8090	(George & Ray, 2017)	12.4	78.5	-16.3	GEOROC
1536	26.3	73.0	1.3670	(George & Ray, 2017)	12.4	78.5	-15.2	GEOROC
1537	26.5	73.4	0.7610	(George & Ray, 2017)	12.4	78.5	-16.3	GEOROC
1538	24.9	72.9	0.8570	(George & Ray, 2017)	12.4	78.5	-15.6	GEOROC
1539	24.9	72.9	0.7200	(George & Ray, 2017)	12.4	78.5	-17.8	GEOROC
1540	25.6	73.9	0.7180	(George & Ray, 2017)	12.4	78.5	-13.8	GEOROC

1541	25.6	73.9	0.7970	(George & Ray, 2017)	12.5	78.5	-8.8	GEOROC
1542	25.1	73.9	0.7290	(George & Ray, 2017)	11.7	77.8	-20.1	GEOROC
1543	25.8	74.1	0.8260	(George & Ray, 2017)	12.4	78.5	-16.2	GEOROC
1544	25.6	73.8	0.7980	(George & Ray, 2017)	12.4	78.5	-18.5	GEOROC
1545	25.8	74.0	0.9000	(George & Ray, 2017)	12.5	78.5	-19.1	GEOROC
1546	26.1	74.4	0.7590	(George & Ray, 2017)	12.5	78.5	-16.1	GEOROC
1547	26.1	74.5	0.7360	(George & Ray, 2017)	12.5	78.5	-15.7	GEOROC
1548	26.1	74.6	0.7540	(George & Ray, 2017)	12.5	78.5	-17.4	GEOROC
1549	26.1	74.6	0.7770	(George & Ray, 2017)	12.5	78.5	-23.9	GEOROC
1550	25.1	75.1	0.8680	(Shukla, 2011)	17.4	80.3	-30.8	GEOROC
1551	25.0	75.1	1.0780	(Shukla, 2011)	17.6	81.6	-24.6	GEOROC
1552	25.0	75.1	0.7860	(Shukla, 2011)	16.8	80.1	-24.9	GEOROC
1553	25.5	75.6	1.0530	(Shukla, 2011)	15.5	77.3	-29.4	GEOROC
1554	25.5	75.9	0.7420	(Shukla, 2011)	16.9	80.1	-23.0	GEOROC
1555	24.8	74.6	0.8850	(Shukla, 2011)	17.6	80.1	-25.0	GEOROC
1556	24.8	74.6	0.8180	(Shukla, 2011)	17.0	80.0	-24.3	GEOROC
1557	24.4	74.7	0.8300	(Shukla, 2011)	17.1	77.3	-25.2	GEOROC
1558	25.1	75.1	0.9630	(Shukla, 2011)	15.0	77.5	-23.9	GEOROC
1559	24.9	75.6	0.9000	(Shukla, 2011)	16.8	77.3	-14.5	GEOROC
1560	25.6	76.1	0.8010	(Shukla, 2011)	16.8	77.4	-12.3	GEOROC
1561	25.5	76.0	0.7830	(Shukla, 2011)	16.8	77.4	-12.9	GEOROC
1562	25.7	76.2	0.8650	(Shukla, 2011)	16.8	77.4	-13.1	GEOROC
1563	25.7	76.2	0.8050	(Shukla, 2011)	16.8	77.4	-12.7	GEOROC
1564	25.7	76.3	0.7720	(Shukla, 2011)	16.8	77.4	-12.2	GEOROC
1565	25.6	77.0	0.8240	(Shukla, 2011)	16.8	77.4	-12.3	GEOROC
1566	25.0	74.7	0.7860	(Shukla, 2011)	16.8	77.4	-12.1	GEOROC
1567	24.9	74.7	0.8120	(Shukla, 2011)	16.8	77.5	-11.1	GEOROC
1568	25.0	75.6	0.8490	(Shukla, 2011)	16.8	77.5	-13.4	GEOROC
1569	24.9	74.7	0.7290	(Shukla, 2011)	16.7	77.6	-11.2	GEOROC
1570	24.9	74.7	0.8100	(Shukla, 2011)	16.8	77.7	-12.2	GEOROC
1571	24.8	74.6	0.8270	(Shukla, 2011)	16.8	77.6	-12.1	GEOROC
1572	24.9	74.6	0.8650	(Shukla, 2011)	16.8	77.1	-18.9	GEOROC
1573	28.6	84.4	0.9394	GEOROC	16.8	77.1	-13.8	GEOROC
1574	28.6	84.4	0.7141	GEOROC	16.7	77.1	-12.3	GEOROC
1575	28.6	84.3	0.7346	GEOROC	16.7	77.1	-12.3	GEOROC
1576	28.6	84.5	0.7475	GEOROC	16.6	77.1	-11.6	GEOROC
1577	28.6	84.3	0.7451	GEOROC	16.6	77.1	-10.8	GEOROC
1578	28.6	84.6	0.7331	GEOROC	16.6	77.1	-11.2	GEOROC
1579	28.6	84.3	0.7336	GEOROC	15.0	77.4	-12.9	GEOROC

1580	28.6	84.7	0.7550	GEOROC	15.0	77.4	-12.7	GEOROC
1581	28.6	84.3	0.7332	GEOROC	15.0	77.5	-13.4	GEOROC
1582	28.6	84.7	0.7460	GEOROC	15.0	77.5	-13.2	GEOROC
1583	28.7	84.3	0.7453	GEOROC	14.9	77.3	-13.8	GEOROC
1584	28.6	84.7	0.7380	GEOROC	14.9	77.3	-13.6	GEOROC
1585	28.6	84.7	0.7344	GEOROC	14.8	77.3	-12.9	GEOROC
1586	28.6	84.3	0.7311	GEOROC	14.8	77.3	-12.4	GEOROC
1587	28.6	84.3	0.7393	GEOROC	14.5	77.7	-12.7	GEOROC
1588	28.6	84.7	0.7305	GEOROC	14.5	77.7	-13.0	GEOROC
1589	28.6	84.6	0.7290	GEOROC	14.5	77.6	-13.0	GEOROC
1590	28.7	84.3	0.8065	GEOROC	14.5	77.6	-12.6	GEOROC
1591	28.7	84.4	0.7519	GEOROC	14.5	77.6	-12.5	GEOROC
1592	28.6	84.7	0.7732	GEOROC	14.5	77.6	-12.4	GEOROC
1593	28.7	84.5	0.7443	GEOROC	14.8	77.3	-11.9	GEOROC
1594	28.7	84.7	0.7487	GEOROC	16.8	77.3	-13.6	GEOROC
1595	28.7	84.3	0.7890	GEOROC	16.8	77.3	-13.8	GEOROC
1596	28.6	84.7	0.7741	GEOROC	14.5	77.7	-6.8	GEOROC
1597	28.6	84.3	0.7807	GEOROC	14.8	77.3	-13.0	GEOROC
1598	28.7	84.7	0.7396	GEOROC	15.0	77.4	-15.0	GEOROC
1599	28.7	84.7	0.7647	GEOROC	12.2	77.8	-21.2	GEOROC
1600	28.8	84.8	0.7619	GEOROC	12.2	77.8	-24.0	GEOROC
1601	28.2	85.5	0.8255	GEOROC	12.2	77.8	-27.3	GEOROC
1602	28.2	85.4	0.7835	GEOROC	12.2	77.8	-25.8	GEOROC
1603	28.2	85.6	0.8036	GEOROC	12.2	77.8	-26.1	GEOROC
1604	28.3	85.6	0.8143	GEOROC	12.2	77.8	-26.8	GEOROC
1605	28.3	85.7	0.8305	GEOROC	12.2	77.8	-38.2	GEOROC
1606	28.3	85.6	0.8316	GEOROC	12.2	77.8	-42.6	GEOROC
1607	28.2	85.5	0.8770	GEOROC	12.2	77.8	-44.8	GEOROC
1608	28.2	85.5	0.7577	GEOROC	12.2	77.8	-40.2	GEOROC
1609	28.2	85.8	0.7504	GEOROC	12.2	77.8	-43.3	GEOROC
1610	28.2	85.7	0.7529	GEOROC	12.4	78.5	-15.0	GEOROC
1611	28.2	86.7	0.7526	GEOROC	12.4	78.5	-15.8	GEOROC
1612	28.2	85.6	0.7623	GEOROC	12.4	78.5	-15.4	GEOROC
1613	28.2	85.6	0.7608	GEOROC	12.4	78.5	-16.1	GEOROC
1614	28.2	85.7	0.7661	GEOROC	12.4	78.5	-13.8	GEOROC
1615	28.4	85.7	0.7720	GEOROC	12.4	78.5	-14.6	GEOROC
1616	28.3	80.3	0.8332	GEOROC	15.5	78.2	-9.1	GEOROC
1617	28.4	81.0	0.9641	GEOROC	15.5	78.2	-17.7	GEOROC
1618	28.3	82.0	0.8257	GEOROC	15.4	78.1	-9.4	GEOROC
1619	28.4	83.0	1.0176	GEOROC	14.5	79.0	-8.9	GEOROC
1620	28.4	84.0	0.8996	GEOROC	15.6	77.9	-13.1	GEOROC
1621	28.5	85.0	0.9370	GEOROC	14.5	78.8	-19.1	GEOROC
1622	23.0	89.0	0.7834	(Goodbred et al., 2014)	14.4	78.2	-18.2	GEOROC

1623	23.6	89.0	0.7750	(Goodbred et al., 2014)	14.4	78.2	-18.8	GEOROC
1624	23.9	89.1	0.7795	(Goodbred et al., 2014)	15.0	79.0	-23.4	GEOROC
1625	23.5	89.5	0.7737	(Goodbred et al., 2014)	17.1	77.3	-24.7	GEOROC
1626	23.1	89.6	0.7620	(Goodbred et al., 2014)	16.8	80.2	-24.1	GEOROC
1627	22.7	89.8	0.7688	(Goodbred et al., 2014)	16.9	80.1	-25.0	GEOROC
1628	22.0	90.3	0.7703	(Goodbred et al., 2014)	15.0	79.0	-24.7	GEOROC
1629	22.8	90.3	0.7204	(Goodbred et al., 2014)	16.8	80.3	-30.4	GEOROC
1630	23.1	90.9	0.7172	(Goodbred et al., 2014)	16.8	80.2	-26.5	GEOROC
1631	24.4	90.9	0.7300	(Goodbred et al., 2014)	17.0	80.0	-22.6	GEOROC
1632	24.5	91.2	0.7250	(Goodbred et al., 2014)	16.9	80.1	-24.2	GEOROC
1633	24.9	91.5	0.7290	(Goodbred et al., 2014)	16.8	80.2	-23.7	GEOROC
1634	28.6	78.8	0.7730	(Tripathi et al., 2013)	16.8	78.0	-7.4	GEOROC
1635	20.0	78.5	0.7843	(Tripathi et al., 2013)	16.8	78.0	-6.5	GEOROC
1636	26.4	79.8	0.7321	(Tripathi et al., 2013)	16.9	77.7	-25.1	GEOROC
1637	29.4	77.2	0.7705	(Tripathi et al., 2013)	16.8	77.7	-9.5	GEOROC
1638	28.4	77.1	0.7306	(Tripathi et al., 2013)	16.8	77.7	-11.7	GEOROC
1639	28.6	77.2	0.7300	(Tripathi et al., 2013)	16.1	79.9	-17.6	GEOROC
1640	28.3	75.9	0.7305	(Tripathi et al., 2013)	16.1	79.9	-20.7	GEOROC
1641	28.5	76.3	0.7315	(Tripathi et al., 2013)	16.1	79.9	-20.5	GEOROC
1642	29.5	76.7	0.7291	(Tripathi et al., 2013)	16.1	79.9	-21.3	GEOROC
1643	29.6	76.6	0.7305	(Tripathi et al., 2013)	16.1	79.9	-21.2	GEOROC
1644	30.0	75.7	0.7344	(Tripathi et al., 2013)	16.1	79.9	-22.4	GEOROC
1645	29.9	76.0	0.7419	(Tripathi et al., 2013)	16.1	79.9	-23.4	GEOROC
1646	27.4	85.2	0.7511	(Jain et al., 2022)	16.1	79.9	-23.2	GEOROC
1647	27.5	85.1	0.7436	(Jain et al., 2022)	16.1	79.9	-22.9	GEOROC
1648	27.4	85.1	0.7347	(Jain et al., 2022)	16.1	79.9	-22.9	GEOROC
1649	27.4	85.1	0.7970	(Jain et al., 2022)	16.1	79.9	-22.5	GEOROC

1650	27.4	85.2	0.7802	(Jain et al., 2022)	16.1	79.9	-21.3	GEOROC
1651	25.5	85.1	0.7321	(Jain et al., 2022)	16.1	79.9	-22.5	GEOROC
1652	25.5	85.1	0.7228	(Jain et al., 2022)	16.1	79.9	-21.4	GEOROC
1653	25.5	85.1	0.7190	(Jain et al., 2022)	16.1	79.9	-21.9	GEOROC
1654	25.5	85.1	0.7206	(Jain et al., 2022)	16.1	79.9	-22.9	GEOROC
1655	25.5	85.1	0.7447	(Jain et al., 2022)	16.1	79.9	-23.1	GEOROC
1656	25.5	85.1	0.7406	(Jain et al., 2022)	12.2	77.8	-29.3	GEOROC
1657	26.7	80.5	0.7789	(Shukla, 2011)	12.2	77.8	-27.3	GEOROC
1658	25.5	74.8	0.9133	(Shukla, 2011)	12.4	78.5	-15.6	GEOROC
1659	25.6	74.1	0.7858	(Tobisch et al., 1994)	12.4	78.5	-15.0	GEOROC
1660	26.5	75.0	0.7270	(Tobisch et al., 1994)	12.5	78.5	-15.7	GEOROC
1661	27.5	75.6	0.7848	(Tobisch et al., 1994)	12.5	78.5	-12.0	GEOROC
1662	26.0	77.1	0.7525	(Tobisch et al., 1994)	12.5	78.5	-16.1	GEOROC
1663	25.9	76.9	0.7254	(Tobisch et al., 1994)	11.7	77.8	-22.7	GEOROC
1664	28.6	84.4	0.9394	(Deniel et al., 1987)	11.7	77.8	-28.3	GEOROC
1665	28.6	84.4	0.7141	(Deniel et al., 1987)	16.8	77.3	-13.6	GEOROC
1666	28.6	84.3	0.7346	(Deniel et al., 1987)	14.9	77.4	-12.7	GEOROC
1667	28.6	84.5	0.7475	(Deniel et al., 1987)	14.9	77.4	-14.3	GEOROC
1668	28.6	84.3	0.7451	(Deniel et al., 1987)	14.0	78.0	-9.1	GEOROC
1669	28.6	84.6	0.7331	(Deniel et al., 1987)	14.0	78.0	-25.0	GEOROC
1670	28.6	84.3	0.7336	(Deniel et al., 1987)	14.0	78.0	-28.9	GEOROC
1671	28.6	84.7	0.7550	(Deniel et al., 1987)	14.0	78.0	-31.3	GEOROC
1672	28.6	84.3	0.7332	(Deniel et al., 1987)	14.0	78.0	-34.2	GEOROC
1673	28.6	84.7	0.7460	(Deniel et al., 1987)	14.0	78.0	-9.1	GEOROC
1674	28.7	84.3	0.7453	(Deniel et al., 1987)	14.0	76.3	-17.8	GEOROC
1675	28.6	84.7	0.7380	(Deniel et al., 1987)	14.0	76.3	-28.6	GEOROC
1676	28.6	84.7	0.7344	(Deniel et al., 1987)	14.0	76.3	-19.2	GEOROC

1677	28.6	84.3	0.7311	(Deniel et al., 1987)	14.0	76.3	-19.6	GEOROC
1678	28.6	84.3	0.7393	(Deniel et al., 1987)	13.8	78.5	-4.6	GEOROC
1679	28.6	84.7	0.7305	(Deniel et al., 1987)	13.8	78.4	-5.2	GEOROC
1680	28.6	84.6	0.7290	(Deniel et al., 1987)	14.0	78.4	-27.5	GEOROC
1681	28.7	84.3	0.8065	(Deniel et al., 1987)	14.1	78.4	-23.0	GEOROC
1682	28.7	84.4	0.7519	(Deniel et al., 1987)	14.2	78.4	-8.5	GEOROC
1683	28.6	84.7	0.7732	(Deniel et al., 1987)	14.2	78.4	-8.1	GEOROC
1684	28.7	84.5	0.7443	(Deniel et al., 1987)	14.2	78.4	-12.4	GEOROC
1685	28.7	84.7	0.7487	(Deniel et al., 1987)	14.2	78.4	-19.5	GEOROC
1686	28.7	84.3	0.7890	(Deniel et al., 1987)	13.8	78.5	-25.4	GEOROC
1687	28.6	84.7	0.7741	(Deniel et al., 1987)	14.0	78.5	-12.3	GEOROC
1688	28.6	84.3	0.7807	(Deniel et al., 1987)	14.0	78.5	-29.7	GEOROC
1689	28.7	84.7	0.7396	(Deniel et al., 1987)	14.0	78.5	-29.7	GEOROC
1690	28.7	84.7	0.7647	(Deniel et al., 1987)	13.8	78.5	-4.6	GEOROC
1691	28.8	84.8	0.7619	(Deniel et al., 1987)	14.2	78.4	-6.5	GEOROC
1692	28.2	85.5	0.8255	(Inger & Harris, 1993)	14.1	78.4	-23.1	GEOROC
1693	28.2	85.4	0.7835	(Inger & Harris, 1993)	14.0	75.5	-13.5	GEOROC
1694	28.2	85.6	0.8036	(Inger & Harris, 1993)	14.0	75.5	-29.0	GEOROC
1695	28.3	85.6	0.8143	(Inger & Harris, 1993)	14.0	75.5	-29.1	GEOROC
1696	28.3	85.7	0.8305	(Inger & Harris, 1993)	14.0	75.5	-5.8	GEOROC
1697	28.3	85.6	0.8316	(Inger & Harris, 1993)	14.0	75.5	-12.9	GEOROC
1698	28.2	85.5	0.8770	(Inger & Harris, 1993)	14.0	75.5	-7.0	GEOROC
1699	28.2	85.5	0.7577	(Inger & Harris, 1993)	14.0	75.5	-11.3	GEOROC

1700	28.2	85.8	0.7504	(Inger & Harris, 1993)	14.3	77.6	-23.0	GEOROC
1701	28.2	85.7	0.7529	(Inger & Harris, 1993)	14.3	77.5	-20.5	GEOROC
1702	28.2	86.7	0.7526	(Inger & Harris, 1993)	14.3	77.6	-25.3	GEOROC
1703	28.2	85.6	0.7623	(Inger & Harris, 1993)	14.3	77.6	-25.2	GEOROC
1704	28.2	85.6	0.7608	(Inger & Harris, 1993)	14.3	77.5	-13.1	GEOROC
1705	28.2	85.7	0.7661	(Inger & Harris, 1993)	14.3	77.6	-14.4	GEOROC
1706	28.4	85.7	0.7720	(Inger & Harris, 1993)	14.3	77.6	-39.8	GEOROC
1707	28.3	80.3	0.8332	(Inger & Harris, 1993)	14.3	77.6	-33.9	GEOROC
1708	28.4	81.0	0.9641	(Inger & Harris, 1993)	13.1	78.1	-11.2	GEOROC
1709	28.3	82.0	0.8257	(France-Lanord & Le Fort, 1988)	13.1	78.1	-9.7	GEOROC
1710	28.4	84.0	0.8996	(France-Lanord & Le Fort, 1988)	13.1	78.1	-12.4	GEOROC
1711	28.5	85.0	0.9370	(France-Lanord & Le Fort, 1988)	13.1	78.1	-9.4	GEOROC
1712	28.9	88.4	0.7661	(Zhang et al., 2004)	13.1	78.1	-11.3	GEOROC
1713	28.9	88.4	0.7715	(Zhang et al., 2004)	13.1	76.4	-15.8	GEOROC
1714	28.9	88.4	0.7852	(Zhang et al., 2004)	13.1	76.4	-22.2	GEOROC
1715	28.9	88.4	0.7831	(Zhang et al., 2004)	13.1	76.4	-18.2	GEOROC
1716	28.8	88.1	0.7385	(Zhang et al., 2004)	13.1	76.4	-22.6	GEOROC
1717	28.8	88.1	0.7384	(Zhang et al., 2004)	13.1	76.4	-21.0	GEOROC
1718	28.8	88.1	0.7377	(Zhang et al., 2004)	13.1	76.4	-20.1	GEOROC
1719	28.8	88.1	0.7373	(Zhang et al., 2004)	13.1	76.4	-16.5	GEOROC
1720	28.7	87.8	0.8785	(Zhang et al., 2004)	13.1	76.4	-22.7	GEOROC
1721	28.7	87.8	0.8533	(Zhang et al., 2004)	13.1	76.4	-15.9	GEOROC
1722	28.7	87.8	0.8532	(Zhang et al., 2004)	13.1	76.4	-15.6	GEOROC
1723	28.7	87.8	0.8547	(Zhang et al., 2004)	13.1	76.4	-17.8	GEOROC
1724	28.8	92.0	0.7156	(Zeng et al., 2015)	13.1	76.4	-14.7	GEOROC
1725	28.8	92.0	0.7147	(Zeng et al., 2015)	15.1	76.7	-8.8	GEOROC
1726	28.8	92.0	0.7163	(Zeng et al., 2015)	13.1	78.1	-10.5	GEOROC
1727	28.8	92.0	0.7205	(Zeng et al., 2015)	13.1	78.1	-9.2	GEOROC
1728	28.8	92.0	0.7155	(Zeng et al., 2015)	14.3	77.6	-20.2	GEOROC
1729	28.8	92.0	0.7154	(Zeng et al., 2015)	14.3	77.6	-23.2	GEOROC
1730	28.8	92.0	0.7151	(Zeng et al., 2015)	14.3	77.6	-19.4	GEOROC
1731	28.8	92.0	0.7154	(Zeng et al., 2015)	14.3	77.6	-20.9	GEOROC
1732	28.7	92.2	0.7121	(Zeng et al., 2015)	14.3	77.6	-13.5	GEOROC

1733	28.7	92.2	0.7120	(Zeng et al., 2015)	14.3	77.6	-18.6	GEOROC
1734	28.7	92.2	0.7189	(Zeng et al., 2015)	14.3	77.6	-24.4	GEOROC
1735	28.7	92.2	0.7152	(Zeng et al., 2015)	14.3	77.6	-24.2	GEOROC
1736	28.4	92.2	0.7292	(Zeng et al., 2015)	14.3	77.6	-21.7	GEOROC
1737	28.4	92.2	0.7208	(Zeng et al., 2015)	14.3	77.6	-17.9	GEOROC
1738	28.4	92.2	0.7248	(Zeng et al., 2015)	14.3	77.6	-26.9	GEOROC
1739	28.4	92.2	0.7236	(Zeng et al., 2015)	14.0	76.3	-15.2	GEOROC
1740	28.4	92.2	0.7223	(Zeng et al., 2015)	14.0	76.3	-9.3	GEOROC
1741	28.4	92.2	0.7291	(Zeng et al., 2015)	13.5	76.5	-20.9	GEOROC
1742	28.4	92.2	0.7264	(Zeng et al., 2015)	12.9	78.3	-20.5	GEOROC
1743	30.2	81.6	0.7564	(Murphy, 2007)	13.1	76.4	-14.9	GEOROC
1744	30.4	81.4	0.7500	(Murphy, 2007)	14.2	76.4	-33.3	GEOROC
1745	30.5	81.4	0.7573	(Murphy, 2007)	14.2	79.7	-9.1	GEOROC
1746	30.4	81.6	0.9051	(Murphy, 2007)	14.2	79.7	-11.4	GEOROC
1747	30.3	81.7	0.9840	(Murphy, 2007)	14.2	79.7	-10.6	GEOROC
1748	30.1	81.9	0.8115	(Murphy, 2007)	14.2	79.7	-14.1	GEOROC
1749	30.0	82.2	0.8011	(Murphy, 2007)	14.2	79.7	-10.1	GEOROC
1750	30.0	82.5	0.7602	(Murphy, 2007)	14.2	79.7	-13.6	GEOROC
1751	30.1	82.3	0.8907	(Murphy, 2007)	14.2	79.7	-13.8	GEOROC
1752	30.4	73.2	0.7198	(Le Fort, et al., 1983)	14.2	79.7	-11.3	GEOROC
1753	31.7	76.9	0.7180	(Jager, et al., 1971)	14.2	79.7	-11.4	GEOROC
1754	32.0	77.4	0.7190	(Bhanot, et al., 1979)	14.2	79.7	-13.1	GEOROC
1755	32.0	77.1	0.7200	(Fank, et al., 1977)	14.2	79.7	-25.7	GEOROC
1756	31.5	78.4	0.7370	(Kwatra, et al., 1999)	14.2	79.7	-27.5	GEOROC
1757	33.8	74.7	0.7170	(Rao, et al., 1990)	14.2	79.7	-27.1	GEOROC
1758	33.2	76.9	0.7175	(Pognante et al., 1990)	14.2	79.7	-16.2	GEOROC
1759	33.2	76.9	0.7365	(Stutz & Thöni, 1987)	14.2	79.7	-16.1	GEOROC
1760	31.7	77.7	0.7244	(Rai, et al., 1993)	14.2	79.7	-12.7	GEOROC
1761	29.3	80.1	0.7109	(Trivedi, et al., 1984)	14.2	79.7	-10.2	GEOROC
1762	29.6	80.6	0.7266	(Einfalt et al., 1993)	14.2	79.7	-13.2	GEOROC
1763	28.3	85.4	0.7205	(Le Fort, et al., 1983)	14.2	79.7	-12.9	GEOROC
1764	29.0	89.7	0.7140	(Debon, et al., 1986)	14.2	79.7	-10.7	GEOROC
1765	29.0	89.7	0.7186	GEOROC	14.2	79.7	-16.1	GEOROC

1766	31.8	77.1	0.7135	(Miller et al., 2001)	14.2	79.7	-9.3	GEOROC
1767	32.3	77.5	0.8413	(Miller et al., 2001)	14.2	79.7	-27.3	GEOROC
1768	32.3	77.4	0.7986	(Miller et al., 2001)	14.2	79.7	-21.0	GEOROC
1769	32.3	77.3	0.8887	(Miller et al., 2001)	16.3	76.8	-26.2	GEOROC
1770	32.3	77.3	0.8085	(Miller et al., 2001)	16.3	76.8	-8.8	GEOROC
1771	32.2	77.2	1.3843	(Miller et al., 2001)	16.3	76.8	-34.4	GEOROC
1772	32.2	77.3	1.0333	(Miller et al., 2001)	16.3	76.8	-31.2	GEOROC
1773	32.2	77.4	0.8248	(Miller et al., 2001)	16.3	76.8	-27.7	GEOROC
1774	32.1	77.4	0.9382	(Miller et al., 2001)	15.1	76.8	-37.8	GEOROC
1775	32.1	77.4	0.7909	(Miller et al., 2001)	15.1	76.8	-41.4	GEOROC
1776	32.2	77.4	0.8696	(Miller et al., 2001)	15.1	76.8	-34.1	GEOROC
1777	32.2	77.3	0.7769	(Miller et al., 2001)	15.9	76.2	-30.5	GEOROC
1778	32.1	77.5	0.8276	(Miller et al., 2001)	15.9	76.2	-30.4	GEOROC
1779	32.8	75.7	0.7884	(Miller et al., 2001)	15.9	76.2	-24.5	GEOROC
1780	32.9	75.6	0.7631	(Miller et al., 2001)	16.1	76.8	-31.3	GEOROC
1781	33.0	75.5	0.8979	(Miller et al., 2001)	16.1	76.8	-27.3	GEOROC
1782	33.0	75.5	0.7695	(Miller et al., 2001)	16.1	76.8	-34.2	GEOROC
1783	33.0	75.6	0.8691	(Miller et al., 2001)	15.1	76.8	-36.2	GEOROC
1784	32.9	75.6	0.8629	(Miller et al., 2001)	15.1	76.8	-31.9	GEOROC
1785	33.5	76.8	0.7959	(Miller et al., 2001)	15.9	76.2	-33.9	GEOROC
1786	33.5	76.8	0.9036	(Miller et al., 2001)	15.9	76.2	-42.1	GEOROC
1787	33.5	76.8	0.8216	(Miller et al., 2001)	15.9	76.2	-31.1	GEOROC
1788	32.3	77.1	0.7474	(Miller et al., 2001)	16.1	76.8	-26.5	GEOROC
1789	32.6	76.1	0.8060	(Miller et al., 2001)	16.1	76.8	-46.0	GEOROC
1790	31.6	78.4	0.8939	(Miller et al., 2001)	16.1	76.8	-36.1	GEOROC
1791	31.5	78.4	0.7570	(Miller et al., 2001)	16.1	78.8	-9.8	GEOROC
1792	31.6	78.3	0.7476	(Miller et al., 2001)	16.1	78.8	-7.0	GEOROC
1793	31.7	78.2	0.8216	(Miller et al., 2001)	16.1	78.8	-7.6	GEOROC
1794	31.4	77.2	1.2130	(Miller et al., 2001)	16.1	78.8	-5.4	GEOROC
1795	31.4	77.1	1.1758	(Miller et al., 2001)	16.1	78.8	-4.7	GEOROC
1796	31.5	77.0	0.7616	(Miller et al., 2001)	16.1	78.8	-26.7	GEOROC
1797	31.5	77.0	0.7560	(Miller et al., 2001)	16.1	78.8	-32.8	GEOROC
1798	31.6	76.9	0.7248	(Miller et al., 2001)	16.1	78.8	-28.1	GEOROC
1799	31.7	76.9	0.7117	(Miller et al., 2001)	16.1	78.8	-27.8	GEOROC
1800	31.6	77.0	0.7081	(Miller et al., 2001)	16.1	78.8	-25.4	GEOROC
1801	31.5	77.0	0.7055	(Miller et al., 2001)	16.1	78.8	-25.7	GEOROC
1802	31.5	77.1	0.7120	(Miller et al., 2001)	16.1	78.8	-29.4	GEOROC
1803	31.5	77.2	0.7075	(Miller et al., 2001)	16.1	78.8	-32.9	GEOROC

1804	32.8	77.0	1.0265	(Miller et al., 2001)	16.1	78.8	-28.9	GEOROC
1805	31.2	77.2	0.7281	(Miller et al., 2001)	14.3	76.3	-30.0	GEOROC
1806	31.1	77.2	0.7731	(Miller et al., 2001)	14.3	76.3	-31.4	GEOROC
1807	32.9	76.7	0.7345	(Miller et al., 2001)	14.3	76.3	-26.8	GEOROC
1808	31.9	77.2	0.7417	(Miller et al., 2001)	14.3	76.3	-36.8	GEOROC
1809	31.1	77.2	0.7447	(Miller et al., 2001)	12.9	78.3	-35.7	GEOROC
1810	31.1	77.4	0.7640	(Miller et al., 2001)	12.9	78.3	-33.4	GEOROC
1811	33.0	76.8	0.7501	(Miller et al., 2001)	12.9	78.3	-38.7	GEOROC
1812	25.1	67.6	0.7245	(Clift et al., 2010)	12.9	78.3	-25.3	GEOROC
1813	25.1	67.6	0.7277	(Clift et al., 2010)	14.0	78.0	-32.4	GEOROC
1814	25.1	67.6	0.7193	(Clift et al., 2010)	14.0	78.0	-33.6	GEOROC
1815	25.1	67.6	0.7200	(Clift et al., 2010)	14.0	78.5	-29.6	GEOROC
1816	25.1	67.6	0.7107	(Clift et al., 2010)	15.3	77.6	-21.0	GEOROC
1817	25.1	67.6	0.7145	(Clift et al., 2010)	16.7	79.2	-21.1	GEOROC
1818	25.1	67.6	0.7148	(Clift et al., 2010)	11.2	78.3	-12.0	GEOROC
1819	25.2	68.2	0.7214	(Clift et al., 2010)	11.3	78.3	-31.1	GEOROC
1820	25.2	68.2	0.7198	(Clift et al., 2010)	11.4	78.1	-32.8	GEOROC
1821	25.2	68.2	0.7252	(Clift et al., 2010)	11.3	78.3	-28.4	GEOROC
1822	29.4	74.2	0.7429	(Singh et al., 2016)	11.3	78.3	-29.7	GEOROC
1823	29.4	74.2	0.7474	Singh et al., 2016)	11.3	78.3	-15.0	GEOROC
1824	29.4	74.1	0.7491	Singh et al., 2016)	11.3	78.3	-25.7	GEOROC
1825	29.4	74.1	0.7498	Singh et al., 2016)	9.7	77.8	-9.3	GEOROC
1826	28.8	69.1	0.7117	(Roddaz et al., 2011)	10.0	77.8	-18.9	GEOROC
1827	28.8	69.1	0.7169	(Roddaz et al., 2011)	10.1	76.7	-33.0	GEOROC
1828	29.0	68.9	0.7131	(Roddaz et al., 2011)	9.6	77.5	-7.8	GEOROC
1829	29.0	68.9	0.7119	(Roddaz et al., 2011)	9.3	77.5	-18.3	GEOROC
1830	29.0	68.9	0.7177	(Roddaz et al., 2011)	10.0	76.4	-18.5	GEOROC
1831	29.0	68.9	0.7215	(Roddaz et al., 2011)	9.9	76.5	-22.2	GEOROC
1832	28.8	69.1	0.7176	(Roddaz et al., 2011)	10.2	76.5	-34.0	GEOROC
1833	28.9	69.1	0.7244	(Roddaz et al., 2011)	9.8	76.5	-22.7	GEOROC
1834	28.9	69.1	0.7129	(Roddaz et al., 2011)	9.6	76.8	-26.7	GEOROC
1835	28.9	69.1	0.7181	(Roddaz et al., 2011)	8.7	76.9	-28.3	GEOROC
1836	28.9	69.1	0.7081	(Roddaz et al., 2011)	8.9	77.3	-14.7	GEOROC
1837	28.9	69.1	0.7081	(Roddaz et al., 2011)	8.9	77.5	-23.6	GEOROC

1838	28.9	69.2	0.7082	(Roddaz et al., 2011)	8.7	77.5	-11.5	GEOROC
1839	28.9	69.2	0.7103	(Roddaz et al., 2011)	8.8	77.8	-6.6	GEOROC
1840	29.1	69.0	0.7122	(Roddaz et al., 2011)	8.7	77.8	-10.4	GEOROC
1841	29.1	69.0	0.7101	(Roddaz et al., 2011)	8.2	77.5	-27.5	GEOROC
1842	25.1	94.3	0.7097	(Kingson et al., 2019)	8.2	77.5	-28.3	GEOROC
1843	25.1	94.3	0.7098	(Kingson et al., 2019)	8.2	77.4	-30.2	GEOROC
1844	25.0	94.3	0.7076	(Kingson et al., 2019)	10.6	78.8	-27.3	GEOROC
1845	25.0	94.3	0.7069	(Kingson et al., 2019)	10.5	78.8	-27.1	GEOROC
1846	25.0	94.3	0.7074	(Kingson et al., 2019)	10.4	78.7	-22.5	GEOROC
1847	25.2	94.5	0.7072	(Kingson et al., 2019)	10.4	78.7	-29.4	GEOROC
1848	25.2	94.5	0.7053	(Kingson et al., 2019)	10.4	78.7	-27.0	GEOROC
1849	25.2	94.5	0.7053	(Kingson et al., 2019)	10.5	78.8	-26.8	GEOROC
1850	25.2	94.5	0.7054	(Kingson et al., 2019)	10.6	78.8	-27.2	GEOROC
1851	28.7	95.9	0.7053	(Haproff et al., 2019)	10.4	78.7	-29.8	GEOROC
1852	28.3	95.9	0.7042	(Haproff et al., 2019)	10.5	78.8	-23.9	GEOROC
1853	28.6	95.9	0.7052	(Haproff et al., 2019)	10.6	78.8	-35.0	GEOROC
1854	28.6	95.9	0.7045	(Haproff et al., 2019)	10.6	78.8	-34.5	GEOROC
1855	28.6	95.8	0.7053	(Haproff et al., 2019)	12.0	77.1	-45.5	GEOROC
1856	28.6	95.8	0.7055	(Haproff et al., 2019)	12.0	77.1	-39.5	GEOROC
1857	28.5	95.9	0.7124	(Haproff et al., 2019)	12.0	77.1	-39.1	GEOROC
1858	28.2	95.9	0.9116	(Haproff et al., 2019)	12.4	77.2	-29.3	GEOROC
1859	28.2	95.9	0.7153	(Haproff et al., 2019)	12.4	77.3	-29.8	GEOROC
1860	28.2	95.9	0.7569	(Haproff et al., 2019)	12.4	77.3	-36.2	GEOROC

1861	28.2	95.8	0.8945	(Haproff et al., 2019)	12.5	77.3	-30.1	GEOROC
1862	28.2	95.9	0.7441	(Haproff et al., 2019)	12.1	77.2	-33.3	GEOROC
1863	28.2	95.8	0.7812	(Haproff et al., 2019)	12.3	77.1	-17.8	GEOROC
1864	28.2	95.8	0.7117	(Haproff et al., 2019)	12.0	77.1	-33.5	GEOROC
1865	25.1	94.3	0.7097	(Singh, 2018,)	12.3	77.7	-36.8	GEOROC
1866	25.1	94.3	0.7098	Singh et al., 2016)	11.9	76.7	-39.9	GEOROC
1867	25.0	94.4	0.7078	Singh et al., 2016)	11.8	76.6	-41.4	GEOROC
1868	25.0	94.4	0.7073	Singh et al., 2016)	11.9	76.6	-36.5	GEOROC
1869	25.0	94.3	0.7076	Singh et al., 2016)	11.8	76.8	-40.6	GEOROC
1870	25.0	94.3	0.7069	Singh et al., 2016)	11.8	76.7	-4.1	GEOROC
1871	25.0	94.3	0.7074	Singh et al., 2016)	11.9	76.6	-13.0	GEOROC
1872	25.2	94.5	0.7052	Singh et al., 2016)	11.8	76.7	-30.6	GEOROC
1873	25.2	94.5	0.7053	Singh et al., 2016)	12.1	76.4	-11.8	GEOROC
1874	25.2	94.5	0.7053	Singh et al., 2016)	12.0	76.4	-18.9	GEOROC
1875	25.2	94.5	0.7054	Singh et al., 2016)	12.0	76.4	-6.5	GEOROC
1876	28.1	96.5	0.7040	(Bikramaditya et al., 2020)	12.0	76.4	-23.6	GEOROC
1877	28.0	96.4	0.7038	(Bikramaditya et al., 2020)	12.0	76.4	-19.6	GEOROC
1878	28.6	95.8	0.7046	(Bikramaditya et al., 2020)	12.2	76.5	-39.7	GEOROC
1879	28.6	95.8	0.7045	(Bikramaditya et al., 2020)	12.2	76.5	-29.5	GEOROC
1880	21.8	94.8	0.7147	(Licht et al., 2013)	12.2	76.5	-30.5	GEOROC
1881	21.8	94.8	0.7156	(Licht et al., 2013)	12.2	76.5	-36.7	GEOROC
1882	21.7	94.8	0.7055	(Licht et al., 2013)	12.2	76.5	-37.1	GEOROC
1883	21.7	94.7	0.7057	(Licht et al., 2013)	12.2	76.5	-34.1	GEOROC

1884	21.7	94.7	0.7172	(Licht et al., 2013)	12.5	75.3	-29.5	GEOROC
1885	21.7	94.7	0.7141	(Licht et al., 2013)	12.5	75.4	-31.6	GEOROC
1886	21.8	94.6	0.7178	(Licht et al., 2013)	12.5	75.5	-29.8	GEOROC
1887	21.8	94.6	0.7059	(Licht et al., 2013)	12.4	75.8	-22.6	GEOROC
1888	21.7	94.6	0.7088	(Licht et al., 2013)	12.1	75.8	-34.9	GEOROC
1889	21.8	94.6	0.7152	(Licht et al., 2013)	12.1	75.8	-36.3	GEOROC
1890	21.7	94.7	0.7112	(Licht et al., 2013)	12.1	75.8	-39.1	GEOROC
1891	23.3	94.9	0.7118	(Licht et al., 2013)	14.0	76.3	-33.3	GEOROC
1892	23.3	94.9	0.7121	(Licht et al., 2013)	13.8	76.3	-36.2	GEOROC
1893	21.7	94.7	0.7098	(Licht et al., 2013)	13.9	76.3	-37.8	GEOROC
1894	21.7	94.7	0.7085	(Licht et al., 2013)	13.9	76.3	-38.2	GEOROC
1895	21.7	94.7	0.7132	(Licht et al., 2013)	13.9	76.3	-38.1	GEOROC
1896	19.7	96.6	0.7270	(Brook, & Snelling, 1976)	14.0	76.3	-35.4	GEOROC
1897	19.7	96.6	0.7990	Singh et al., 2016)	13.9	76.3	-38.2	GEOROC
1898	19.7	96.6	0.7230	Singh et al., 2016)	13.9	76.3	-38.7	GEOROC
1899	19.7	96.6	0.7400	Singh et al., 2016)	13.9	76.3	-33.3	GEOROC
1900	22.9	96.0	0.711	Singh et al., 2016)	13.9	76.3	-39.4	GEOROC
1901	22.9	96.3	0.7170	Singh et al., 2016)	13.9	76.3	-28.9	GEOROC
1902	31.6	78.4	0.7430	(Richards et al., 2005)	27.9	91.9	-18.2	GEOROC
1903	31.6	78.4	0.7752	(Richards et al., 2005)	27.9	91.9	-15.5	GEOROC
1904	31.6	78.3	0.7501	(Richards et al., 2005)	27.9	91.9	-18.1	GEOROC
1905	31.6	78.3	0.7423	(Richards et al., 2005)	27.9	91.9	-15.6	GEOROC
1906	31.6	78.3	0.7432	(Richards et al., 2005)	27.9	91.9	-17.7	GEOROC
1907	31.5	78.2	0.7694	(Richards et al., 2005)	27.9	91.8	-19.3	GEOROC
1908	31.5	78.2	0.7497	(Richards et al., 2005)	27.9	91.8	-19.8	GEOROC
1909	31.5	78.2	0.7311	(Richards et al., 2005)	28.6	78.8	-15.8	(Tripathi et al., 2013)
1910	31.6	78.0	0.9638	(Richards et al., 2005)	20.0	78.5	-17.5	(Tripathi et al., 2013)
1911	31.6	77.8	0.8845	(Richards et al., 2005)	26.4	79.8	-15.4	(Tripathi et al., 2013)
1912	31.5	77.7	0.7824	(Richards et al., 2005)	29.4	77.2	-17.7	(Tripathi et al., 2013)

1913	31.5	77.8	1.2438	(Richards et al., 2005)	28.4	77.1	-15.4	(Tripathi et al., 2013)
1914	31.5	77.8	0.8744	(Richards et al., 2005)	28.6	77.2	-14.7	(Tripathi et al., 2013)
1915	31.4	77.6	1.0413	(Richards et al., 2005)	28.3	75.9	-14.4	(Tripathi et al., 2013)
1916	31.4	77.6	0.9496	(Richards et al., 2005)	28.5	76.3	-13.4	(Tripathi et al., 2013)
1917	31.4	77.5	0.8372	(Richards et al., 2005)	29.5	76.7	-13.2	(Tripathi et al., 2013)
1918	31.4	77.7	0.7756	(Richards et al., 2005)	29.9	76.0	-15.4	(Tripathi et al., 2013)
1919	31.3	77.4	0.7527	(Richards et al., 2005)	27.4	85.2	-17.4	(Jain et al., 2022)
1920	31.3	77.5	0.7639	(Richards et al., 2005)	27.4	85.2	-18.5	(Jain et al., 2022)
1921	31.2	77.4	0.9451	(Richards et al., 2005)	27.4	85.2	-17.8	(Jain et al., 2022)
1922	31.1	77.3	0.7696	(Richards et al., 2005)	27.4	85.2	-18.8	(Jain et al., 2022)
1923	31.1	77.2	0.8040	(Richards et al., 2005)	27.4	85.2	-17.9	(Jain et al., 2022)
1924	31.0	77.2	0.7605	(Richards et al., 2005)	25.5	85.1	-17.7	(Jain et al., 2022)
1925	31.0	77.1	0.8303	(Richards et al., 2005)	25.5	85.1	-18.1	(Jain et al., 2022)
1926	31.0	77.1	0.7509	(Richards et al., 2005)	25.5	85.1	-17.9	(Jain et al., 2022)
1927	30.6	77.6	0.8189	(Richards et al., 2005)	25.5	85.1	-18.1	(Jain et al., 2022)
1928	31.6	78.4	0.7646	(Richards et al., 2005)	25.5	85.1	-18.9	(Jain et al., 2022)
1929	31.8	78.4	0.7341	(Richards et al., 2005)	25.5	85.1	-18.4	(Jain et al., 2022)
1930	31.7	78.5	0.7639	(Richards et al., 2005)	26.7	80.5	-17.6	(Shukla, 2011)
1931	31.6	78.4	0.7366	(Richards et al., 2005)	25.1	78.9	-34.0	(Shukla, 2011)
1932	32.7	76.5	0.7631	(Richards et al., 2005)	25.5	74.8	-32.1	(Shukla, 2011)
1933	32.8	76.4	0.7937	(Richards et al., 2005)	25.6	74.1	-21.3	(Tobisch et al., 1994)

1934	32.3	76.6	0.7777	(Richards et al., 2005)	26.5	75.0	-3.0	(Tobisch et al., 1994)
1935	32.3	76.6	0.7560	(Richards et al., 2005)	27.5	75.6	-28.2	(Tobisch et al., 1994)
1936	32.4	76.7	0.7790	(Richards et al., 2005)	23.3	79.6	-16.9	(Tobisch et al., 1994)
1937	32.5	76.4	0.7808	(Richards et al., 2005)	23.4	79.9	-14.7	(Tobisch et al., 1994)
1938	32.6	76.2	0.7718	(Richards et al., 2005)	23.6	79.6	-15.4	(Tobisch et al., 1994)
1939	32.6	76.2	0.7592	(Richards et al., 2005)	23.1	79.4	-16.4	(Tobisch et al., 1994)
1940	30.1	78.8	0.8230	(Ahmad & Harris, 2000)	26.0	77.1	-14.6	(Tobisch et al., 1994)
1941	30.1	78.9	0.7709	(Ahmad & Harris, 2000)	25.9	76.9	-16.9	(Tobisch et al., 1994)
1942	30.1	78.9	0.8004	(Ahmad & Harris, 2000)	28.1	96.5	5.1	(Bikramaditya et al., 2020)
1943	30.2	78.8	0.8151	(Ahmad & Harris, 2000)	28.0	96.4	5.1	(Bikramaditya et al., 2020)
1944	30.2	78.7	0.7499	(Ahmad & Harris, 2000)	28.6	95.9	3.2	(Bikramaditya et al., 2020)
1945	30.1	78.6	0.7993	(Ahmad & Harris, 2000)	28.6	95.8	3.2	(Bikramaditya et al., 2020)
1946	30.4	79.4	0.7331	(Ahmad & Harris, 2000)	25.1	75.1	-17.8	(Shukla, 2011)
1947	30.4	79.4	0.7412	(Ahmad & Harris, 2000)	25.0	75.1	-16.4	(Shukla, 2011)
1948	30.4	79.4	0.7329	(Ahmad & Harris, 2000)	25.0	75.1	-15.2	(Shukla, 2011)
1949	30.5	79.5	0.9309	(Ahmad & Harris, 2000)	25.5	75.6	-14.8	(Shukla, 2011)
1950	30.5	79.5	1.1765	(Ahmad & Harris, 2000)	25.5	75.9	-15.5	(Shukla, 2011)
1951	30.5	79.5	0.7158	(Ahmad & Harris, 2000)	24.8	74.6	-23.4	(Shukla, 2011)
1952	30.3	79.0	0.9224	(Ahmad & Harris, 2000)	24.8	74.6	-16.4	(Shukla, 2011)
1953	30.4	79.0	0.9300	(Ahmad & Harris, 2000)	24.4	74.7	-18.5	(Shukla, 2011)

1954	30.3	79.3	0.8245	(Ahmad & Harris, 2000)	25.1	75.1	-15.5	(Shukla, 2011)
1955	30.5	79.5	1.0470	(Ahmad & Harris, 2000)	24.9	75.6	-17.0	(Shukla, 2011)
1956	30.5	79.6	0.7369	(Ahmad & Harris, 2000)	25.6	76.1	-17.8	(Shukla, 2011)
1957	30.5	79.6	0.9205	(Ahmad & Harris, 2000)	25.5	76.0	-20.2	(Shukla, 2011)
1958	30.5	79.6	0.8779	(Ahmad & Harris, 2000)	25.7	76.2	-19.4	(Shukla, 2011)
1959	30.5	79.5	0.9804	(Ahmad & Harris, 2000)	25.7	76.2	-18.6	(Shukla, 2011)
1960	30.5	79.5	0.8294	(Ahmad & Harris, 2000)	25.7	76.3	-14.2	(Shukla, 2011)
1961	30.5	79.6	1.0437	(Ahmad & Harris, 2000)	25.6	77.0	-17.6	(Shukla, 2011)
1962	30.5	79.6	0.7769	(Ahmad & Harris, 2000)	25.0	74.7	-15.2	(Shukla, 2011)
1963	30.5	79.5	0.7488	(Ahmad & Harris, 2000)	24.9	74.7	-17.8	(Shukla, 2011)
1964	30.5	79.8	0.7780	(Ahmad & Harris, 2000)	25.0	75.6	-17.2	(Shukla, 2011)
1965	30.6	79.8	0.7578	(Ahmad & Harris, 2000)	24.9	74.7	-18.2	(Shukla, 2011)
1966	30.8	79.5	0.7844	(Ahmad & Harris, 2000)	24.9	74.7	-17.1	(Shukla, 2011)
1967	30.8	79.5	0.7902	(Ahmad & Harris, 2000)	24.8	74.6	-22.6	(Shukla, 2011)
1968	30.7	79.9	0.7414	(Ahmad & Harris, 2000)	24.9	74.6	-19.2	(Shukla, 2011)
1969	30.5	79.6	0.7515	(Ahmad & Harris, 2000)	28.6	84.3	-14.3	(Deniel et al., 1987)
1970	30.5	79.6	0.7451	(Ahmad & Harris, 2000)	28.7	84.3	-14.3	(Deniel et al., 1987)
1971	30.5	79.6	0.9062	(Ahmad & Harris, 2000)	28.6	84.4	-13.5	(Deniel et al., 1987)
1972	30.6	79.8	0.7617	(Ahmad & Harris, 2000)	28.6	84.3	-16.0	(Deniel et al., 1987)
1973	30.7	79.9	0.7723	(Ahmad & Harris, 2000)	28.6	84.5	-16.2	(Deniel et al., 1987)
1974	35.3	74.6	0.7433	(Argles et al., 2003)	28.6	84.3	-14.0	(Deniel et al., 1987)
1975	35.2	74.6	0.7269	(Argles et al., 2003)	28.6	84.6	-15.1	(Deniel et al., 1987)
1976	35.3	74.7	0.7339	(Argles et al., 2003)	28.6	84.3	-15.5	(Deniel et al., 1987)

1977	35.2	74.6	0.7367	(Argles et al., 2003)	28.6	84.7	-16.8	(Deniel et al., 1987)
1978	35.2	74.4	0.7860	(Argles et al., 2003)	28.6	84.3	-15.3	(Deniel et al., 1987)
1979	35.2	74.5	0.7662	(Argles et al., 2003)	28.6	84.7	-14.9	(Deniel et al., 1987)
1980	35.3	74.7	0.7506	(Argles et al., 2003)	28.7	84.3	-18.2	(Deniel et al., 1987)
1981	35.2	74.5	0.7609	(Argles et al., 2003)	28.6	84.7	-18.0	(Deniel et al., 1987)
1982	35.3	74.7	0.7109	(Argles et al., 2003)	28.7	84.3	-15.5	(Deniel et al., 1987)
1983	35.2	74.6	0.7191	(Argles et al., 2003)	28.6	84.3	-15.4	(Deniel et al., 1987)
1984	35.3	74.6	0.7164	(Argles et al., 2003)	28.7	84.7	-10.6	(Deniel et al., 1987)
1985	35.3	74.5	0.7066	(Argles et al., 2003)	28.8	84.8	-14.2	(Deniel et al., 1987)
1986	35.3	74.6	0.7150	(Argles et al., 2003)	27.7	88.1	-13.1	(Imayama & Arita, 2008)
1987	35.5	74.7	0.7117	(Argles et al., 2003)	27.7	88.1	-10.0	(Imayama & Arita, 2008)
1988	35.3	74.8	0.7067	(Argles et al., 2003)	27.7	88.1	-16.2	(Imayama & Arita, 2008)
1989	35.4	74.8	0.7107	(Argles et al., 2003)	27.7	88.1	-17.9	(Imayama & Arita, 2008)
1990	35.2	74.8	0.8226	(Argles et al., 2003)	28.7	83.5	-18.1	(Imayama & Arita, 2008)
1991	35.5	75.1	0.8675	(Gazis, et al., 1998)	28.7	83.5	-14.9	(Imayama & Arita, 2008)
1992	35.4	75.5	0.8660	(Gazis, et al., 1998)	27.6	86.6	-17.5	(Imayama & Arita, 2008)
1993	35.4	76.0	0.8236	(Gazis, et al., 1998)	27.6	86.6	-16.4	(Imayama & Arita, 2008)
1994	35.3	75.9	1.0642	(Gazis, et al., 1998)	27.6	86.6	-18.0	(Imayama & Arita, 2008)
1995	34.9	76.0	0.8839	(Gazis, et al., 1998)	27.6	86.6	-16.3	(Imayama & Arita, 2008)
1996	34.6	75.8	0.9126	(Gazis, et al., 1998)	27.6	86.6	-17.8	(Imayama & Arita, 2008)

1997	34.6	75.2	0.8870	(Gazis, et al., 1998)	26.9	87.2	-20.2	(Imayama & Arita, 2008)
1998	34.8	75.2	0.8252	(Gazis, et al., 1998)	26.9	87.2	-18.5	(Imayama & Arita, 2008)
1999	35.0	75.6	0.7721	(Gazis, et al., 1998)	27.8	86.3	-21.9	(Imayama & Arita, 2008)
2000	35.1	75.3	0.7681	(Gazis, et al., 1998)	27.8	86.3	-23.3	(Imayama & Arita, 2008)
2001	34.7	75.6	0.8528	(Gazis, et al., 1998)	27.8	86.3	-26.2	(Imayama & Arita, 2008)
2002	35.2	76.2	0.8183	(Gazis, et al., 1998)	27.8	86.3	-22.2	(Imayama & Arita, 2008)
2003	34.6	76.2	0.8510	(Gazis, et al., 1998)	27.8	86.3	-22.6	(Imayama & Arita, 2008)
2004	35.3	75.6	0.8170	(Gazis, et al., 1998)	27.3	86.5	-25.6	(Imayama & Arita, 2008)
2005	28.5	86.1	0.7082	(Oliver et al., 2003)	27.4	87.7	-26.9	(Imayama & Arita, 2008)
2006	28.4	86.1	0.7148	(Oliver et al., 2003)	27.4	87.7	25.4	(Imayama & Arita, 2008)
2007	28.4	86.1	0.7524	(Oliver et al., 2003)	27.4	87.7	-26.6	(Imayama & Arita, 2008)
2008	28.0	86.0	0.8053	(Oliver et al., 2003)	27.4	87.7	-25.7	(Imayama & Arita, 2008)
2009	28.2	86.0	0.7151	(Oliver et al., 2003)	27.4	87.7	-22.0	(Imayama & Arita, 2008)
2010	28.2	86.0	0.7100	(Oliver et al., 2003)	27.4	87.7	-17.2	(Imayama & Arita, 2008)
2011	28.2	86.0	0.7134	(Oliver et al., 2003)	28.2	83.9	-13.9	(Imayama & Arita, 2008)
2012	28.2	86.0	0.7107	(Oliver et al., 2003)	28.2	83.9	-17.0	(Imayama & Arita, 2008)
2013	28.2	86.0	0.7139	(Oliver et al., 2003)	28.2	83.9	-25.9	(Imayama & Arita, 2008)
2014	28.2	86.0	0.7173	(Oliver et al., 2003)	28.2	83.9	-23.8	(Imayama & Arita, 2008)
2015	28.0	85.9	0.8542	(Oliver et al., 2003)	28.2	83.9	-26.2	(Imayama & Arita, 2008)

2016	27.9	85.9	1.1161	(Oliver et al., 2003)	28.0	84.0	-25.6	(Imayama & Arita, 2008)
2017	27.9	85.9	0.9232	(Oliver et al., 2003)	28.0	84.0	-25.3	(Imayama & Arita, 2008)
2018	27.9	85.9	0.7712	(Oliver et al., 2003)	27.8	85.4	-25.0	(Imayama & Arita, 2008)
2019	27.9	85.9	0.8461	(Oliver et al., 2003)	27.8	85.4	-25.3	(Imayama & Arita, 2008)
2020	27.8	85.9	1.1613	(Oliver et al., 2003)	28.0	85.2	-23.4	(Imayama & Arita, 2008)
2021	27.9	85.9	0.9302	(Oliver et al., 2003)	27.8	84.8	-21.9	(Imayama & Arita, 2008)
2022	27.9	85.9	1.0742	(Oliver et al., 2003)	27.8	84.8	-20.0	(Imayama & Arita, 2008)
2023	27.9	85.9	1.1114	(Oliver et al., 2003)	28.2	83.9	-17.2	(Imayama & Arita, 2008)
2024	27.9	85.9	1.1061	(Oliver et al., 2003)	28.2	83.9	-17.7	(Imayama & Arita, 2008)
2025	27.9	85.9	0.7974	(Oliver et al., 2003)	28.2	83.9	-14.4	(Imayama & Arita, 2008)
2026	27.9	85.9	0.9137	(Oliver et al., 2003)	28.2	83.9	-24.6	(Imayama & Arita, 2008)
2027	27.9	85.9	1.0381	(Oliver et al., 2003)	28.2	83.9	-12.4	(Imayama & Arita, 2008)
2028	27.9	85.9	0.9080	(Oliver et al., 2003)	28.2	83.9	-23.8	(Imayama & Arita, 2008)
2029	27.9	85.9	0.9735	(Oliver et al., 2003)	28.2	83.9	-25.2	(Imayama & Arita, 2008)
2030	27.7	85.8	0.8502	(Oliver et al., 2003)	28.2	83.9	-25.8	(Imayama & Arita, 2008)
2031	27.6	85.7	0.7292	(Oliver et al., 2003)	28.3	83.8	-14.8	(Martin et al., 2005)
2032	27.6	85.7	0.7702	(Oliver et al., 2003)	28.3	83.8	-17.6	(Martin et al., 2005)
2033	27.6	85.7	0.9258	(Oliver et al., 2003)	28.3	83.8	-15.5	(Martin et al., 2005)
2034	27.7	85.7	0.8918	(Oliver et al., 2003)	28.3	83.8	-16.8	(Martin et al., 2005)
2035	27.9	85.9	1.0561	(Oliver et al., 2003)	28.2	84.0	-16.7	(Martin et al., 2005)

2036	27.9	85.9	0.7505	(Oliver et al., 2003)	28.2	84.0	-13.4	(Martin et al., 2005)
2037	27.9	85.9	0.7969	(Oliver et al., 2003)	28.2	84.2	-15.0	(Martin et al., 2005)
2038	27.9	85.9	0.8692	(Oliver et al., 2003)	28.2	84.2	-13.8	(Martin et al., 2005)
2039	27.9	85.9	0.9937	(Oliver et al., 2003)	28.2	84.2	-14.2	(Martin et al., 2005)
2040	27.9	85.9	0.9159	(Oliver et al., 2003)	28.2	84.0	-14.0	(Martin et al., 2005)
2041	27.9	85.9	0.9160	(Oliver et al., 2003)	28.2	84.0	-16.0	(Martin et al., 2005)
2042	27.9	85.9	0.9334	(Oliver et al., 2003)	28.2	84.0	-17.5	(Martin et al., 2005)
2043	27.9	85.9	0.9637	(Oliver et al., 2003)	28.2	84.0	-13.8	(Martin et al., 2005)
2044	27.9	85.9	0.9110	(Oliver et al., 2003)	28.7	83.9	-13.8	(Martin et al., 2005)
2045	27.9	85.9	0.9648	(Oliver et al., 2003)	28.7	83.9	-16.5	(Martin et al., 2005)
2046	27.9	85.9	0.8354	(Oliver et al., 2003)	28.7	83.9	-18.9	(Martin et al., 2005)
2047	27.9	85.9	0.8994	(Oliver et al., 2003)	28.7	83.9	-18.5	(Martin et al., 2005)
2048	27.9	85.9	0.9735	(Oliver et al., 2003)	28.7	83.9	-17.3	(Martin et al., 2005)
2049	27.9	85.9	0.7119	(Oliver et al., 2003)	28.2	85.4	-24.8	(Parrish and Hodges, 1996)
2050	27.9	85.9	0.7926	(Oliver et al., 2003)	28.1	85.4	-24.9	(Parrish and Hodges, 1996)
2051	27.9	85.9	0.8182	(Oliver et al., 2003)	28.1	85.4	-23.4	(Parrish and Hodges, 1996)
2052	27.9	85.9	0.7633	(Oliver et al., 2003)	28.1	85.4	-25.3	(Parrish and Hodges, 1996)
2053	27.9	85.9	0.7270	(Oliver et al., 2003)	28.1	85.4	-25.9	(Parrish and Hodges, 1996)
2054	27.9	85.9	0.9106	(Oliver et al., 2003)	28.1	85.4	-23.5	(Parrish and Hodges, 1996)
2055	27.9	85.9	0.9085	(Oliver et al., 2003)	28.1	85.4	-21.4	(Parrish and Hodges, 1996)
2056	27.9	85.9	0.7970	(Oliver et al., 2003)	28.1	85.4	-16.3	(Parrish and Hodges, 1996)

2057	27.9	85.9	0.7976	(Oliver et al., 2003)	28.1	85.4	-17.5	(Parrish and Hodges, 1996)
2058	27.9	85.9	0.9725	(Oliver et al., 2003)	28.1	85.4	-15.6	(Parrish and Hodges, 1996)
2059	27.7	85.6	0.7116	(Oliver et al., 2003)	28.1	85.4	-14.6	(Parrish and Hodges, 1996)
2060	27.7	85.6	0.7173	(Oliver et al., 2003)	28.1	85.5	-15.8	(Parrish and Hodges, 1996)
2061	27.7	85.6	0.7144	(Oliver et al., 2003)	28.1	85.5	-18.5	(Parrish and Hodges, 1996)
2062	27.7	85.6	0.7206	(Oliver et al., 2003)	29.7	71.8	-15.0	(Inger and Harris, 1993)
2063	27.7	85.6	0.7106	(Oliver et al., 2003)	30.3	75.0	-14.0	(Inger and Harris, 1993)
2064	27.3	83.4	0.7482	(Szulc et al., 2006)	30.5	75.7	-13.4	(Inger and Harris, 1993)
2065	27.3	83.4	0.7384	(Szulc et al., 2006)	28.9	84.0	-6.2	(Robinson et al., 2001)
2066	27.3	83.4	0.7338	(Szulc et al., 2006)	28.9	83.9	-16.2	(Robinson et al., 2001)
2067	27.3	83.4	0.7424	(Szulc et al., 2006)	28.8	83.9	-18.8	(Robinson et al., 2001)
2068	27.3	83.4	0.7407	(Szulc et al., 2006)	28.7	83.8	-18.9	(Robinson et al., 2001)
2069	27.3	83.4	0.7359	(Szulc et al., 2006)	28.7	83.7	-17.3	(Robinson et al., 2001)
2070	27.3	83.4	0.7371	(Szulc et al., 2006)	29.3	80.8	-17.6	(Robinson et al., 2001)
2071	29.0	89.7	0.70669	(Williams, 2004)	29.3	80.7	-20.1	(Robinson et al., 2001)
2072	29.0	89.7	0.70676	(Williams, 2004)	28.4	83.7	-19.9	(Robinson et al., 2001)
2073	29.0	89.7	0.70695	(Williams, 2004)	28.5	83.7	-18.0	(Robinson et al., 2001)
2074	29.0	89.7	0.71137	(Williams, 2004)	28.6	83.6	-9.8	(Robinson et al., 2001)
2075	32.9	80.5	0.71527	(Williams, 2004)	29.2	80.6	-11.8	(Robinson et al., 2001)

2076	32.9	80.5	0.71528	(Williams, 2004)	29.3	80.6	-7.6	(Robinson et al., 2001)
2077	32.9	80.5	0.71505	(Williams, 2004)	27.5	87.0	-16.1	(Robinson et al., 2001)
2078	32.9	80.5	0.73515	(Williams, 2004)	27.6	87.1	-13.5	(Robinson et al., 2001)
2079	29.6	85.8	0.70722	(Williams, 2004)	27.5	87.1	-15.6	(Robinson et al., 2001)
2080	35.2	83.0	0.70837	(Williams, 2004)	27.2	87.3	-25.3	(Robinson et al., 2001)
2081	35.2	83.0	0.71018	(Williams, 2004)	27.3	87.4	-19.7	(Robinson et al., 2001)
2082	35.2	83.0	0.71018	(Williams, 2004)	27.4	87.3	-20.7	(Robinson et al., 2001)
2083	35.8	89.5	0.70816	(Williams, 2004)	27.4	87.2	-23.6	(Robinson et al., 2001)
2084	35.8	89.5	0.70824	(Williams, 2004)	27.7	84.8	-24.7	(Robinson et al., 2001)
2085	35.8	89.5	0.70823	(Williams, 2004)	27.7	84.9	-21.9	(Robinson et al., 2001)
2086	35.8	89.5	0.70794	(Williams, 2004)	27.8	85.1	-24.2	(Robinson et al., 2001)
2087	33.3	90.3	0.71416	(Williams, 2004)	27.9	83.5	-23.0	(Robinson et al., 2001)
2088	33.3	90.3	0.70898	(Williams, 2004)	28.0	83.5	-17.5	(Robinson et al., 2001)
2089	33.3	90.3	0.70906	(Williams, 2004)	28.1	83.6	-19.7	(Robinson et al., 2001)
2090	29.0	89.7	0.70669	(Williams, 2004)	28.2	83.6	-25.3	(Robinson et al., 2001)
2091	28.9	89.0	0.70720	(Zhao et al., 2001)	28.3	83.6	-19.3	(Robinson et al., 2001)
2092	29.0	89.3	0.70614	(Zhao et al., 2001)	28.4	83.6	-20.8	(Robinson et al., 2001)
2093	29.2	89.5	0.70673	(Zhao et al., 2001)	29.5	80.7	-15.9	(Robinson et al., 2001)
2094	29.2	89.1	0.70571	(Zhao et al., 2001)	29.4	80.8	-23.3	(Robinson et al., 2001)

2095	29.2	88.8	0.70704	(Zhao et al., 2001)	29.5	80.9	-21.1	(Robinson et al., 2001)
2096	29.0	89.1	0.70950	(Zhao et al., 2001)	29.5	81.0	-21.8	(Robinson et al., 2001)
2097	28.8	89.5	0.71002	(Zhao et al., 2001)	29.6	81.1	-18.1	(Robinson et al., 2001)
2098	29.0	89.5	0.70801	(Zhao et al., 2001)	26.8	87.1	-8.1	(Robinson et al., 2001)
2099	30.9	86.4	0.71852	(Hao et al., 2022)	26.8	87.1	-10.7	(Robinson et al., 2001)
2100	31.0	86.4	0.71788	(Hao et al., 2022)	26.8	87.1	-14.9	(Robinson et al., 2001)
2101	31.0	86.4	0.72294	(Hao et al., 2022)	27.7	86.4	-16.0	(Robinson et al., 2001)
2102	31.0	86.4	0.71849	(Hao et al., 2022)	27.7	86.4	-16.8	(Robinson et al., 2001)
2103	31.0	86.4	0.72083	(Hao et al., 2022)	27.7	86.4	-15.9	(Robinson et al., 2001)
2104	30.9	86.7	0.71907	(Hao et al., 2022)	27.7	84.4	-16.4	(Robinson et al., 2001)
2105	30.9	86.7	0.71917	(Hao et al., 2022)	27.7	84.4	-15.5	(Robinson et al., 2001)
2106	30.8	86.7	0.71923	(Hao et al., 2022)	27.7	84.4	-17.7	(Robinson et al., 2001)
2107	30.8	86.7	0.71958	(Hao et al., 2022)	27.7	84.4	-16.4	(Robinson et al., 2001)
2108	30.8	86.8	0.71944	(Hao et al., 2022)	27.7	84.4	-15.5	(Robinson et al., 2001)
2109	30.8	86.8	0.71926	(Hao et al., 2022)	27.7	84.4	-18.0	(Robinson et al., 2001)
2110	30.7	86.8	0.72027	(Hao et al., 2022)	27.7	84.4	-16.5	(Robinson et al., 2001)
2111	30.7	86.8	0.71919	(Hao et al., 2022)	27.7	84.4	-16.1	(Robinson et al., 2001)
2112	30.1	86.4	0.71972	(Hao et al., 2022)	27.9	91.9	-18.2	GEOROC
2113	30.1	86.4	0.71675	(Hao et al., 2022)	27.9	91.9	-15.5	GEOROC
2114	30.2	86.4	0.71648	(Hao et al., 2022)	27.9	91.9	-18.1	GEOROC
2115	30.1	86.4	0.71659	(Hao et al., 2022)	27.9	91.9	-15.6	GEOROC

2116	30.1	86.4	0.72638	(Hao et al., 2022)	27.9	91.9	-17.7	GEOROC
2117	30.1	86.4	0.73461	(Hao et al., 2022)	27.9	91.8	-19.3	GEOROC
2118	30.1	86.5	0.73025	(Hao et al., 2022)	27.9	91.8	-19.8	GEOROC
2119	30.2	86.5	0.73627	(Hao et al., 2022)	28.6	78.8	-15.8	GEOROC
2120	30.2	86.5	0.73649	(Hao et al., 2022)	20.0	78.5	-17.5	GEOROC
2121	29.7	89.6	0.70679	(Hao et al., 2022)	26.4	79.8	-15.4	GEOROC
2122	29.7	89.6	0.71106	(Hao et al., 2022)	29.4	77.2	-17.7	GEOROC
2123	29.7	89.6	0.71479	(Hao et al., 2022)	28.4	77.1	-15.4	GEOROC
2124	29.7	89.6	0.70687	(Hao et al., 2022)	28.6	77.2	-14.7	GEOROC
2125	29.7	89.6	0.70688	(Hao et al., 2022)	28.3	75.9	-14.4	GEOROC
2126	29.7	89.6	0.70652	(Hao et al., 2022)	28.5	76.3	-13.4	GEOROC
2127	29.7	89.6	0.70715	(Hao et al., 2022)	29.5	76.7	-13.2	GEOROC
2128	29.9	91.1	0.70485	(Lee et al., 2012)	29.6	76.6	-13.3	GEOROC
2129	29.9	91.1	0.70508	(Lee et al., 2012)	30.0	75.7	-15.8	GEOROC
2130	29.9	90.6	0.70628	(Lee et al., 2012)	29.9	76.0	-15.4	GEOROC
2131	30.4	87.1	0.73998	(Lee et al., 2012)	27.4	85.2	-17.4	GEOROC
2132	30.4	87.1	0.71312	(Lee et al., 2012)	27.4	85.2	-18.5	GEOROC
2133	30.4	87.1	0.73760	(Lee et al., 2012)	27.4	85.2	-17.8	GEOROC
2134	29.9	91.0	0.70518	(Lee et al., 2012)	27.4	85.2	-18.8	GEOROC
2135	30.0	91.1	0.70897	(Lee et al., 2012)	27.4	85.2	-17.9	GEOROC
2136	29.2	88.8	0.70378	(Lee et al., 2012)	25.5	85.1	-17.7	GEOROC
2137	29.8	92.9	0.70724	(Lee et al., 2012)	25.5	85.1	-18.1	GEOROC
2138	30.8	88.7	0.70856	(Lee et al., 2012)	25.5	85.1	-17.9	GEOROC
2139	29.6	91.1	0.70534	(Lee et al., 2012)	25.5	85.1	-18.1	GEOROC
2140	29.9	89.0	0.70584	(Lee et al., 2012)	25.5	85.1	-18.9	GEOROC
2141	30.8	88.7	0.70595	(Lee et al., 2012)	25.5	85.1	-18.4	GEOROC
2142	29.6	89.0	0.70604	(Lee et al., 2012)	25.1	78.9	-34.0	GEOROC
2143	29.9	89.0	0.70642	(Lee et al., 2012)	25.5	74.8	-32.1	GEOROC
2144	29.9	89.0	0.70578	(Lee et al., 2012)	25.6	74.1	-21.3	GEOROC
2145	29.7	89.9	0.70553	(Lee et al., 2012)	26.5	75.0	-3.0	GEOROC
2146	29.7	89.9	0.70556	(Lee et al., 2012)	27.5	75.6	-28.2	GEOROC
2147	29.9	89.0	0.70516	(Lee et al., 2012)	23.3	79.6	-16.9	GEOROC
2148	29.7	86.7	0.70597	(Lee et al., 2012)	23.4	79.9	-14.7	GEOROC
2149	29.7	86.7	0.71580	(Lee et al., 2012)	23.6	79.6	-15.4	GEOROC
2150	29.9	89.0	0.70736	(Lee et al., 2012)	23.1	79.4	-16.4	GEOROC
2151	29.7	89.9	0.70775	(Lee et al., 2012)	26.0	77.1	-14.6	GEOROC
2152	31.4	91.9	0.71317	(Lee et al., 2012)	25.9	76.9	-16.9	GEOROC
2153	31.1	87.3	0.72773	(Lee et al., 2012)	28.1	96.5	5.1	GEOROC
2154	31.4	91.9	0.71286	(Lee et al., 2012)	28.0	96.4	5.1	GEOROC
2155	30.5	87.4	0.71313	(Lee et al., 2012)	28.6	95.9	3.2	GEOROC
2156	29.8	85.9	0.70686	(Lee et al., 2012)	28.6	95.8	3.2	GEOROC
2157	29.0	80.1	0.76020	(Lee et al., 2012)	25.1	75.1	-17.8	GEOROC
2158	28.9	80.5	0.73226	(Lee et al., 2012)	25.0	75.1	-16.4	GEOROC

2159	29.1	79.8	0.74745	(Gao & Zeng, 2014)	25.0	75.1	-15.2	GEOROC
2160	29.0	80.1	0.74732	(Gao & Zeng, 2014)	25.5	75.6	-14.8	GEOROC
2161	28.9	80.3	0.74835	(Gao & Zeng, 2014)	25.5	75.9	-15.5	GEOROC
2162	30.5	82.3	0.70940	(Lin et al., 2021)	24.8	74.6	-23.4	GEOROC
2163	30.5	82.3	0.70942	(Lin et al., 2021)	24.8	74.6	-16.4	GEOROC
2164	30.5	82.3	0.70947	(Lin et al., 2021)	24.4	74.7	-18.5	GEOROC
2165	30.5	82.3	0.70945	(Lin et al., 2021)	25.1	75.1	-15.5	GEOROC
2166	29.5	89.6	0.70520	(Chu et al., 2006)	24.9	75.6	-17.0	GEOROC
2167	30.0	93.0	0.71339	(Chu et al., 2006)	25.6	76.1	-17.8	GEOROC
2168	30.1	89.1	0.71329	(Chu et al., 2006)	25.5	76.0	-20.2	GEOROC
2169	29.3	91.8	0.70504	(Chu et al., 2006)	25.7	76.2	-19.4	GEOROC
2170	28.6	92.3	0.72235	(Hu et al., 2018)	25.7	76.2	-18.6	GEOROC
2171	28.8	84.8	0.74952	(Hu et al., 2018)	25.7	76.3	-14.2	GEOROC
2172	28.9	92.0	0.71333	(Hu et al., 2018)	25.6	77.0	-17.6	GEOROC
2173	30.0	95.4	0.71749	(Lin et al., 2012)	25.0	74.7	-15.2	GEOROC
2174	29.5	96.6	0.71676	(Lin et al., 2012)	24.9	74.7	-17.8	GEOROC
2175	29.5	96.6	0.71542	(Lin et al., 2012)	25.0	75.6	-17.2	GEOROC
2176	29.5	96.6	0.71478	(Lin et al., 2012)	24.9	74.7	-18.2	GEOROC
2177	29.4	96.9	0.74112	(Lin et al., 2012)	24.9	74.7	-17.1	GEOROC
2178	29.3	97.1	0.71387	(Lin et al., 2012)	24.8	74.6	-22.6	GEOROC
2179	29.7	96.0	0.70686	(Lin et al., 2012)	24.9	74.6	-19.2	GEOROC
2180	29.8	95.7	0.71187	(Lin et al., 2012)	28.9	88.4	-13.7	(Zhang et al., 2004)
2181	29.8	95.7	0.72264	(Lin et al., 2012)	28.9	88.4	-13.4	(Zhang et al., 2004)
2182	29.5	96.6	0.70656	(Lin et al., 2012)	28.9	88.4	-13.8	(Zhang et al., 2004)
2183	29.5	96.8	0.70645	(Lin et al., 2012)	28.9	88.4	-13.1	(Zhang et al., 2004)
2184	29.7	96.0	0.70624	(Lin et al., 2012)	28.8	88.1	-13.7	(Zhang et al., 2004)
2185	29.7	96.0	0.70617	(Lin et al., 2012)	28.8	88.1	-14.1	(Zhang et al., 2004)
2186	29.7	96.0	0.70609	(Lin et al., 2012)	28.8	88.1	-13.5	(Zhang et al., 2004)
2187	28.6	97.1	0.71643	(Lin et al., 2012)	28.8	88.1	-13.3	(Zhang et al., 2004)
2188	28.6	97.2	0.74917	(Lin et al., 2012)	28.7	87.8	-19.5	(Zhang et al., 2004)
2189	28.7	97.5	0.75054	(Lin et al., 2012)	28.7	87.8	-19.3	(Zhang et al., 2004)
2190	28.5	97.0	0.70789	(Lin et al., 2012)	28.7	87.8	-18.3	(Zhang et al., 2004)
2191	28.5	97.0	0.70796	(Lin et al., 2012)	28.7	87.8	-19.0	(Zhang et al., 2004)
2192	30.13	78.33	0.78388	(Lupker et al., 2012)	28.8	92.0	-10.8	(Zeng et al., 2015)

2193	30.13	78.33	0.78384	(Lupker et al., 2012)	28.8	92.0	-11.3	(Zeng et al., 2015)
2194	30.52	78.35	0.78652	(Singh et al., 2008)	28.8	92.0	-13.2	(Zeng et al., 2015)
2195	30.52	78.35	0.77489	(Singh et al., 2008)	28.8	92.0	-12.5	(Zeng et al., 2015)
2196	26.43	80.35	0.77989	(Singh et al., 2008)	28.8	92.0	-9.8	(Zeng et al., 2015)
2197	25.43	81.88	0.77726	(Singh et al., 2008)	28.8	92.0	-10.4	(Zeng et al., 2015)
2198	25.50	81.87	0.77164	(Singh et al., 2008)	28.8	92.0	-10.2	(Zeng et al., 2015)
2199	25.50	81.87	0.77485	(Singh et al., 2008)	28.8	92.0	-10.9	(Zeng et al., 2015)
2200	25.30	84.00	0.77137	(Singh et al., 2008)	28.7	92.2	-13.0	(Zeng et al., 2015)
2201	25.30	83.00	0.74807	(Singh et al., 2008)	28.7	92.2	-12.9	(Zeng et al., 2015)
2202	25.30	83.00	0.78280	(Singh et al., 2008)	28.7	92.2	-9.6	(Zeng et al., 2015)
2203	25.53	83.20	0.78089	(Singh et al., 2008)	28.7	92.2	-13.1	(Zeng et al., 2015)
2204	25.73	84.82	0.78168	(Singh et al., 2008)	28.4	92.2	-13.6	(Zeng et al., 2015)
2205	25.62	85.15	0.76887	(Singh et al., 2008)	28.4	92.2	-13.2	(Zeng et al., 2015)
2206	25.62	85.15	0.76830	(Singh et al., 2008)	28.4	92.2	-13.5	(Zeng et al., 2015)
2207	25.38	86.00	0.75769	(Singh et al., 2008)	28.4	92.2	-13.2	(Zeng et al., 2015)
2208	25.37	86.00	0.75527	(Singh et al., 2008)	28.4	92.2	-13.7	(Zeng et al., 2015)
2209	25.37	86.00	0.76225	(Singh et al., 2008)	28.4	92.2	-13.8	(Zeng et al., 2015)
2210	25.06	87.83	0.76179	(Singh et al., 2008)	28.4	92.2	-13.4	(Zeng et al., 2015)
2211	25.06	87.83	0.76482	(Singh et al., 2008)	30.2	81.6	-10.5	(Murphy, 2007)
2212	25.06	87.83	0.76355	(Singh et al., 2008)	30.4	81.4	-17.6	(Murphy, 2007)
2213	24.05	89.02	0.78392	(Lupker et al., 2012)	30.5	81.4	-14.4	(Murphy, 2007)
2214	24.05	89.02	0.78461	(Lupker et al., 2012)	30.4	81.6	-22.8	(Murphy, 2007)
2215	24.05	89.02	0.79196	(Lupker et al., 2012)	30.3	81.7	-21.3	(Murphy, 2007)
2216	24.05	89.02	0.80176	(Lupker et al., 2012)	30.1	81.9	-23.0	(Murphy, 2007)
2217	24.05	89.02	0.77358	(Lupker et al., 2012)	30.0	82.2	-23.4	(Murphy, 2007)
2218	24.05	89.02	0.77752	(Lupker et al., 2012)	30.0	82.5	-14.0	(Murphy, 2007)
2219	24.05	89.02	0.77965	(Lupker et al., 2012)	30.1	82.3	-21.3	(Murphy, 2007)
2220	24.05	89.02	0.77135	(Lupker et al., 2012)	32.1	77.5	-15.6	(Miller et al., 2001)

2221	24.05	89.02	0.77789	(Lupker et al., 2012)	33.5	76.8	-12.8	(Miller et al., 2001)
2222	24.05	89.02	0.77111	(Lupker et al., 2012)	32.3	77.1	-14.0	(Miller et al., 2001)
2223	24.05	89.02	0.77825	(Lupker et al., 2012)	31.6	78.4	-14.6	(Miller et al., 2001)
2224	24.05	89.02	0.77297	(Lupker et al., 2012)	31.5	78.4	-11.7	(Miller et al., 2001)
2225	24.05	89.02	0.77185	(Lupker et al., 2012)	31.4	77.2	-13.4	(Miller et al., 2001)
2226	24.05	89.02	0.77230	(Lupker et al., 2012)	31.4	77.1	-13.3	(Miller et al., 2001)
2227	24.05	89.02	0.77252	(Lupker et al., 2012)	31.5	77.0	-13.9	(Miller et al., 2001)
2228	24.05	89.02	0.75780	(Lupker et al., 2012)	31.7	76.9	-6.1	(Miller et al., 2001)
2229	24.05	89.02	0.76642	(Lupker et al., 2012)	31.6	77.0	-1.3	(Miller et al., 2001)
2230	24.05	89.02	0.77228	(Lupker et al., 2012)	31.5	77.0	-2.1	(Miller et al., 2001)
2231	24.05	89.02	0.76864	(Lupker et al., 2012)	32.8	77.0	-12.1	(Miller et al., 2001)
2232	24.05	89.02	0.75757	(Lupker et al., 2012)	31.2	77.2	-14.9	(Miller et al., 2001)
2233	24.05	89.02	0.76914	(Lupker et al., 2012)	31.1	77.2	-17.0	(Miller et al., 2001)
2234	25.42	81.88	0.76241	(Singh et al., 2008)	32.9	76.7	-18.6	(Miller et al., 2001)
2235	25.42	81.88	0.75338	(Singh et al., 2008)	31.9	77.2	-11.3	(Miller et al., 2001)
2236	28.08	95.34	0.7206	(Singh et al., 2006)	31.1	77.2	-13.6	(Miller et al., 2001)
2237	27.5	94.85	0.71866	(Singh et al., 2006)	31.1	77.4	-15.4	(Miller et al., 2001)
2238	26.61	92.85	0.72848	(Singh et al., 2006)	33.0	76.8	-18.8	(Miller et al., 2001)
2239	26.61	92.85	0.7192	(Singh et al., 2006)	25.1	67.6	-13.5	(Clift et al., 2010)
2240	26.19	91.74	0.72105	(Singh et al., 2006)	25.1	67.6	-15.2	(Clift et al., 2010)
2241	26.19	91.74	0.72186	(Singh et al., 2006)	25.1	67.6	-12.7	(Clift et al., 2010)
2242	26.02	90	0.73439	(Singh et al., 2006)	25.1	67.6	-14.0	(Clift et al., 2010)
2243	27.8	95.59	0.7053	(Singh et al., 2006)	25.1	67.6	-11.8	(Clift et al., 2010)
2244	27.8	95.6	0.70881	(Singh et al., 2006)	25.1	67.6	-12.4	(Clift et al., 2010)

2245	27.45	94.25	0.73563	(Singh et al., 2006)	25.1	67.6	-10.8	(Clift et al., 2010)
2246	27.45	94.26	0.73013	(Singh et al., 2006)	25.2	68.2	-14.2	(Clift et al., 2010)
2247	27.2	94.06	0.73065	(Singh et al., 2006)	25.2	68.2	-13.8	(Clift et al., 2010)
2248	27.23	94.06	0.73812	(Singh et al., 2006)	25.2	68.2	-13.2	(Clift et al., 2010)
2249	26.81	92.88	0.77705	(Singh et al., 2006)	29.2	71.9	-14.7	(East et al., 2015)
2250	26.81	92.88	0.77682	(Singh et al., 2006)	29.2	71.9	-15.3	(East et al., 2015)
2251	26.5	90.92	0.75867	(Singh et al., 2006)	29.2	71.9	-14.5	(East et al., 2015)
2252	26.5	90.94	0.7703	(Singh et al., 2006)	29.2	72.3	-14.8	(East et al., 2015)
2253	26.37	91.6	0.7644	(Singh et al., 2006)	29.2	72.3	-13.7	(East et al., 2015)
2254	26	91.6	0.76005	(Singh et al., 2006)	29.2	72.3	-13.9	(East et al., 2015)
2255	26.22	90.14	0.78452	(Singh et al., 2006)	29.2	72.3	-13.9	(East et al., 2015)
2256	26.63	93.73	0.73342	(Singh et al., 2006)	29.2	72.3	-15.1	(East et al., 2015)
2257	27.31	94.88	0.73252	(Singh et al., 2006)	29.2	72.3	-15.4	(East et al., 2015)
2258	26.16	92.35	0.71814	(Singh et al., 2006)	29.1	71.6	-14.8	(East et al., 2015)
2259	26.16	92.35	0.72742	(Singh et al., 2006)	29.1	71.6	-15.9	(East et al., 2015)
2260	28.08	95.34	0.7206	(Singh et al., 2006)	29.1	71.8	-14.5	(East et al., 2015)
2261	27.5	94.85	0.71866	(Singh et al., 2006)	29.1	71.8	-14.8	(East et al., 2015)
2262	28.02	88.76	0.75073	(Das et al., 2022)	29.1	71.8	-14.7	(East et al., 2015)
2263	28.05	88.69	0.75185	(Das et al., 2022)	29.1	71.8	-14.8	(East et al., 2015)
2264	27.94	88.55	0.75123	(Das et al., 2022)	29.1	71.8	-14.6	(East et al., 2015)
2265	27.84	88.55	0.74867	(Das et al., 2022)	29.1	71.8	-14.8	(East et al., 2015)
2266	27.64	88.62	0.75073	(Das et al., 2022)	28.8	69.1	-9.25	(Roddaz et al., 2011)

2267	27.55	88.64	0.81076	(Das et al., 2022)	28.8	69.1	-11.88	(Roddaz et al., 2011)
2268	27.41	88.52	0.82288	(Das et al., 2022)	29.0	68.9	-12.27	(Roddaz et al., 2011)
2269	27.21	88.49	0.81178	(Das et al., 2022)	29.0	68.9	-10.69	(Roddaz et al., 2011)
2270	27.17	88.53	0.80816	(Das et al., 2022)	29.0	68.9	-9.85	(Roddaz et al., 2011)
2271	26.88	88.48	0.80221	(Das et al., 2022)	29.0	68.9	-11.7	(Roddaz et al., 2011)
2272	26.75	88.59	0.79568	(Das et al., 2022)	28.8	69.1	-12.5	(Roddaz et al., 2011)
2273	26.34	88.88	0.7981	(Das et al., 2022)	28.9	69.1	-13.3	(Roddaz et al., 2011)
2274	27.76	88.54	0.75765	(Das et al., 2022)	28.9	69.1	-12.0	(Roddaz et al., 2011)
2275	27.81	88.63	0.76832	(Das et al., 2022)	28.9	69.1	-9.6	(Roddaz et al., 2011)
2276	27.69	88.74	0.80816	(Das et al., 2022)	28.9	69.1	-9.4	(Roddaz et al., 2011)
2277	27.54	88.63	0.90529	(Das et al., 2022)	28.9	69.1	-9.8	(Roddaz et al., 2011)
2278	27.53	88.61	0.8357	(Das et al., 2022)	28.9	69.2	-9.8	(Roddaz et al., 2011)
2279	27.52	88.53	0.89287	(Das et al., 2022)	28.9	69.2	-9.3	(Roddaz et al., 2011)
2280	27.23	88.50	0.90011	(Das et al., 2022)	29.1	69.0	-8.5	(Roddaz et al., 2011)
2281	27.19	88.59	0.85148	(Das et al., 2022)	29.1	69.0	-9.5	(Roddaz et al., 2011)
2282	27.19	88.61	0.81813	(Das et al., 2022)	25.1	94.3	2.9	(Kingson et al., 2019)
2283	27.17	88.53	0.80791	(Das et al., 2022)	25.1	94.3	3.0	(Kingson et al., 2019)
2284	27.22	88.34	0.79899	(Das et al., 2022)	25.0	94.3	9.9	(Kingson et al., 2019)
2285	27.13	88.28	0.77635	(Das et al., 2022)	25.0	94.3	9.6	(Kingson et al., 2019)

2286	27.11	88.33	0.82662	(Das et al., 2022)	25.0	94.3	8.7	(Kingson et al., 2019)
2287	26.82	88.60	0.86235	(Das et al., 2022)	25.2	94.5	3.2	(Kingson et al., 2019)
2288	28.02	88.76	0.75073	(Das et al., 2022)	25.2	94.5	2.9	(Kingson et al., 2019)
2289					25.2	94.5	3.2	(Kingson et al., 2019)
2290					25.2	94.5	3.2	(Kingson et al., 2019)
2291					14.2	98.4	-11.4	(Li et al., 2019)
2292					14.2	98.4	-10.9	(Li et al., 2019)
2293					14.2	98.4	-10.6	(Li et al., 2019)
2294					14.2	98.4	-14.5	(Li et al., 2019)
2295					14.3	98.2	-11.0	(Li et al., 2019)
2296					14.3	98.3	-11.1	(Li et al., 2019)
2297					13.9	98.1	-5.5	(Li et al., 2019)
2298					13.9	98.1	-5.6	(Li et al., 2019)
2299					13.9	98.1	-5.8	(Li et al., 2019)
2300					13.9	98.1	-8.6	(Li et al., 2019)
2301					14.1	98.1	-7.6	(Li et al., 2019)
2302					14.1	98.1	-7.0	(Li et al., 2019)
2303					13.9	99.1	-14.6	(Li et al., 2019)
2304					13.9	99.1	-8.5	(Li et al., 2019)
2305					13.7	99.4	-10.6	(Li et al., 2019)
2306					12.7	98.7	-9.5	(Li et al., 2019)
2307					12.5	98.4	-9.6	(Li et al., 2019)
2308					12.5	98.7	-9.5	(Li et al., 2019)
2309					28.7	95.9	3.2	(Haproff et al., 2019)

2310					28.3	95.9	3.2	(Haproff et al., 2019)
2311					28.6	95.9	5.1	(Haproff et al., 2019)
2312					28.6	95.9	3.2	(Haproff et al., 2019)
2313					28.6	95.8	7.1	(Haproff et al., 2019)
2314					28.6	95.8	1.2	(Haproff et al., 2019)
2315					28.5	95.9	-6.6	(Haproff et al., 2019)
2316					28.2	95.9	-18.3	(Haproff et al., 2019)
2317					28.2	95.9	-16.3	(Haproff et al., 2019)
2318					28.2	95.9	-10.5	(Haproff et al., 2019)
2319					28.2	95.9	-18.3	(Haproff et al., 2019)
2320					28.2	95.8	-18.3	(Haproff et al., 2019)
2321					28.2	95.9	-28.1	(Haproff et al., 2019)
2322					28.2	95.8	-16.3	(Haproff et al., 2019)
2323					28.2	95.8	-10.5	(Haproff et al., 2019)
2324					25.1	94.3	2.9	(Singh 2018 thesis work)
2325					25.1	94.3	3.0	(Singh 2018 thesis work)
2326					25.0	94.4	8.5	(Singh 2018 thesis work)
2327					25.0	94.4	8.7	(Singh 2018 thesis work)
2328					25.0	94.3	9.9	(Singh 2018 thesis work)

2329					25.0	94.3	9.6	(Singh 2018 thesis work)
2330					25.0	94.3	8.7	(Singh 2018 thesis work)
2331					25.2	94.5	3.2	(Singh 2018 thesis work)
2332					25.2	94.5	2.9	(Singh 2018 thesis work)
2333					25.2	94.5	3.2	(Singh 2018 thesis work)
2334					25.2	94.5	3.2	(Singh 2018 thesis work)
2335					25.6	94.3	-8.8	(Singh 2018 thesis work)
2336					25.2	94.4	0.7	(Singh 2018 thesis work)
2337					25.2	94.4	8.3	(Singh 2018 thesis work)
2338					25.2	94.5	1.4	(Singh 2018 thesis work)
2339					25.1	94.5	-9.6	(Singh 2018 thesis work)
2340					25.1	94.5	10.5	(Singh 2018 thesis work)
2341					25.0	94.5	12.5	(Singh 2018 thesis work)
2342					25.0	94.5	-0.9	(Singh 2018 thesis work)
2343					25.0	94.5	16.0	(Singh 2018 thesis work)
2344					24.3	94.3	8.2	(Singh 2018 thesis work)
2345					24.3	94.3	10.4	(Singh 2018 thesis work)
2346					24.3	94.3	6.8	(Singh 2018 thesis work)
2347					24.3	94.3	11.9	(Singh 2018 thesis work)

2348					24.3	94.3	11.7	(Singh 2018 thesis work)
2349					24.3	94.3	13.7	(Singh 2018 thesis work)
2350					24.3	94.3	-4.2	(Singh 2018 thesis work)
2351					24.2	94.3	10.9	(Singh 2018 thesis work)
2352					31.6	78.4	-17.6	(Richards et al. 2005)
2353					31.6	78.4	-8.1	(Richards et al. 2005)
2354					31.6	78.3	-15.8	(Richards et al. 2005)
2355					31.6	78.3	-13.2	(Richards et al. 2005)
2356					31.6	78.3	-12.9	(Richards et al. 2005)
2357					31.5	78.2	-16.5	(Richards et al. 2005)
2358					31.5	78.2	-15.8	(Richards et al. 2005)
2359					31.5	78.2	-16.2	(Richards et al. 2005)
2360					31.6	78.0	-22.0	(Richards et al. 2005)
2361					31.6	77.8	-23.1	(Richards et al. 2005)
2362					31.5	77.7	-23.3	(Richards et al. 2005)
2363					31.5	77.8	-22.8	(Richards et al. 2005)
2364					31.5	77.8	-20.7	(Richards et al. 2005)
2365					31.4	77.6	-23.6	(Richards et al. 2005)
2366					31.4	77.6	-26.6	(Richards et al. 2005)
2367					31.4	77.5	-24.5	(Richards et al. 2005)
2368					31.4	77.7	-14.3	(Richards et al. 2005)
2369					31.3	77.4	-10.5	(Richards et al. 2005)

2370					31.3	77.5	-16.4	(Richards et al. 2005)
2371					31.2	77.4	-11.1	(Richards et al. 2005)
2372					31.1	77.3	-13.7	(Richards et al. 2005)
2373					31.1	77.2	-16.2	(Richards et al. 2005)
2374					31.0	77.2	-12.2	(Richards et al. 2005)
2375					31.0	77.1	-13.4	(Richards et al. 2005)
2376					31.0	77.1	-12.2	(Richards et al. 2005)
2377					30.6	77.6	-15.8	(Richards et al. 2005)
2378					31.6	78.4	-18.9	(Richards et al. 2005)
2379					31.8	78.4	-17.0	(Richards et al. 2005)
2380					31.7	78.5	-14.0	(Richards et al. 2005)
2381					31.6	78.4	-7.8	(Richards et al. 2005)
2382					32.7	76.5	-14.3	(Richards et al. 2005)
2383					32.8	76.4	-17.0	(Richards et al. 2005)
2384					32.3	76.6	-16.4	(Richards et al. 2005)
2385					32.3	76.6	-12.0	(Richards et al. 2005)
2386					32.4	76.7	-13.5	(Richards et al. 2005)
2387					32.5	76.4	-15.5	(Richards et al. 2005)
2388					32.6	76.2	-13.6	(Richards et al. 2005)
2389					32.6	76.2	-14.0	(Richards et al. 2005)
2390					30.0	91.7	-8.6	(Dai et al. 2008)
2391					30.0	91.7	-8.2	(Dai et al. 2008)
2392					30.0	91.7	-9.8	(Dai et al. 2008)

2393					29.1	90.4	-5.4	(Dai et al. 2008)
2394					28.3	91.2	-16.8	(Dai et al. 2008)
2395					28.2	91.2	-16.9	(Dai et al. 2008)
2396					28.2	91.2	-17.5	(Dai et al. 2008)
2397					28.1	91.1	-8.0	(Dai et al. 2008)
2398					28.2	91.0	-18.0	(Dai et al. 2008)
2399					35.3	74.6	-10.7	(Argles et al. 2003)
2400					35.2	74.6	-12.2	(Argles et al. 2003)
2401					35.3	74.7	-16.9	(Argles et al. 2003)
2402					35.2	74.6	-9.9	(Argles et al. 2003)
2403					35.2	74.4	-13.9	(Argles et al. 2003)
2404					35.2	74.5	-16.2	(Argles et al. 2003)
2405					35.3	74.7	-13.1	(Argles et al. 2003)
2406					35.2	74.5	-14.0	(Argles et al. 2003)
2407					35.3	74.7	-8.3	(Argles et al. 2003)
2408					35.2	74.6	-13.8	(Argles et al. 2003)
2409					35.3	74.6	-14.7	(Argles et al. 2003)
2410					35.3	74.5	0.6	(Argles et al. 2003)
2411					35.3	74.6	-15.1	(Argles et al. 2003)
2412					35.5	74.7	-18.1	(Argles et al. 2003)
2413					35.3	74.8	-1.0	(Argles et al. 2003)
2414					35.4	74.8	-14.5	(Argles et al. 2003)
2415					35.2	74.8	-15.0	(Argles et al. 2003)
2416					35.5	74.7	-16.5	(Argles et al. 2003)

2417					35.7	74.8	-12.3	(Argles et al. 2003)
2418					35.7	75.3	-17.5	(Argles et al. 2003)
2419					35.5	74.9	-18.8	(Argles et al. 2003)
2420					35.5	75.1	-28.8	(Gazis et al. 1998)
2421					35.4	75.5	-28.7	(Gazis et al. 1998)
2422					35.4	76.0	-25.5	(Gazis et al. 1998)
2423					35.3	75.9	-26.5	(Gazis et al. 1998)
2424					34.9	76.0	-28.4	(Gazis et al. 1998)
2425					34.6	75.8	-26.2	(Gazis et al. 1998)
2426					34.6	75.2	-27.1	(Gazis et al. 1998)
2427					29.6	80.1	-22.0	(Mackenzie et al. 2011)
2428					30.7	77.8	-16.0	(Mackenzie et al. 2011)
2429					29.4	79.4	-16.0	(Mackenzie et al. 2011)
2430					30.6	77.8	-16.9	(Mackenzie et al. 2011)
2431					27.3	83.4	-16.5	(Szulc et al. 2006)
2432					27.3	83.4	-17.3	(Szulc et al. 2006)
2433					27.3	83.4	-16.9	(Szulc et al. 2006)
2434					27.3	83.4	-16.9	(Szulc et al. 2006)
2435					27.3	83.4	-17.6	(Szulc et al. 2006)
2436					27.3	83.4	-17.2	(Szulc et al. 2006)
2437					27.3	83.4	-16.9	(Szulc et al. 2006)
2438					30.0	95.3	-12.1	(Lin et al., 2012)
2439					29.5	96.6	-8.4	(Lin et al., 2012)
2440					29.5	96.6	-9.1	(Lin et al., 2012)
2441					29.5	96.6	-8.5	(Lin et al., 2012)
2442					29.3	96.9	-7.3	(Lin et al., 2012)

2443					29.2	97.0	-8.3	(Lin et al., 2012)
2444					29.7	96.0	-5.1	(Lin et al., 2012)
2445					29.8	95.7	-4.6	(Lin et al., 2012)
2446					29.8	95.7	-13.9	(Lin et al., 2012)
2447					29.5	96.6	-5.2	(Lin et al., 2012)
2448					29.7	96.0	-3.6	(Lin et al., 2012)
2449					29.7	96.0	-2.4	(Lin et al., 2012)
2450					29.7	96.0	-3.5	(Lin et al., 2012)
2451					29.4	96.9	-10.7	(Lin et al., 2012)
2452					29.4	96.9	-11.7	(Lin et al., 2012)
2453					29.4	96.9	-11.5	(Lin et al., 2012)
2454					29.4	96.9	-11.5	(Lin et al., 2012)
2455					29.4	96.9	-11.4	(Lin et al., 2012)
2456					28.5	97.0	-11.1	(Lin et al., 2012)
2457					28.5	97.2	-11.1	(Lin et al., 2012)
2458					28.6	97.5	-8.9	(Lin et al., 2012)
2459					28.5	97.0	-2.0	(Lin et al., 2012)
2460					28.5	97.0	-2.3	(Lin et al., 2012)
2461					28.6	97.5	-13.5	(Lin et al., 2012)

Table S3: $^{87}\text{Sr}/^{86}\text{Sr}$ and ε_{Nd} data used for the characterisation of Dust end member, used in Binary mixing plot.

Sr. No.	$^{87}\text{Sr}/^{86}\text{Sr}$	ε_{Nd}	References	Comments
1	0.7193	-14.1	(Grousset et al., 1998)	Saharan aerosol
2	0.7225	-13.2	(Grousset et al., 1998)	Saharan aerosol
3	0.7223	-11.9	(Grousset et al., 1998)	Saharan aerosol
4	0.7287	-11.3	(Grousset et al., 1998)	Saharan aerosol
5	0.7144	-14.2	(Grousset et al., 1992)	Saharan aerosol
6	0.717	-12.8	(Grousset et al., 1992)	Saharan aerosol
7	0.7148	-14.5	(Grousset et al., 1992)	Saharan aerosol
8	0.715	-13.9	(Grousset et al., 1992)	Saharan aerosol
9	0.7154	-12.7	(Grousset et al., 1992)	Saharan aerosol
10	0.7167	-12.7	(Grousset et al., 1992)	Saharan aerosol
11	0.7155	-11.2	(Grousset et al., 1992)	Saharan aerosol
12	0.7302	-15.9	(Tripathi et al., 2013)	Delhi Loess
13	0.7304	-15	(Tripathi et al., 2013)	Delhi Loess
14	0.7313	-15.3	(Tripathi et al., 2013)	Delhi Loess
15	0.7294	-14	(Tripathi et al., 2013)	Delhi Loess
16	0.7306	-15.3	(Tripathi et al., 2013)	Delhi Loess
17	0.729	-15.1	(Tripathi et al., 2013)	Delhi Loess
18	0.732	-13.7	(Tripathi et al., 2013)	Thar sands
19	0.7294	-12.6	(Tripathi et al., 2013)	Thar sands
20	0.7332	-14.6	(Tripathi et al., 2013)	Thar sands
21	0.7318	-12.9	(Tripathi et al., 2013)	Thar sands
22	0.7292	-12.7	(Tripathi et al., 2013)	Thar sands
23	0.729	-13.7	(Tripathi et al., 2013)	Thar sands
24	0.739	-14.5	(Tripathi et al., 2013)	Thar sands
25	0.7305	-13.3	(Tripathi et al., 2013)	Thar sands
26	0.7344	-15.8	(Tripathi et al., 2013)	Thar sands
28	0.7115	-6.4	(Kunkelova et al., 2022)	Arabian Peninsula
29	0.7228	-8.4	(Grousset & Biscaye, 2005)	South African Desert
30	0.723	-8	(Grousset & Biscaye, 2005)	South African Desert

31	0.7254	-10.1	(Grousset & Biscaye, 2005)	South African Desert
32	0.7248	-10.7	(Grousset & Biscaye, 2005)	South African Desert
33	0.7217	-3.1	(Grousset & Biscaye, 2005)	South African Desert
34	0.7169	-12.5	(Grousset & Biscaye, 2005)	South African Desert
35	0.7219	-3.8	(Grousset & Biscaye, 2005)	South African Desert
36	0.7464	-5.2	(Grousset & Biscaye, 2005)	South African Desert
37	0.7472	-5.2	(Grousset & Biscaye, 2005)	South African Desert
38	0.7397	-14.4	(Zhao et al., 2018)	North Africa dust
39	0.7325	-12.3	(Zhao et al., 2018)	North Africa dust
40	0.7173	-17.3	(Zhao et al., 2018)	North Africa dust
41	0.724	-14.4	(Zhao et al., 2018)	North Africa dust
42	0.7218	-13.7	(Zhao et al., 2018)	North Africa dust
43	0.7269	-15.9	(Zhao et al., 2018)	North Africa dust
44	0.728	-18.7	(Zhao et al., 2018)	North Africa dust
45	0.7335	-17.8	(Zhao et al., 2018)	North Africa dust
46	0.7344	-18.2	(Zhao et al., 2018)	North Africa dust
47	0.7302	-18.6	(Zhao et al., 2018)	North Africa dust
48	0.7298	-18.4	(Zhao et al., 2018)	North Africa dust
49	0.724	-14.8	(Zhao et al., 2018)	North Africa dust
50	0.7306	-17.1	(Zhao et al., 2018)	North Africa dust
51	0.725	-17.1	(Zhao et al., 2018)	North Africa dust
52	0.7121	-16.4	(Zhao et al., 2018)	North Africa dust
53	0.7395	-12.7	(Zhao et al., 2018)	North Africa dust
54	0.7208	-11.9	(Zhao et al., 2018)	North Africa dust
55	0.73	-13.0	(Zhao et al., 2018)	North Africa dust
56	0.7234	-12.0	(Zhao et al., 2018)	North Africa dust
57	0.7217	-11.2	(Zhao et al., 2018)	North Africa dust
58	0.7205	-10.9	(Zhao et al., 2018)	North Africa dust
59	0.7212	-12.1	(Zhao et al., 2018)	North Africa dust
60	0.7187	-11.6	(Zhao et al., 2018)	North Africa dust
61	0.7177	-10.5	(Zhao et al., 2018)	North Africa dust
62	0.7223	-13.3	(Zhao et al., 2018)	North Africa dust
63	0.7223	-12.6	(Zhao et al., 2018)	North Africa dust
64	0.7245	-13.0	(Zhao et al., 2018)	North Africa dust
65	0.7305	-11.7	(Zhao et al., 2018)	North Africa dust
66	0.7305	-12.9	(Zhao et al., 2018)	North Africa dust
67	0.7254	-12.6	(Zhao et al., 2018)	North Africa dust
68	0.7321	-13.3	(Zhao et al., 2018)	North Africa dust
69	0.7279	-14.0	(Zhao et al., 2018)	North Africa dust
70	0.7288	-13.1	(Zhao et al., 2018)	North Africa dust

71	0.7289	-13.5	(Zhao et al., 2018)	North Africa dust
72	0.7129	-9.9	(Zhao et al., 2018)	North Africa dust
73	0.7138	-10.1	(Zhao et al., 2018)	North Africa dust
74	0.7218	-9.7	(Zhao et al., 2018)	North Africa dust
75	0.7248	-10.0	(Zhao et al., 2018)	North Africa dust
76	0.7129	-13.3	(Zhao et al., 2018)	North Africa dust
77	0.7307	-15.3	(Zhao et al., 2018)	North Africa dust
78	0.7113	-14.5	(Zhao et al., 2018)	North Africa dust
79	0.7142	-12.2	(Zhao et al., 2018)	North Africa dust
80	0.7139	-11.8	(Zhao et al., 2018)	North Africa dust
81	0.7094	-4.8	(Zhao et al., 2018)	North Africa dust
82	0.7127	-9.5	(Zhao et al., 2018)	North Africa dust
83	0.7124	-9.99	(Zhao et al., 2018)	North Africa dust
84	0.7098	-9.5	(Zhao et al., 2018)	North Africa dust
85	0.7092	-11.6	(Zhao et al., 2018)	North Africa dust
86	0.7097	-10.9	(Zhao et al., 2018)	North Africa dust
87	0.7088	-10.9	(Zhao et al., 2018)	North Africa dust
88	0.7108	-9.9	(Zhao et al., 2018)	North Africa dust
89	0.7106	-8.8	(Zhao et al., 2018)	North Africa dust
90	0.7106	-8.6	(Zhao et al., 2018)	North Africa dust
91	0.7108	-4.5	(Zhao et al., 2018)	North Africa dust
92	0.7092	-9.3	(Zhao et al., 2018)	North Africa dust
93	0.7094	-7.3	(Zhao et al., 2018)	North Africa dust
94	0.708	-6.8	(Zhao et al., 2018)	North Africa dust
95	0.7139		(Skonieczny et al., 2011)	North Africa dust
96	0.7173		(Skonieczny et al., 2011)	North Africa dust
97	0.7147		(Skonieczny et al., 2011)	North Africa dust
98	0.715		(Skonieczny et al., 2011)	North Africa dust
99	0.7136		(Skonieczny et al., 2011)	North Africa dust
100	0.715		(Skonieczny et al., 2011)	North Africa dust
101	0.7124		(Skonieczny et al., 2011)	North Africa dust
102	0.712		(Skonieczny et al., 2011)	North Africa dust
103	0.7124		(Skonieczny et al., 2011)	North Africa dust
104	0.711		(Skonieczny et al., 2011)	North Africa dust
105	0.7132		(Skonieczny et al., 2011)	North Africa dust
106	0.7143		(Skonieczny et al., 2011)	North Africa dust
107	0.7205		(Skonieczny et al., 2011)	North Africa dust
108	0.7194		(Skonieczny et al., 2011)	North Africa dust
109	0.7123	-11.3	(Gili et al., 2022)	South Africa dust
110	0.7138	-10.3	(Gili et al., 2022)	South Africa dust
111	0.7127	-9.8	(Gili et al., 2022)	South Africa dust

112	0.7224	-10.9	(Gili et al., 2022)	South Africa dust
113	0.7157	-10.1	(Gili et al., 2022)	South Africa dust
114	0.7265	-10.9	(Gili et al., 2022)	South Africa dust
115	0.7283	-9.7	(Gili et al., 2022)	South Africa dust
116	0.7285	-10.6	(Gili et al., 2022)	South Africa dust
117	0.7306	-10.2	(Gili et al., 2022)	South Africa dust
118	0.7282	-11.5	(Gili et al., 2022)	South Africa dust
119	0.7252	-12.6	(Gili et al., 2022)	South Africa dust
120	0.724	-12.3	(Gili et al., 2022)	South Africa dust
121	0.7244	-12.4	(Gili et al., 2022)	South Africa dust
122	0.7246	-12.1	(Gili et al., 2022)	South Africa dust
123	0.7305	-11.6	(Gili et al., 2022)	South Africa dust
124	0.7329	-10.6	(Gili et al., 2022)	South Africa dust
125	0.7384	-10.2	(Gili et al., 2022)	South Africa dust
126	0.7261	-17.9	(Gili et al., 2022)	South Africa dust
127	0.7255	-17.1	(Gili et al., 2022)	South Africa dust
128	0.7254	-16.3	(Gili et al., 2022)	South Africa dust
129	0.7257	-15.9	(Gili et al., 2022)	South Africa dust
130	0.7261	-15.6	(Gili et al., 2022)	South Africa dust
131	0.7268	-16.1	(Gili et al., 2022)	South Africa dust
132	0.7272	-16.5	(Gili et al., 2022)	South Africa dust
133	0.7278	-16.2	(Gili et al., 2022)	South Africa dust
134	0.7276	-16.7	(Gili et al., 2022)	South Africa dust
135	0.7278	-16.9	(Gili et al., 2022)	South Africa dust
136	0.7281	-17	(Gili et al., 2022)	South Africa dust
137	0.725	-16.4	(Gili et al., 2022)	South Africa dust
138	0.7253	-16.6	(Gili et al., 2022)	South Africa dust
139	0.725	-17.6	(Gili et al., 2022)	South Africa dust
140	0.7208	-12.8	(Gili et al., 2022)	South Africa dust
141	0.7219	-12.8	(Gili et al., 2022)	South Africa dust
142	0.7217	-12.5	(Gili et al., 2022)	South Africa dust
143	0.7218	-12.1	(Gili et al., 2022)	South Africa dust
144	0.7253	-11.8	(Gili et al., 2022)	South Africa dust
145	0.7288	-10.9	(Gili et al., 2022)	South Africa dust

References

- Ahmad, T., & Harris, N. (2000). Isotopic constraints on the structural relationships between the Lesser Himalayan Series and the High Himalayan Crystalline Series, Garhwal Himalaya. *Geological Society of America Bulletin*, 111. [https://doi.org/10.1130/0016-7606\(2000\)112<0467:ICOTSR>2.3.CO;2](https://doi.org/10.1130/0016-7606(2000)112<0467:ICOTSR>2.3.CO;2)
- Argles, T., Foster, G., Whittington, A., Harris, N., & George, M. (2003). Isotope studies reveal a complete Himalayan section in the Nanga Parbat syntaxis. *Geology*, 31(12), 1109. <https://doi.org/10.1130/G19937.1>
- Ayalew, D., Jung, S., Romer, R. L., & Garbe-Schönberg, D. (2018). Trace element systematics and Nd, Sr and Pb isotopes of Pliocene flood basalt magmas (Ethiopian rift): A case for Afar plume-lithosphere interaction. *Chemical Geology*, 493, 172–188. <https://doi.org/10.1016/j.chemgeo.2018.05.037> <https://doi.org/10.1130/G19937>
- Bhanot, V. B, Bhandari, A. K, Singh, V. P., & Kansal, A. K. (1979). Geochronological and geological studies on a granite of Higher Himalaya, northeast of Manikaran, Himachal Pradesh. *Journal of the Geological Society of India*, 20, 90. Retrieved from <https://www.geosocindia.org/index.php/jgsi/article/view/64591>
- Bikramaditya, R. K., Chung, S.L., Singh, A. K., Lee, H.-Y., Lin, T.-H., & Iizuka, Y. (2020). Age and isotope geochemistry of magmatic rocks of the Lohit Plutonic Complex, eastern Himalaya: implications for the evolution of Transhimalayan arc magmatism. *Journal of the Geological Society*, 177(2), 379–394. <https://doi.org/10.1144/jgs2018-214>
- Brook, M. & Snelling, N.J. (1976). K/Ar and Rb/Sr Age Determinations on Rocks and Minerals from Burma. Report of the Isotope Geology Unit 76/12. Institute of Geological Sciences, Keyworth, Nottingham, UK.
- Chu, M. F., Chung, S.L., Song, B., Liu, D., O'Reilly, S. Y., Pearson, N. J. (2006). Zircon U-Pb and Hf isotope constraints on the Mesozoic tectonics and crustal evolution of southern Tibet. *Geology*, 34(9), 745. <https://doi.org/10.1130/G22725.1>
- Clift, P. D., Giosan, L., Carter, A., Garzanti, E., Galy, V., Tabrez, A. R. (2010). Monsoon control over erosion patterns in the Western Himalaya: possible feed-back into the tectonic evolution. *Geological Society, London, Special Publications*, 342(1), 185–218. <https://doi.org/10.1144/SP342.12>
- Dai, J., Yin, A., Liu, W., and Wang, C. (2008). Nd Isotopic Compositions of the Tethyan Himalayan Sequence in Southeastern Tibet. *Science in China Series D: Earth Sciences*, 51, 1306-1316. <https://doi.org/10.1007/s11430-008-0103-7>
- Das, S., Rai, S. K., Rahaman, W., Singhal, S., & Sarangi, S. (2022). Chemical weathering and Sr flux from the silicate lithology dominated fluvial system: Insights from major ions, dissolved Sr and $^{87}\text{Sr}/^{86}\text{Sr}$ of the Teesta headwaters, Sikkim Himalaya. *Applied Geochemistry*, 137, 105171. <https://doi.org/10.1016/j.apgeochem.2021.105171>

Debon, F, Le Fort, P, & Sonet, J. (1986). Granitoid belts West and South of Tibet. About their geochemical trends and Rb-Sr isotopic studies. Science Press, Beijing, 1(395–4). [https://doi.org/10.1016/0040-1951\(87\)90248-4](https://doi.org/10.1016/0040-1951(87)90248-4)

Deniel, C., Vidal, P., Fernandez, A., Le Fort, P., & Peucat, J.J. (1987). Isotopic study of the Manaslu granite (Himalaya, Nepal): inferences on the age and source of Himalayan leucogranites. Contributions to Mineralogy and Petrology, 96(1), 78–92. <https://doi.org/10.1007/BF00375529>

Derry, L. A., & France-Lanord, C. (1996). Neogene Himalayan weathering history and river⁸⁷Sr/⁸⁶Sr: impact on the marine Sr record. Earth and Planetary Science Letters, 142(1–2), 59–74. [https://doi.org/10.1016/0012-821X\(96\)00091-X](https://doi.org/10.1016/0012-821X(96)00091-X)

DIGIS Team, (2021), "GEOROC Compilation: Archaean Cratons", Goettingen Research Online, <https://doi.org/10.25625/1KRR1P>

DIGIS Team, (2021), "GEOROC Compilation: Continental Flood Basalts", Goettingen Research Online, <https://doi.org/10.25625/WSTPOX>

DIGIS Team, (2021), "GEOROC Compilation: Intraplate Volcanic Rocks", Goettingen Research Online, <https://doi.org/10.25625/RZZ9VM>

East, A. E., Clift, P. D., Carter, A., Alizai, A., & VanLanhingham, S. (2015). Fluvial–eolian interactions in sediment routing and sedimentary signal buffering: an example from the Indus Basin and Thar Desert. Journal of Sedimentary Research, 85, 715–728. <https://doi.org/10.2110/jsr.2015.42>

Einfalt, H. C., Hoehndorf, A., & Kaphle, K. P. (1993). Radiometric age determination of the Dadeldhura granite, Lesser Himalaya, far western Nepal. Schweizerische Mineralogische und Petrographische Mitteilungen, 73(1), 97–106. <https://doi.org/10.5169/SEALS-55564>

Fank, W., Thoni, M., & Purtscheller, F. (1977). Geology and petrography of Kullu–south Lahul area. Science de La Terre, 268, 147–72.

France-Lanord, C., & Le Fort, P. (1988). Crustal melting and granite genesis during the Himalayan collision orogenesis. Earth and Environmental Science Transactions of the Royal Society of Edinburgh, 79(2–3), 183–195. <https://doi.org/10.1017/S0263593300014206>

France-Lanord, C., Derry, L., & Michard, A. (1993). Evolution of the Himalaya since Miocene time: isotopic and sedimentological evidence from the Bengal Fan. Geological Society, London, Special Publications, 74(1), 603–621. <https://doi.org/10.1144/GSL.SP.1993.074.01.40>

Goddard Earth Sciences Data and Information Services Center (2016), TRMM (TMPA-RT) Near Real-Time Precipitation L3 1 day 0.25 degree x 0.25 degree V7, TMPA (3B42RT_Daily) [Dataset] Goddard Earth Sciences Data and Information Services Center (GES DISC). <https://doi.org/10.5067/TRMM/TMPA/DAY-E/7>

Gao, L. E., & Zeng, L. (2014). Fluxed melting of metapelite and the formation of Miocene high-CaO two-mica granites in the Malashan gneiss dome, southern Tibet. *Geochimica et Cosmochimica Acta*, 130, 136–155. <https://doi.org/10.1016/j.gca.2014.01.003>

Gazis, C.A, Blum, J.D, Chamberlain, C.P, & Poage, M. (1998). Isotope systematics of granites and gneisses of the Nanga Parbat massif, Pakistan Himalaya.pdf. *American Journal of Science*, 298, 673–698. <https://doi.org/10.2475/ajs.298.8.673>

George, B. G., & Ray, J. S. (2017). Provenance of sediments in the Marwar Supergroup, Rajasthan, India: Implications for basin evolution and Neoproterozoic global events. *Journal of Asian Earth Sciences*, 147, 254–270. <https://doi.org/10.1016/j.jseas.2017.07.027>

Gili, S. A., Vanderstraeten, A. Chaput, J. King, D. M. Gaiero, B. Delmonte, & Mattielli, N. (2022). South African dust contribution to the high southern latitudes and East Antarctica during interglacial stages. *Communications Earth & Environment*, 3 (1), 129. <https://doi.org/10.1038/s43247-022-00464-z>

Goddard Earth Sciences Data and Information Services Center (2016), TRMM (TMPA-RT) Near Real-Time Precipitation L3 1 day 0.25 degree x 0.25 degree V7, TMPA (3B42RT_Daily) [Dataset] Goddard Earth Sciences Data and Information Services Center (GES DISC). <https://doi.org/10.5067/TRMM/TMPA/DAY-E/7>

Goodbred, S. L., Paolo, P. M., Ullah, M. S., Pate, R. D., Khan, S. R., Kuehl, S. A. (2014). Piecing together the Ganges-Brahmaputra-Meghna River delta: Use of sediment provenance to reconstruct the history and interaction of multiple fluvial systems during Holocene delta evolution. *Geological Society of America Bulletin*, 126(11–12), 1495–1510. <https://doi.org/10.1130/B30965.1>

Goswami, V., Singh, S. K., Bhushan, R., & Rai, V. K. (2012). Temporal variations in $^{87}\text{Sr}/^{86}\text{Sr}$ and ϵNd in sediments of the southeastern Arabian Sea: Impact of monsoon and surface water circulation. *Geochemistry, Geophysics, Geosystems*, 13(1). <https://doi.org/10.1029/2011GC003802>

Grousset, F. E., & Biscaye, P. E. (2005). Tracing dust sources and transport patterns using Sr, Nd and Pb isotopes: Chemical Geology, 222, 149-167. <https://doi.org/10.1016/j.chemgeo.2005.05.006>

Grousset, F. E., Parra, M., Bory, A., Martinez, P., Bertrand, P., Shimmield, G., & Ellam, R. M. (1998). Saharan wind regimes traced by the Sr–Nd isotopic composition of subtropical Atlantic sediments: last glacial maximum vs today: *Quaternary Science Reviews*, 17, 395–409. [https://doi.org/10.1016/S0277-3791\(97\)00048-6](https://doi.org/10.1016/S0277-3791(97)00048-6)

Grousset, F. E., Rognon, P., Coudé-Gaussen, G., & Pédemay, P. (1992). Origins of peri-Saharan dust deposits traced by their Nd and Sr isotopic composition. *Palaeogeography, Palaeoclimatology, Palaeoecology*, 93, 203-212. [https://doi.org/10.1016/0031-0182\(92\)90097-O](https://doi.org/10.1016/0031-0182(92)90097-O)

Hao, L.L., Wang, Q., Kerr, A. C., Wei, G.J., Huang, F., Zhang, M.Y. (2022). Contribution of continental subduction to very light B isotope signatures in post-collisional magmas: Evidence from southern Tibetan ultrapotassic rocks. *Earth and Planetary Science Letters*, 584, 117508. <https://doi.org/10.1016/j.epsl.2022.117508>

Haproff, P. J., Zuza, A. V., Yin, A., Harrison, T. M., Manning, C. E., Dubey, C. S. (2019). Geologic framework of the northern Indo-Burma Ranges and lateral correlation of Himalayan-Tibetan lithologic units across the eastern Himalayan syntaxis. *Geosphere*. <https://doi.org/10.1130/GES02054.1>

Harris, N. B. W., Santosh, M., & Taylor, P. N. (1994). Crustal Evolution in South India: Constraints from Nd Isotopes. *The Journal of Geology*, 102(2), 139–150. <https://doi.org/10.1086/629659>

Hu, G., Zeng, L., Gao, L.E., Liu, Q., Chen, H., & Guo, Y. (2018). Diverse magma sources for the Himalayan leucogranites: Evidence from B-Sr-Nd isotopes. *Lithos*, 314–315, 88–99. <https://doi.org/10.1016/j.lithos.2018.05.022>

Imayama, T., & Arita, K. (2008). Nd isotopic data reveal the material and tectonic nature of the Main Central Thrust zone in Nepal Himalaya. *Tectonophysics*, 451(1–4), 265–281. <https://doi.org/10.1016/j.tecto.2007.11.051>

Inger, S., & Harris, N. (1993). Geochemical Constraints on Leucogranite Magmatism in the Langtang Valley, Nepal Himalaya. *Journal of Petrology*, 34(2), 345–368. <https://doi.org/10.1093/petrology/34.2.345>

Jager, E., Bhandari, A. K., & Bhanot, V. (1971). Rb-Sr age determinations on biotites and Whole Rock samples from Mandi and Chor granites, Himachal Pradesh. India. *Eclogae Geologicae Helvetiae*. <https://doi.org/10.5169/seals-163993>

Jain, V., Wasson, R., McCulloch, M., Kaushal, R. K., & Singhvi, A. K. (2022). Controls on sediment provenance in the Baghmati river catchment, Central Himalaya, India. *Journal of Earth System Science*, 131(1), 14. <https://doi.org/10.1007/s12040-021-01759-z>

Jayananda, M., Moyen, J. F., Martin, H., Peucat, J. J., Auvray, B., & Mahabaleswar, B. (2000). Late Archaean (2550–2520 Ma) juvenile magmatism in the Eastern Dharwar craton, southern India: constraints from geochronology, Nd–Sr isotopes and whole rock geochemistry. *Precambrian Research*, 99(3–4), 225–254. [https://doi.org/10.1016/S0301-9268\(99\)00063-7](https://doi.org/10.1016/S0301-9268(99)00063-7)

Kessarkar, P. M., Rao, V. P., Ahmad, S. M., & Babu, G. A. (2003). Clay minerals and Sr–Nd isotopes of the sediments along the western margin of India and their implication for sediment provenance. *Marine Geology*, 202(1–2), 55–69. [https://doi.org/10.1016/S0025-3227\(03\)00240-8](https://doi.org/10.1016/S0025-3227(03)00240-8)

Kingson, O., Bhutani, R., Balakrishnan, S., Dash, J. K., & Shukla, A. D. (2019). Subduction-related Manipur Ophiolite Complex, Indo-Myanmar Ranges: elemental and isotopic record of mantle metasomatism. *Geological Society, London, Special Publications*, 481(1), 195–210. <https://doi.org/10.1144/SP481.9>

Kunkelova, T., Crocker, A. J., Jewell, A. M., Breeze, P. S., Drake, N. A., Cooper, M. J., et al. (2022). Dust sources in Westernmost Asia have a different geochemical fingerprint to those in the Sahara. *Quaternary Science Reviews*, 294, 107717. <https://doi.org/10.1016/j.quascirev.2022.107717>

Kwatra, S. K., Singh, S., Singh, V.P, Sharma, R. K., Rai, B., & Kishor, N. (1999). Geochemical and geochronological characteristics of the Early Palaeozoic granitoids from Sutlej-Baspa Valleys, Himachal Himalaya. *Gondwana Research Group Memoirs*, 6, 145–58.

Le Fort, P, Debon, F, & Sonet, J. (1983). The Lower palaeozoic Lesser Himalayan granitic belt: emphasis of the Simchar pluton of Central Nepal. In *Granites of Himalayas Karakorum and Hindu Kush*, 235–255.

Lee, H. Y., Chung, S. L., Ji, J., Qian, Q., Gallet, S., Lo, C. H., et al. (2012). Geochemical and Sr–Nd isotopic constraints on the genesis of the Cenozoic Linzizong volcanic successions, southern Tibet. *Journal of Asian Earth Sciences*, 53, 96–114. <https://doi.org/10.1016/j.jseaes.2011.08.019>

Li, J. X., Fan, W. M., Zhang, L. Y., Evans, N. J., Sun, Y. L., Ding, L., & Sein, K. (2019). Geochronology, geochemistry and Sr–Nd–Hf isotopic compositions of Late Cretaceous–Eocene granites in southern Myanmar: Petrogenetic, tectonic and metallogenic implications. *Ore Geology Reviews*, 112, 103031. <https://doi.org/10.1016/j.oregeorev.2019.103031>

Licht, A., France-Lanord, C., Reisberg, L., Fontaine, C., Soe, A. N., & Jaeger, J. J. (2013). A palaeo Tibet–Myanmar connection? Reconstructing the Late Eocene drainage system of central Myanmar using a multi-proxy approach. *Journal of the Geological Society*, 170(6), 929–939. <https://doi.org/10.1144/jgs2012-126>

Lin, C., Zhang, J., Wang, X., Huang, T., Zhang, B., & Fan, Y. (2021). Himalayan Miocene adakitic rocks, a case study of the Mayum pluton: Insights into geodynamic processes within the subducted Indian continental lithosphere and Himalayan mid-Miocene tectonic regime transition. *GSA Bulletin*, 133(3–4), 591–611. <https://doi.org/10.1130/B35640.1>

Lin, I. J., Chung, S. L., Chu, C. H., Lee, H. Y., Gallet, S., Wu, G. (2012). Geochemical and Sr–Nd isotopic characteristics of Cretaceous to Paleocene granitoids and volcanic rocks, SE Tibet: Petrogenesis and tectonic implications. *Journal of Asian Earth Sciences*, 53, 131–150. <https://doi.org/10.1016/j.jseaes.2012.03.010>

Lupker M., France-Lanord C., Galy V., Lave' J., Gaillardet J., Gajurel A.P., Guilmette C. , Rahman M., Singh S.K. and Sinha R. (2012) Predominant floodplain over mountain weathering of Himalayan sediments (Ganga basin). *Geochimica et Cosmochimica Acta* 84, 410–432. <https://doi.org/10.1016/j.gca.2012.02.001>

Martin, A. J., DeCelles, P.G., Gehrels, G. E., Patchett, P. J., and Isachsen, C. (2005). Isotopic and Structural Constraints on the Location of the Main Central Thrust in the Annapurna Range, Central Nepal Himalaya. *Geological Society of America Bulletin*, 117, 926–944. <https://doi.org/10.1130/B25646.1>

McKenzie, N. R., Hughes, N. C., Myrow, P. M., Xiao, S., and Sharma, M. (2011). Correlation of Precambrian-Cambrian Sedimentary Successions across Northern India and the Utility of Isotopic Signatures of Himalayan Lithotectonic Zones. *Earth and Planetary Science Letters*, 312, 471–483. <https://doi.org/10.1016/j.epsl.2011.10.027>

Miller, C., Thöni, M., Frank, W., Grasemann, B., Klötzli, U., Guntli, P., & Draganits, E. (2001). The early Palaeozoic magmatic event in the Northwest Himalaya, India: source, tectonic setting and age of emplacement. *Geological Magazine*, 138(3), 237–251. <https://doi.org/10.1017/S0016756801005283>

Murphy, M. A. (2007). Isotopic characteristics of the Gurla Mandhata metamorphic core complex: Implications for the architecture of the Himalayan orogen. *Geology*, 35(11), 983. <https://doi.org/10.1130/G23774A.1>

Nesbitt, H. W., & Young, G. M. (1982). Early Proterozoic climates and plate motions inferred from major element chemistry of lutites. *Nature*, 299(5885), 715–717. <https://doi.org/10.1038/299715a0>

Oliver, L., Harris, N., Bickle, M., Chapman, H., Dise, N., & Horstwood, M. (2003). Silicate weathering rates decoupled from the $^{87}\text{Sr}/^{86}\text{Sr}$ ratio of the dissolved load during Himalayan erosion. *Chemical Geology*, 201(1–2), 119–139. [https://doi.org/10.1016/S0009-2541\(03\)00236-5](https://doi.org/10.1016/S0009-2541(03)00236-5)

Pandey, B. K., Gupta, J. N., Sarma, K. J., & Sastry, C. A. (1997). Sm-Nd, Pb-Pb and Rb-Sr geochronology and petrogenesis of the mafic dyke swarm of Mahbubnagar, South India: implications for Paleoproterozoic crustal evolution of the Eastern Dharwar Craton. *Precambrian Research*, 84(3–4), 181–196. [https://doi.org/10.1016/S0301-9268\(97\)00027-2](https://doi.org/10.1016/S0301-9268(97)00027-2)

Parrish, R.R., and Hodges, V. (1996). Isotopic Constraints on the Age and Provenance of the Lesser and Greater Himalayan Sequences, Nepalese Himalaya. *Geological Society of America Bulletin*, 108, 904–911. [https://doi.org/10.1130/0016-7606\(1996\)108<0904:ICOTAA>2.3.CO;2](https://doi.org/10.1130/0016-7606(1996)108<0904:ICOTAA>2.3.CO;2)

Peketi, A., Mazumdar, A., Pillutla, S. P. K., Sawant, B., & Gupta, H. (2021). Climatic and Tectonic Control on the Bengal Fan Sedimentation Since the Pliocene. *Geochemistry, Geophysics, Geosystems*, 22(3). <https://doi.org/10.1029/2020GC009448>

Peucat, J. J., Vidal, P., Bernard-Griffiths, J., & Condie, K. C. (1989). Sr, Nd, and Pb Isotopic Systematics in the Archean Low- to High-Grade Transition Zone of Southern India: Syn-Accretion vs. Post-Accretion Granulites. *The Journal of Geology*, 97(5), 537–549. <https://doi.org/10.1086/629333>

Pognante, U., Castelli, D., Benna, P., Genovese, G., Oberli, F., Meier, M., & Tonarini, S. (1990). The crystalline units of the High Himalayas in the Lahul-Zanskar region (northwest India): metamorphic-tectonic history and geochronology of the collided and imbricated Indian plate. *Geological Magazine*, 127(2), 101–116. <https://doi.org/10.1017/S0016756800013807>

Rai, B., Kwatra, S. K., Singh, V. P., & Sharma, N. K. (1993). Whole rock Rb–Sr age for granitic rocks of Khadrala area, district Shimla, Himachal Pradesh, India. Preprint Volume 6th National Symposium Mass Spectrometry, 8, 1–4.

- Ramaswamy, V., & Nair, R. R. (1994). Fluxes of material in the Arabian Sea and Bay of Bengal Sediment trap studies. *Journal of Earth System Science*, 103(2), 189–210. <https://doi.org/10.1007/BF02839536>
- Rao, D. R., Sharma, K. K., Sivaraman, T. V., Gopalan, K., & Trivedi, J. R. (1990). Rb/Sr dating and petrochemistry of Hante granite (Baramulla area) Kashmir Himalaya. *Journal of Himalayan Geology*, 1, 57–63.
- Richards, A., Argles, T., Harris, N., Parrish, R., Ahmad, T., Darbyshire, F., & Draganits, E. (2005). Himalayan architecture constrained by isotopic tracers from clastic sediments. *Earth and Planetary Science Letters*, 236(3–4), 773–796. <https://doi.org/10.1016/j.epsl.2005.05.034>
- Robinson, D. M., DeCelles, P. G., Patchett, P. J., and Garzione, C. N., (2001). The Kinematic Evolution of the Nepalese Himalaya Interpreted from Nd Isotopes. *Earth and Planetary Science Letters*, 192, 507-521. [https://doi.org/10.1016/S0012-821X\(01\)00451-4](https://doi.org/10.1016/S0012-821X(01)00451-4)
- Roddaz, M., Said, A., Guillot, S., Antoine, P.-O., Montel, J.-M., Martin, F., & Darrozes, J. (2011). Provenance of Cenozoic sedimentary rocks from the Sulaiman fold and thrust belt, Pakistan: implications for the palaeogeography of the Indus drainage system. *Journal of the Geological Society*, 168(2), 499–516. <https://doi.org/10.1144/0016-76492010-100>
- Shukla. (2011). Geochemical and isotopic studies of some sedimentary sequences of the vindhyan supergroup India. M.S. University of Baroda, Vadodara, Gujarat, India. <http://hdl.handle.net/10603/58046>
- Singh, A., Paul, D., Sinha, R., Thomsen, K. J., & Gupta, S. (2016). Geochemistry of buried river sediments from Ghaggar Plains, NW India: Multi-proxy records of variations in provenance, paleoclimate, and paleovegetation patterns in the Late Quaternary. *Palaeogeography, Palaeoclimatology, Palaeoecology*, 449, 85–100. <https://doi.org/10.1016/j.palaeo.2016.02.012>
- Singh D. P. (2019), Foraminiferal distribution off the southern tip of India to understand its response to cross basin water exchange and to reconstruct seasonal monsoon intensity during the Late Quaternary, PhD thesis, Goa University, Goa, India. <http://hdl.handle.net/10603/281649>
- Singh, K. (2018). Sr, Nd isotopic and geochemical studies of the rocks in the Manipur Ophiolite complex, Indo-Myanmar Range, India. Pondicherry University, Pondicherry. <http://hdl.handle.net/10603/284323>
- Singh, S. K., Kumar, A., & France-Lanord, C. (2006). Sr and $^{87}\text{Sr}/^{86}\text{Sr}$ in waters and sediments of the Brahmaputra river system: silicate weathering, CO₂ consumption and Sr flux. *Chemical Geology*, 234(3-4), 308-320. <http://doi.org/10.1016/j.chemgeo.2006.05.009>
- Singh, S. K., Rai, S. K., & Krishnaswami, S. (2008). Sr and Nd isotopes in river sediments from the Ganga Basin: Sediment provenance and spatial variability in physical erosion. *Journal of Geophysical Research*, 113(F3), F03006. <https://doi.org/10.1029/2007JF000909>
- Sirocko, F. (1995). Abrupt Change in Monsoonal Climate: Evidence from the Geochemical Composition of Arabian Sea Sediments. habilitation thesis. Univ. of Kiel, Kiel, Germany. <https://epic.awi.de/id/eprint/21173/1/Sir1994a.pdf>

Sirocko, F., & Sarnthein, M. (1989). Wind-Borne Deposits in the Northwestern Indian Ocean: Record of Holocene Sediments Versus Modern Satellite Data. In M. Leinen & M. Sarnthein (Eds.), *Paleoclimatology and Paleometeorology: Modern and Past Patterns of Global Atmospheric Transport* (pp. 401–433). Dordrecht: Springer Netherlands. https://doi.org/10.1007/978-94-009-0995-3_17

Skonieczny, C., Bory, A., Bout-Roumazeilles, V., Abouchami, W., Galer, S. J., Crosta, X., & Ndiaye, T. (2011). The 7–13 March 2006 major Saharan outbreak: Multiproxy characterization of mineral dust deposited on the West African margin. *Journal of Geophysical Research: Atmospheres*, 116(D18). <https://doi.org/10.1029/2011JD016173>

Stutz, E., & Thöni, M. (1987). The lower Paleozoic Nyimaling Granite in the Indian Himalaya (Ladakh): New Rb/Sr data versus zircon typology. *Geologische Rundschau*, 76(2), 307–315. <https://doi.org/10.1007/BF01821076>

Szulc, A. G., Najman, Y., Sinclair, H. D., Pringle, M., Bickle, M., Chapman, H., et al. (2006). Tectonic evolution of the Himalaya constrained by detrital 40Ar-39Ar, Sm-Nd and petrographic data from the Siwalik foreland basin succession, SW Nepal: Tectonic evolution of the Himalaya. *Basin Research*, 18(4), 375–391. <https://doi.org/10.1111/j.1365-2117.2006.00307.x>

Taylor, P. N., Chadwick, B., Moorbath, S., Ramakrishnan, M., & Viswanatha, M. N. (1984). Petrography, chemistry and isotopic ages of Peninsular Gneiss, Dharwar acid volcanic rocks and the Chitradurga granite with special reference to the late Archean evolution of the Karnataka craton, southern India. *Precambrian Research*, 23(3), 349–375. [https://doi.org/10.1016/0301-9268\(84\)90050-0](https://doi.org/10.1016/0301-9268(84)90050-0)

Tobisch, O. T., Collerson, K. D., Bhattacharyya, T., & Mukhopadhyay, D. (1994). Structural relationships and Sr-Nd isotope systematics of polymetamorphic granitic gneisses and granitic rocks from central Rajasthan, India: implications for the evolution of the Aravalli craton. *Precambrian Research*, 65(1–4), 319–339. [https://doi.org/10.1016/0301-9268\(94\)90111-2](https://doi.org/10.1016/0301-9268(94)90111-2)

Tripathi, J. K., Bock, B., & Rajamani, V. (2013). Nd and Sr isotope characteristics of Quaternary Indo-Gangetic plain sediments: Source distinctiveness in different geographic regions and its geological significance. *Chemical Geology*, 344, 12–22. <https://doi.org/10.1016/j.chemgeo.2013.02.016>

Tripathy, G. R., Singh, S. K., Bhushan, R., & Ramaswamy, V. (2011). Sr–Nd isotope composition of the Bay of Bengal sediments: Impact of climate on erosion in the Himalaya. *Geochem. J.*, 45, 175–186. <https://doi.org/10.2343/geochemj.1.0112>

Trivedi, J. R., Gopalan, K., & Valdiya, K. S. (1984). Rb-Sr ages of granitic rocks within the Lesser Himalayan nappes, Kumaun, India. *Journal of the Geological Society of India*, 25, 641–654. Retrieved from <https://www.geosocindia.org/index.php/jgsi/article/view/65318>

Vimal R., Banerjee R., Gupta S., Krishna V., Achar K.K., Babu P.V., Parihar, P. S., Maithani, P. B. (2012). Geochemistry and Sr and Pb isotope systematics of basement granitoids from north and west of Palnad Sub-basin, Guntur and Nalgonda districts, Andhra Pradesh: *Journal of Applied Geochemistry*, 14(3), 295–315.

Williams, H. M. (2004). Nature of the Source Regions for Post-collisional, Potassic Magmatism in Southern and Northern Tibet from Geochemical Variations and Inverse Trace Element Modelling. *Journal of Petrology*, 45(3), 555–607. <https://doi.org/10.1093/petrology/egg094>

Zeng, L., Gao, L. E., Tang, S., Hou, K., Guo, C., & Hu, G. (2015). Eocene magmatism in the Tethyan Himalaya, southern Tibet. *Geological Society, London, Special Publications*, 412(1), 287–316. <https://doi.org/10.1144/SP412.8>

Zhang, H., Harris, N., Parrish, R., Kelley, S., Zhang, L., Rogers, N. (2004). Causes and consequences of protracted melting of the mid-crust exposed in the North Himalayan antiform. *Earth and Planetary Science Letters*, 228(1–2), 195–212. <https://doi.org/10.1016/j.epsl.2004.09.031>

Zhao, W., Balsam, W., Williams, E., Long, X., & Ji, J. (2018). Sr-Nd-Hf isotopic fingerprinting of transatlantic dust derived from North Africa. *Earth and Planetary Science Letters*, 486, 23–31. <https://doi.org/10.1016/j.epsl.2018.01.004>

Zhao, Z., Mo, X., Zhang, S., Guo, T., Zhou, S., Dong, G., & Wang, Y. (2001). Post-collisional magmatism in Wuyu basin, central Tibet: evidence for recycling of subducted Tethyan oceanic crust. *Science in China Series D: Earth Sciences*, 44(S1), 27–34. <https://doi.org/10.1007/BF02911968>